School of Biological Sciences

# Development of Soft Modular Robotics

by

Victoria Wumi Oguntosin

Thesis submitted for the degree of Doctor of Philosophy

**Electronics Engineering**

**Biomedical Engineering Section, School of Biological Sciences**

**November 2017**

University of Reading

# Abstract

This thesis covers the development and validation of soft robots in providing upper limb assistive motion. The main purpose of this research is to develop highly compliant and resilient actuators that generate motion for elbow and shoulder movements. To accomplish the purpose of the study, the fabrication, geometric construction along with experimental data of pressure, torque and range of motion of all developed actuators are described.

The main contribution of this thesis is the development of soft actuators that transfer force via elastic deformation in order to generate assistive motion; features such as flexibility and soft contact with the skin ensure excellent safety potential of the actuators. To reduce the instability phenomenon attributed to the elastic response of rubber under large deformations that leads to bulging, the implementation of a pleated network design and embedded braided mesh network is presented. Bulging was reduced and torque output was increased with the integration of braided mesh into the silicone rubber actuator. The soft actuators developed for elbow and shoulder motion was tested on ten healthy participants thereby demonstrating its comfort, ease of use, fitting and removal as well as its practicality as an assistive apparatus for stroke patients. The use of soft robotics to provide shoulder motion was also assessed by the integration of soft robotics with a gravity compensated exoskeleton. The developed soft actuators were powered with electro-pneumatic hardware components presented in a compact, embedded form. Positive and negative air pressure control was implemented by a piecewise linear control algorithm with the performance of the controller shown.

The design of a novel muscle made entirely of silicone rubber that contract upon actuation was described together with the manufacturing procedure, design parameters and measurement results of performance of these muscles such as the velocity of shortening, isometric contraction and maximal obtainable muscle force (without shortening). The muscles are manufactured to mimic the skeletal muscles present in the human body.

These muscles are composed of a number of wedge-like units in series, the number of these wedge units increase the contraction. The soft muscles were characterized in order to find optimum design parameters that results in more contraction and speed; the muscles were tested on a model hinge joint to execute flexion/extension of the forearm at the elbow. Aside from contracting, the muscle has an interesting capability of producing bidirectional bending by the regulation of internal positive and negative air pressure in each wedge unit.

In order to measure performance data relating to range of motion from bending, rotary and muscle actuators, computer vision processing was made use of. Soft robots are made with materials that experience large deformations, the sensors used to obtain measurement data can either be through the use of embedded sensors or visual processing. The use of embedded sensors can be cumbersome, resulting in limitation of its performance. The visual processing algorithms implemented to measure performance data such as angle of motion, bending angle and contraction ratio in real-time using a Webcam is described. Visual processing concepts such as colour tracking, template matching, camera calibration were applied. The developed vision system was applied to execute vision based motion control which is able to move the soft robot to a desired position using high level vision control and lower level pressure control.

The material described in the preceding paragraphs are presented in an interrelated format. A concise introduction to the thesis is presented in the first chapter. An extensive survey of the field of soft robotics including materials, manufacturing procedure, actuation principles, primary accomplishments, control and challenges are presented in the literature review chapter, together with a review of rehabilitation devices. Since this work focused on the use of silicone rubber as actuator material, a brief introduction to working with silicone rubber as an engineering material is presented in the third chapter. The conclusions of the work and suggestions for future research are provided at the last chapter of this thesis.

# Declaration of Originality

I confirm that this is my own work and the use of all material from other sources has been properly and fully acknowledged.

Victoria Wumi Oguntosin

# Acknowledgment

I would like to thank my supervisors, Dr Yoshikatsu Hayashi and Prof. Slawomir Nasuto for their supervisory guidance and for fruitful discussions during the meetings. I thank Prof. William Harwin and Prof. Sadao Kawamura for the support and contribution. Mr Guy Haworth together with Mr Ben Haworth also supported me during the starting phase of this project by providing me with relevant advise. I also want to thank members of the Brain Embodiment Lab (BEL) for the platform for development.

I gratefully acknowledge the contribution of Mr Peter Tolson in the mechanical arrangement of the exoskeleton; Mr Steve Gould and Mr Nick Dove for technical support.

My gratitude goes to Mr Jonathan Adedeji for his encouragement, involvement and contribution to my work.

My appreciation goes to my siblings: Mide, Sumbo, Dunni and Yinka for providing me with inspiration, emotional support and for their endurance throughout this study period.

I am greatly indebted to my parents, Emmanuel & Marion Oguntosin, for their intervention, enormous investment and for being a source of inspiration.

I thank God that I had these people, guiding and supporting me through this journey.

# Table of Contents

# Chapter 1

# Introduction

> The softest things in the world
> overcome the hardest things.
>
> *Lao Tzu*

Until recent times, majority of the robots described today are made of rigid links connected by joints actuated with motors or servos. Ongoing research work in the field of soft robotics has therefore found the need to differentiate between traditional robots made of metals and rigid links as "hard robots" while those made of flexible materials are freely termed "soft robots". Soft robot and soft robotics has become a rapidly growing field, hence the need to coin the phrase "hard robot" so as to distinguish it from the more familiar rigid type robots [1].

The first robots were soft: the first usage of the word "robot" was that of an autonomous machine moulded in humanoid form [2]. It is also intuitive to imagine robots not just in humanoid form but also from living organisms. This intuition is arrived at because living organisms composed of completely deformable bodies perform excellent locomotory feats that exceeds the motion of humans or organisms with skeletal support [3]. Soft robotics inspired by nature and biology, therefore represents a fascinating new alternative. Figure 1.1 shows a diagram of the comparison between hard and soft robots. While hard robots draw inspiration from mammalian limbs, soft robots are inspired by muscular hydrostats with no skeletal system.

A lot of the motivation for soft robotics is an actuation method that is closer to nature. Nature does not use metal or servos, therefore, bio-inspired mechanisms of actuation points to some very interesting alternatives. Soft robotic structures display continuum

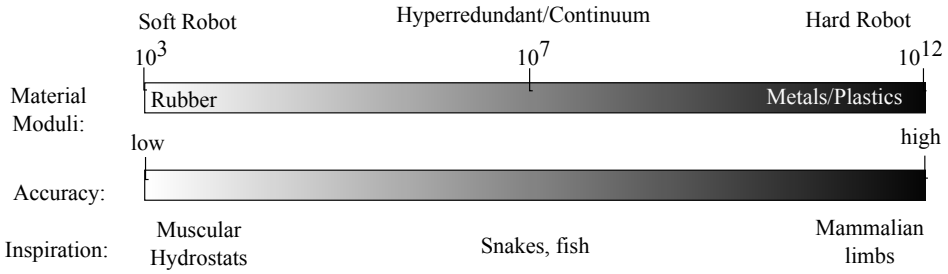


Figure 1.1: Trends from hard and soft robots

motion, large deformation, comparatively high compliance and resilience when compared to traditional rigid-bodied robots [4]. Soft robots have a number of advantages over "hard" robots, such as the ability to handle irregularly-shaped objects comparable to how primates grasp objects; squeeze into tight spaces like a lizard, rat or octopus; and easily recover from collisions. A major advantage of soft robotics is that their design and fabrication together with their actuation components are relatively inexpensive compared to hard robots. Furthermore, when robots are soft, they are safer to interact with making them a lot more comfortable to wear and handle. Researchers have begun to explore the design and control of soft-bodied robots composed of compliant materials. In fact, the main motivation behind this research work is to make use of soft structures through the development of soft robotic actuators to provide assistive force to individuals with weakness of their upper limb. The use of these soft assistive devices are particularly targeted towards recovering stroke patients.

## 1.1 Aims

The aim of this work is the design of soft, wearable robotic assistive devices for the rehabilitation of stroke patients. The device will assist the patient in a compliant way, thereby delivering assistive force in a gentle way. In achieving this aim, the following contributions to research were achieved:

1. Design and validation of entirely soft silicone rubber actuators to effect angle change

2. The development and application of visual processing algorithms to act as sensor for soft robots and to measure parameters of the robot during actuation.

3. Development, fabrication and characterisation of novel soft robotic muscles made completely of silicone rubber that contract upon actuation.

4. A novel concept of producing bending motion with soft silicone rubber actuators.

## 1.2 Background

This thesis is comprised of several projects explored during research while working towards the main aim of the project which is novel designs and implementations of soft robots to provide assistance motion to individuals with weakened upper limb, patients recovering from stroke in particular. The focus on stroke patients is because there is a substantial number people that would experience and survive a stroke owing to the fact that age is a risk factor and the baby boom of the 1950s [5]. These patients would require hand and arm rehabilitation devices to recover muscle function. This is because upper-limb weakness that arises from stroke is due to damage to the motor and somatosensory cortex of the brain resulting in the loss of muscle function in some parts of the upper limb [6]. Stroke patients are encouraged to exercise their damaged limb to facilitate the regrowth of a pattern of neurons that would aid recovery through brain plasticity [7]. These exercises are often delivered with assistive robotic devices.

The thesis is organized as follows - After providing background introductory information (Chapter 1), Chapter 2 reviews recent advances in the fields of soft robotics and rehabilitation robotics. This work is based on using silicone rubber to develop soft robots, so introductory concepts that pertain to rubber material science is given in Chapter 3. Chapter 4 then describes the detailed manufacturing process of the produced soft robotic actuators from schematic drawings to final production. Chapter 5 presents the visual processing algorithms used to provide measurement data on the performance of the soft robot; and then Chapter 6 describes the performance of the soft actuators developed in Chapter 4 in terms of air pressure, range of movement and torque characterisation. In Chapter 7, the implementation of an embedded hardware controller and novel software controller that drives the actuation components was detailed; The anatomy of the upper limb is described in Chapter 8 alongside qualitative study of the use of the developed actuators on healthy participants. In Chapter 9, a practical use of soft robots in providing active motion for a passive exoskeleton is detailed. Finally, the conclusion and possible future direction of this work is provided in Chapter 10.

This thesis is largely based on work that appeared in the UKSIM-AMSS International Conference on Modelling and Simulation; International Journal of Simulation Systems, Science & Technology (IJSSST); and 2015 IEEE International Conference on Rehabilitation Robotics (ICORR) [8, 9, 10, 11].

# Chapter 2

# Literature Review

The field of soft robotics is multidisciplinary: the fields of material science, biology, chemistry, electronics, robotics, mechanical design and control engineering are closely allied with soft robotics. Its application branches into a large number of potential fields including health care, soft sensors and assistive devices. In this literature review, research work in the field of soft actuators has been described with particular emphasis to the main application of this research work which is the development of soft actuators to aid assistive motion.

This review chapter is divided into two parts - the first part provides an overview on the field of soft robotics detailing its motivation, methods of actuation, control, fabrication, soft sensors and challenges. The second part gives a review of rehabilitation robotics then narrow it down to work that has been done using soft robotics for rehabilitation. It also provides a review of hardware and software controllers applied for robots. At the conclusion of this chapter, there will be an understanding about actuation mechanisms, manufacturing, sensors and controllers of soft materials, the primary accomplishments in the field of soft robotics till date and the current challenges the field faces. There will also be an awareness of the systems developed in rehabilitation of persons with upper limb disabilities, with the review of soft rehabilitation devices.

## 2.1 Part I - Soft Robotics

This part will discuss the field of soft robotics in general while giving a focus on the major achievements of the field over its short history. There is a focus on robots that are intrinsically soft. These robots are compliant and resilient: they are compliant in that

they possess an inherent ability to transfer force by deformation, and exhibit resilience due to their ability to recover from the deformation.

## 2.2 What is Soft Robotics?

A novel design paradigm for robots is to design robots that provide safety in an intrinsic way or by means of control components [12]. The term "soft" may refer to the compliance of a structure, it can also refer to its inherent material properties. In other words, soft can be via intrinsic material properties or via extrinsic mechanical design or software induced. 'Soft' is an extrinsic property, depending on robot's architecture; Even metal actuators can be "soft" relative to object/actuator interaction. In compliant robotic actuation systems, compliance is added to conventional drives by adding elastic elements to the drive chain [13]. One example of such is the Baxter robot, it is compliant and can safely share its workspace with humans due to its mechanical design and combination of sensors that makes Baxter aware of where humans are and how to safely interact with people. Its softness is generated by the geometrical arrangement of its composed structure.

There is therefore the need to provide a formal definition of soft robots. The RoboSoft Coordination Action community proposed and agreed on the following definition of soft robots during its first plenary meeting [14]: *"Soft robots are devices which can actively interact with the environment and which can undergo 'large' deformations relying on inherent or structural compliance"*. In order words, soft robots comprises of deformable devices that possess sensing, control and actuation components. From Figure 2.1, the materials from which soft robots are manufactured from will generally fall below the $10GPa$ young's modulus line and $10000Kgm^{-3}$ density line.

### 2.2.1 Soft robots draw inspiration from biology

Research in robotic manipulators has focused mainly on designs that bear a resemblance to the human arm in structure. But in nature, this is not the only design that can perform complex feats of locomotion. Nature uses soft materials frequently and stiff materials sparingly [15]. Animals such as snakes, elephants, and octopuses make use of soft bodies that allow them to effectively manipulate objects, even though they are very different in structure compared to the human arm [16]. Soft materials play a critical role

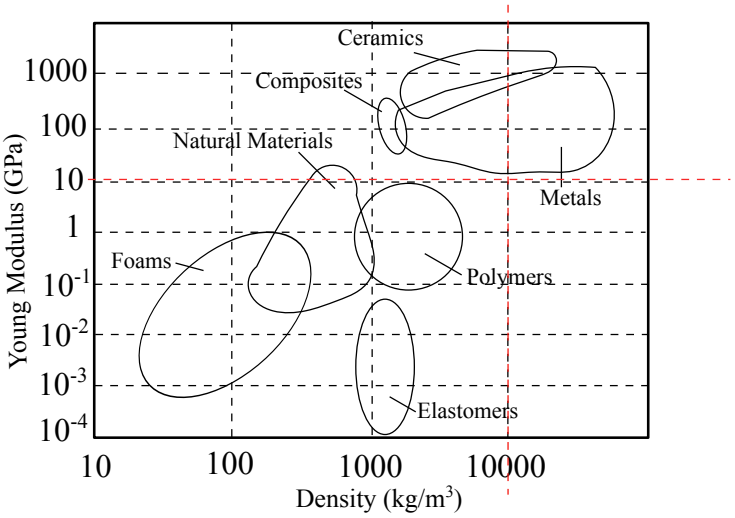


Figure 2.1: Modulus density graph of engineering materials.

in the mechanical design of animals, these soft components provide numerous benefits, helping animals negotiate and adapt to its ever changing, complex environment [17].

Biological living organisms are one motivation behind soft robotics. The huge majority of animals are soft bodied, even those with stiff skeletons are largely composed of soft materials. For example, the human skeleton (with a Young's Modulus of 20 - 30GPa) is about 11% of the body mass while the soft skeletal muscles contributes an average of 42% of body mass in a typical human. Moreover, other organs of vertebrates such as heart, tendons, ligaments, skin are all soft and flexible. The mammalian tongue is entirely composed of soft structure and yet able to achieve complex feats of locomotion such as elongation, shortening, bending, stiffening and torsion.

The fluidic (gaseous or liquid) actuation principle of soft robots has a strong background in biomimetics [18], for example, in hydrostatic skeletons. The pressure of fluid in an hydrostatic skeleton is used to change the organism's shape and produce movement. In contrast to hydrostats, muscular hydrostats are composed mainly of muscle tissue with no skeletal support. The mechanisms of elongation, bending, stiffening and torsion in muscular hydrostats work on the principle of water incompressibility at physiological pressures. This same principle is used by worms, elephant trunks, squids, octopuses, mammalian and reptile tongues for motion.

### 2.2.2 Design motivation for soft robots

Aside the highlighted benefits described thus far, soft robots possess many other interesting benefits by virtue of their nature. These include the following:

1. Safe interaction − due to high flexibility, soft robots possess high safety integrity when handling them.
2. They are suitable for use in open (unconstrained) as well as constrained environments because they conform better to obstacles [16].
3. Soft structures manipulate and grasp objects with their body, so no need of specialised end-effectors.
4. Soft structures can be repaired when damaged owing to their non linear elastic behaviour and resilience.
5. They are relatively inexpensive compared to discrete manipulators [16]..
6. Characteristic high power to weight ratio − robotic designs with inflatable structures aim at space applications since they have a small shipping volume when unactuated [19].
7. Shock absorbing − shock forces are reduced with soft elements, collision forces cannot be minimised when the joints are stiff.

Just as George Whitesides, a soft robotics expert at Harvard University says *"Soft robotics is going to be a very big deal. It provides a set of capabilities that just cannot be performed with hard robots"* [1]

## 2.3 Actuation Mechanisms of Soft Materials

The body of soft robots are manufactured from a wide variety of engineering materials which include polymers, composites and natural materials [18]. Polymers constitute a higher percentage of soft materials that have been explored in soft robotics till date. Metal alloys have surprisingly been explored as soft materials, but in liquid form and millimeter sized thickness. Table 2.1 shows a list of engineering materials with example soft materials that have been used to achieve soft material actuation.

Table 2.1: Engineering materials with example soft materials that have been explored in soft robotics for actuation purposes, polymers constitute a large fraction of engineering materials that have been explored in soft robotics.

| **Engineering Material** | **Example soft material** |
|---|---|
| Foams | Silicone foam prepolymers [20] |
| | Polystyrene foam [21] |
| | Urethane foam [22] |
| Polymers | Polyester [23] |
| | Elastomers [24] |
| | Latex rubber [18] |
| | Polythene [17] |
| | Hydrogel [25] |
| | Electroactive Polymers [26] |
| | Silly putty® [27] |
| | Sewing thread [28] |
| | Fishing line [28] |
| | Braided mesh sleeve [29] |
| | Polypropylene [30] |
| | Nylon [31] |
| | Thermoplastic urethane [32] [33] |
| Metals | Shape Memory Alloys [34] |
| | EGaIn (Liquid Metal) [35] |
| Natural origin | Onion epidermal cells [36] |
| | Coffee beans [37] |
| | Cotton [38] |
| | Wood pulp [39] |
| Composites | Fiber reinforced rubber [40] |
| | Filled rubber [23] |
| | Nano-sheet infused polymer [23] |
| Ceramics | Piezo [41] |
| Glass | Not yet studied for actuation purposes. |

The body of a soft robot can be actuated by chemical, mechanical or electrical means, their actuators and/or power transmission systems are usually integrated within and distributed throughout their soft body. For example, air operated soft actuators have a air cavity inside its body which produces motion when filled with compressed gas. One type of soft actuator, called Flexible Fluidic Actuators (FFA) generally consist of a soft flexible body that transmits potential energy, delivered by a pressurized fluid, into a mechanical force, which then can be used to create motion [23]. Therefore, actuation power can be delivered mechanically through hydraulic or pneumatic means or powering mechanical components electrically. FFAs are fabricated with materials such as silicone elastomers [24], vulcanized elastomers [32], thermoplastic urethanes [31], fire hose material [30], kevlar® fabrics [19], multi-lumen hose material [40] and other composite materials. Research into soft structures has spawned many different designs and actuation modes. The most popular design is driven by pneumatic or fluidic actuation, other designs use electrical energy, thermal and chemical energy. Pneumatic actuation normally requires compressed air which is easier to store, readily available and environmentally friendly. The various designs are explained in the following subsections.

### 2.3.1 Shape Memory Alloys

he motion experienced by Shape Memory Alloy (SMA) actuators, are due to variation of its crystalinity and material properties. SMAs have special memory characteristics and can be trained to "remember" a shape by means of annealing. The most commonly used shape memory alloy is Nickel Titanium (NiTi) alloy. Nitinol wire can act as a muscle wire because it becomes shorter when heated above a transition temperature, contraction ratio is typically 5-8%. Superelastic nitinol is also used as superelastic wire which becomes resilient and would spring back to its original shape when deformed without the use of heat. A nitinol shape memory wire would return to its pretrained shape only with the application of heat. When heated by electric current, the wire bends to its trained shape with a usable amount of force. The nitinol SMA provides a relatively large force and movement when actuated. SMA actuation is accomplished by embedding the trained alloy into silicone rubber and passing electric current through the wire to produce heat that deforms the robot to the trained shape. A soft hand with five fingers and a palm was fabricated [42] for grasping, actuated by NiTi SMA strip pre-trained to a circular shape. NiTi coil spring was modelled and fabricated for use in soft actuators [34]. An octopus arm prototype [33, 15] was built and actuated with

cables and SMA springs. NiTi coil actuators arranged in flexible braided mesh-tube structure was used to achieve peristaltic locomotion [43]. A crawling inchworm inspired robot [44] was actuated by means of SMA coil spring to bend its body into an omega shape. SMA coil springs were also used [45] to generate complex gaits with the use of a soft body. Though SMAs have low contraction ratio in straight form, they can be trained into other different shapes such as circular or in form of wedges to produce varying contraction strains. A major advantage of SMAs is extremely low mass of the wire or sheet.

### 2.3.2 McKibben Artificial Muscles

Artificial muscles are a class of flexible fluidic contraction actuators, they generate a tensile force when air pressure is applied due to anisotropic membrane stiffness [23]. Artificial muscles are designed to mimic the skeletal muscles in humans and animals to achieve locomotion. There have been increasing research in designing structures that mimic the skeletal muscle. These muscles are generally referred to as Pneumatic Artificial Muscles (PAM). Driving pressures for these actuators are typically higher than elastomer based soft actuators. The first research work in PAM was done in 1930 [46]. Joseph McKibben is the inventor of the most popular PAM who used it for his daughter named Karen, who was paralyzed from the neck down as a result of polio in 1950. The most developed and highly studied type of artificial muscles are the pneumatic muscles commonly referred to as the McKibben muscles [29, 47]. McKibben-type muscles have their interior composed of highly elastic inner membrane through which compressed air enters; this inner membrane is surrounded with a helically wound fiber reinforcement such that actuation via air pressurization would cause contraction. When pressurized, the muscle increases in surface area with the axial contraction coupled to a radial expansion such that some of the energy is then used for membrane deformation [23]. Pneumatic muscles have been used to actuate the fingers for gripping [48], they are used in many applications such as in prosthesis, exoskeletons and rehabilitation [29, 47, 48]. A diagram of the McKibben muscle is shown in Figure 2.2.

Pneumatic muscles allow for compliant and light weight construction of assistive devices. McKibben muscles can generate a pulling force of up to 1000-1500N and typically have a contraction ratio between 30-35% [49]. This relatively small contraction ratio is one of major disadvantages of PAMs. Due to small contraction ratio coupled with the generation of one axis linear motion, realizing bidirectional revolute joints is complex

(a) Unactuated (b) Contracted

Figure 2.2: Actuation via compressed air of the McKibben muscle produces shortening of the muscle.

and results in a bulky setup [38, 50]. Artificial muscles made by twist insertion from sewing thread and fishing line have been developed [28]. These muscles have been shown to have little hysteresis, cheap, strong, capable of lifting weights more than 100 times their own weight while delivering up to 5kW/kg of work.

A much more recent work on artificial muscles are work carried out [51] where multi filament muscle fibers were fabricated using thin McKibben muscles. These muscles were applied to give a musculoskeletal robot in order to mimic the muscles responsible for knee and ankle motions in the human body. Advantages of these muscles include its miniature size, therefore, summation of contraction in each muscle fiber will lead to increase in contraction. Disadvantages include bulky and tedious arrangement to realise rotary motion of the elbow and shoulder. Commercially available McKibben muscles are sold by FESTO AG&Co. in Germany, and Shadow Robot Company in the U.K.

### 2.3.3 Elastomer-based soft robots

Apart from PAMs, the most popular design of soft robots are the elastomer-based designs. Soft elastomer actuators are another class of compliant structures capable of producing different motions through inflation of internal network channels with compressed air. They usually operate at lower pneumatic pressures compared to McKibben artificial muscles [4]. As opposed to McKibben-type actuators, they are made almost entirely out of stretchable materials such as silicone-rubber [52]. They can be actuated electrically (by SMAs) or through fluidic pressure (using pneumatics or hydraulics) by (Flexible Fluidic Actuators or FFAs). They are capable of executing extending, contracting, twisting, angular change and bending motions [52].

Bending motions are created by adding structural constraints implemented by gluing

two different grades soft elastomer layers: one is highly extensible while the other is highly inextensible [24, 53]. The inextensible layer can be realised with embedding a soft layer with constraining material such as paper [54], braided weave or other fabric. The constraint serves to transform channel deformation into segment curvature by providing a neutral axis around which the segment bends [55]. The bending soft robot operates on the same principle of a bimetallic strip: gluing two metals having different expansion coefficient produces bending when temperature rises. Similarly, gluing two rubber layers together having different elastic modulus with air channels in between produces bending when inflated. Investigations of ways to increase the bending curvature is achieved by designing multichannel networks [54] or reinforcement with an helically wound thread [56]. A design was proposed [57] with only axial fiber reinforcements, thus, actuation of the rubber section only leads to radial stretching. This principle was also applied in this research work by using an interwoven net as the fiber reinforcement to prevent bulging of the designed soft actuator. Muscles composed of only silicone rubber were developed for the production of contraction linear motion [58].

### 2.3.4 Inflatable air bag structures

Inflatable structural elements are another class of soft actuators, these structures are not elastomer based but are composed of fabrics such as composite sheets, polyurethane, polythene and other plastic materials that can be joined via thermal welding or sewing. Inflatable robot links having structural members were proposed [59] to provide safe physical interaction. A arm constructed with plastic elements such as inflatable links and air bag was designed [31]. Otherlab [19] specializes in using inflatables for developing robots, orthosis as well as exoskeletons which compares favorably in applications hard robots are designed to achieve.

Apart from robotic applications, air bag structures have widely been employed in safety systems especially in vehicles as shock absorber during collision following a road accident. Airbags consist of a flexible fabric bag and are often used as part of safety feature in a vehicle. A combination of the air and flexible material help to protect against forward momentum by providing a soft cushioning in the event of a crash by absorbing large impact forces.

### 2.3.5 Electroactive Polymers

Another way to classify soft actuators is based on its response to stimulation. Polymers that change shape or size in response to electrical stimulus are called ElectroActive Polymers (EAPs) actuators. EAPs operate on the principle of polarization, ion transfer, molecular shape change and phase change in active conducting polymer layers. Ionic-type conducting polymer actuators change shape by diffusion of ions and the mobility of their conjugated substances. Dielectric Elastomer Actuators (DEA) are a type of EAP made with an incompressible and highly deformable dielectric medium. When an electric field is applied across the parallel plates of a capacitor, coulombic forces in between generate a stress, making the electrodes to move closer. This movement squeezes the elastomer, causing an expansion in the lateral direction [26]. EAPs are compliant, bio-compatible, not affected by magnetic field, have low power consumption and the ability to be miniaturized [60]. Ionic EAPs operate in electrolytic solution which limits the range of practical applications. However, because the actuation of EAP is by directly controlling the applied voltage, the implementation of a software controller can be easily implemented. A planar bending motion inspired by the locomotion movement of cilia, a nano-sized organelle, was synthesized [61] using dry-type electroactive polymer actuator.

A soft gripper made from a thin silicone layer sandwiched between two soft electrodes was designed [62] to grasp objects possessing different shapes and material properties such as flat and deformable objects. The gripper made of DEA structure with an interdigitated electrode geometry is shape adaptable and can firmly grip fragile objects and objects up to 80 times its weight. The principle to achieve bending, holding and manipulation of objects is based on electrostatic actuation with electroadhesion force.

### 2.3.6 Hydrogel

Hydrogel is a soft, highly water absorbent polymer material and the amount of water that can be absorbed into it can approach up to 99 wt% of the hydrogel mass [63]. Hydrogels are a suitable material for soft robots because the tissues present in the human body and other soft-bodied animals contains 70% water. Hydrogels can be used to imitate these natural tissues because they are able to absorb the 70% water which natural tissues are composed of by regulating the amount of water absorbed into the hydrogel.

An hydrogel's movement is induced with chemicals and electric current. For example, copper ions injected into an hydrogel creates copper-linked polymer molecules that bends and stiffens the hydrogel. They transform chemical energy into mechanical motion [25]. Apart from their application in soft actuation, hydrogels are used as scaffolds for tissue engineering, drug delivery and biological modelling [64].

### 2.3.7 Granular material jamming

Granular jamming has been practiced in the agricultural industry [65] with the use of granular food products. When particles of a granular material like sand or coffee grounds are tightly packed together, they "jam" or lock into one another. But when they are loosely packed, they become deformable, soft and pliable. This approach to actuation is due to stiffness resulting from variation in mechanical properties of the system. The number, shape and dimensions of particles have been identified as key factors affecting the jamming mechanism. A soft bag containing a granular material is shaped around an object and can efficiently sustain the grasp firmly by vacuum-packing. Friction, suction and mechanical interlocking connects gripper and object. One of the first robotics research to exploit the jamming of granular material concept was presented by Brown et al [37]. The reliability of this simple concept has now led to their use for unconventional applications, and well suited for gripping objects whose shape is unknown prior to grasping. Another design [66] used the jamming of granular material principle to achieve reversible stiffness of manipulator joints since the gripper can transition from soft state to rigid state. Granular material jamming method of actuation is simple, feasible, low-cost and highly adaptable but current research suggest that stiffness values are low [65, 67].

## 2.4 Inflation Sources

Inflation source commonly used for powering pneumatic soft actuators is compressed air. Sodium azide explosion [68] has been studied as a source of inflation. Propane is another potential gas that has not yet been explored for inflating soft robots. These highlighted inflation sources are listed:

1. Compressed air: The primary merits of using air as the source of pneumatic actuation are unlimited abundance, free availability, portability, damage resistance, no environmental pollution, light weight and low viscosity [69].

2. Explosion of Sodium azide: An electronic controller detonates the mixture of oxidizers and sodium azide to release nitrogen which causes inflation pressure in the reaction: $2NaN_3 \rightarrow 2Na + 3N_2$. This high temperature reaction of approximately 300°C requires ignitors and accelerants. This is commonly used to inflate vehicular airbags [68].

3. Propane: This is a potential gas that can be used as a source of inflation but it is 1.5 times denser than air, this limits its use as inflation source compared to air that is lighter and more freely available [69].

## 2.5 Fabrication

Soft roboticists often have to fabricate and build every aspect of their robot from scratch including the actuator body and geometry, almost nothing exists off the shelf [70]. This section focuses on the fabrication methods used for manufacturing soft robots. Table 2.2 presents a summary description of standard manufacturing processes of engineering materials with example soft materials that have been produced using these techniques. Standard manufacturing techniques of engineering materials includes machining, injection moulding, thermoforming, sheet metal forming, casting, additive manufacturing and welding. The materials from which soft actuators are made of have great influence on the fabrication process. The two main processes for soft actuator fabrication are moulding and welding. Casting can be achieved through soft lithography, lost-wax casting or compression moulding. Welding can be achieved via thermal lamination or sewing. Soft actuators produced with clothing fabric material are sewn, internal bladder is required which together with sewing, produces an air tight volume. A third, newly developed method is production of a soft robot via rapid prototyping such as 3D printing the soft robot using projection stereolithography [71]. Methods that have been studied for the fabrication of soft robots are explored in this section.

### 2.5.1 Compression moulding

In compression moulding [23], a preheated liquid rubber material is poured into a heated mould cavity. The mould is then closed with pressure and heat maintained until the material has fully cured. The first step in compression moulding involves moulding the inner shell. For the second step, the inner shell is covered with a braided fiber

sleeve as reinforcement using Vectran® yarn. The fiber reinforcement determines the pressure resistance of the actuator. After insertion of metal connectors and adapters for connection with compressed air source, a thin layer of rubber is added to the surface and cured. Compression moulding requires the production of moulds with specialized geometry, this limits variation in shape but provides actuators with higher operating pressures, hence more force.

### 2.5.2 Casting

Fabrication of a soft robot via casting also makes use of a two-step moulding process, however, it does not require the use of high pressure and temperature as in compression moulding. In the first step, the inner cavity that comprise the main actuator geometry is made by curing in a master mould which is designed to be a negative of the desired channel structure. The second step closes the actual actuator chamber by covering the main cavity with a bottom layer to create an enclosed structure. Casting techniques that have been widely explored include soft lithography and lost-wax casting.

**Soft lithography:** Soft lithography is similar to compression moulding except that it does not involve the use of pressure. Soth lithography can be done by hand casting and would not require the use of specialized or industrial equipment and can be implemented under standard atmospheric temperature and pressure. The mould is 3D-printed with Acrylonitrile Butadiene Styrene (ABS) or Polylactic Acid (PLA) plastic material to form the actuator's cavity, the design of which requires the use of 3D CAD software and printing technology. Limitations of this approach include restrictions in the demoulding process; soft robots produced using soft lithography largely constrained to a planar morphology [4] except when more complex geometry are involved. Soft lithography provides a convenient and low-cost method for the formation and manufacturing of soft actuators [72]. A fundamental downside of this fabrication procedure is that the produced soft robot is prone to failure at the site of joining due to the points of weakness created by the 2-step fabrication process.

**Lost-wax casting** Here, soft actuators are moulded as one piece rather than using a multi-layer moulding process. First, liquid rubber is poured into the top mould and allowed to cure. A wax core supported with an embedded rod is then affixed to the mould together with the bottom mould. Strain limiting liquid rubber is

poured into the assembled mould to form a constraint layer. The cured actuator is then removed from the mould. The wax cure is melted out from the actuator within an oven. Tubing is then inserted with the soft robot ready for actuation [73]. Lost-wax casting is advantageous because it eliminates the rupture-prone connection between channels and constraint layer associated with soft lithography.

### 2.5.3 Thermal Welding

Another way of manufacturing soft actuators is via welding to create a hermetically sealed structure. Fabrication of soft actuators by welding entails the fusion of thermoplastic materials together to form an enclosed structure of varied shapes that can be actuated with compressed air. The impulse sealer or ultrasonic welder is mostly used for this purpose. The machine allows the welding of only straight seams between layers of plastic film. Hot air welding machine allows for producing curved seams and more complex actuator geometry. One advantage of this fabrication process is that it does not require the design and use of very complicated moulds. Example of soft actuators produced using this method are inflatable air bag actuators [31, 59].

### 2.5.4 Additive and Subtractive Manufacturing

The application of rapid prototyping described so far has been in the design of moulds to cast the rubber elastomer. Here, the soft robot itself is manufactured directly using additive or subtractive process or a combination of both.

**3D-Printing the soft robot:** The commonly used method of casting rubber a multistep approach before the final actuator is arrived at, it offers a low cost way to progress from prototypes to final products [74]. 3D printing the soft robot provides an alternative because the actuator is printed out in a single step process. 3D printing technology was commercially developed circa 1980 but recently became popular due to the advent of open source 3D printers. Application of this technology ranges from manufacturing countless products such as toys, decorations, furnitures, enclosures to applications in assistive technology [75].

A soft robot has been produced via 3D-printing using Projection Stereolithography (SLA) [71]. The soft robot is printed with a photopolymerizable elastomeric material with a SLA 3D printer. A projector directs light on to the desired areas

for selective polymerization. Upon curing, the build platform repositions along the Z-axis of the printer layer-by-layer and the process is repeated until all layers are cured. The produced design are more prone to fracture compared to casted rubbers, they have a relatively low strain but offer an area for further research and exploration because they offer a new fabrication process for soft actuators and promising direction to making sophisticated, biomimetic systems.

Another work on 3D printing the soft robot using Fused Deposition Modeling (FDM) technology was carried out [76]. The printed robot was capable of bidirectional bending and showed high power to weight ratio. NinjaFlex®, a thermoplastic urethane based material from Fenner Drives possesses rubbery properties and can be used as printer filament. The properties of NinjaFlex that makes it suitable as a soft material are its flexibility, strength and quality. It is capable of stretching, bending, twisting and folding without causing permanent deformation. NinjaFlex material is suited for high endurance applications due to its sufficiently large Young's modulus of about 2200psi (15.2MPa).

**Shape Deposition Manufacturing (SDM):** SDM is a layered manufacturing method in which parts are built through cycling alternating layers of structural and support material. This involve alternative steps of subtractive manufacturing with the use of a CNC machine to shape each layer of material after deposition (additive manufacturing). The layered addition of sacrificial support material allows for the construction of nearly arbitrary geometries and facilitates the inclusion of embedded components [77] such as sensors, motors or structural reinforcements. A grasper manufactured via alternating layers of stretchy and stiff materials with a cable embedded was described [78]. This technology has application in medical application such as for performing surgical operation [79].

## 2.6 Soft skin and sensors

Silicone rubber possesses many distinct features which make it suitable for a number of novel applications. These features include the following:

(i) It is soft and deformable, conforms to surfaces, and releases from features of a mould without damaging them or itself depending on the mould material.

Table 2.2: Standard manufacturing processes of engineering materials showing examples of soft materials that have been fabricated using such process.

| **Manufacturing process** | **Description** |
|---|---|
| Machining | - a group of processes that comprises of material removal and surface modification after production by other methods<br>- involves a subtractive process, such as milling, drilling<br>- commonly used for metals<br>- explored in soft robotics under SDM [78, 79] |
| Injection moulding | - involves heat and pressure; used to produce polymers<br>- in soft robotics: elephant trunks are produced [23] |
| Thermoforming | - involves heat and pressure of a plastic sheet into a pliable forming temperature against a mould<br>- similar to injection moulding, but thermoformed parts are thinner, e.g. the manufacturing of polythene plastic bags<br>- types: vacuum forming and blow moulding<br>- in soft robotics: to manufacture inflatable bag actuators |
| Sheet metal forming | - involves bending and/or die cutting and/or stretching an already manufactured material<br>- commonly used for metals, not yet explored in soft robotics |
| Casting | - a process involving solidification of a material (from liquid state) to take the shape of the mould.<br>- for producing complex geometries and internal cavities<br>- common process of manufacturing soft robots [4]<br>- types: (i) sand; (ii) die; (iii) investment 'lost wax' casting |
| Additive manufacturing | - refers to a process by which digital 3D design is used to build up a component in layers by depositing material.<br>- commonly referred to as 3D printing.<br>- have recently been explored in soft robotics [71, 76]<br>(i) Extrusion: also known as Fused Filament Fabrication (FFF); material is selectively dispensed through a nozzle and solidifies.<br>(ii) Photopolymerization: also known as Stereolithography (SLA); material is cured by light activation<br>(iii) Powder bed fusion: energy (in form of laser or electron beam) is used to selectively fuse regions of a powder bed; also referred to as Selective Laser Sintering/Melting (SLS/SLM) |
| Welding | - materials are joined together, under high temperatures<br>- used commonly for metals and thermoplastics<br>- in soft robotics, plastic bags are thermally welded together to produce complex shapes [31, 59] |

(ii) Irreversible Sealing: Liquid silicone adheres to cured silicone without requiring high temperatures, pressures or voltages.

(iii) Reversible Sealing: Silicone rubber makes reversible conformal contact (van der Waals contact) with smooth, non silicone surfaces. It can therefore be demountable multiple times without degradation to itself.

(iv) Non toxic: Biocompatible silicone rubber are not harmful to proteins and cells in biological organisms; it is permeable to oxygen and carbon dioxide, but only slowly permeable to water. Silicone rubber possesses excellent biocompatibility properties, and thus used in implants and suitable for culturing mammalian cells [80].

Silicone rubber has been integrated into a variety of designs to be used in soft skin and sensors. This section would describe some other novel soft robot sensors and actuators that have been developed.

**Eutectic Gallium-Indium (EGaIn) Sensors:** One approach to sensing in soft-bodied systems is with EGaIn alloy [35] injected into flexible microfluidic channels of silicone rubber. Gallium-Indium alloy is an electrically conductive fluid metal. Its rheological property at room temperature makes it suitable for use as a soft sensor to be embedded into an elastic material. EGaIn behaves like an elastic material until it experiences a critical surface stress, at which point it yields and flows readily [81]. This behaviour facilitates its injection into microchannels as a liquid at room temperature after which it becomes elastic.

The basic principle behind the EGaIn sensor is: when the elastomer is stretched, the geometry of the channel changes (reduction in cross-sectional area and increase in length) resulting in a change of resistance. By measuring this change in resistance, it becomes possible to calculate the strain. EGaIn sensors are well suited for large strain applications owing to their elastic nature [82].

**Tactile array sensors:** It consists of a barometric pressure sensor and the associated tactile array circuit built on a flexible membrane [83]. This design allows the measurement of touch through a soft interface by integration into designs like robot finger structures to provide a robust and compliant grasping surface [84]. Unlike the EGaIn sensor, tactile array sensors are not designed to measure strain or stretch but to sense grasping events and detect object shape.

**Smart Braids:** The reinforcing braid of a McKibben artificial muscle is manufactured using conductive and insulated wires that form a solenoid-like circuit whose inductance and resistance changes with muscle contraction. Hence, the measured inductance indicates the contraction ratio [85, 86]. A particular advantage of smart braids is that sensing is embedded in the structural material itself so no requirement for additional materials to the actuator.

**Soft skin innovations:** Rubber actuators have been made to emit light which changes in both luminance and capacitance under deformation. A soft and stretchable electroluminescent display [87] was made with silicone rubber by also mixing with appropriate fillers.

In another design, a soft electronic artificial skin, called iSkin was developed [88]. iSkin is a thin, flexible, stretchable touch sensor that can be worn directly on the skin at different locations opening up possibilities for mobile interactions that have not been possible with traditional touch sensors. Combining capacitive and resistive touch sensing, a major advantage is that the soft sensor remains functional under typical and extreme deformations that occur on the human body. Another soft skin sensor [41] was manufactured by embedding piezoelectric transducer into silicone rubber to achieve pneumatic vibrotactile actuation.

The elasticity of silicone rubber have been used as valves to open and close air channels. The mode of operation is through the application of a force by piezoelectric actuators that pinches and releases a fluidic channel made of PDMS in order to close or open it at a precise location [69].

A soft elastic battery, made from wood and pulp material making it light and porous has been fabricated [39]. Wood fibers were used to increase strength and create covalent bonding in the fiber–fiber joint [89]. The spongy material was coated with an electrically conductive ink to give it the ability to store energy within the aerogel. The soft, 3D energy storage device was fabricated based on layer by layer self assembly of interdigitated thin films on the surface of an electrically conductive substrate. Graphene, a 2D carbon sheet with monoatomic layer thickness, offers great potential to be used with soft materials for creating energy storage devices. A 100% soft battery made completely of stretchable silicone rubber have been fabricated to generate electric power. In this way, the body of a soft robot can be used to power sensors attached to its body [90].

## 2.7 Soft actuators controller

Soft robotics is currently an active area of research [24, 53, 4, 91, 68, 92]. The compliant structure of soft robots allows novel motion and grasping tasks that are difficult to implement with rigid parts [93]. Their compliant nature allows them to be placed in direct contact with the surface of the skin [94] to provide the necessary assistive force through pressure control. These robots are considered soft due to their intrinsic property: the materials from which they are made are compliant and resilient. Soft robots are actuated by electrical or mechanical means to provide a deformation in their shape. FEAs are actuated by compressed air and are capable of producing multiple degrees of freedom using a single actuation source and each degree of freedom cannot be controlled directly. Therefore, pressure control becomes very important when actuating these robots.

Previous work on methods of driving soft actuators is with the use on/off solenoid valves [24, 53], syringes [95] and cylinders [55] to control the flow of pressurized air to the actuators. The use of cylinders is superior to on/off solenoid valves since it enables precise analogue control of airflow into and out soft robots [55]. The effectiveness of pneumatic pressure controllers has been confirmed through step response experiments, both for PWM-controlled on/off valves [96] as well as for different types of servo valves [97, 98]. A feedback control loop with an angle filter was implemented for a fiber reinforced soft bending actuator [99]. Using information about the measured input air pressure from a pressure sensor, the angle filter of the feedback loop estimated the required soft actuator bending angle.

A soft pneumatic system that requires the multiplexing of many fluids, ranges of pressure and changes in flow rate has been implemented [69]. This system utilized elastomeric valves that open and close using piezoelectric actuators of a commercial Braille display. This Braille display had 64 individually addressable pins and therefore controlled 32 expandable outputs. The micro fluidic device having elastomeric valves was fabricated using soft lithography. As the piezoelectric actuator present in the Braille display moved a pin upward, the elastomeric membrane closes the micro channel and vice versa. Figure 2.3 shows a diagram of elastomer valves arrangement for pressurizing and depressurizing an air channel. This work served to identify serial, embedded and parallel connection possible with air valves for soft pneumatic actuation because the connection of solenoid valves for a multichannel soft robot would later be used in this

work will be used for inflation and deflation task. While mentioned applications of this system include control of medical assistive soft machines and untethered soft robots, no work has so far been done to apply the principle of elastomeric valves with soft, pneumatic, non-microfluidic actuators.

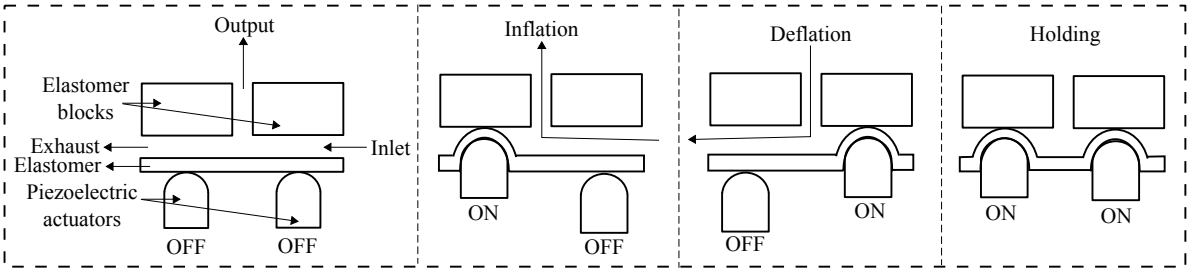


Figure 2.3: Four different states are possible with two elastomer valves: unactuated, inflation, deflation and holding state [69].

## 2.8 Challenges of soft structures

The strengths of soft actuators have been described so far. Unfortunately, the soft robots' greatest strength also becomes its weakness. The design, fabrication and precise control of soft robots are considerably challenging. These core challenges are listed:

**Design:** Soft robots require specialist knowledge to design because they are continuum by design with multiple DoF which is different from conventional robotic manipulators, connected with kinematic joints having lesser DoF. Designed soft actuators suffer from hysteresis and non linearity due to multiple DoF and air flow dynamics [100]. Rubber, a common material associated with soft robotics, is subject to wear and fatigue, it retains episodes of excessive stretch (temperature effect).

**Fabrication:** Casting elastomer into moulds still requires considerable design and effort. The traditional method of manufacturing by machining and assembly simply does not apply in soft robotics. Manufactured designs of exactly the same specification could differ significantly from one other in performance. Silicone rubbers are difficult to bond with other materials, making compound structures difficult. Though soft robots may be inexpensive to fabricate, creating a hermetically air sealed actuator could be a challenge and undermine performance.

**Strength:** Soft robots transmit forces in proportion to the air pressure requirements. They have been unable to generate the large amounts of torque comparable with rigid-bodied robots.

**Motion:** In nature, it can seem effortless and uncomplicated to move and explore the environment, but not in the world of soft robotics. It has proved very difficult to create robots that can exhibit the smart, agility and dexterity seen in nature [101]. Pneumatic actuation requires air compressors which are noisy. Solving the inverse kinematics of soft robots are considerably challenging thereby presenting demanding requirements for actuation [102].

**Control:** The precise control of soft robots is considerably challenging because they possess infinite degrees of freedom as they navigate based on deformation of their structure [42]. Through the compliance benefits and soft interaction offered by soft robots, they are more difficult to control when compared with rigid manipulators [103]. Soft robots' high degree of flexibility makes precise control of its position, configuration, output force and movement a difficult task since its kinematics is not easily described. There are still no standard sensors: a robust, standardized, stable measurement and control system is still a challenge. Although several types of soft sensors have been developed as explained in Section 2.6, there is still the need to adapt and integrate these sensors to a specified design at prototypes scale because researchers still have to fabricate their soft robots from scratch. Because soft robots have notional infinite DoF and rely on material deformation for controlling their position, control is still difficult even when feedback sensors are present [42]. Furthermore, pneumatic systems are known to generally suffer from nonlinearity due to air compressibility. They are also difficult to control since identifying a precise system model is cumbersome due to unknown disturbances [104].

In this thesis, Chapter 4 addresses the design, fabrication of soft robots for different types of motion. The problem of strength is also addressed by introduction of fabric reinforcement. Chapter 7 addresses the specific problem of pressure control in pneumatic soft robots.

## 2.9 Part I - Conclusion

The aim of this work is to utilise soft robots to provide assistive force for the movement of the upper limb. McKibben soft actuators have undergone numerous early research in rehabilitation robotics but are posed with severe limitations: they are limited by the inability to miniaturize and also limited due to their ability to generate only linear motion. Therefore, conversion of this linear motion into the rotary motion commonly present in human joints result in complex and voluminous arrangement. The developed actuators that would be described in this work therefore presents interesting and novel alternatives.

The applications of soft structures designs is not only limited to assistive devices and prosthesis alone, designs can be developed to mimic the motion of reptiles, the way they walk, grasp objects, etc. through bending actuators [4]. The increased degree of freedom provided by the softness can also allow for achieving flexible human-like movements such as smiling. They can be used to do dangerous tasks, i.e. in nuclear applications and in general work that requires the flexibility of human control. Since they are bio-compatible, they can also be used for neural implants and can be applied for the design of stretchable electronic circuits.

The accomplishments and innovations in the field of soft robotics continue to increase in number as advances in materials, hardware and software control, higher robustness, novel sensors and actuators allow designers to attempt new ways of developing smart materials and devices with novel capabilities.

## 2.10 Part II - Rehabilitation Robotics

This part will provide a review of rehabilitation robotic systems that have been developed for the upper limb with a discussion of major innovations in the field. Rehabilitation robotics is generally aimed at improving the quality of life for disabled persons and can be categorized into therapy and assistive robots. Assistive robots can be grouped based on manipulation, mobility, or cognition abilities. Robotic rehabilitation systems aim to provide robotic assistance for persons with upper and lower limb disability so they can engage in Activities for Daily Living (ADL), or to improve physical or cognitive function by providing therapy [5]. Rehabilitation robotics also includes the disciplines of prosthetics, Functional Neural Stimulation (FNS) and Brain

Computer Interface (BCI) technologies. Prostheses are artificial limbs designed for use to replace amputated ones. FNS systems employ electrical stimulation of nerve and muscle in order to move weak or paralyzed limbs. BCI systems seek to record brain activity which could help in diagnosing and monitoring people during ADLs. In this part, focus is on systems that have been studied for upper limb rehabilitation. A focus and critical review of soft robots in upper limb rehabilitation is also carried out. Figure 2.5 shows a diagram to give an overview of the field of rehabilitation robotics.

## 2.11 Robots for assistive motion

In order to execute physical motion support for disabled persons, daily life assistance and motion therapy devices for function recovery are required. Daily life assistance robots can be machines that substitute for movement to perform day-to day tasks while function recovery devices are machines used for exercises to train the damaged part to quicken recovery. Function recovery robots are classified as end-effector type or wearable. In end-effector type assistance, the patient holds the end effector of a robot, movement of the end-effector will produce a corresponding movement of the arm. Wearable assistance involves the patient wearing the device through attachments such that controlled movement of the robot will lead to movement of the arm.

The descending motor pathway of the neuromuscular system is the most important tract of the motor system. It starts at the pre-central gyrus (motor cortex) and sends an axon that goes to the posterior limb of the internal capsule. At the junction of the brainstem and upper cervical spinal cord, 90% of these axons cross (Figure 2.4). The neuromuscular system of the body exhibits use dependent plasticity - this implies that use modifies function by changing the properties of neurons and muscles, including the pattern of their connectivity [6]. Using this feature, patients can relearn how to move by engaging in therapy activities following a neuro-muscular damage such as stroke [105]. Typically, rehabilitation therapies are either highly human intensive requiring skilled therapists or involve attachment of rigid robotic controls to the upper limb. The use of human therapists can be labor intensive and time consuming because daily, intensive and repetitive movements are needed over a long period.

Robot-based rehabilitation has been shown to have positive effects by lessening of impairment [107]. Robots provide an acceptable performance measurement test; and control of the amount of exercise delivered to the subject [108]. Since the amount

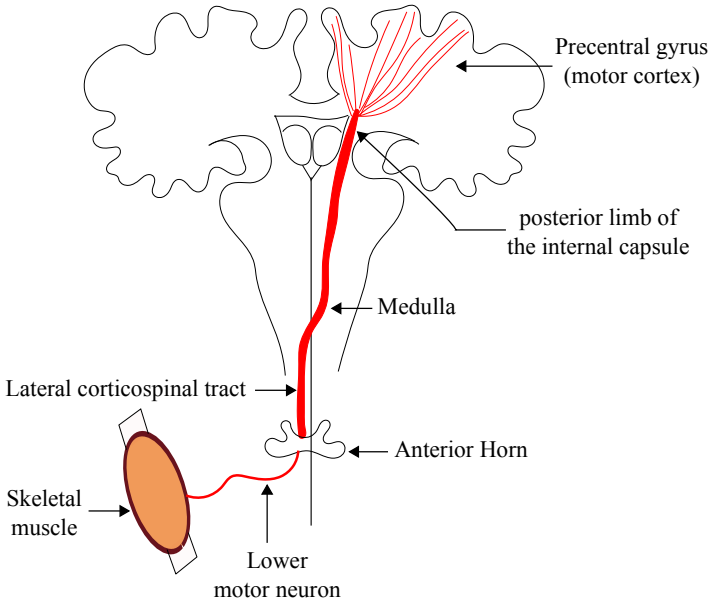


Figure 2.4: The neuromuscular system showing signal flow from the motor cortex to a muscle [106].

of recovery is linked with the amount of repetition, robots are able to deliver a set of repetitive movement at lower cost than human therapists, increasing chances of patients' recovery. Robots also provide well controlled patterns of assistive therapy, therefore, the possibility of studying brain plasticity during therapy is possible using robot-based approach.

Hard robotic structures are often based on joints connected by rigid links; this makes them heavy with expensive and complicated control. In addition, these robotic controls are less compliant than the joints they themselves actuate, making it difficult to be directly attached to the human body unless through the use of specialized end effectors [109], thereby mitigating their use for personal use by patients. To overcome these challenges, safe human robotic interactions can be achieved through soft wearable robots [29].

### 2.11.1 Robot Exoskeletons for Upper Extremity

The history of rehabilitation robotics dates back to the late 1950s. Then, robots were large manipulators used to replace workers in factories for dirty, dangerous, and undesirable tasks [5]. Hence, this design crept into rehabilitation robotics thereby giving

rise to rigid exoskeletons.

A 5 degree-of freedom exoskeleton termed Motorized Upper Limb Orthotic System (MULOS) consisting of 3 DoF movements at the shoulder and 2 DoF at the elbow joint was designed [110]. The problems with MULOS are due to difficulty in moving the shoulder through a large workspace due to risks of arm dislocation. The hard nature of the exoskeleton could lead to injury and pain over prolonged use and must therefore follow strict supervision during usage. The center of rotation of the 3 Revolute Revolute Revolute (RRR) shoulder joints should not move in MULOS, but in everyday life, this center of rotation is normally moved. Motion at the sternoclavicular and acromioclavicular joints of the shoulder girdle permits gliding of the scapula over the chest wall and considerably enhances the mobility and reach of the upper limb, and as a result, makes the center of rotation move, so usage of MULOS would cause misalignment with the robot and lead to long term wearing of the human shoulder joint and greater chances of dislocation. This is the reason 3RRR articulate design to assist shoulder motion is not suitable since it does not consider the joints at the shoulder girdle.

More popular upper extremity devices are MIT-MANUS and ARMin. The MIT-MANUS is an end-effector type planar robot with two active degrees of freedom, that makes use of the Selective Compliant Assembly Robot Arm (SCARA) configuration. MIT-MANUS is the first robotic exoskeleton to undergo great success in clinical trials of stroke patients [111] and attain commercial success. It has a simple mechanical design that allows planar movement of the arm across a tabletop while a patient plays simple video games involving moving a cursor to a target that changes locations on a computer screen. The clinical version is called InMotion ARM. The ARMin combines a haptic display with a four active and two passive degrees of freedom exoskeleton [112]. They support spatial arm movements and account for weight of the subject's extremity to compliantly move against gravity.

The Mirror Image Movement Enhancer (MIME) [113] system from Stanford uses a Puma-560 robot arm to provide assistive movement of the upper arm by attaching to the hand through a customized splint and connector designed to break away when high interaction forces are applied.

The GENTLE/s system [114] from EU project uses a commercial robot, the Haptic-Master to allow for 4 DoF movement and achieves a high bandwidth of force control using force feedback. This system makes use of gravity compensating mechanism and robot driven interactive interface to assist patients while performing therapy.

The MIT-MANUS, ARMIn, MIME and GENTLE/s robots are advantageous in their own rights: entirely rigid robots are fast and accurate but not intrinsically soft. These rigid robots rely on user vigilance and explicit control to be safe. As an ethical concern, if a user does not possess the capability of assessing the robot's safety, then the positive value of a robot is nullified by the harm that it could inflict on the user, hence the need for an intrinsically safe robot.

### 2.11.2 Gravity Compensation

Articulated robots suffer from adverse effects of gravity loading. Robots can be designed such that gravity has minimal effect. To make a rigid robot safe while maintaining performance and payload, a solution is the division of tasks into two: compensating for gravity and moving the mass as high amounts of torque are usually required in robot manipulators just to overcome gravity. For example, the SCARA robot plane of motion is horizontal, so vertical (gravity) effects are eliminated. A gravity balanced arm is essentially in indifferent equilibrium, meaning that no joint actuator inputs are required to keep the system in equilibrium for any configuration. Gravity compensation method equilibrates a rotational mechanism for all postures so that effects of varying torques due to gravity is passively negated [115]. Methods of countering gravity effect can be achieved by adding counterweights such that the mass center coincides with the pivot point or by using stored energy in springs.

The combination of a parallelogram structure together with the introduction of linear springs which produces a non-linear restoring force that opposes gravity are uniquely suited for counterbalancing applications [116]. This design is used in robot assistance by providing support to the arm against gravity using elastic bands, while still allowing a large range of motion of the arm. The gravity compensation mechanism is the same as that in an anglepoise lamp. Ideally, a zero free length spring whose ends are connected to the link is sufficient to offset gravity effects. However, zero free length springs can be replaced by cable-pulley system combined with a non-zero free length spring or the use of a preloaded spring. A passive device called Wilmington Robotic Exoskeleton (WREX) was developed at the Alfred I. duPont Hospital in Delaware [75] to balance out the effects of gravity in three dimensions. The WREX uses a parallelogram linkage and elastic bands to allow users move their arms against gravity by providing a sense of flotation. Children with arthrogryposis were able to navigate their hands through space [117] with WREX. The device attaches parallel to the arm and forearm and can be

worn via a wheel chair or back brace. Commercial companies such as Neater Solutions Ltd, Armeo Spring and JAECO Orthopedic produce and markets various designs of WREX. T-WREX or Therapy-Wilmington Robotic Exoskeleton allows substantially weakened patients to practise simple virtual reality exercises that simulate functional tasks such as shopping and cooking [118]. Another different design called Freebal [119] compensates for gravity using a spring and sling system. Springs are more favorable for gravity compensation because they use stored energy, whereas counterweights add weight and inertia.

### 2.11.3 Series Elastic Actuators (SEA) and Variable Stiffness Actuators (VSA)

Compliant robotic actuators have different principles of operation which can be pneumatic, elastomeric or joint stiffness variation. Rigid robots can be made compliant with the introduction of elasticity into the drives. It has been proposed that for natural tasks such as manipulation, the interface between the actuator and load should be less stiff [120]. Series Elastic Actuators (SEAs) and Variable Stiffness Actuators (VSAs) introduce passive compliance into electromechanical drives by the addition of elastic elements between the drive and actuator output. VSAs control joint stiffness mechanically or by the controller. Stiffness is changed with a spring unit while impedance is adjusted with a damper unit. Contrary to the intuitive notion otherwise, robots based on SEAs and VSAs are easy to control, accurate, have good reproducibility and repeatability [121, 120]. These, of course will depend on the accuracy of the sensors used.

Actuation systems for robotic exoskeletons that combine Bowden cables with SEA have been developed [13]. The Bowden cables allow the motors to be mounted remotely in a fixed position in order to reduce transmitted mass on exoskeleton links. SEAs help to reduce the negative effects associated with static friction and also the effects which unmodelled dynamics have on the stability of force control. A robot based on SEA concept can execute stiff, robot-in-charge mode and compliant, low-impedance assist-as-needed mode.

### 2.11.4 Assistive control of motion

The procedure followed by physiotherapists when exercising the limb of a stroke patient involves discharge of weight, guidance of motion path and guided assistance relative to patient's muscular strength. Therefore, robot-assisted control of assistive force to be delivered to a patient is implemented as either patient-cooperative or continuous passive therapy. In patient-cooperative therapy, the effort or muscular strength of the patient is measured and accounted for in delivering exercises. This therapy is also called assist-as-needed, that is, the robot is controlled such that patients are able to engage in exercises as much as possible. This method have been found to reduce the treatment period and enhance recovery because movement effort by the patient is a key factor for recovery. Continuous Passive Motion (CPM) does not take into account the patient's effort, so exercises are delivered to move a joint through its range of motion without the patient's muscles being considered.

Series elastic elements are used to deliver compliant control to robots. But actuators operated pneumatically are already compliant by virtue of air compressibility. Pneumatic actuators are attractive because of this inherent feature of compliance but their control is difficult, limiting their use [100]. ON/OFF control air valves possesses just two states. A better analogue control of air inflow and outflow in soft actuators is with piston cylinders, although non-linear effects associated with pneumatics still hold. A two-staged cascaded control involving a lower level pressure controller and high level control using visual information can be implemented [4]. Another work [122] devised a cooperative control strategy to ensure the robot act in unison with the patient's arm while providing customized assistance in proportion to the patient needs. Another pneumatic actuator control scheme was developed [30] to guarantee sufficient safety and account for unforeseen circumstances during assistive therapy. Another control law of soft robots based on desired trajectories, actual distances to targets together with desired and estimated direction of patient's motion was developed [50].

## 2.12 Brain Computer Interfaces (BCI) and Functional Neural Stimulation (FNS)

Research work on decoding movement related brain signals in real time [7] has made it possible to control an assistive device. Using signal processing to decode brain activity,

a user is able to control the rehabilitation robot through decoding intended movement. Brain Computer Interfaces (BCI) can be classified into invasive and non-invasive methods. Non-invasive method employs the recording of electrical activity of the brain by means of surfaces electrodes. This is known as Electroencephalogram (EEG). A user of EEG can control the amplitude of the EEG signal as a function of time or the amplitude of specific frequency components of the EEG signal through training. Four degrees of control has been achieved with BCI to control assistive devices and also the movement of a computer cursor to a desired target. Invasive approach of BCI requires the implantation of electrode to measure the amplitude and frequency of brain signals.

Rehabilitation robotics also involve neural stimulation. For individuals that have their limbs paralyzed due to neurological injury, the actuator (the natural limbs itself) is still present but the control system that drives it is not functional. Functional Neural Stimulation (FNS) seeks to take advantage of this by making use of external electrical signals directly delivered to the innervating muscle to produce limb movement.

## 2.13 Soft robotics in rehabilitation

### 2.13.1 Motivation

Rehabilitation robots are such that they must share the same workspace with humans and require attachment with humans for transmission of interaction forces from the robot to the user. Rigid robots are powerful enough to manipulate the limbs of the user, which implies that they are consequently strong enough to cause injury to the user either by accidental collision or movement of the limbs inappropriately. Safety is therefore a source of serious concern [5]. It is possible to place limits on the range of motion, strength and speed of rigid robots, control strategies can also be adapted to introduce mechanical compliance. An actuator material that is inherently compliant with the use of soft and deformable body like the human skin is desired in rehabilitation robotic systems to assist in necessary movements.

When physiotherapists are delivering physiotherapy exercises to the upper arm, muscles are stretched and joints are rotated. To make use of soft robots for rehabilitation is to allow for a soft wearable interface while delivering the assistive force. Soft robotics will also make the robot conform to the user's workspace through a combination of weight reduction as well as material choice. However, the achievement of inherent safety comes

at the expense of sacrificing high performance and adequate payload. Behaviors that are intelligent, adaptive and safe through the use of smart materials can easily be introduced into a soft, deformable body [85]. Therefore, soft robots characterized by high levels of redundancy, cognition and adaptability are required for rehabilitation.

Given that characteristics such as force and range of motion meets the design requirements, soft pneumatic actuators can permit the development of new class of actuators as a rehabilitation device in place of traditional robots composed of hard structures. Soft robots can take advantage of its inherent compliant nature and are therefore highly recommended as a neuro-rehabilitation device for physiotherapy. In contrast to conventional assistive devices [107, 108] which are made of rigid heavy metal, and as a result, require the constrain of the body trunk, this PhD work is aimed at wearable and lightweight assistive modules which can provide appropriate degrees of assistive force depending on clinical stages of patients. The modules made of soft inflatable structures allow to provide assistive force while ensuring safe human-robotic interaction [29] required for neuro-rehabilitation.

### 2.13.2 Locomotory movements of soft robots

The various forms of locomotory movements possible with soft robots are bending, angular change, rotation, contraction, expansion and combined motion. These generated movements have made it attractive for use in rehabilitation purposes.

**Bending movement:** These class of soft actuators manipulate objects in an adaptive and compliant way by generating a bending motion when pressurized. They are applied by integrating into a wearable structure to assist disabled patients in performing thumb and finger movement and for grasping and gripping objects [123, 54]. They are applied in generating crawling and different gait movements [53] by making use of air channels embedded in elastomers to perform bending motions similar to the motion of human fingers.

**Contraction and Expansion:** Contraction type actuators contract when pressurized such as McKibben artificial muscles while expansion actuators will increase in length upon actuation. Some EAP artificial muscles expand when a voltage is applied and contract when the voltage is removed. Rubber-based designs can be designed in a corrugated form to expand with pressurization.

**Rotary movement:** Rotational movements are effected in soft actuators through the

bidirectional design arrangement of antagonist system of contraction and expansion actuators [38, 50] or by rotary soft actuators [8, 52].

**Combined motion:** A flexible electro-pneumatic micro-actuator with three degrees of freedom (yaw, pitch and stretch) has been studied [124]. A soft bag containing a granular material generates gripping movement by vacuum packing.

### 2.13.3 Soft Exoskeletons

A relatively novel approach to rehabilitation is making use of inexpensive and soft actuators. SMA actuation, accomplished by embedding trained alloy into silicone rubber and using an electric current to produce heat which deforms the rubber to the trained shape was applied [42] to make a gripping tool. McKibben artificial muscles have also been used to produce compliant motion similar to the skeletal muscles [29, 47], and has been used for more than fifty years. Another approach uses embedded pneumatic networks of channels in elastomers [24] to achieve bending and crawling motions [53]. Soft rehabilitation robots to generate assistive force for grasping [54, 91] and gait rehabilitation [125] have been developed. Other robots composed of silicone rubber for angular displacement [52] and as 2D [55] or 3D [109] manipulators have been developed.

There have been previous research work done using soft robots for rehabilitation. A device [52] that aims to facilitate hip joint movement for a rodent with spinal cord injury has been fabricated completely with silicone rubber. Couplings of the soft actuator to the rat is also through custom made elastic rubber, positioning to the musculoskeletal structure of the animal for weight support is by 3D printed ABS plastic. The study focused on providing tailored rehabilitation for a rat in place of human intervention. Results show the soft actuator to be able to meet the design requirement of producing an actuation cycle at 1Hz, capable of achieving a linear extension displacement of 30mm, could generate a sufficient interaction force of 2N to the hind limb while imposing negligible twisting resistance to the joint. Evaluation with a live rat showed good integration as well as comfortable interaction with the soft robot. Safety concerns were kept at minimum because of the inherent softness of silicone rubber, thereby ensuring a safe interaction with soft skin and tissues. However, there is still a need for effective coupling to the animal since the elastomer attachment slipped out of position when pressurized. Also, the low interaction force means unsuitability for humans and high weighted animals.

Another set of soft rehabilitation actuator called the soft hand glove [54, 91] aims to articulate the natural bending motions of the fingers and thumb by providing a task-oriented therapeutic device. This soft glove is similar to Rutgers hand robotic device that uses low-friction pneumatic cylinders to help extend or flex the fingers [126]. With the design of a comfortable and controllable rehabilitation system composed entirely of soft silicone rubber, the study focused on replicating the motion path of bend, twist and extension in a healthy subject for grasping tasks. Results show the device was able to achieve grasp and pick up everyday objects by varying pressure in the elastomer device. In stroke patients, there is a dramatic decrease in the ability to open the hand than to close it. But the soft hand glove is pressurized to close the hand, actuation to open the hand will be by releasing the pressure, so a soft device that works be opening the hand would be more advantageous. Also, the implemented design would not be suitable for rotary movements of other parts of the upper limb such as the elbow and shoulder.

Other soft exoskeletons have been designed to enhance or assist motion. Orthosis with McKibben pneumatic muscles have also been used to augment normal muscle functions for walking in healthy individuals [127]. Similarly, a soft exosuit actuated by Bowden cables [102] was built to comfortably transmit joint torques to the hip, knee and ankle thereby improving strength, speed, and endurance while walking.

There have been a lot of research work in using pneumatic muscles for rehabilitation. A pleated form of PAM, called Pleated Pneumatic Artificial Muscle (PPAM), are distinguished from PAMs in that they are strong, have large stroke and able to inflate without material stretching [128]. They have been found to generate a torque of 60Nm under an operating pressure of 4 bar [129]. PAMs have the unique advantage of being able to be controlled using an open loop concepts reqring no feedback path. These features could offer these muscles a promising approach for use as a motion therapy apparatus to deliver exercise. However, converting the linear motion produced by these muscles into rotary motion requires complex arrangement and transmission [50].

While the use of conventional electromechanical actuators in form of DC, stepper motors in combination with gear trains requires using complex force/torque controllers, PAM soft actuators can be easily controlled with open loop concepts. PAMs have high torque but relatively small contraction ratios (between 25%–30%). Another limiting factor that strongly restricts their use in upper limb rehabilitation is that the attainment of bidirectional rotary motion to drive the elbow and shoulder joints using the one-axis linear motion generated by PAMs requires non-compact and voluminous arrangement

such as the muscles getting in the way of movement.

Besides this thesis, other prior attempts to use soft actuators for elbow and shoulder assistive movements was through mechanical transmission with an exoskeleton [30]. Fire hose, fabricated from polyester was utilized as soft actuator material with benefit of high torque output of about 40Nm. A upper limb orthosis called Orthojacket composed of an hybrid of flexible actuators actuated by pneumatics and rigid transmission links for elbow rehabilitation has also been developed [130].

### 2.13.4 Controller software

Control systems can either be open loop or closed loop. An open-loop control system implements no feedback path providing information about the current state of the system. The more advanced closed loop control system uses a sensor to measure the current state variable and uses this information as feedback to check if the desired value has become equal to the current value. A portable and wearable control system implemented with a bang-bang controller for actuating the Bowden cable of a soft robot using a microcontroller system has been demonstrated [131]. The bang-bang controller unfortunately suffers from large errors or very slow response times[132]. The design parameters for a PID controller $(K_p, K_i, K_d)$ are carefully obtained experimentally or though a process reaction curve [132]. PID controllers work extremely fast, accurate and stable given that the physical plant can be modeled with a set of linear differential equations [133].

Fuzzy logic controllers are another way of executing closed loop control. Fuzzy logic was invented by Zadeh [134] in 1965 and has since been applied for a variety of practical and commercial applications such as in the operation and programming of temperature control of a shower head [132], air conditioners, washing machine and rice cookers [135]. A fuzzy controller optimized by genetic algorithm to control pressure and level of drum boilers has also been designed [136] which had the overall effect of reducing both the settling and rise time. A neural-network based learning algorithm [137] which can self adjust weights of fuzzy rules has been implemented to improve timing parameters of the controller. Fuzzy logic controllers are a way of executing closed loop control and is more intuitive, following more closely the way a human would control the system. Fuzzy logic is an algebra and similar to Boolean logic. While Boolean logic defines only two states (true and false), conditions exist in the continuum between true and false for a fuzzy logic system.

### 2.13.5 Visual control and measurement

Vision has been applied in a wide range of applications such as industrial uses for inspecting manufactured objects, surveillance and in robotics. Vision can also be used to measure a soft robot's parameters. Color intensity values of a soft robot that changes color upon actuation was measured using a digital camera [138]. Curvature formula was derived and used in curvature calculation of a continuum robot that is similar in design to an elephant's trunk [16, 139]. Vision was employed to determine the curvature of a soft robot segment that undergoes deformation to a curved shape [55]. With the use of this visual information, a control law was applied to achieve a desired curvature. Vision-based motion control systems have been used in robotic applications to measure and control plate positions of pneumatic powered actuators [140]; to rotate a humanoid robotic head [141]; to implement controlled movements of a flexible robot through accurate 3D shape reconstruction and spatial localisation in real time [142]; for real-time visual tracking [143]. Motion of the arm was tracked through visual recording of markers attached to the arm itself [144].

Visual tracking of objects in motion can be discriminatory or generative, while a discriminatory approach reduces the tracking to binary classification, generative approach makes use of a region of interest to locate a subsequent frame. Visual tracking relies on intensity and texture information. To determine the position of a marker, a template-based matching algorithm implemented using absolute or squared difference or normalised cross correlation or ridge regression can be applied [145]. Template matching is a robust method that excels with low textured objects but comes with increased computational cost and therefore not well adapted for real-time applications [146]. A type of matching cost, that applied normalized cross correlation was developed [147] to handle noise, color variation, inconsistent shadow, reflection from object and to consider texture information in order to get reliable feature points. Zero Normalized Cross Correlation (ZNCC) is robust to lighting intensity, compensates for local gain and offset changes between matched image regions with great precision and provides the ability to handle large radiometric differences in an input image [148]. It was used to match points of interest across two images [149]. This cost computation method was applied for dense stereo matching using frame-to-frame tracking [150]. Though ZNCC is more conservative than other methods of matching such as sum of absolute or square differences in uniform regions, it is more tolerant in textured areas where noise might be important.

A more popular and widely used method of determining the position of a particular tracked point is using only color space information to reduce the tracking into binarised form using thresholding. It makes use of luminance and color intensity information. Color measurements vary considerably over an image sequence due to illuminance, shadows, shading and specularity variations [151]. These variations are normally eliminated with several preprocessing prior to object identification.

Other methods applied to track features with a camera can be linear [152] or Ridge Regression [153]. Ridge regression minimizes a cost function comprising mean-square-error and Tikhonov regularisation term. This method was applied [154] to track myography movements on the surface of the forearm. Some other feature point detection algorithms include SURF [155], SIFT [156], amongst others. Marker systems for object detection are template-based markers or 2D fiducial digital based markers such as ARTag [157]. They both provide precise and robust tracking methods. Commercially available vision tracking systems include OptiTrack (Corvallis, United States) and Vicon (Oxford, United Kingdom)

A robot can be controlled using visual information from a camera, although encoders are primarily used as internal sensors in control of rigid robots by making use of forward and inverse kinematics [158]. An encoder and camera combination [159] can also be used with the benefit that through the combination, measurement information can be collected from the encoder which will be needed only if the target falls outside the viewspace of the camera. If the camera image is lost because its view is limited, the robot cannot be controlled, therefore encoder information is used only when outside the view of the camera. Though the sampling time of visual feedback control is large when compared with the internal sensors, it presents a method for end-point tracking as encoders may create kinematic errors and information from it would be unreliable for endpoint control.

## 2.14 Part II - Conclusion

A major problem with rehabilitation robotics is that disability has a highly individualized effect. This means that given the same disability, a solution that works for one person may not work for another. Soft robotics will help in this regard since it allows for the fabrication of custom actuators that would be designed to suit a specified user.

The problem of designing a wearable, high DoF, high bandwidth robotic assistive ex-

oskeleton that is comparable to the flexibility of a human therapist is yet unsolved in rehabilitation robotics [5]. There is still no device that can assist in both upper and lower extremity movement or can match the intelligence of a human by providing real time tailored movements such as stretching, resisting and disturbing motions. This challenge can be met through the multidisciplinary research efforts from the field of clinical neuroscience, soft robotics and rehabilitation robotics. Just like soft robotics, various types of rehabilitation systems continue to increase in number and complexity with advancement in robust materials and controllers. This will allow roboticists and designers to venture into new ways of improving the quality of life of disabled persons.

Introducing soft robotics into rehabilitation engineering research will facilitate the design and development of intrinsically safe robots that can coexist with people in a natural setting and yet exhibit a certain amount of autonomy while performing useful work. Ongoing research to develop intrinsically safe robots without a decrease of function in terms of strength and speed of rigid robots will be a major accomplishment in rehabilitation robotics.

## 2.15 Chapter Conclusion

After this review chapter which focuses on manufacturing, actuator mechanism, control and design of soft robots; and rehabilitation since the focus of this work is using soft robots for rehabilitation, the next chapter is based on the study of engineering concepts with rubber because the actuators designed in this work were composed of stretchable silicone rubber.

Figure 2.5: Diagram showing summary of the overview of rehabilitation robotics.

# Chapter 3

# Engineering with Silicone Rubber Material

In this work, silicone rubber was primarily made use of to design the actuators. Therefore, this chapter is solely dedicated to introduce background information about elasticity which explains the properties of silicone rubber that will be exhibited while working with the material. Also, uniaxial tensile tests and modelling to characterize silicone rubber is described in this chapter.

Natural rubber consists of polymers isoprene including other organic compounds. Forms of polyisoprene that are used as natural rubbers are classified as elastomers. Rubber is harvested mainly in the form of latex from the rubber tree and known as latex rubber. Silicone rubber is an elastomer. Unlike other elastomers which have carbon-carbon backbones, silicone rubbers contain very flexible siloxane backbones, and have very low glass transition temperatures. The most common silicone elastomer is Polydimethyl Siloxane (PDMS). it contains repeating units of $-O-Si(CH_3)_2-$ groups.

## 3.1 Rubber Elasticity

### 3.1.1 Atomistic basis for elasticity

Consider a cubic element (Figure 3.1). Defining the terms: $\delta u$ as the change in internal energy; $\delta W$ as the work done on material by stress, $\sigma_{11}$; and $\delta q$ as the heat absorbed

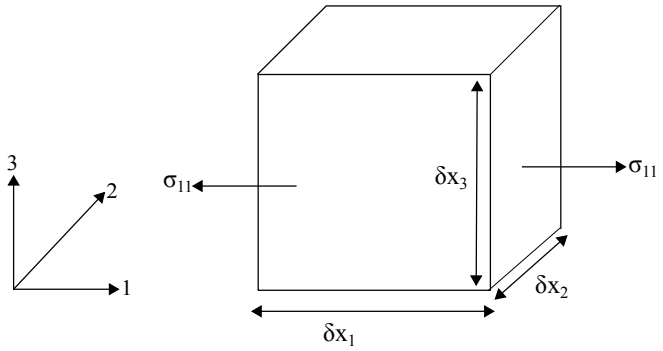


Figure 3.1: A cubic element.

by the material, define:

$$\delta u = \delta W + \delta q \tag{3.1}$$

The work done $\delta W$, is given by force multiplied by distance, $Fd$ which is given by:

$$\delta W = \sigma_{11}\delta x_2 \delta x_3 \delta \epsilon_{11} \delta x_1 \tag{3.2}$$

$$= \sigma_{11}\delta\epsilon_{11}V \tag{3.3}$$

Where $V$ is the volume, the stress is constant is over the volume. For a reversible process, the heat absorbed $\delta q$ is given as:

$$\delta q = T\delta S \tag{3.4}$$

Where $T$ = temperature, $\delta S$ = change in entropy. Combining the equations together, the change in internal energy is given as:

$$\delta u = V\sigma\delta\epsilon + T\delta S \tag{3.5}$$

Solving for the stress $\sigma$:

$$\sigma = \frac{1}{V}\frac{\delta u}{\delta \epsilon} - \frac{T}{V}\frac{\delta S}{\delta \epsilon} \tag{3.6}$$

Considering the internal energy per atom or molecule of volume, $\Omega$:

$$\text{Stress}, \sigma = \frac{1}{\Omega}\frac{\delta u}{\delta \epsilon} - \frac{T}{\Omega}\frac{\delta S}{\delta \epsilon} \tag{3.7}$$

Therefore, the stress is related to the change in internal energy as the material is deformed and also the change in the entropy. For crystalline and amorphous materials at $T < T_g$, when deforming the material, bonds are being stretched so the $\frac{\delta u}{\delta \epsilon}$ term dominates, it relates to bond stretching. Rubbers are made up of polymer chains that are occasionally crosslinked. When rubber is pulled, the chains can slide over each other and there is a reconfiguration of chain geometry so $\frac{\delta S}{\delta \epsilon}$ term is dominant because the bonds are not being stretched.

Deriving the Young's modulus as the derivative of the stress with respect to strain:

$$\text{Young Modulus}, E = \frac{\delta \sigma}{\delta \epsilon} = \frac{1}{\Omega}\frac{\delta^2 u}{\delta \epsilon^2} - \frac{T}{\Omega}\frac{\delta^2 S}{\delta \epsilon^2} \tag{3.8}$$

### 3.1.2 Moduli of Rubbers

Young modulus or stiffness is the amount of deformation per unit load while strength is the amount of load it takes to break a material. Strength is not the same as stiffness. For example, aluminum and glass have about the same Young modulus of ≈70GPa but obviously, glass has a lower strength than aluminum. Rubbers would generally have a lower Young modulus compared to most metals.

Polymers at $T > T_g$ are rubbers. The model of rubber can be considered as an entangled strand of wool or spaghetti. At $T < T_g$, rubber structure is at random $C - C$ chains, covalently bonded along the length, with occasional covalent and van der waals crosslinks between the chains. At $T_g$, the van der waals bonds melt and the structure has only occasional covalent crosslinks. Just like cooked spaghetti, segments of polymer chain between cross-links can slide over one another. If rubber is loaded in tension or compression or shear, the chains slide over one another and the structure becomes more oriented, straightens out and become less random, entropy then decreases, i.e. the chains move relative to one another but the $C - C$ bonds do not stretch (Figure 3.2a).

Since $E = \frac{1}{\Omega}\frac{\delta^2 u}{\delta \epsilon^2} - \frac{T}{\Omega}\frac{\delta^2 S}{\delta \epsilon^2}$, with the first term, $\frac{1}{\Omega}\frac{\delta^2 u}{\delta \epsilon^2}$ relating to bond stretching and the second term $\frac{T}{\Omega}\frac{\delta^2 S}{\delta \epsilon^2}$ corresponding to the change in entropy (disorder). Therefore, in rubbers, the Young Modulus, $E$, has its entropy term greater than the bond stretching term. Therefore:

$$E = \frac{T}{\Omega}\frac{\delta^2 S}{\delta \epsilon^2} \tag{3.9}$$

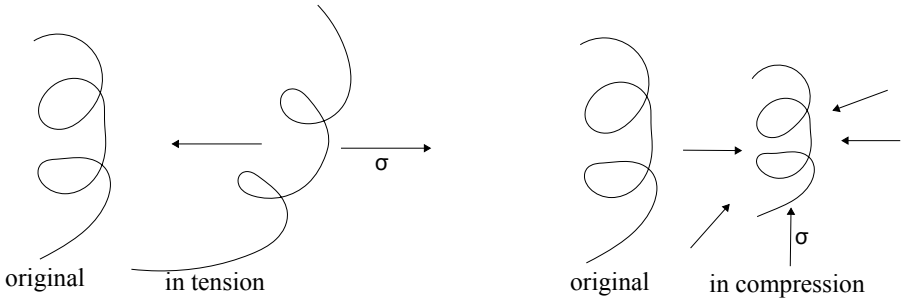


a. sliding of crosslinks chains of rubber b. loading C-C bonds of rubber

Figure 3.2: a. Rubber loaded in tension, polymer chains between crosslinks slide over one another, structure straightens out, becomes less random and entropy decreases. b. Rubber loaded hydrostatically, C-C bonds are loaded

In contrast, if rubber is loaded hydrostatically, $\sigma x = \sigma y = \sigma z = \sigma$, the entire structure contracts uniformly without changing its configuration. The relative position of atoms remains unchanged. There is little change in entropy, instead, the $C - C$ bonds are loaded along the chain (Figure 3.2b). This relates to the Bulk modulus.

$$\text{Bulk modulus}, K = \frac{1}{\Omega}\frac{\delta^2 u}{\delta \Delta^2} \tag{3.10}$$

$$K = \frac{\text{stress}}{\text{volumetric strain}} = \frac{\sigma}{\frac{\Delta}{V_0}} \tag{3.11}$$

$$\text{Volumetric strain}, \frac{\Delta V}{V_0} = \Delta \tag{3.12}$$

For rubbers, the bulk modulus, $K$, relates to the bond stretching term. Therefore, the bulk modulus is always greater than the Young's modulus ($K >> E$) since bond stretching is greater than chain sliding. The bulk modulus for rubber being greater than the Young's modulus has an implication on the Poissons ratio.

For isotropic materials (rubber is isotropic), there are only two independent elastic constants. So there is a relationship between the Poissons ratio, bulk modulus and Youngs modulus. The relationship is given by:

$$\text{Poissons ratio}, v = \frac{1}{2} - \frac{1}{6}\frac{E}{K} \tag{3.13}$$

Since $E/K$ is small, (E is related to sliding the chains over each other while K is related

to stretching the C-C bonds along the chains), $v \longrightarrow \frac{1}{2}$ for rubber.

### 3.1.3 Hyper-elastic model of rubber

Hyper-elastic models describe the stress-strain ($\sigma - \lambda$) relations of rubber-like solids in terms of strain energy functions rather than using Young's modulus and Poisson's ratio. This stress-strain relationship can be described by hyper-elastic models such as Polynomial, Ogden, Mooney-Rivlin and Yeoh strain energy functions. A brief study of the basis of these hyper-elastic models [160] are presented here.

Rubber is isotropic in elastic behavior in the unstrained state and incompressible in bulk, three strain invariants $J_1$, $J_2$ and $J_3$ are defined:

$$\begin{aligned} J_1 &= \lambda_1^2 + \lambda_2^2 + \lambda_3^2 - 3 \\ J_2 &= \lambda_1^2\lambda_2^2 + \lambda_2^2\lambda_3^2 + \lambda_1^2\lambda_3^2 - 3 \\ J_3 &= \lambda_1^2\lambda_2^2\lambda_3^2 - 1 \end{aligned} \tag{3.14}$$

These strain invariants are chosen so that they become zero in the unstrained state when $\lambda_1 = \lambda_2 = \lambda_3 = 1$. For an incompressible material, $J_3 = 0$, hence, only 2 independent measures of strain, $J_1$ and $J_2$ remain. Strain energy density, $W$, is given as $W(J_1, J_2)$. Stress, $\sigma$, can then be obtained as the derivative of $W$ with respect to strain, $\lambda$. To determine the derivatives of strain energy function, measurements of $\lambda_1 = \lambda_2 = \lambda_3 = 1$ relations under different types of strain is obtained. When $W$ is expanded as a power series, it becomes:

$$W = C_1 J_1 + C_2 J_2 \tag{3.15}$$

$C_1$ and $C_2$ are constants. This strain energy function is called the Mooney-Rivlin equation. Agreement with experimental data is obtained using a simple 2-coefficient form for $W$ as:

$$W = C_1 J_1 + k_2 \ln \frac{J_2 + 3}{3} \tag{3.16}$$

Strain hardening is introduced by a simple modification to the first term in eqn 3.15, by incorporating a maximum possible value for the strain measure, $J_1$, denoted by $J_m$

as:

$$J_m = (\lambda_1^2 + \lambda_2^2 + \lambda_3^2 - 3)_{max} \tag{3.17}$$

Equation 3.15 then becomes:

$$W = -C_1 J_m \ln(1 - \frac{J_1}{J_m}) + k_2 \ln \frac{J_2 + 3}{3} \tag{3.18}$$

Equation 3.18 reduces to equation 3.15 for sufficiently small strains and when the ratio $\frac{J_1}{J_m}$ is small.

The Yeoh model [160] is another form of strain energy potential polynomial model, which has been found to excel when describing elastic behavior over large ranges of strain and therefore, well suited to model soft robots since they are composed of silicone rubber which exhibits high strain. A simple expansion of the strain energy function in terms of only $J_1$ will give rise to Yeoh's model:

$$W = C_{11} J_1 + C_{12} J_1^2 + C_{13} J_1^3 \tag{3.19}$$

## 3.2 Uniaxial Tensile Test

Table 3.1: Ecoflex 0030 and Addition Cure 33 specifications

| **Rubber** | **Property** | **Specification** |
|---|---|---|
| Ecoflex 0030 | Mixed Viscosity | 3000 mPa-s |
| | Cure Time | 4 hours |
| | Shore Hardness | 00-30 |
| | Tensile Strength | 200psi |
| | Elongation at break | 900% |
| Addition Cure 33 | Mixed Viscosity | 50000 mPa-s |
| | Cure Time | 3 hours |
| | Shore Hardness | A 40 |
| | Tensile Strength | 856psi |
| | Elongation at break | 370% |

Ecoflex 0030 and Addition Cure 33 are the two silicone rubbers used in this work, these

are platinum catalysed rubbers that cure at room temperature. Table 3.1 show the specifications of these rubber from their datasheets [161, 162].

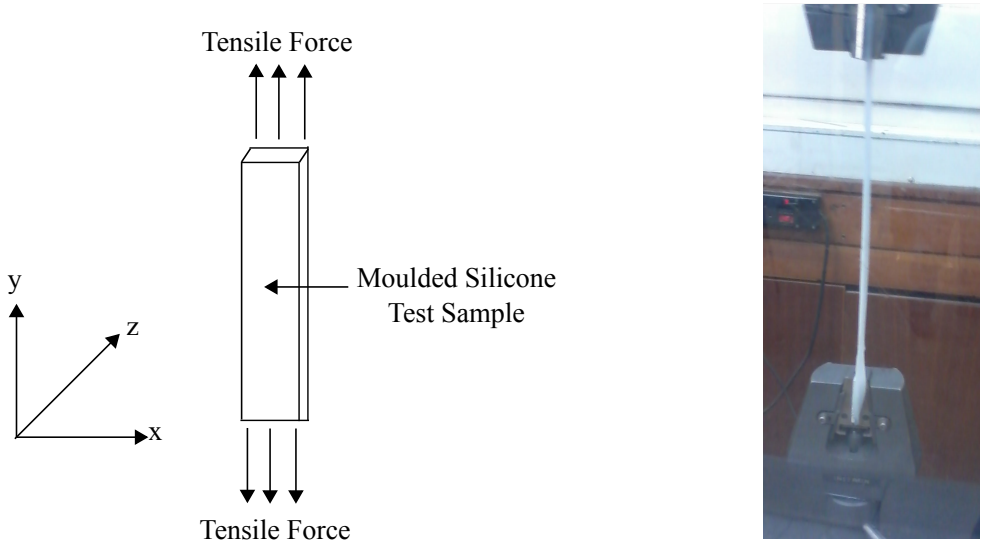


Figure 3.3: Uniaxial tensile test measurement system (a) Schematic representation (b) Moulded silicone test sample with Instron tensile testing machine.

There are different methods that can be used to obtain material data for silicone rubber. The method selected will depend on several factors such as the accuracy needed for the modelling, the type of material, time and amount of funding available. Uniaxial tensile test (Figure 3.3) of Ecoflex 0030 and Addition Cure 33 test samples were carried out at room temperature by applying predefined tensile force and measuring the elongation. Silicone rubber test samples with 60mm by 30mm in length and breath, with a thickness of 4mm were used. Instron tensile testing machine was used for this purpose and the test was carried out at a speed of 30mm/min. The tensile testing used can only generate tensile force from 5N so for Ecoflex 0030 there were fewer data points since it has a lower tensile strength. Because silicone based soft robots are hyperelastic in nature, their large strain elastic response is modeled using strain energy potential [160]. The nominal stress and strain of the tensile data was plotted as well as making use of Polynomial, Ogden and Yeoh models to fit the data using a general purpose Finite Element program, ABAQUS. As observed in Figures 3.4 and 3.5, the models provided a good fit to the experimental data, this was because the strain from experimental data remained within the strain magnitude where the data and hyperelastic model fit well.

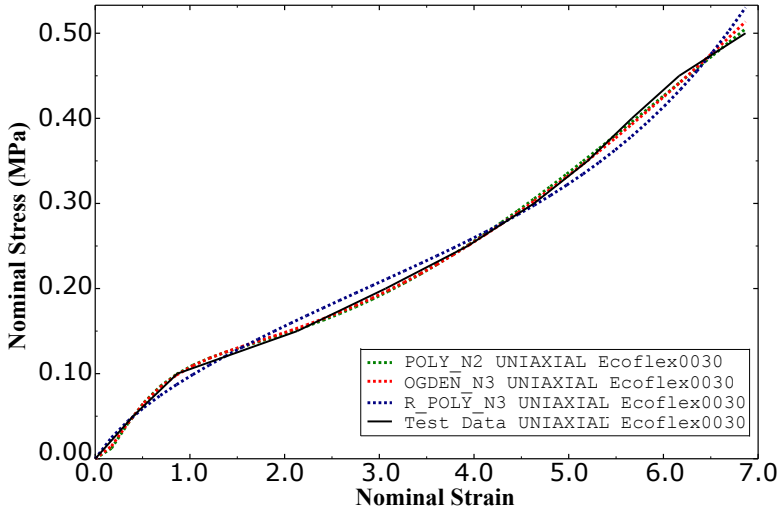


Figure 3.4: $\sigma - \lambda$ curves of Ecoflex 0030 silicone rubber. Experimental data is fitted with Polynomial, Ogden and Yeoh model for one sample.

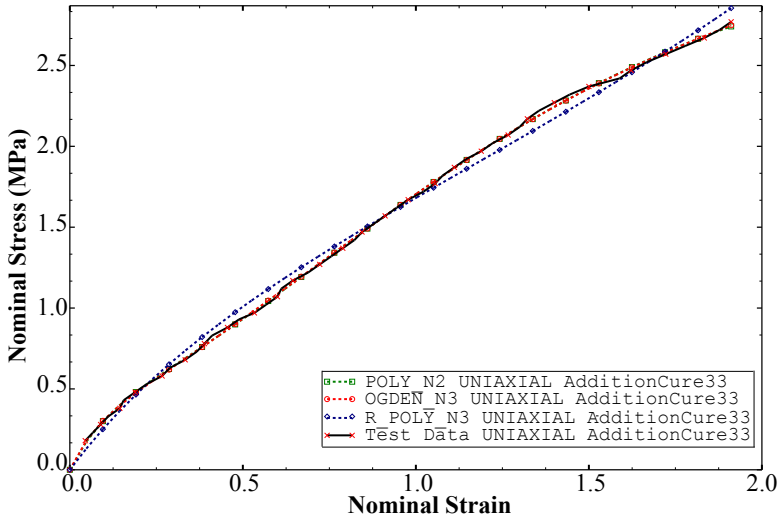


Figure 3.5: $\sigma - \lambda$ curves of Addition Cure 33 silicone rubber. Experimental data is fitted with Polynomial, Ogden and Yeoh model for one sample.

For these models, computational simulation and experimental results have been shown to match well for uniaxial tension tests at strains less than 100%. Thus, obtaining sufficient material data points at strains less than 100% will be required in order to perform Finite Element Analysis (FEA) so as to compare experimental observations with simulation results. Because the instrument that was used to conduct uniaxial test could not produce data points at strains less than 100%, FEM modelling was not carried out on the actuators that were produced in this work. Furthermore, FEM simulation of soft actuators manufactured in this work was not carried out due to limitation of the FEM ABAQUS Student Version to 1000 nodes which is insufficient to analyse non linear models required for rubber. Also, FEM characterization of rubbers is rather costly because of the effort and care required, therefore, FEM simulation of the actuators designed in this work were not performed in this thesis.

## 3.3 Chapter Conclusion

This chapter served to provide background introductory information to lay a foundation for working with silicone rubber as an engineering material because majority of the soft actuators developed and studied in this work were composed of silicone rubber. Details of its theoretical and experimental properties in terms of chemical structure, elasticity, modulus and tensile strength was given. In the succeeding chapter, work carried out in terms of the description and development of all manufactured actuators for different movement modes is detailed.

# Chapter 4

# Development of soft actuators for motion

In line with the contribution of this work which is to develop soft robots to deliver assistance for upper limb motion, the development of these actuators are presented here. This chapter describes the manufacturing procedure for all the soft actuators produced in this work, which includes silicone rubber and plastic bag actuators. They are able to achieve different movements such as bending, rotation and contraction. The geometry design variables of all the actuators are also presented.

## 4.1 Rubber Actuators Fabrication

Silicone rubber actuators were fabricated by a 2-part moulding process with the moulds built by free form fabrication technique (3D printing). The other materials required for producing rubber actuators are measuring scale, gloves, mixing sticks and cups. The general sequence for moulding with silicone rubber are: (i) Pattern or mould making; (ii) Mould preparation; (iii) Mould filling with liquid silicone rubber; (iv) Curing; and (v) Removal of cured part.

A 3D Computer-Aided Design (CAD) program, SolidWorks®, was used to design the geometry of all moulds. The top mould serves to establish the geometrical structure of the actuator while bottom moulds are required to create an enclosed structure for the air channels. Top moulds constitute the actuator geometry while bottom moulds are flat bases through which the structure forms an enclosed, air tight structure. The moulds were printed out with a HP Designjet® 3D printer using Acrylonitrile Butadi-

ene Styrene (ABS) plastic material filament.

Silicone rubber actuators were manufactured using two grades of silicone: a highly extensible and a high stiffness silicone. Ecoflex 0030 with a lower elastic modulus was used as the soft silicone while Addition Cure 33 Silicone Rubber with a higher elastic modulus was used as the hard silicone. Each of the silicone grades come in two parts - Parts A and B, to achieve moulding, both parts were mixed in equal quantity (by weight), poured into 3D printed moulds and allowed to cure at room temperature for 4 hours. During curing, cross linking takes place in the presence of air and standard temperature to form a flexible resilient silicone rubber.

To facilitate release of cured silicone from the mould, mould release spray in form of clear acrylic lacquer or petroleum jelly is applied to the interior mould surface prior to pouring the liquid silicone into it. In order to realize a better adhesion between two layers to be joined together, the main structure is first moulded and cured, it is then removed from the mould and allowed to sit on the bottom layer of liquid silicone. This ensured seamless closure since cured silicone bonds well with liquid silicone and the result produces an ideal continuous structure. A silicone tube is then inserted into each of the air channels to create air passages from a pressure source to the designed soft robot. This was done by creating a hole on the body of the soft robot into the air channel. After insertion of the tubing, additional liquid silicone was used to seal ends of the holes in order to minimize air leakage.

### 4.1.1 Mould making process

The general sequence for fabricating moulds that will form the design of the soft actuators using rapid prototyping is given by the following processes:

(a) CAD Design of mould using a 3D modeling CAD software such as AutoCAD, Sketchup or SolidWorks;

(b) Conversion of CAD design to *.stl* format;

(c) Conversion of the *.stl* file into g-code using a slicer software;

(d) Transfer of file to 3D printer machine via a wireless network, USB or MicroSD card;

(e) Loading plastic filament and printer setup;

(f) Layer by layer building of the mould part (printing) via heated plastic extrusion from the nozzles;

(g) Removal of mould from the 3D printer;

(h) Post processing of the printed mould (involving removal of support material); and

(i) Using the mould (application).

3D printing with plastic filaments such as ABS or PolyLactic Acid (PLA) plastic was used to produce the moulds – a primary advantage of 3D printing is its ability to produce very complicated or intricate geometries with relative ease when compared to the other fabrication methods. Complex shapes such as a hollow structure can be built with the introduction of another printer material to act as a supporting material which can be easily dissolved away during the post processing of the part. PolyVinyl Alcohol (PVA) was used as a support structure because it is water soluble and can be dissolved after the 3D printed structure has been soaked in water after few hours (this depends on the density and location of the support material).

Several other designs were made in this fashion – these included moulds, 3D casing to house control components, dummy structures to model elbow and shoulder joints. The representation of these parts in SolidWorks, actual ABS printed structures and silicone robots produced are illustrated in Appendix D, Figures D.1, D.2 and D.3.

During the process of mixing both parts of liquid silicone and subsequent pouring to fill the internal cavities of a printed mould, bubbles result which was removed by pouring gently and very slowly into a corner of a given mould so that it fills up and flows across the surface of the mould. Additionally, when the mixed silicone liquid is allowed to sit for some time, the entrapped bubbles located beneath the mould would begin to move up to the top surface, these floating bubbles can then be easily ruptured.

The following sections will describe the rubber actuators developed using the fabrication procedure detailed in this section. These are bending, triangular, embedded mesh, corrugated, rotary and muscle actuators.

## 4.2 Bending Actuators

Soft robots that can generate bending motion were manufactured. The principle used to achieve bending motion is the same as that of a bimetallic strip, i.e. two materials of

different expansion coefficient or young modulus glued together will bend when heated. For the case of a soft robot fabricated for the purpose of bending, a high stiffness silicone rubber is used as the bottom layer while a lower stiffness silicone with higher extensibility is used as the top layer. These two silicone layers are then bounded together to create air channel(s). To produce bending motion, compressed air from a pressure source is fed into the air channels via air tubing. The soft robot is then able to bend because of the difference in young modulus between top and bottom silicone layers. In place of using an inextensible but continuously deformable rubber as bottom layer, another material e.g. paper, fabric or braided weave (Figure 4.14) can instead be embedded inside the soft silicone layer to act as a constrain. These embedded constraint will serve to transform deformation into curvature by providing a neutral axis around which the robot can bend. The highly extensible part is in tension and the stiffer/constraining layer results in the generation of bending motion as illustrated in Figure 4.1.

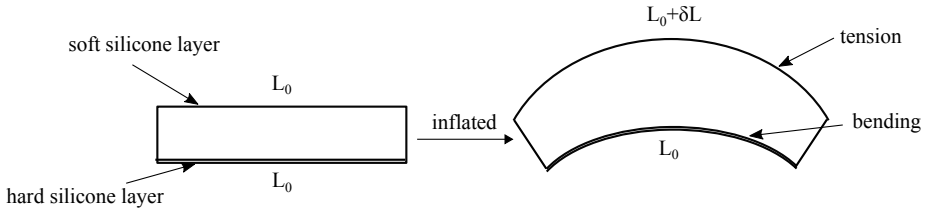


Figure 4.1: Operating principle of a bending elastomer segment. One surface of the rubber is strained, while the opposite side remains unextended. When inflated with air, the difference in length caused by tension on the soft silicone layer produces bending on the hard silicone layer.

Plain and corrugated bending actuators were manufactured. The geometry variables for the plain bending actuators are given by: base, $b$, length, $l$, height of air channel, $h$.

The geometry variables for the corrugated bending actuators (Figure 4.2) are given by: base, $b$, length, $l$, height of air channel, $h$, number of corrugations, $n$, height of corrugation, $d$. The geometric equations describing the area, surface area and volume is given as:

$$\begin{aligned}
\text{Area:} \quad A &= lb + 2bd(n-1) \\
&= \text{Area without corrugation} + 2bd(n-1) \\
\text{Surface Area:} \quad SA &= 2(lb + bh + hl) + 2d(n-1)(2b + h) \\
&= \text{Surface Area without corrugation} + 2d(n-1)(2b + h) \\
\text{Volume:} \quad V &= lbh + 2bhd(n-1) \\
&= \text{Volume without corrugation} + 2bhd(n-1)
\end{aligned} \tag{4.1}$$

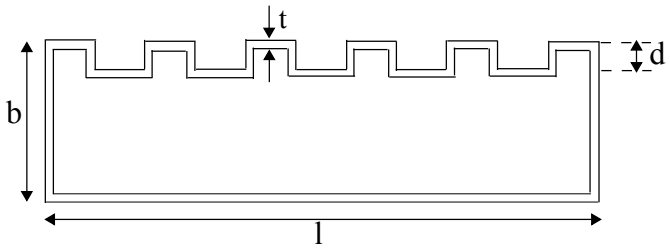


Figure 4.2: Corrugated Rectangle Sketch

The different bending soft actuators produced in this work are shown in Figure 4.3.


Figure 4.3: Different bending actuators produced (a) soft robot has internal corrugations (b) robot has external corrugations (c) robot has a plain structure. All robots have a single air channel.

## 4.3 Triangular Actuators

Soft actuators for rotary motion were fabricated which comprises of triangular or wedge-shaped structure consisting of one or more segments that form air channels. Five types

of soft triangular actuators were developed in this work: a single 20° actuator, four 20° actuators concatenated to produce 80° wedge, a single 80° actuator, a 45° corrugated actuator and a 90° corrugated actuator. For these triangular soft robots, their main structure were casted with high stiffness silicone rubber while the low stiffness but highly extensible silicone was used for casting the other layers to crease an enclosed structure. For the pleated (corrugated) triangle robots, all the layers were casted with soft silicone because the realisation of complex corrugation geometry requires casting all layers with the same material characteristics. To actuate the soft modules, compressed air fed from a pressure source is directed into separate air channels from each corresponding air tubing.

Plain (20°, four concatenated 20° and 80° segments) and corrugated (45° and 90° segments) triangular actuators were manufactured. The geometric parameters for these actuators are shown in Figures 4.5 and 4.8 and are presented in Tables 4.1 and 4.2. Rotation is achieved by inflation of the embedded air channels which results in the soft silicone layers deforming under inflation pressure which in turn leads to an increase of its wedge angle, $\theta$.

Table 4.1: Geometric Parameters of 20° and four concatenated 20° actuators

| | $\theta$ | $n$ | $h_c$ | $l$ | $t$ |
|---|---|---|---|---|---|
| 20° Triangle | 20° | 1 | $60mm$ | $100mm$ | $3.5mm$ |
| 80° Triangle | 80° | 4 | $60mm$ | $120mm$ | $3.5mm$ |

Table 4.2: Varying Parameters of corrugated triangle actuators for fabrication

| | $\theta$ | $n_c$ | $h_c$ | $l$ | $t$ | $d$ |
|---|---|---|---|---|---|---|
| Corrugation 1 | 45° | 7 | $120mm$ | $100mm$ | $2.5mm$ | $5mm$ |
| Corrugation 2 | 90° | 15 | $60mm$ | $110mm$ | $2.5mm$ | $5mm$ |

The geometry variables for the 20° triangle actuator are given by: defining angle of wedge, $\theta$, base length, $l$, height of air channel, $h_c$, thickness of wall, $t$. The geometric equations describing the area, surface area and volume are given as:

Figure 4.4: Produced 20° triangle actuator for angular movement.

$$\begin{aligned} \text{Area:} \quad A &= \frac{1}{2} l^2 \tan\theta \\ \text{Surface Area:} \quad SA &= l^2 \tan\theta + l h_c(\cos\theta + \tan\theta + 1) \\ \text{Volume:} \quad V &= \frac{1}{2} l^2 h_c \tan\theta \end{aligned} \tag{4.2}$$

To manufacture a single 80° wedge-shaped structure, three moulds are required - the top mould that comprises the geometrical structure of the actuator and bottom moulds to create an enclosed structure for the air channels. The values of these parameters are presented in Table 4.1. The actuator is made of a complete isosceles triangle with four individual air channels (Figure 4.5).

The geometry variables for the 80° triangle actuator (Figures 4.5 and 4.6) are given by: defining angle of wedge, $\theta$, number of wedges, $n$, side length, $l$, height of air channel, $h_c$, thickness of wall, $t$. The geometric equations describing the area, surface area and volume are given as:

$$\begin{aligned} \text{Area:} \quad A &= \frac{1}{2} l^2 \sin\theta \\ \text{Surface Area:} \quad SA &= l^2 \sin\theta + 2 l h_c \sin\frac{\theta}{2} + 2 l h_c \\ \text{Volume:} \quad V &= \frac{1}{2} l^2 h_c \sin\theta \end{aligned} \tag{4.3}$$

Figure 4.6 shows a single 80° triangle actuator with 4 individual air channels. The design process of producing a single 80° actuator rather than concatenating four 20° actuator in series (Figure 4.7) offers significant improvement in terms of weight. This enhanced design manufacture process significantly reduced the weight from 340g to 180g. This

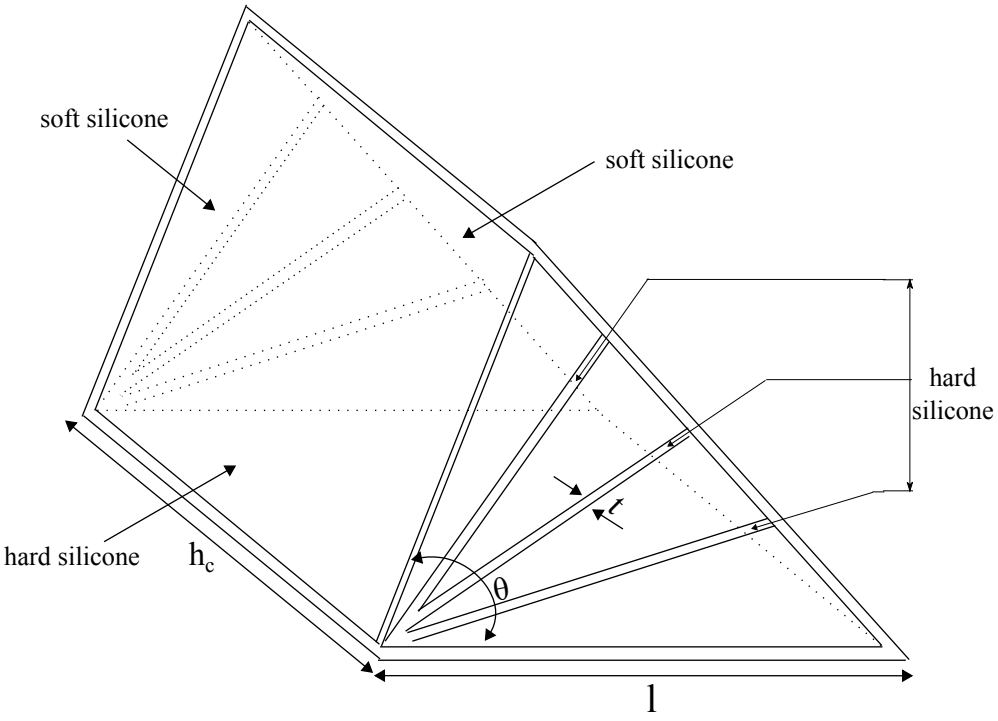


Figure 4.5: Sketch of 80° Triangle Actuator

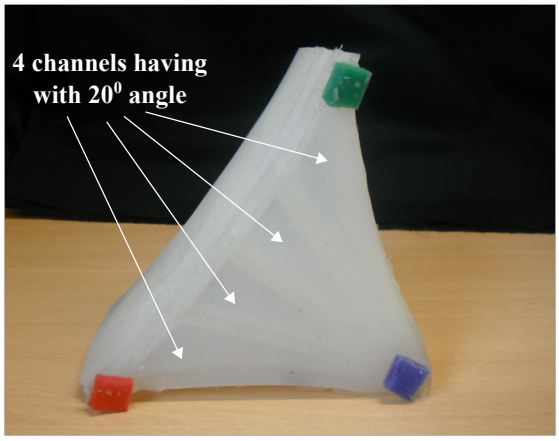


Figure 4.6: Soft module showing the four embedded air channels having 20° triangle segments separated by 3.5mm thick walls.

results from the derived geometry formulas indicated by the sin and tan terms. So given the same parameters, the single 80° triangle produced lower area, surface area and volume, hence, a reduction in its weight. As would be seen, this feature is useful when creating a wearable assistive device to be worn on the human body.

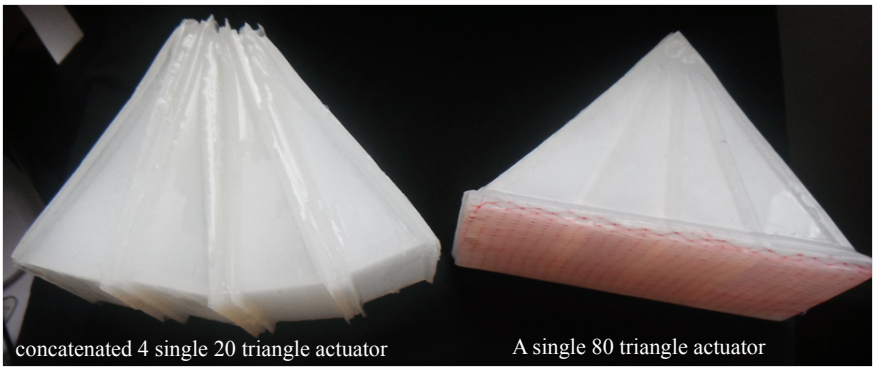


Figure 4.7: A single 80° actuator replaced with concatenating four single 20° triangle actuator to produce a 80° actuator.

Another novel design made up of a pleated or corrugated structure in the wedge-shaped modules was implemented. Therefore, inflation of the embedded air channels will first lead to unwinding of the pleats, then followed by deformation of the silicone layer. The design of a pleated structure is aimed at increasing the range of motion by unwinding of the pleats under inflation pressure. Given a pleated structure where $d$ is height of corrugation, $n$ is the number of corrugations, $l$ is the unstretched length; the stretched length is therefore given by $l + 2nd$. With the corrugated structure, when the wedge-shaped triangle is inflated, $l$ is unwound and increases in length to $l + 2nd$. The geometry variables for pleated triangle actuator (Figure 4.8) are given by: defining angle of wedge, $\theta$, side length, $l$, number of corrugations, $n_c$, height of corrugation, $d$, height of air channel, $h_c$, thickness of wall, $t$ :. The geometric equations describing the area, surface area and volume is given as:

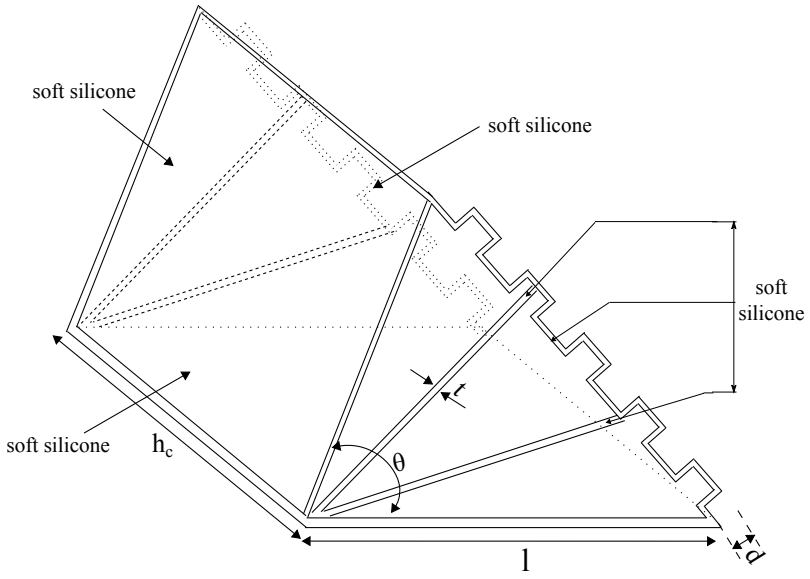


Figure 4.8: Corrugated Triangle Actuator Sketch

$$
\begin{aligned}
A &= \frac{1}{2}l^2 \sin\theta + l n_c d \cos(\frac{\theta}{2}) \\
A &= \text{Area without corrugation} + l n_c d \cos(\frac{\theta}{2}) \\
SA &= l^2 \sin\theta + 2lh_c \sin\frac{\theta}{2} + 2lh_c + 2n_c d(l\cos(\frac{\theta}{2}) + h_c) \\
SA &= \text{ Surface area without corrugation} + 2n_c d(l\cos(\frac{\theta}{2}) + h_c) \\
V &= \frac{1}{2}l^2 h_c \sin\theta + l n_c h_c d \cos(\frac{\theta}{2}) \\
V &= \text{ Volume without corrugation} + l n_c h_c d \cos(\frac{\theta}{2})
\end{aligned} \tag{4.4}
$$

## 4.4 Braided Mesh Network Designs

A study that introduced the bulging phenomenon of rubber under large deformations was conducted [160]. Rubbers under inflation shows new elastic instabilities evidenced by non-uniform deformation of the structure. Therefore, at a critical inflation pressure, one portion of the rubber structure becomes highly distended as an aneurysm while the rest remains less inflated. This occurrence arises from the particular ability of rubber

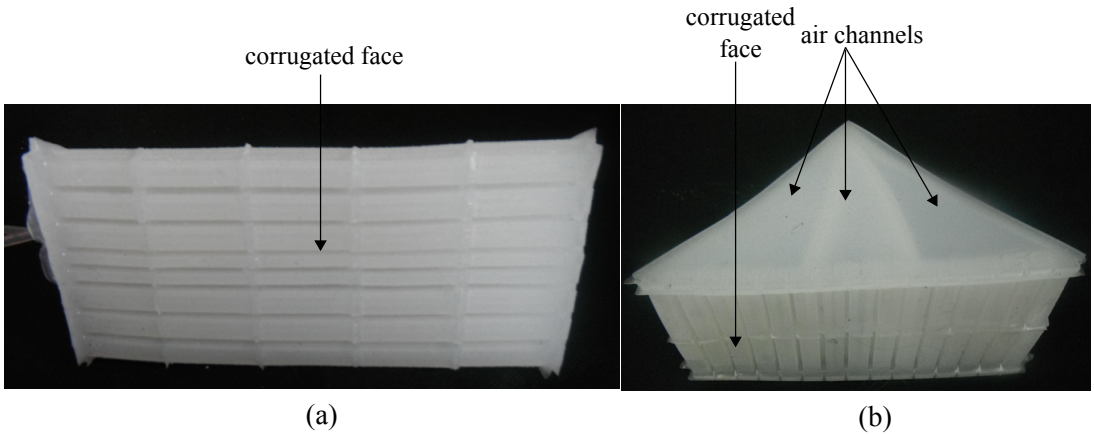


Figure 4.9: Produced (a) 45° and (b) 90° corrugated triangle actuators for angular movement.

to undergo large elastic deformations. This phenomenon was described by Gent [163] where the relationship between Inflating pressure $P$ and volume expansion ratio $V$ of a thin-walled tube is given by:

$$\frac{Pr}{wC_1} = \frac{2[V^2-2][2V(V^2+1)]^{\frac{1}{3}}}{V^2[1-\frac{J_1}{J_m}]} \tag{4.5}$$

$P$ is the inflation pressure, $w$ is the wall thickness, $C_1$ is the material parameter, $V$ is the ratio of the volume contained by the tube in the inflated and uninflated states, $J_1$ is the strain invariant parameter and a function of the strain, $J_m$ is the maximum possible value for the stain invariant $J_1$. Gent [163] observed that by plotting the relations between $P$ and $V$ for various limiting strain measure $J_m$, the inflating pressure passes through a maximum at a $V$ value of about 60%, indicating that larger expansions will be unstable. In practice, pneumatic rubber actuators undergo the same phenomenon under inflation as a portion of the wall becomes highly distended as an aneurysm while the rest portion remains less inflated resulting in bulging.

When triangle segments were inflated, soft silicone layers increase in length in both axial and biaxial directions, thereby increasing the angle $\theta$. This increase in both axial and biaxial directions creates a bulge (Figure 4.10). In order to reduce the effect of the bulge, interwoven mesh was embedded inside soft silicone layers. It was also found out that the division of an actuator into four parts, thereby making 4 separate air channel so that each segment is separated by a layer of hard silicone also led to

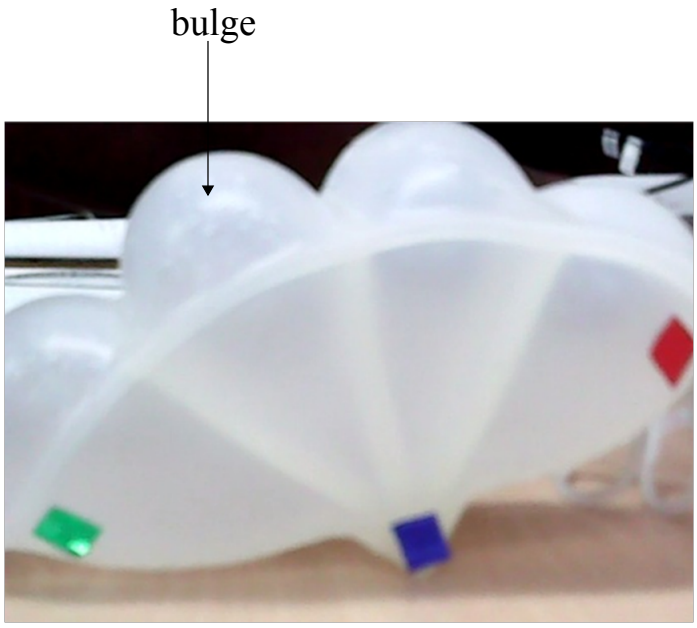


Figure 4.10: Wedge-shaped soft actuator showing rotary motion produced, caused by increase in angle upon inflation, a visible bulge can be seen.

reduce the bulge. As seen in Figure 4.11, the 80° triangle actuator with braided mesh reinforcement comprises 20° triangle segments separated by hard silicone layers.

The bulge produced reduced the efficiency of the soft modules and was minimized through the introduction of embedded braided mesh into the faces of the actuator. The diagram of the interwoven mesh is illustrated in Figure 4.12. The braided mesh is made of Polypropylene (PP) net and composed of cylindrical shape twine with a thickness of about $50\mu m$. The PP net is commonly used in packaging of fruits in grocery stores. The structure of the PP net is different to the polymeric sleeve in form of a braided helical weave used in McKibben-type muscles in that the braided mesh does not slide. Additionally, the McKibben braided sleeve is an expandable and flexible cable composed of polyester.

The mesh network consists of a planar mesh structure having a longitudinal and lateral direction. The mesh undergoes strain only in one direction (longitudinal) but does not strain in the lateral direction. This property was used to reduced bulging of the soft modules. In other words, the asymmetry of the braided mesh was used to constrain the tension. The constrained tension of the walls introduced by the braided mesh resulted in applying tension in the circumferential direction with the condition that the width in the other direction is prevented from altering under deformation, that is, the strain

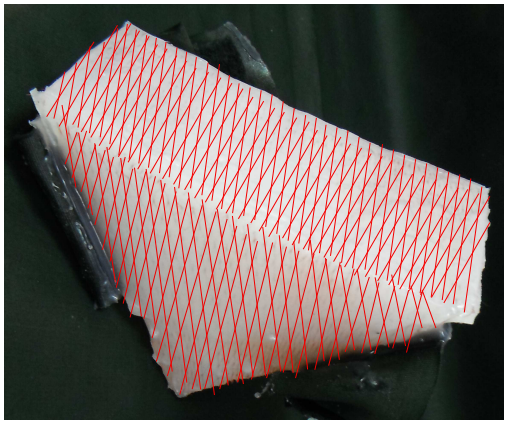

Figure 4.11: Soft module showing the 80° triangle actuator having embedded interwoven anisotropic mesh to reduce bulging of the module. Mesh direction is indicated in the diagram. The characteristic thickness of the mesh is $50\mu m$.

in the other direction is unity. The braided mesh characteristics is shown in Table 4.3. The braided mesh is embedded in the silicone rubber as a flat, single layer as shown in Figures 4.11, 4.12 and 4.13. The triangular faces of the soft module has the mesh placed as a flat, single layer rather than in form of a fan shape. A fan-shaped mesh may produce the same effect as a flat layer mesh because a fan shaped mesh will also have a single layer at the opposite sides of the tip of the fan.

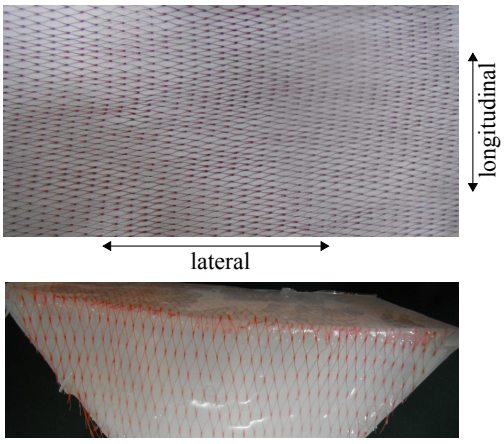


Figure 4.12: Weave pattern of the braided mesh network. The weave undergoes little strain in the lateral direction with the application of a tensile force but strains maximally in the longitudinal direction. The close up picture shows the weave embedded into the body of the silicone rubber actuator.

Figure 4.10 shows the bulge created as a result of inflation without the mesh while

Table 4.3: Braided mesh characteristics

| **Value** | **Characteristics** |
|---|---|
| Direction of motion | Longitudinal (in the direction of motion) |
| | Lateral (in the direction of bulging) |
| Thickness | $50\mu m$ |
| Structure | Planar |
| Mode of integration | Embedded inside silicone rubber |
| Material | Polypropylene |
| Symmetry | Anisotropic |
| Placement | Flat, not folded |
| Layers | Single (1) layer |

Figure 4.13: Soft modules inflated with embedded interwoven mesh. Notice visible reduction in bulging of the front face of the wedge-shaped modules compared to Figure 4.10.

Figure 4.13 shows a reduction in bulging with the addition of a braided mesh. It was discovered that the braided weave can be employed as a constraining layer by embedding the weave in the direction at which the weave fabric undergoes less strain on the constraining layer as shown in Figure 4.14a.

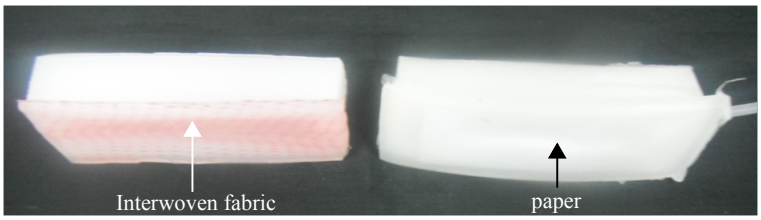


Figure 4.14: Braided mesh fabric and paper were employed as a constraining layer.

A theoretical examination of the soft modules involves an energy analysis. An energy analysis equates the work done by the compressed air in the air channels to the work done by the rubber because of the elastic strain energy accompanying wedge angle change. For the case of bulging and as illustrated in Figure 4.15, assume circle between $PQ$, Hooke's law for rubber is given as:

$$F(r,\theta) = k(r\theta - r_0\theta_0)\Delta h = k(r\theta - r_0\theta_0)$$

Work done by elastic rubber is given as:

$$dW_R = k(r\theta - r_0\theta_0)dr$$

Work done by inner air pressure, $P$, is given as:

$$\begin{aligned} dW_R = P(r,\theta)dV &= P(r,\theta)[\frac{\theta + d\theta}{2\pi}\pi(r+dr)^2 - \frac{\theta}{2\pi}\pi r^2]\Delta h \\ &= P(r,\theta)[r^2\theta + 2r\theta dr + (dr)^2\theta + 2rd\theta dr + (drd\theta)^2]\Delta h \end{aligned}$$

First order elements are: $r^2 d\theta + 2r\theta dr$ while second order elements are $2rd\theta dr + (dr)^2\theta$. Taking only first order elements and $d\theta \approx dr$ and $dW_R = dW_P$

$$\begin{aligned} P(r,\theta)(r^2 + 2r\theta)dr &= k(r\theta - r_0\theta_0)dr \\ P(r,\theta) &= \frac{k(r\theta - r_0\theta_0)}{r^2 + 2r\theta} \end{aligned} \tag{4.6}$$

The equation of a circle is given as: $x^2 + (y - y_0)^2 = r^2$. From the conditions: $(x, y) =$

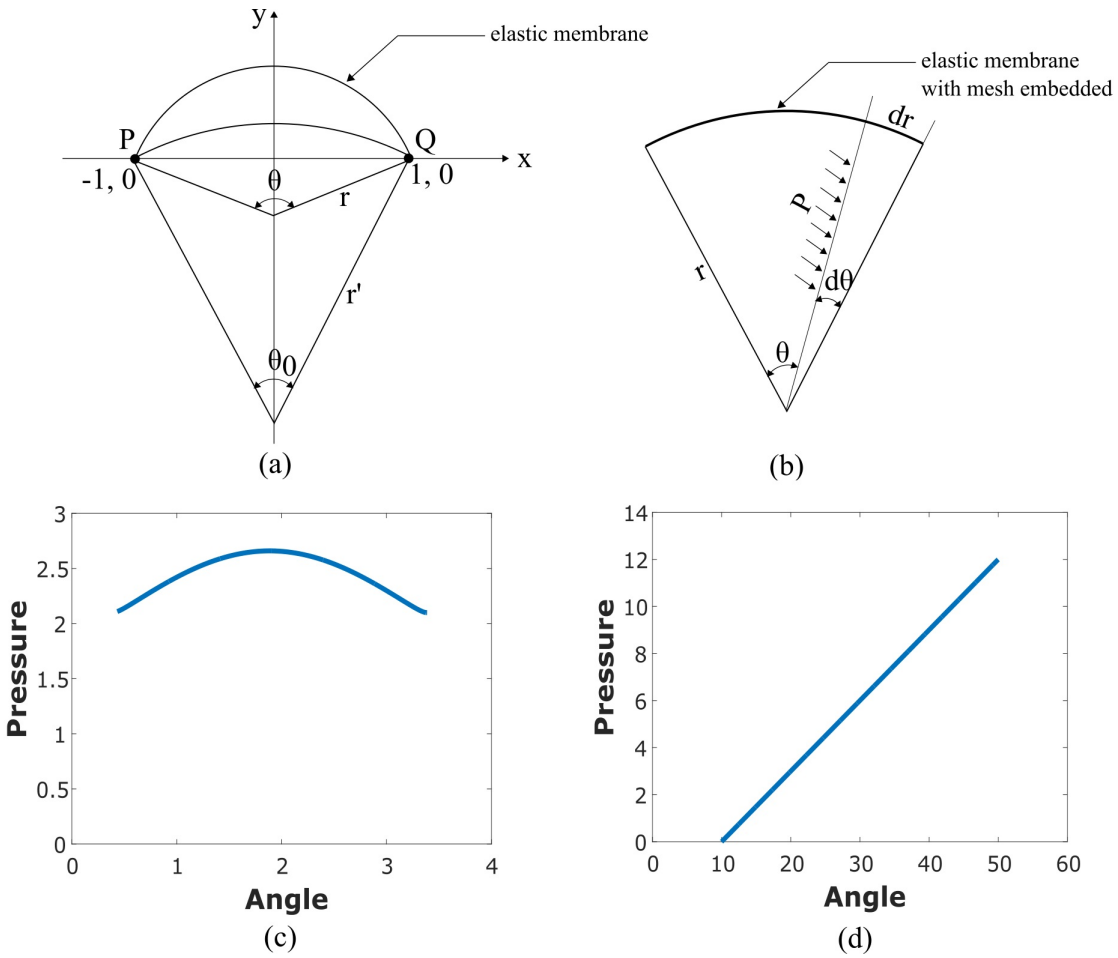


Figure 4.15: Theoretical explanation of soft modules based on 2D geometrical model (a) case of bulging (b) case of embedded mesh (c) Plot of pressure as a function of angle for the case of bulging model (d) Plot of pressure as a function of angle for the case of embedded mesh model.

$(1, 0)$, the equation becomes: $1 + y_0^2 = r^2$. Substituting $y_0 = r\cos\theta$, gives:

$$r = \frac{1}{\sin\theta} \tag{4.7}$$

Combining eqn(4.6) and eqn(4.7) and plotting $P(r)$ as a function of $\theta$ produces a circular curve (Figure 4.15c) indicating the bulge.

The case of the mesh structure as illustrated in Figure 4.15b is now described. Hooke's law is given as:

$$F(\theta) = k(\pi r\theta - \pi r\theta_0)\Delta h = k(\theta - \theta_0), \text{where } r \text{ is a constant}$$

Work done by rubber is given as $dW_R = k(\theta - \theta_0)d\theta$. Work done by inner air pressure, $P$, is given as:

$$dW_P = P(r)dV = P(r)[\frac{(\theta + d\theta)}{2\pi}\pi r^2\Delta h - \frac{\theta}{2\pi}\pi r^2\Delta h] = P(r)Ad\theta$$

Equating $dW_R = dW_P$,

$$P(r)Ad\theta = k(\theta - \theta_0)d\theta$$
$$P(r) = B(\theta - \theta_0)$$

The plot of $P(r)$ as a function of $\theta$ (Figure 4.15) is a linear function indicating the absence of a bulge. This theoretical study is based on considering a 2D geometrical case of expansion of rubber.

## 4.5 Rotary Actuators

Soft rotary actuators perform the same function with triangular actuators but their shape are in a different configuration. Because their fabrication demands casting the actuator body as a single piece, their entire body were casted with soft silicone while the layers separating each air channel was made inextensible by embedding with paper inside (Figure 4.17). The geometry variables for the rotary actuators (Figure 4.16) are given by: big radius, $R_1$, Small radius, $R_2$, offset distance from center of circle, $d$, height of air channel, $h$, thickness of wall, $t$. The geometric equations describing the area, surface area and volume are described by the following equations:

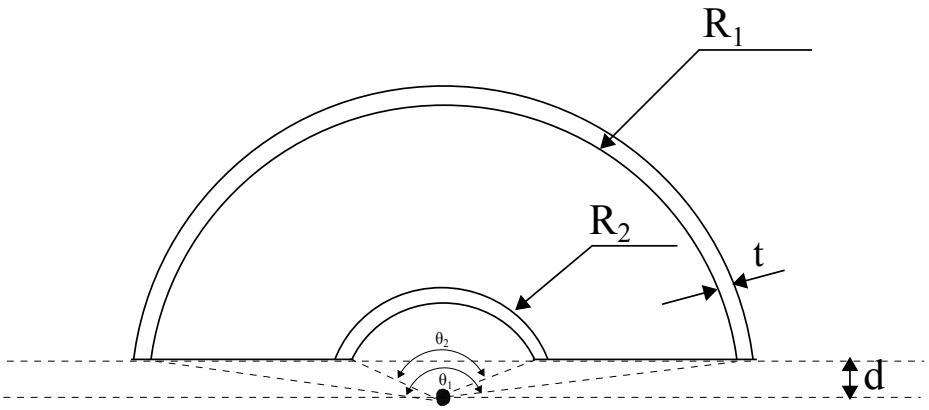


Figure 4.16: Simplified Rotary Actuator Sketch

$$\theta_1 = \arccos\frac{d}{R_1}$$
$$\theta_2 = \arccos\frac{d}{R_2}$$
$$A = R_1^2\theta_1 - R_2^2\theta_2 - (R_1^2 - d^2)^{\frac{1}{2}} + (R_2^2 - d^2)^{\frac{1}{2}}$$
$$SA = R_1^2\theta_1 - R_2^2\theta_2 - (R_1^2 - d^2)^{\frac{1}{2}} + (R_2^2 - d^2)^{\frac{1}{2}} + 2(R_1^2 - R_2^2) + h(R_1\theta_1 + R_2\theta_2)$$
$$V = [R_1^2\theta_1 - R_2^2\theta_2 - (R_1^2 - d^2)^{\frac{1}{2}} + (R_2^2 - d^2)^{\frac{1}{2}}]h \quad (4.8)$$

Table 4.4 shows the geometric values of the rotary actuators produced in the work.

Table 4.4: Varying Parameters of Rotary Actuator for fabrication.

| | $R_1$ | $R_2$ | $d$ | $h$ | $t$ |
|---|---|---|---|---|---|
| Rotary Actuator I | $150mm$ | $50mm$ | $80mm$ | $40mm$ | $2.5mm$ |
| Rotary Actuator II | $150mm$ | $105mm$ | $40mm$ | $50mm$ | $2.5mm$ |

## 4.6 Muscle Actuators

The fundamental property of a muscle is contractility. Skeletal muscle fibers are very long multinuclear cells specialized for forceful short duration contractions. The type of artificial muscle produced in this work is similar to the fusiform muscle present

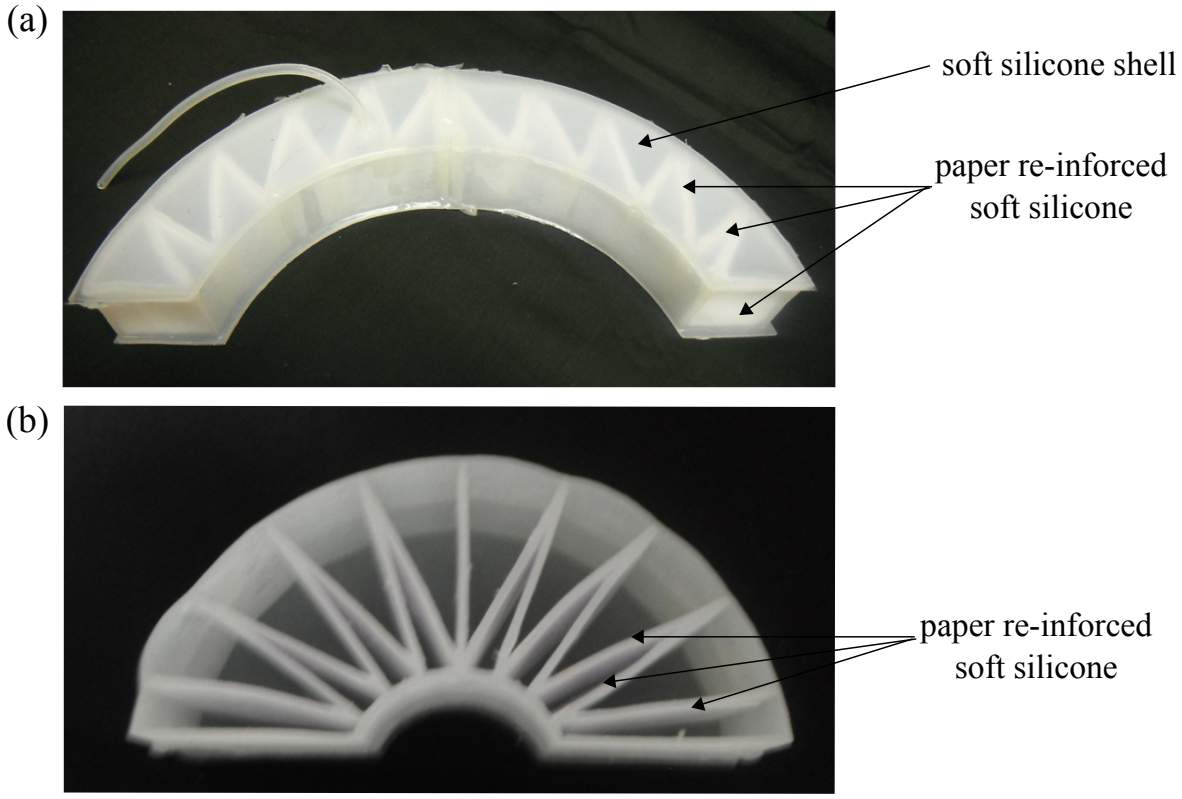


Figure 4.17: Silicone rubber muscle actuators designed for rotary motion (a) Rotary Actuator I (b) Rotary Actuator II. Parameters for these actuators are specified in Table 4.4. These actuators have their entire body casted with soft silicone while the layers separating each air channel was made inextensible by embedding with paper inside.

in the human body but its makeup comprises wedge-shaped segments connected in series (Figure 4.18). Like the human skeletal muscles, each of the wedges represents the function of the sarcomeres. It is each of the sarcomeres that will contract, so the number of sarcomeres contracting at the same time would have effect on the extent of shortening of the muscle.

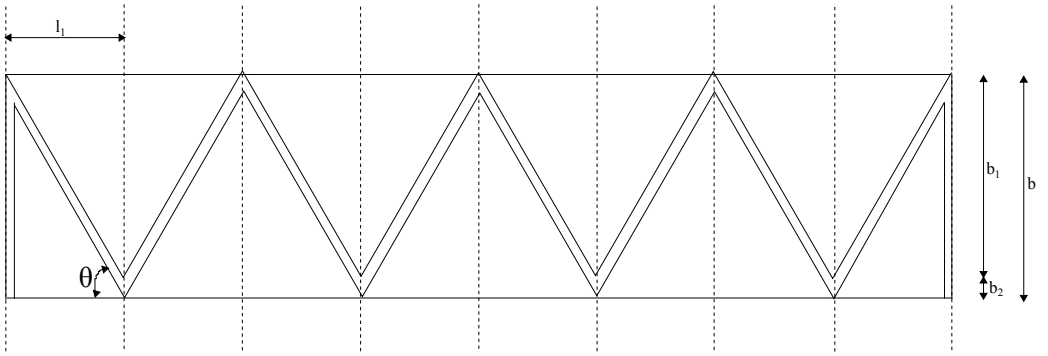


Figure 4.18: Soft Muscle Sketch

Soft muscle actuators were fabricated to contract in length with the application of vacuum air pressure. The wedges were casted with hard silicone while the remaining layers were casted in soft silicone. The geometry variables for the produced muscle actuators (Figure 4.18) are given by: defining angle of wedge, $\theta$, number of wedges, $n$, length of a wedge, $l_1$, total length of muscle, $l$, height of air channel, $h_c$, thickness of wall, $t$. The geometric equations describing the area, surface area and volume are described by the following equations:

$$\begin{aligned} A &= (n-1)l_1 \tan\theta(l_1 + \frac{t}{\sin\theta}) \\ SA &= 2lb + 2lh_c + 2bh_c \\ &\Rightarrow l = (n-1)l_1 \\ &\Rightarrow b = \tan\theta(l_1 + \frac{t}{\sin\theta}) \\ V &= (n-1)h_c l_1 \tan\theta(l_1 + \frac{t}{\sin\theta}) \end{aligned} \tag{4.9}$$

Another muscle actuator, which is made of straight air channels instead of wedges is shown in Figure 4.19. The geometry variables for the produced muscle actuators are given by: base, $b$, total length, $l$, length of each air channels, $l_c$, height of air channel,

$h$, number of channels, $n$, thickness of wall, $t$. The geometric equations describing the area, surface area and volume are described by the following equations:

$$\begin{aligned} \text{Area:} \quad A &= lb \\ \Rightarrow l &= nl_c + (n+1)t \\ \text{Surface Area:} \quad SA &= 2(lb + bh + hl) \\ \text{Volume:} \quad V &= lbh \end{aligned} \tag{4.10}$$

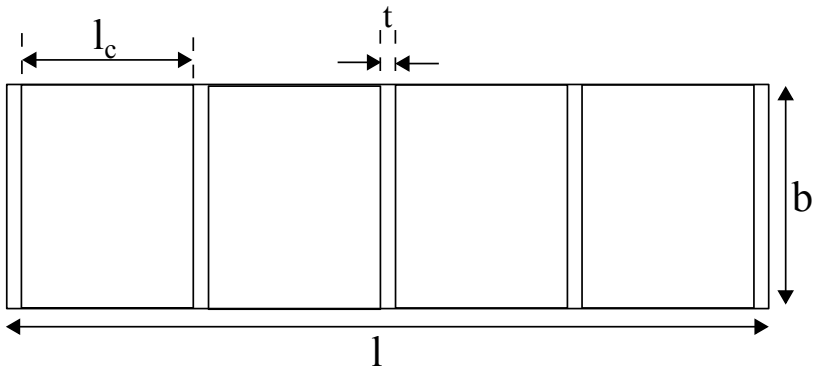


Figure 4.19: Rectangular Muscle Sketch

The geometry variables of all the muscle actuators are represented in Table 4.5, while the manufactured muscle actuators are shown in Figure 4.20. The notation M1-M8 denotes a representation of eight different soft muscles fabricated with varying parameters of defining angle of wedge, $\theta$, length of wedge, $l_1$, number of wedges, $n$, height of air channel, $h_c$, and the total length of muscle, $l$ as shown in Table 4.5. M1 is specified by an angle of 60°, a length of $160mm$ and height of $40mm$. M2 has its angle varied to 67.5° while M3 has its angle changed to 75°. M4 has its air channel height set to $20mm$. M5 has its number of air channels changed to 7. M6 is composed of two M1 muscles joined in parallel to give a total air channel height of $80mm$. M7 is produced by a combination of two M1 muscles in series to give a total length of $320mm$. M8 is a rectangular actuator with an angle of 90°. These parameters were chosen to study the effect of parameter change on the performance of the muscle in terms of isotonic contraction. All the soft muscles have wall thickness, $t$, set to 2.5mm for the wedged-shaped layer and a layer thickness of 1.5mm for the outer layers.

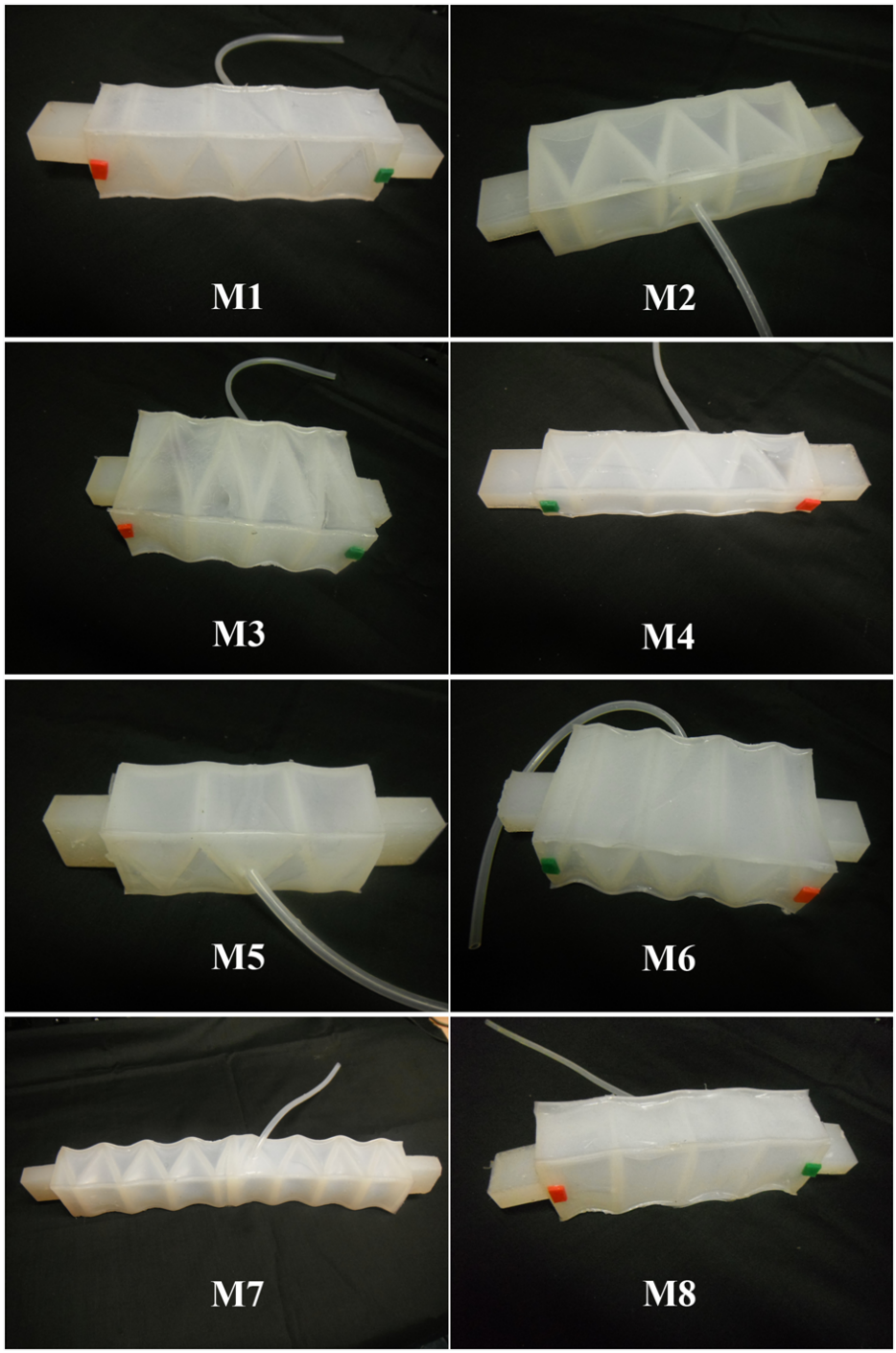


Figure 4.20: M1 is specified by an angle of 60°, a length of 160$mm$ and height of 40$mm$; M2 has its angle varied to 67.5°; M3 has its angle changed to 75°; M4 has its air channel height set to 20$mm$; M5 has its number of air channels changed to 7; M6 is composed of two M1 muscles joined in parallel to give a total air channel height of 80$mm$; M7 is produced by a combination of two M1 muscles in series to give a total length of 320$mm$; M8 is a rectangular actuator with an angle of 90°.

Table 4.5: Varying Parameters of muscles for fabrication

| | $\theta$ | $n$ | $h_c(mm)$ | $l_1(mm)$ | $l(mm)$ | $t(mm)$ |
|---|---|---|---|---|---|---|
| Muscle 1 | 60° | 9 | 40 | 20 | 160 | 2.5 |
| Muscle 2 | 67.5° | 9 | 40 | 20 | 160 | 2.5 |
| Muscle 3 | 75° | 9 | 40 | 20 | 160 | 2.5 |
| Muscle 4 | 60° | 9 | 20 | 20 | 160 | 2.5 |
| Muscle 5 | 60° | 7 | 40 | 20 | 120 | 2.5 |
| Muscle 6 | 60° | 9 | 80 | 20 | 160 | 2.5 |
| Muscle 7 | 60° | 9 | 40 | 20 | 320 | 2.5 |
| Muscle 8 | 90° | 4 | 40 | 30 | 160 | 2.5 |

When the artificial muscle is unactuated, the structure is at standard atmospheric pressure. The actuation via a vacuum pump will expel air from the structure causing the muscle to contract. When air is introduced into the system through an air pump, the muscle goes back to its normal resting length. Figure 4.21 shows a M7 muscle contracting. As shown, the SRM muscles are wedge-like structures in series, a hole that connects a wedge with the next is created so that a single pressure source feeds into all air channels.

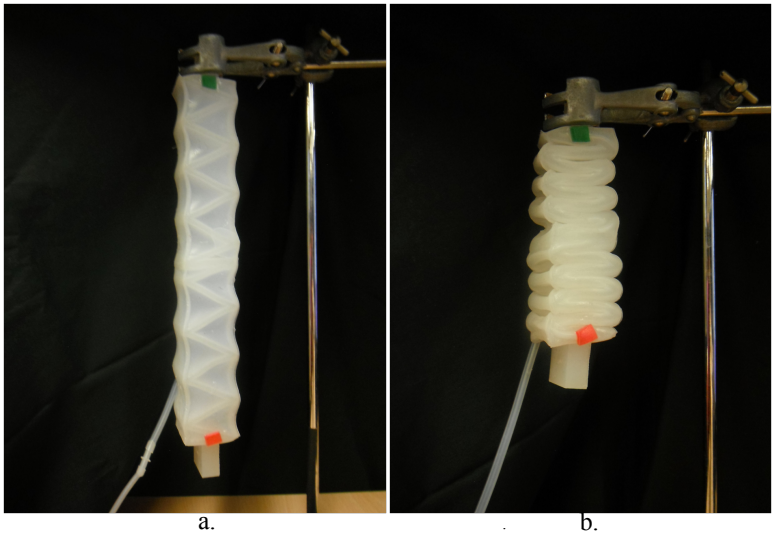


Figure 4.21: M7 muscle (a) Normal muscle length (b) Contracted Muscle

Aside from contraction, the SRM muscle is also capable of bidirectional bending. This is achieved through the control of positive and negative internal air pressure in each of the wedges. Figure 4.22 shows a sketch and picture of the M1 muscle exhibiting bending

motion. As shown in Figure 4.22, the upper air cavities have their internal air pressure $P$, increased to $\delta P$ while the lower air cavities have their internal air pressure decreased by $\delta P$. This difference in pressures in both upper and lower air channels results in tension at the upper part and bending on the lower part. Bidirectional bending is likewise possible by decreasing the pressure in the upper air channels and increasing the pressure in the lower air air channels. Other motions possible as a result of varying pressure distribution are different curves such as s-shaped curve. In this way, more complex bending movements are possible such as how earthworm and snakes crawl.

## 4.7 Plastic bag actuators

Soft robots are generally non rigid robots fabricated from soft and deformable material such as silicone rubber, plastic, fabric, or any other compliant mechanical parts like springs. In this section, the production of plastic bag actuators made of polythene material is given.

Table 4.6: Produced plastic bag actuator parameters and characteristics.

| **Parameter** | **Value** |
|---|---|
| Length | $100mm$ |
| Breadth | $50mm$ |
| Thickness | $50\mu m$ |
| Material | PE film |

The production process of inflatable plastic actuators differs from that of silicone rubber actuator. The inflatable bags are manufactured using a heat welding method to create a hermetically sealed structure while incorporating a masking technique. Fabrication of soft actuators by welding entails the fusion of two thermoplastic materials together to form an enclosed structure of varied shapes that can be actuated with compressed air. Polyethylene (PE) film is the plastic bag material that is used. The impulse sealer is mostly used for this purpose. The machine allows the welding of only straight seams between layers of plastic film. A conventional heat sealer can only seal along a line. Therefore, in order to make complicated shapes to produce multi-layer air chambers, masking technique using cellophane films or paper is made use of to cover the parts that should not be sealed. Cellophane films have higher melting points than PE and so are

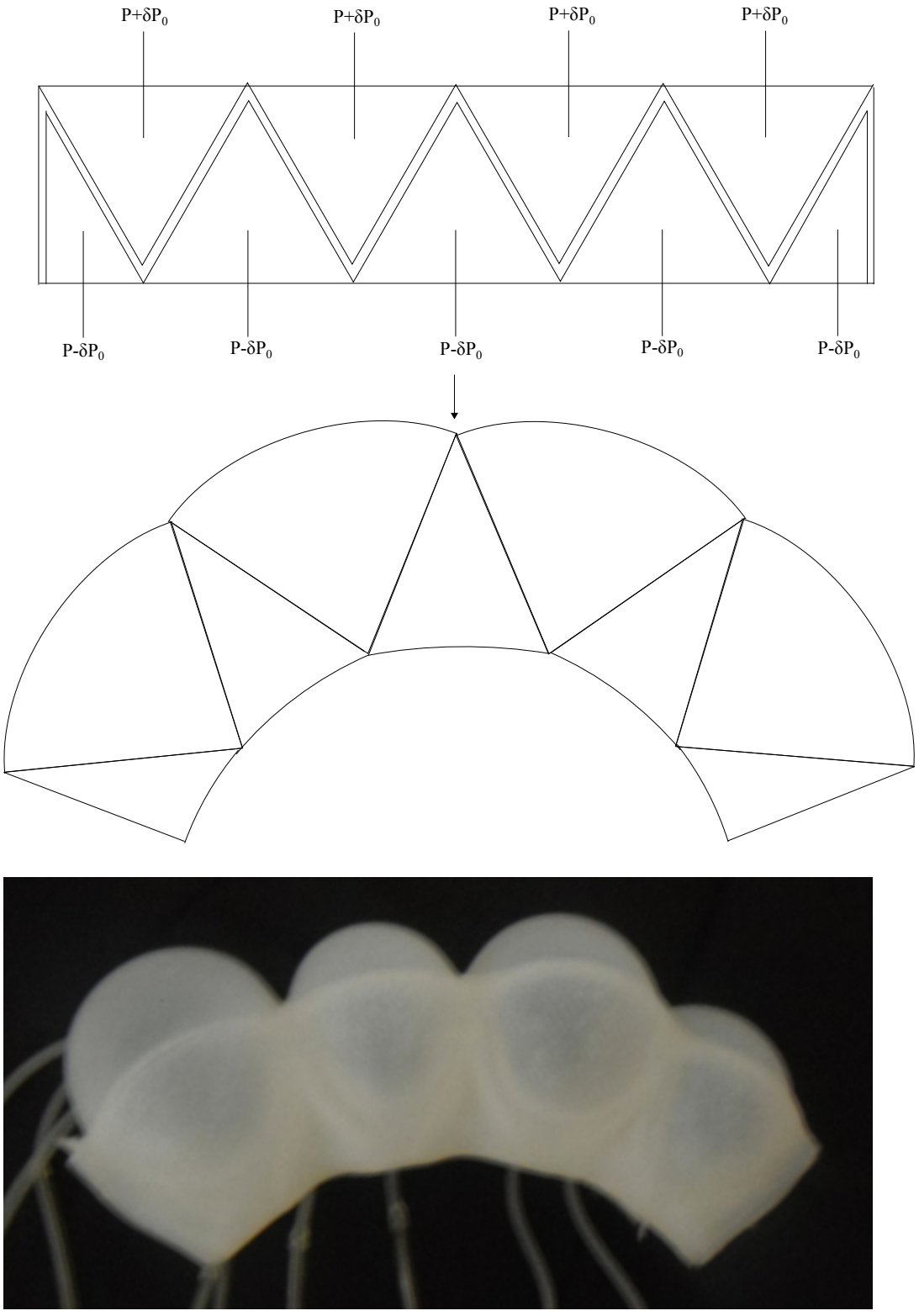


Figure 4.22: M1 muscle undergoing bending motion. This is achieved by the variation of internal positive and negative air pressure in each air channel, the upper air cavities have their internal air pressure $P$, increased to $\delta P$ while the lower air cavities have their internal air pressure decreased by $\delta P$.

used as heat shields. Table 4.6 shows the parameters of the plastic bag produced, figure 4.23 shows a picture of the produced plastic bag actuator. The plastic bag actuator together with the parameters specified were used in Chapter 9 to actively move an exoskeleton.

Figure 4.23: Plastic bag actuator produced.

To further compare with the rubber based designs, plastic bags are ultra-light weight, have a thickness of $50\mu m$ and weigh less than 10g depending on the design. They are not stretchable, actuation with pneumatic air do not deform the material, rather air occupies the chamber, making the plastic films push against each other to give rise to an increase in air chamber. One advantage of the welding fabrication process is that it does not require the design and use of very complicated moulds and therefore inquires a less expensive manufacturing process.

## 4.8 Discussion

The manufacturing, development process, geometric and material parameters of silicone rubber and plastic bag actuators that exhibit bending, rotary and contraction movements have been described in the preceding sections. These actuators were produced with a view to assisting in upper limb motion.

Rubbers have been found to exhibit unstable elastic phenomenon when undergoing large deformations, which results in aneurysm or visible bulging. Braided mesh and

corrugated designs are novel methods employed in this work that helped reduce visible bulging. Embedding a braided mesh to reduce bulging is a novel aspect to this work, which helped to improve overall performance of the actuator.

The corrugated design at first glance is able to reduce bulging, but as would be seen in the characterization chapter (Chapter 6), this does not transfer to improving the overall strength of the actuator. As a result of the corrugated design, there are hindrances in repairing of the structure when damaged because this would lead to covering the corrugation. Demoulding process also requires careful extraction of cured silicone from the mould.

Rubber thins out under tension and thickens under compression, but inflatable plastic bags, rather than deform, work by increasing in area and volume to produce a corresponding movement. Silicone rubber actuators have a higher mass compared with inflatable bags. Due to this, the silicone rubber actuators can be directly attached to the human body to assist as would be presented in Chapter 8 while plastic bag actuators would be attached to an exoskeleton which in turn is attached to a human arm as would be presented in Chapter 9

The soft muscle actuators which work by making use of vacuum to extract air from the actuator are also a novel aspect of this work, as previous soft robots make use of McKibben muscles to achieve contraction. A yet another innovation presented here is the use of a combination of positive and negative air pressure directed within a silicone rubber air chamber to achieve bending. Previous studies have always made use of inextensible rubber or fabric layer to execute bending motion.

To actuate the soft modules developed in this chapter, compressed air and/or vacuum from a pressure source is fed into the air channels via air tubing. Chapter 7 will detail the hardware and software control system setup that was used to actuate all the soft actuators that was developed in this chapter.

## 4.9 Chapter Conclusion

Soft robots are capable of performing a wide variety of tasks owing their flexibility. Additionally, the fabrication of components with silicone rubber is easier and more flexible than in metals. The use of silicone rubber as a material reduces time, complexity and cost of prototyping. But designing a single actuator that performs optimally for

an entire range of tasks is difficult, so a new actuator that meets a given specific design requirement such as producing bending, rotary or contraction motion has to be fabricated as seen in this Chapter. To conclude, silicone rubber presents many attractive features that make it useful for a wide range of applications especially for prototyping in research, though it may not be the ultimate material when it comes to large scale manufacturing.

In this chapter, the detailed description of all soft actuators produced in this work was described from schematic drawing to final production while also providing explanations to the geometry and design choices made through the development process. The characterization of these developed actuators will be carried out next, but first, description of visual processing concepts and algorithms used to obtain visual related data from the soft actuators is carried out.

# Chapter 5

# Visual processing system for tracking soft robots

Before the characterisation of the soft robots that was developed in the previous chapter is presented, this chapter is first used to describe visual processing algorithms used to get vision performance data from the actuators. One downside of soft robots owing their extra flexibility or compliance is that sensors cannot be easily integrated so as to accurately measure its position, hence the need for vision to act as a sensor. Soft robots are made with materials that experience large deformations, the sensors that can be used to obtain motion data is either through the use of embedded sensors or visual tracking information from a camera. The use of embedded sensors can be cumbersome, also limiting movement of the soft robot. Red-Green-Blue (RGB) colour markers made of pigmented silicone rubber were produced and glued unto the robot's body with no hindrance to movement. Visual processing concepts such as RGB colour tracking, template matching and camera calibration was applied.

The contribution of this chapter to the overall aim of the work is the application of vision processing algorithms to track the position (expansion and contraction) of silicone based soft robots. The developed vision processing system can track and measure parameters such as angle of motion, bending angle, degree of bulging and contraction ratio in real-time for bending, wedge-shaped and muscle actuators that were developed in the preceding chapter. The results obtained from the visual measurement system, together with other performance data such as torque and pressure are presented in the succeeding chapter. This vision system was also used to execute a two-stage control law based on vision and pressure information that moves the soft robot to a desired position, this

will be presented in Chapter 7.

## 5.1 Introduction

Vision is a way of sensing the world, using a camera as a sensor is arguably one of the most sophisticated method of sensing an environment. A camera is a passive, exteroceptive sensor meaning that it receives light signal from the environment and measures the amount of light reflected by an object. When it comes to robotics, alternatives from nature is often used and this is another classic example of how nature is borrowed from where real time parameters of soft robots are collected by the use of a camera. Computational requirement is taken care of by the operating PC; a USB connected camera; the weight and size of the camera is such that it is portable and easy to handle.

Soft robots are made with deformable bodies and have a number of advantages such as flexibility, dexterity and inherent compliance. However, one downside to the extra flexibility of a soft robot is that this creates difficulty in accurately measuring movement paths - a challenge in soft robotics is finding a suitable way of measuring their motion, a robust, standardized, stable measurement and control system is still a challenge. This chapter focuses on applying computer vision algorithms in measuring the structural change and motion of soft robots.

## 5.2 Methodology

Visual processing algorithms for color intensity and template-based tracking were used as a means of collecting information about the soft robot's deformation, movement and position.

### 5.2.1 Color intensity tracking

Color intensity tracking is aimed at differentiating a specific colour marker from background information by reducing the scene to a binary image. Color tracking can be achieved by using distinctive colour such as RGB colour markers in the scene and performing thresholding to binarize the image - the image is separated into two pixel classes with a minimal variance, these pixel classes are black and white. White indicates the colors being tracked while black is everything else. The pre-processing and post-processing algorithms for thresholding method include:

1. **Filtering:** Filtering is applied to reduce noise by averaging each pixel of the original image over a odd-number square matrix window. Gaussian kernel is applied to make the averaging isotropic with decreasing weight away from the tracked point. Median operation through ranking can also be used to preserve detail during filtering.

2. **RGB to HSV Conversion:** Hue Saturation Value (HSV) is an intuitive way of specifying colors rather than RGB. The tracking is carried out in the HSV color space in order to separate lumia intensity from chroma intensity. In HSV colour space, hue selects the color; saturation determines how deep and rich the colors are (fully de-saturated is white, fully saturated is pure color); and value behaves like a dimmer. In this color space, hue and saturation are invariant for shadow-shading.

3. **Binarisation:** A logical operation in vectorised form is performed to separate the image into black and white. The logical test is done between every element of the image input matrix and a vector matrix. The vector matrix specifies range of HSV values of the red, green and blue color trackers to produce a logical output matrix (true or false).

4. **Erosion and dilation operation:** This operation is carried out on the binarised image to open and close holes with a square matrix morphological structuring element, $S$, which is sensitive to shape. Erosion and dilation are converse operations. For erosion, the output is true if all pixels in $S$ are true. For dilation, the output is true if any pixels in $S$ are true. A sequence of erosion followed by dilation is called opening, only shapes compatible with the structuring element are maintained while the rest shapes disappear. A sequence of dilation followed by erosion is called closing, holes within the shape are closed up.

5. **Find binary regions:** To determine the geometry of tracked object, blobs have to be determined. A blob is defined as a group of contiguous pixels in a binary image, connected to each other which have the same color. Since multiple colors are being tracked, the image has multiple blobs distinctive from each other by the RGB thresholding operation.

6. **Find centroid of region:** After defining blob regions in the image, the position coordinate of the blobs are found by calculating the zeroth and first moments.

The zeroth moment, $m_{00}$ is the number of white (true) pixels in a region. This specifies the area of the tracked region, given as:

$$m_{00} = \sum_{(m,n)\in I} I[m,n] \tag{5.1}$$

Where $m$ and $n$ coordinates are the $x-y$ locations of pixels in the image and $I[m,n]$ specify the value of the binary pixel at that particular coordinate. The first moments, $m_{10}$ and $m_{01}$ are weighted averages of $m$ and $n$ coordinates, weighted by the color of binary pixels and specified as:

$$m_{10} = \sum_{(m,n)\in I} uI[m,n], \quad m_{01} = \sum_{(m,n)\in I} vI[m,n] \tag{5.2}$$

The coordinate of the geometric center or centroid of the tracked region, $[m_c, n_c]$ is given by:

$$m_c = \frac{m_{10}}{m_{00}}, \quad n_c = \frac{m_{01}}{m_{00}} \tag{5.3}$$

### 5.2.2 Template matching

Location tracking of binarised color markers, whilst efficient requires constant recalibration to account for pose variation. A robust method, although more computationally expensive is using a template or pattern of pixels to find the location of tracked points. Template matching tracks regions by focusing on the search for regions in the image which are the most similar to tracked targets. This is achieved by calculating at each position of the image, a correlation that symbolizes the degree of similarity or dissimilarity to a template patch. This is a spatial operator approach in which an input image is compared with a template image, the template being the image pattern being looked for, the input window is a subset matrix of the input image that would have the same size with the template. A numeric similarity score between a particular input window of the image that matches the template is determined. Its implementation requires usage of distinct markers, this marker is the template that is compared across every single location in the scene. To do achieve this comparison, an image similarity measure is needed.

Sum of Absolute Differences (SAD) is an image similarity measure that takes the ab-

solute difference between corresponding pixels of the two images being compared and sums it up. The similarity measure, $s$, will have a value of zero if the both images are identical and a value greater than zero if dissimilar. In other words, the position where the minimum value of the output similarity matrix is located indicates the position of a perfect match. The equation is specified as:

$$\text{SAD, } s = \arg\min \sum_{(m,n)\in I} |I_1[m,n] - I_2[m,n]| \tag{5.4}$$

A similar approach is the operation called Sum of Squared Differences (SSD), which instead of using absolute difference, uses the sum of squared differences calculated as:

$$\text{SSD, } s = \arg\min \sum_{(m,n)\in I} (I_1[m,n] - I_2[m,n])^2 \tag{5.5}$$

The ZNCC measure varies from $-1$ to $+1$. $+1$ means the images are identical; $-1$ means one image is negative of the other. 0 means the two images are not well correlated. Typically, a value of 0.8 can be considered as a reasonable match. ZNCC tracking algorithm is specified in Algorithm 1. Its equation is given as:

$$\text{ZNCC, } s = \arg\max \frac{\sum_{(m,n)\in I} I_1[m,n] - I_2[m,n]}{\sqrt[2]{\sum_{(m,n)\in I} I_1^2[m,n].\sum_{(m,n)\in I} I_2^2[m,n]}} \tag{5.6}$$

**Algorithm 1** ZNCC Tracking algorithm

1: Get template height and width, $h_t, w_t$
2: Get image height and width, $h, w$
3: $h_{t2} = \frac{h_t - 1}{2}$
4: $w_{t2} = \frac{w_t - 1}{2}$
5: Initialize: $Im_{ZNCC} = [\infty]$
6: **for** $c = [w_{t2} + 1] : [w - w_{t2}]$ **do**
7: **for** $r = [h_{t2} + 1] : [h - h_{t2}]$ **do**
8: $Im_{win} = image(r - h_{t2} : r + h_{t2}, c - w_{t2} : c + w_{t2})$
9: $Im_{ZNCC}[r,c] = \frac{\sum |Im_{win} - tp_{win}|}{\sqrt[2]{\sum Im_{win}^2 . \sum tp_{win}^2}}$ ▷ ZNCC
10: **end for**
11: **end for**
12: $\max Im_{ZNCC}[r,c]$

If an object template is applied to another scene having the same object template but in a different or slightly modified condition such as change in lighting conditions or

camera position to make the tracked point bigger or smaller depending on how closer or farther from the camera the template is, template matching would not work well, hence the need for constant recalibration. Recalibration is easily performed with template matching as tracked regions are selected online prior to tracking.

## 5.3 Implementation

Visual processing was carried out on a PC. The setup employed uses a Webcam to view the scene. RGB tracker markers fabricated with silicone rubber were produced, so that the trackers have same material characteristics with the soft robot to ensure easy integration. These trackers were manufactured by adding and mixing few drops of coloured paint to liquid silicone in order to give rise to red, blue and green soft color trackers. Ecoflex 0030 silicone liquid is transparent and can therefore be coloured as desired with pigment pastes. The pigments are easily blended into the silicone liquid compound during mixing. The soft color markers were glued to the soft robot's body also using silicone liquid as adhesive.

### 5.3.1 Camera Calibration

The amount of light that is reflected off a surface depends not only on the color of the object but also on its roughness, distance of light from the object and most importantly the color of the light source and ambient light. The pixel value of a point in the scene can change even if the camera does not move. A slight change in illumination, perhaps a difference in sunlight or light source can change the exposure of that point in the scene. So calibration is important because of these highlighted factors are constantly changing. To accommodate for all these factors, recalibration is performed each time by selecting the group of pixels to be tracked, that way, ambient light levels is taken care of and other discrepancies. For color intensity tracking, a recalibration of the HSV values of the three colour markers was done at the start of data collecction in order to minimise the effect of change in lighting conditions of the room.

If camera axis is orthogonal to the object plane and the distance between object and camera is fixed, the geometric setting of the camera relative to the object can be chosen such that it is converted from pixel to metric value. A perspective camera (like the human eyes) will always project a straight line to a straight line. It will project a conic section to a conic section, though not necessarily the same conic section, so a

circle (a conic section) could be mapped to a different conic section such as an ellipse. Angles between lines are not preserved which means parallel lines may be projected as converging, and the vertex angles of a planar shape (triangle, square or more generally a polygon) may not be preserved.

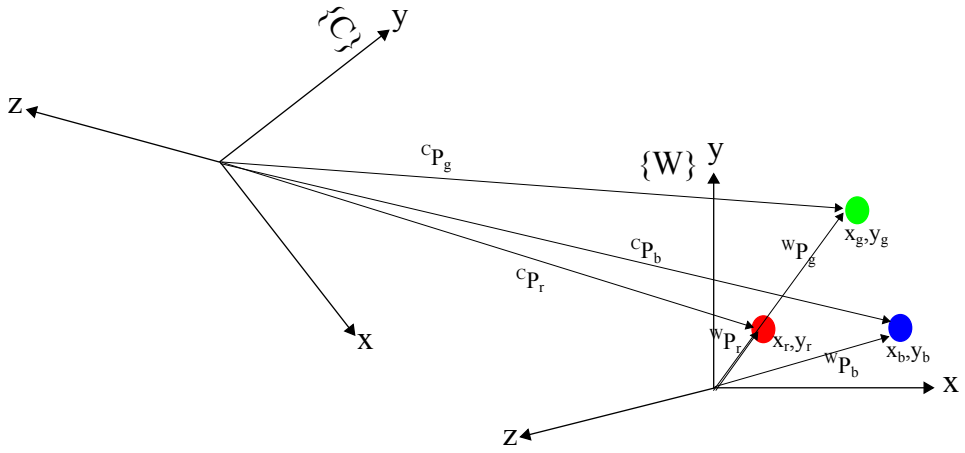


Figure 5.1: Method for obtaining angle data – green, red and blue markers are positioned as indicated, each $x, y$ position represents $[x, y]$ centroid position for each colour marker.

As a way of preserving angles, coordinate frame transformation from camera frame to the workspace (Figure 5.1) is performed. $W$ represents world coordinate frame, measurement from this frame signifies the real position of the RGB colour markers in $mm$ at positions $x_r, y_r, z_r$,$x_g, y_g, z_g$,$x_b, y_b, z_b$. $C$ represents the coordinate frame of the camera, fixed at a position $a_x, a_y, a_z$ from the world coordinate, rotated by an angle $\theta_1$ with respect to the $x-$axis and then rotated by an angle $\theta_2$ with respect to the $y-$axis. The camera frame signifies the view of the camera with respect to the soft robot. The homogeneous transform of the camera from the world frame, ${}^{W}T_{C}$, is given by:

$$ {}^{W}T_{C} = T(a_x, a_y, a_z)R_x(\theta_1)R_y(\theta_2) = \begin{bmatrix} \cos\theta_2 & 0 & \sin\theta_2 & a_x \\ \sin\theta_1 \sin\theta_2 & \cos\theta_1 & -\sin\theta_1 \cos\theta_2 & a_y \\ -\cos\theta_1 \sin\theta_2 & \sin\theta_1 & \cos\theta_1 \cos\theta_2 & a_z \\ 0 & 0 & 0 & 1 \end{bmatrix} \quad (5.7) $$

The transformed vector, representing the position of each of the markers with respect to the world frame is calculated as:

$$ {}^{W}P_{(r,g,b)} = {}^{W}\ T_{C}.{}^{C}P_{(r,g,b)} \quad (5.8) $$

Where ${}^{C}P$ is a vector representing the $[XYZ]$ position of each corresponding marker location with respect to the camera measured in pixel units, these values are obtained by the camera as the centroid of each marker. The vector corresponding to the soft robot's workspace for each marker is calculated as:

$$ {}^{W}P = \begin{bmatrix} X\cos\theta_2 + Z\sin\theta_2 + a_x \\ X\sin\theta_1\sin\theta_2 + Y\cos\theta_1 - Z\sin\theta_1\cos\theta_2 + a_y \\ -X\cos\theta_1\sin\theta_2 + Y\sin\theta_1 + Z\cos\theta_1\cos\theta_2 + a_z \\ 1 \end{bmatrix} \tag{5.9} $$

$X$ and $Y$ are measured directly from the camera, $Z$ is obtained using a 2-camera system placed on the same horizontal surface with $B$ being the distance between both cameras; $f$ the focal length of both cameras; $x$ and $x'$ are the x-positions of both cameras. $Z$ given by:

$$ Z = \frac{Bf}{x - x'} \tag{5.10} $$

After translation to the world frame, angle of the soft robot is calculated as:

$$ q_0 = \cos^{-1}\left(\frac{l_1^2 + l_2^2 - l_3^2}{2l_1 l_2}\right) \tag{5.11} $$

Where lengths $l_1$, $l_2$ and $l_3$ are calculated as the distance between centroid locations of green and red; red and blue; green and blue color markers respectively.

Visual processing was also used to measure deformation parameters for triangular, bending and muscle soft actuators by placing colour markers as illustrated in Figure 5.2.

## 5.4 Results & Discussion

The developed visual processing was written in C++ language and was used for all manufactured soft robots which include SRM muscles, bending and triangular robots as shown in Figure 5.3. The soft color markers which also integrates well with the soft robot's body were fixed to specify tracked points. To ensure accurate data collection from visual processing, measurements of ground truth information was also performed.

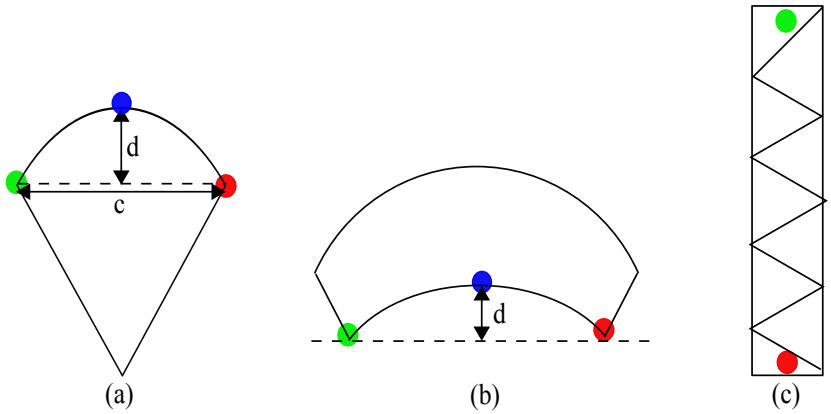


Figure 5.2: Colour markers placed on (a) Wedged-shaped soft robots to measure deformation parameters: arc width, $c$ and arc height, $d$. (b) Bending soft robot to measure bending angle which is defined by the angle made between the green - blue and red - blue colour markers. (c) Soft muscle actuators to measure contraction.

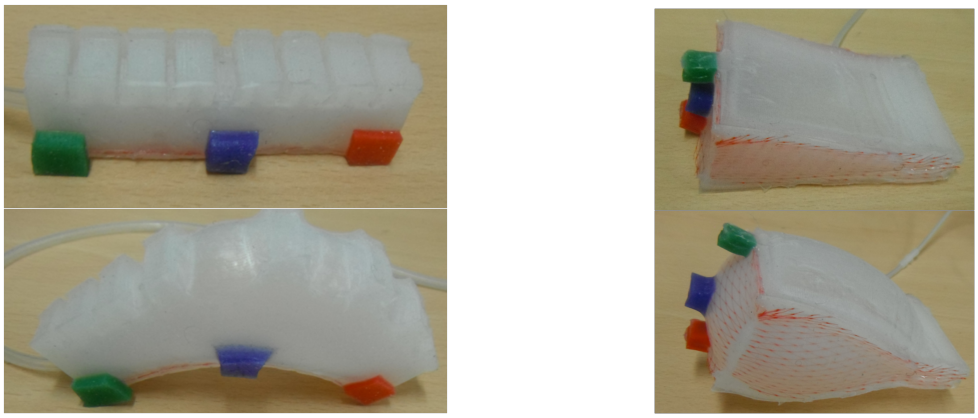

(a) (b)

Figure 5.3: Soft color markers bonded with the soft robots to measure parameters of various soft robots as they undergo deformation through air filling of channels.

Both methods of colour tracking via thresholding and template matching were used. Figure 5.4 shows thresholding procedure from original image to centroid location of marker to measure angle. To achieve better results while using computer vision to get angle measurements, a recalibration of the HSV values of the three colour markers was done at every instance the experiment was conducted in order to minimise the effect of change in lighting conditions of the room. Vision results of angle were compared with ground truth measurements at the start and end of experiments using a digital protractor to ensure correct reading.

Template matching method provided more accuracy in the tracked point, real time calibration was possible using this method as the template was selected using mouse selection though it was more computationally expensive. The time to process an image frame for three color markers for template matching is 600ms while thresholding algorithm was about $280ms$. When the frames were converted from RGB to grayscale, speed of visual processing for template matching improved to between 100 - 120ms. This improved processing time measured was because in RGB color tracking, three different values were being compared but in grayscale, a single number is compared instead of three numbers. This is as a result of grayscale being representative of an image frame as a 1-Dimensional array as opposed to an RGB colour image which is represented as a 3-Dimensional array of pixel values. Another important factor affecting visual processing speed is the size of the image, a larger frame size of 640 by 480 slows down the processing compared with a 320 by 480 image frame.

In general, tracking with template matching approach resulted in better performance as room lighting conditions would have a reduced chance in obtaining the correct location of tracked regions when compared with thresholding. Calibration is also easier with template matching - no need of tedious adjustment and recalibration of HSV values due to changes in the lighting conditions of the room. During experiments, template matching was also found to be a more robost method. As a way of minimising errors while measurement data and control was carried out with template matching approach, a test run was carried out to ensure that position of the marker is tracked through the soft actuator's entire range of motion prior to starting the experiment.

Visual processing was used not only as a sensor but also as an aid to performing control of the soft robots. Based on the current positional measurement, a controller was implemented which produced a control signal to be used as input to a low level pressure controller to represent the desired pressure that should be maintained to allow

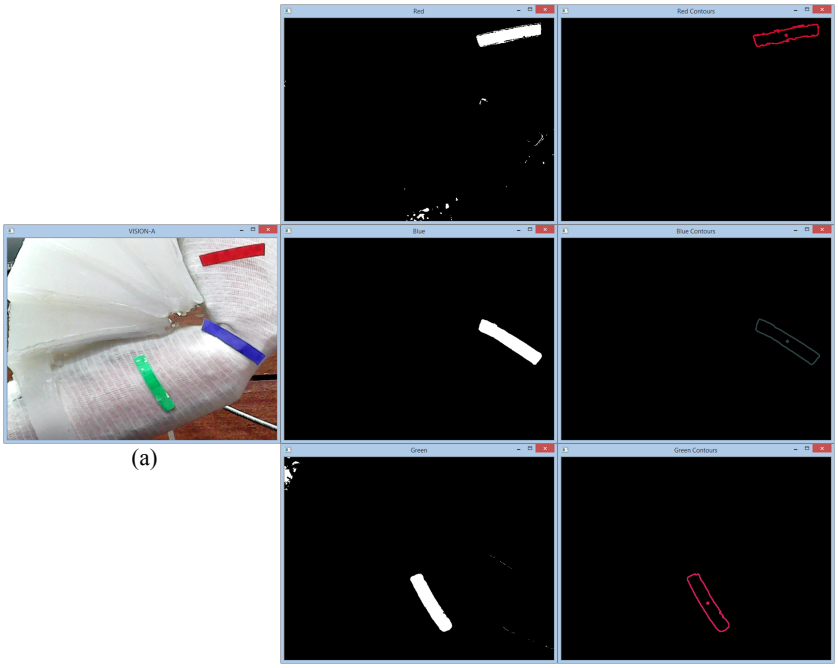


Figure 5.4: Thresholding procedure showing (a) original image, (b) binarised image and (c) centroid location tracking of each red, green and blue colour marker.

the robot reach the desired position, this will be detailed in Chapter 7

## 5.5 Chapter Conclusion

Visual precessing that was adopted in sensing parameters of the developed soft actuators in real-time has been presented in this chapter. Other possibilities of utilizing computer vision for soft robots can be for measuring shape of deformation, which would be achieved by placing markers along the length of the robot. A major advantage of using vision as a sensor is that it can used as a standard approach for measurement. In addition, due to the emerging nature of soft robotics and no standardized sensors have been adopted, computer vision will offer a robost measurement system.

# Chapter 6

# Characterisation of soft actuators for motion

In this chapter, characterisation of developed soft actuators in terms of range of movement such as angle, deformation as well as pressure and torque is presented. First, a presentation of the sensors used to get these measurements are given, then characterisation of bending, triangular and muscle actuators are detailed.

## 6.1 Introduction

The previous chapter focused on the visual processing implementation required for getting deformation parameters from the soft robot. The method used to record angle of motion was through visual processing via camera recording of the position of RGB colour markers in real time. In this section, a discussion of the setup for pressure and torque measurement is discussed. After, the results and discussion based on these measurements are presented.

To measure air and vacuum pressure inside the soft actuators, amplified pressure sensors with analogue interface having a 1ms response time was used to read the pressure. The sensors have been calibrated and compensated for sensitivity, temperature effects, sensor offset and non-linearity. The gauge sensor measures air pressure with its minimum value referenced to atmospheric pressure while the absolute sensor measures pressure with the minimum referenced to complete vacuum. The sensors are produce 12-bit analogue output at a speed of 1kHz, Table 6.1 shows sensor parameters, a datasheet with detailed information is available [164]. All pressure data presented was captured

at a speed of 60Hz using a ADC having a 10-bit resolution because these chosen speed of capture and ADC resolution were the maximum possible available.

Table 6.1: Pressure sensors specification for measuring air and vacuum pressure within soft robots

| **Parameter** | **Value** | **Specification** |
|---|---|---|
| Gauge sensor | Sensor output | Analogue |
| | Maximum operating pressure | 5psi |
| | Minimum operating pressure | 0psi |
| | Pressure measurement type | Gauge |
| | Voltage rating | 5V |
| | Port style | Axial |
| | Supply current | 2.5mA |
| | Manufacturer | Honeywell |
| | Model number | ASDXAVX005PGAA5 |
| | Product range | ASDX Series |
| Absolute sensor | Sensor output | Analogue |
| | Maximum operating pressure | 15psi |
| | Minimum operating pressure | 0psi |
| | Pressure measurement type | Absolute |
| | Voltage rating | 5V |
| | Port style | Axial |
| | Supply current | 2.5mA |
| | External depth | 16.76mm |
| | Manufacturer | Honeywell |
| | Model number | ASDXACX015PAAA5 |
| | Product range | ASDX Series |

A pump, which consists of air and vacuum was used for positive and negative air pressure supply. The parameters of the pump used for the characterisation have the specifications listed in Table 6.2.

A light weight prototype model of an elbow joint was used as a first test of the performance of these soft modules, and to verify the torque output, range of angle and pressure. The links of the elbow joint was made of light weight swimming float material having a diameter of $60mm$ while the hinge joint was composed of 3D printed ABS material. This dummy model was used as a first step in taking measurements. Figure 6.1 illustrates the measurement set up to determine the torque of developed triangular

Table 6.2: Specification of 6V DC air pump.

| Property | Specification |
|---|---|
| Rated voltage | DC 6.0V |
| Rated current | 350 mA |
| Maximum pressure | 8.7psi |
| Air flow rate | 2.0 lpm |
| Noise | $<$ 67dB |
| Pipe diameter | $\oslash$ 4.2mm |
| Model number | AJK-B06A2703 |
| External size | 27x58mm |

soft actuators. This consists of a load cell, the dummy joint and a digital protractor for the exact positioning of the angle.

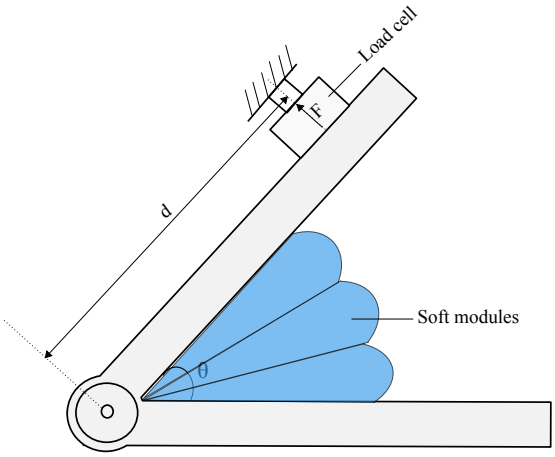


Figure 6.1: Schematic of torque measurement setup. Torque, $T = Fd$. Torque was measured by positioning a dummy joint fixed at a predefined angle $\theta$ and measuring the force obtained by the load cell placed at a fixed distance $d$ from the pivot point of the dummy joint as shown.

## 6.2 Bending actuators

Characterisation of bending soft actuators in terms of bending distance, angle and pressure were performed. When bending soft robots are pressurized, the channel enclosed by soft silicone undergoes high strain and lengthens while the base (stiffer) layer is unextended, therefore, the expansion generates a bending curvature about the stiffer but

extensible layer. To determine the degree of bending, a graph of the bending distance as a function of time was plotted. The bending distance is defined by the distance between the mid-point of the bottom layer of the soft robot and the ground support in its uninflated state and the distance of this mid-point from the ground support when pressurized as illustrated in Figure 5.2. The bending angle is defined by the angle made as a result of the bending at the base (stiffer) layer as shown in Figure 5.2. The bending distance of the bending actuator of Figure 4.3c was plotted as shown in Figure 6.2. Figure 6.2a shows that the time taken to inflate the bending soft robot to its maximum bending is about 10s for the inflation cycle while the deflation time as shown in Figure 6.2b is about 8s. A displacement of 6mm was measured as the distance moved by this soft robot at the maximum bending. Figure 6.3 shows plots of the bending angle and air pressure within the actuator illustrated in of Figure 4.3c as it undergoes inflation as a function of time, as shown, a pressure reading of 4.5psi was obtained at the maximum bending angle.

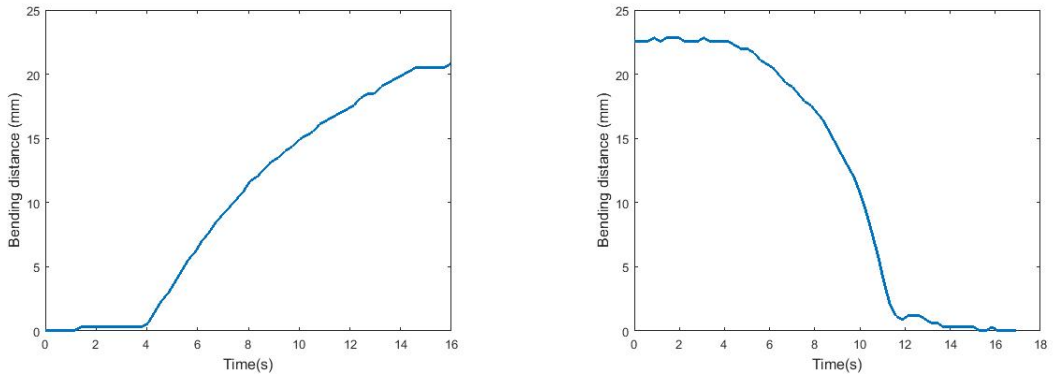


(a) (b)

Figure 6.2: Bending distance of actuator described in Figure 4.3c as a function of time for 1 sample. Geometry of actuator length, $l = 120$mm; breadth $b = 50$mm; thickness $t = 2.5$mm. (a)inflation cycle (b) Deflation cycle

## 6.3 Triangular actuators

The 20° triangular actuator developed in Figure 4.9 of Chapter 4 was characterised in terms of measured angle, bending distance and arc length as a function of time as shown in Figure 6.4. The parameters were obtained by placing colour markers as illustrated in Figures 5.2a and 5.3b.

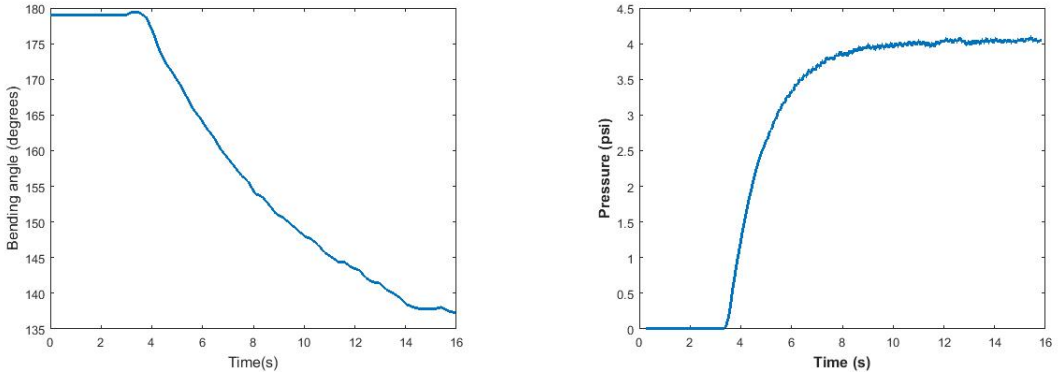


(a) (b)

Figure 6.3: Bending angle and air pressure of actuator described in Figure 4.3c as a function of time for 1 sample. Geometry of actuator length, $l = 120$mm; breadth $b = 50$mm; thickness $t = 2.5$mm(a) Bending angle as a function of time. (b) Pressure as a function of time for the soft robot undergoing inflation for the bending actuator.

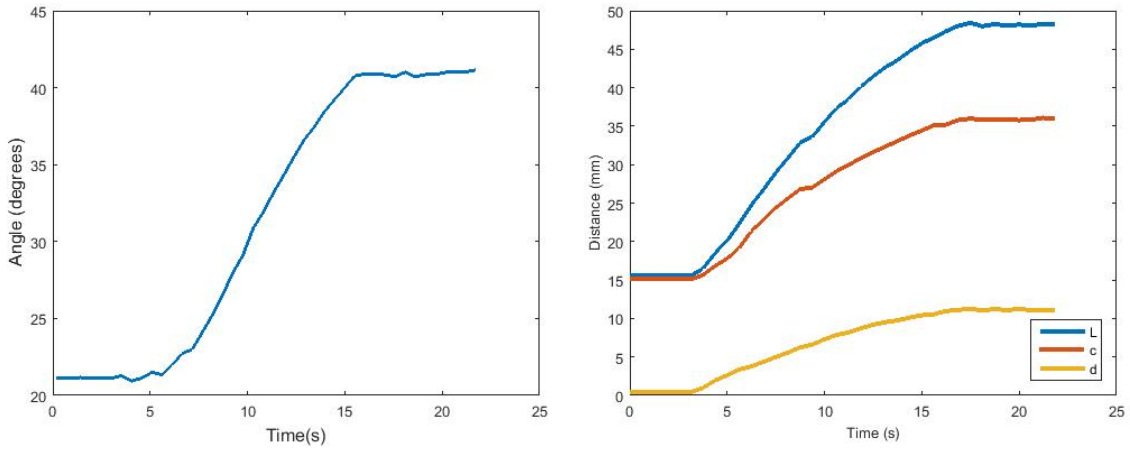


(a) (b)

Figure 6.4: (a) Graph showing angle as a function of time for the 20° wedged shaped soft actuator undergoing inflation; colour markers detect current inflation angle. (b) Graph showing arc width, $c$, arc height, $d$, and arc length, $L$ as a function of time for a 20° soft actuator under inflation pressure.

Three other triangular actuators developed in Chapter 4 are characterised in this section, they include plain 80° (Figure 4.6), embedded mesh 80° (Figure 4.11) and corrugated 90° (Figure 4.9b) actuators. These actuators were characterised in terms of range of motion as well as torque during positive and negative air pressure actuation for a single sample of each. The focus on the characterisation of these actuators is due to their potential use for assisting upper limb motion.

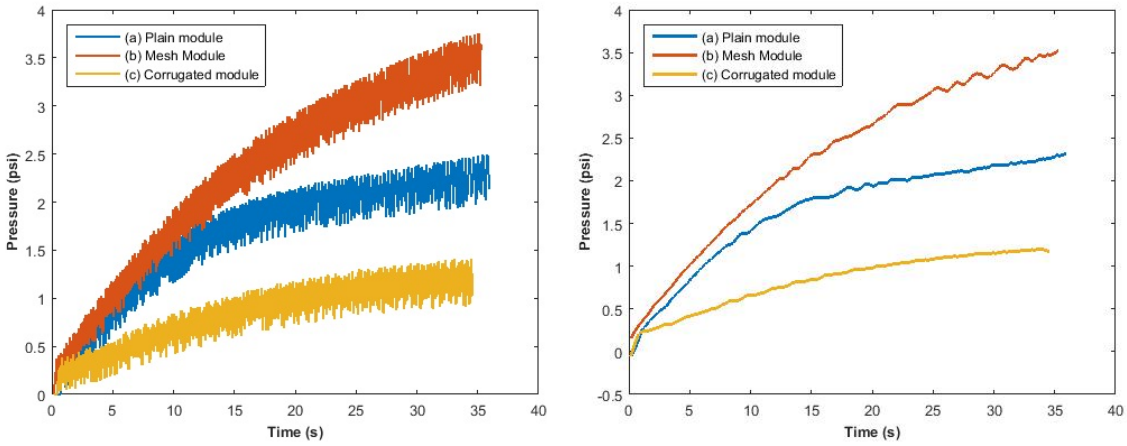


(a) Original (b) Moving average over 5 samples

Figure 6.5: Positive air pressure inside soft modules as a function of time for plain (Figure 4.6), mesh (Figure 4.11) and corrugated modules (Figure 4.9b) for a single sample: For the same actuation control time of 35s, a maximum pressure of 2.6psi is obtained for plain modules, air pressure up to 3.7psi is obtained for mesh modules, and maximum pressure up to 1.3psi is obtained for pleated modules.

Figure 6.5 show graph of the range of output air pressure measured by the pressure sensor inside plain, mesh and corrugated soft modules as a function of time. For the same control time of about 35s, maximum air pressure is up to 2.6psi for plain modules, a high air pressure up to 3.7psi is obtained for meshed modules; air pressure is up to 1.3psi for corrugated modules. It can be observed from the graphs that actuation times is typically slow (30s - 40s), this can be improved using a high pressure system such as an air compressor tank but comes at the expense of the system being bulky and less portable. A slow rate of actuation of 0.2Hz has also been reported [99] so as to avoid dynamic oscillations. As a consequence of slow actuation and limited torque, this designed actuator will be unsuited for assisting lower extremities motion and in shoulder elevation.

Figure 6.5b is a filtered graph of Figure 6.5a that shows the range of output air pressure in plain, mesh and corrugated soft modules as a function of time. The filtering function is a moving average of the pressure over 5 samples to smooth out the pump noise, this filtering function is given by:

$$\text{Moving Average } \bar{P}_{avg} = \frac{P_o + P_{o-1} + ... + P_{o-(n-1)}}{n} = \frac{1}{n}\sum_{i=0}^{n-1} P_{0-i} \tag{6.1}$$

Where $P_o$, $P_{o-1}$, ..., $P_{o-(n-1)}$ are the previous $n$ values of air pressure which will be averaged over $n$ consecutive values. Henceforth, the air pressure readings shown will be the filtered form to smoothen the readings.

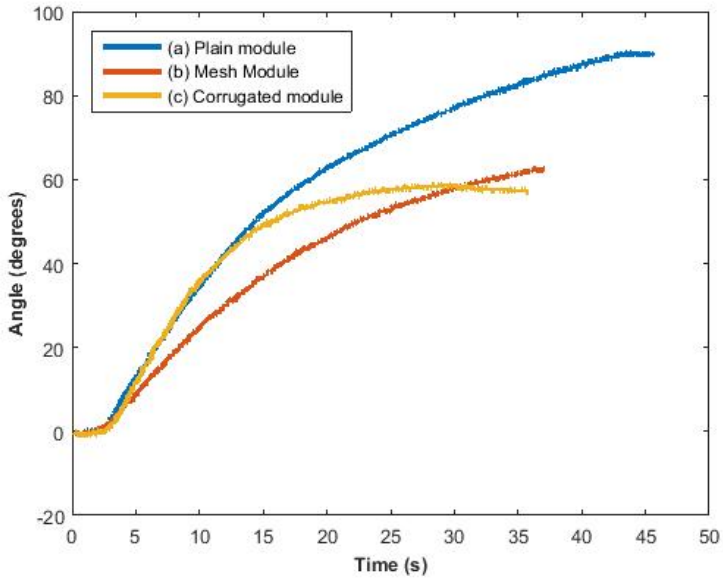


Figure 6.6: Normalised angle measurements of soft modules as a function of time for plain, mesh and corrugated modules: Angle range of $0° - 90°$ is obtained for the plain module, angle range of $0° - 65°$ is obtained for the braided mesh module, angle range of $0° - 59°$ is obtained for the corrugated module.

Figure 6.6 show graph of the range of angle motion as a function of time for plain, mesh and corrugated modules. The range of angle for plain modules is considerably large (between $0° - 90°$), the range of movement is between $0° - 65°$ for meshed modules while the range of angle motion is between $0° - 59°$ for corrugated modules. Figure 6.7 show graphs of the range of air pressure as a function of angle for plain, mesh and corrugated soft modules. It can be observed that while corrugated actuators help to

reduce the visible bulging, it does not produce as much torque and range of motion as the plain modules.

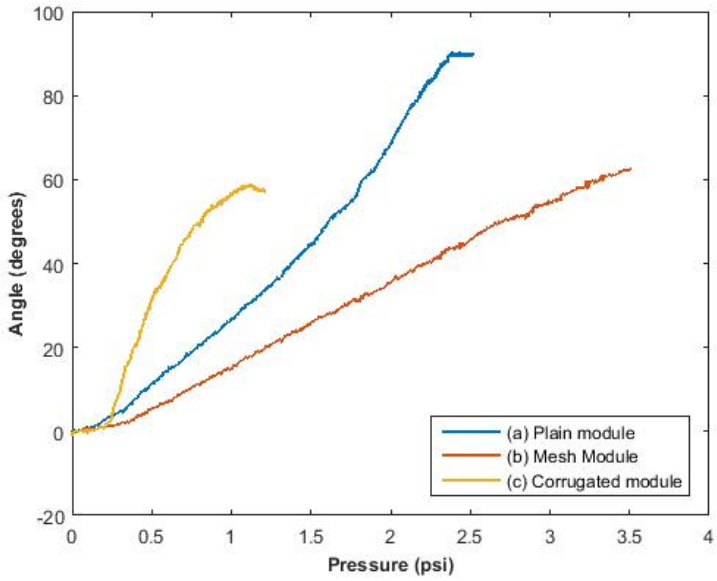


Figure 6.7: Normalised angle as a function of positive air pressure for plain, mesh and corrugated modules: A maximum angle of 90° is obtained for plain modules at 2.6psi, maximum angle of 65° is obtained at 3.7psi for mesh modules. Maximum angle of 59° is obtained at 1.3psi for corrugated modules.

Figure 6.8 show graph of air pressure inside soft modules as a function of torque for plain, mesh and corrugated actuators. A maximum torque output of 3.6Nm is obtained at 4.75psi for mesh soft modules, maximum torque output of 2Nm is obtained at 1.8psi for corrugated modules. To compare the torque output of these three soft triangular actuators, the mesh soft actuator experienced the highest torque and could consequently hold a larger amount of air pressure compared with the remaining actuators. The fiber reinforcement increased pressure resistance of the soft modules. As a consequence of this observation, the mesh actuator significantly helped to improve the torque performance of the soft robot and is the most suitable option for delivering assistive motion to the elbow. Although the plain triangular actuator had a larger range of angle compared with the mesh actuator, this advantage is not particularly useful given the intended purpose of the soft module, which is to provide assistive force for elbow movements.

From these results, the pleated triangular actuator only served to reduce visible bulging but had no overall effect in terms of torque and angle compared with the plain trian-

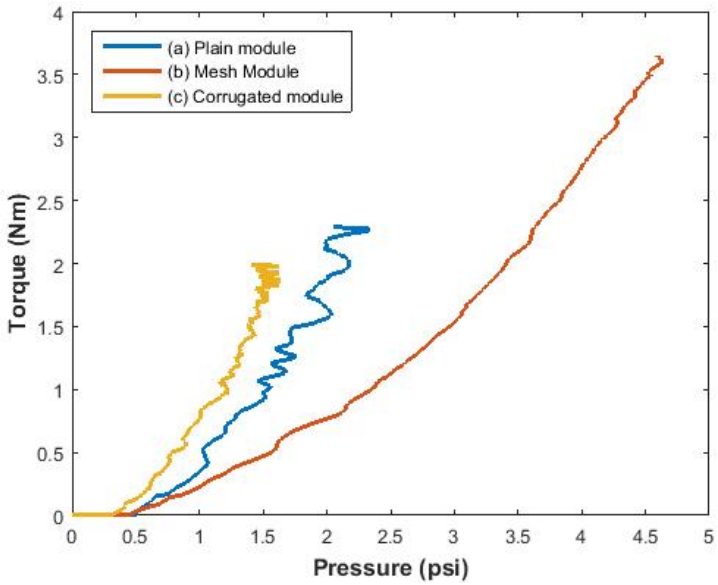


Figure 6.8: Torque as a function of positive air pressure of in soft modules: Maximum torque of $2.4Nm$ is obtained at 2.3psi for plain module at an angle of 80°, maximum torque of $3.7Nm$ is obtained at 4.75psi for meshed module at an angle of 80°, and maximum torque of $2Nm$ is obtained at 1.8psi for corrugated modules at an angle of 90°.

gular actuator. From observation of the corrugated module plots, a low operating air pressure, angle range and torque is seen. This is because there was no hard silicone layer reinforcements introduced, therefore, a combination of hard silicone and mesh reinforcement is needed in order to produce higher operating pressure and hence, higher torque.

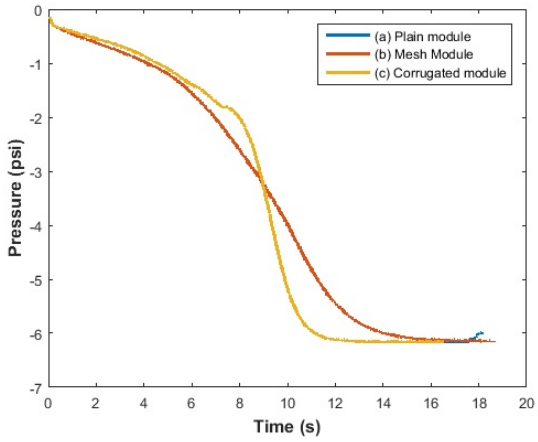


Figure 6.9: Negative air pressure inside soft modules as a function of time for plain, mesh and corrugated modules. Plain and mesh modules have the same path of pressure as a function of time, hence an overlap.

Negative air pressure was also applied to the soft modules to decrease the angle and for flexion motions. Measurements relating to range of motion and torque for negative air pressure results in which the pressure is regulated to -6psi are represented in Figures 6.9, 6.10, 6.11 and 6.12. A range of 15° was obtained for plain modules and a larger range of movement of 30° was obtained for mesh modules. The corrugated modules do not experience buckling when depressurized because of the corrugation network. Therefore, depressurization caused an increase in angle rather than decrease as illustrated from the plot in Figure 6.11. The mesh modules showed a higher negative torque of -2.7Nm compared to other modules as shown in Figure 6.12.

## 6.4 Plastic bag actuators

In this section, the characterisation of plastic bag actuators are described. Figure 6.13 show angle and air pressure readings collected at the same instance as a function of time using the 6V pump defined in Table 6.2. The plastic bags exhibit an interesting

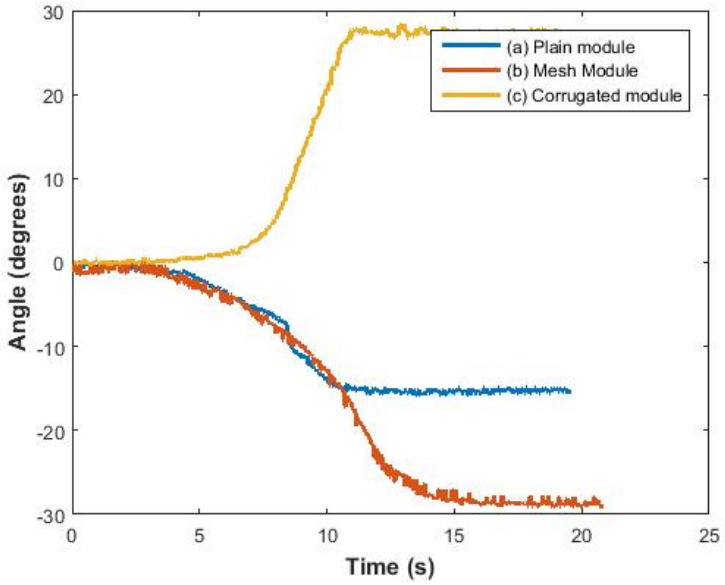


Figure 6.10: Normalised angle measurements of soft modules as a function of time for plain, mesh and corrugated modules for negative air pressure actuation.

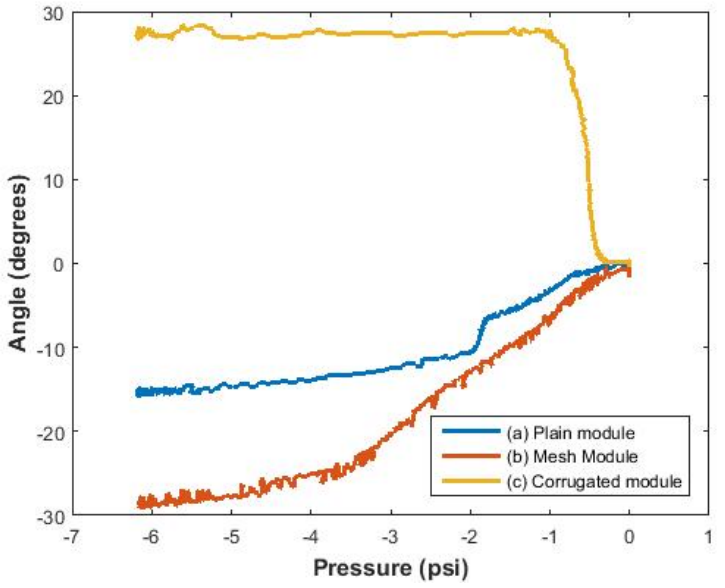


Figure 6.11: Normalised angle as a function of negative air pressure for plain, mesh and corrugated modules.

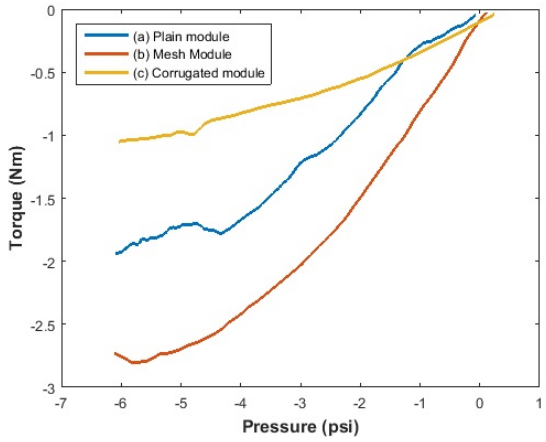


Figure 6.12: Torque as a function of negative air pressure of in soft modules.

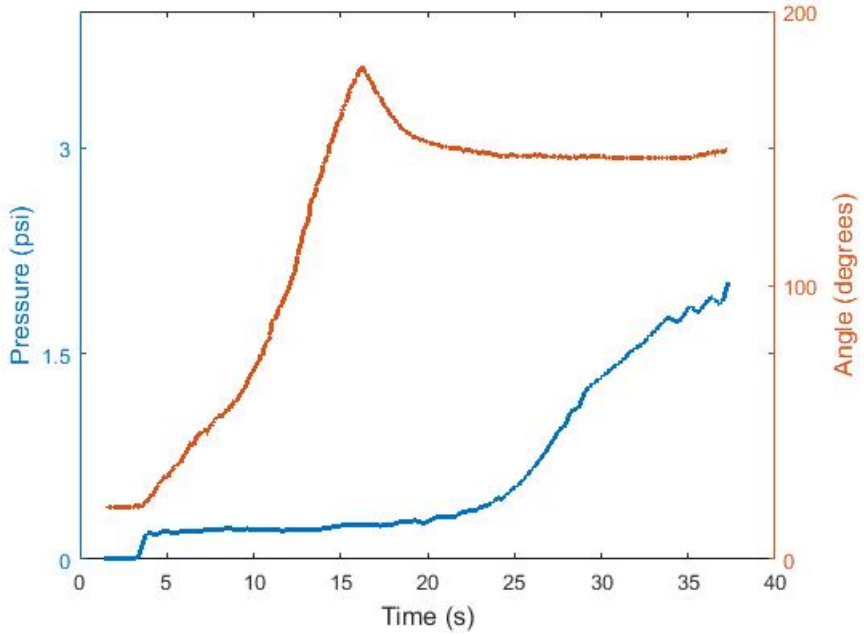


Figure 6.13: Normalised angle and air pressure of plastic bag actuator in Figure 4.23 as a function of time.

behaviour compared with the rubber actuators – as they inflate, there is no noticeable change in readings from the pressure sensor, this continues until it reaches its maximum angle after which the pressure begins to rise. The stage at which there is a 15s period at which pressure reading is not changing is because each plastic bag module is not pushing strongly against each other, as they begin to push strongly, the pressure begins to rise. From this graph, it can be observed that though the angle increased rapidly as it was inflated, it reaches a maximum after which the angle suddenly decreases. Figure 6.14 show plot of air pressure inside the plastic bag actuator as a function of angle obtained from the graph of Figure 6.13, as observed, the pressure-angle relationship is highly non linear, as there was no corresponding increase in angle as air pressure increased. This implies that plastic bag actuators cannot be controlled with a pressure - angle relationship.

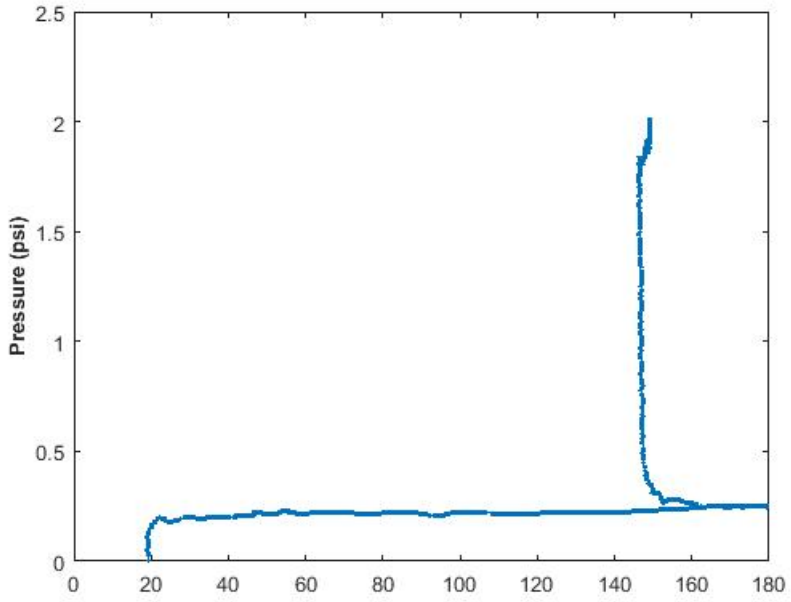


Figure 6.14: Air pressure of plastic bag actuator as a function of angle, pressure-angle relationship is not linear.

Figure 6.15 show air pressure as a function of torque for the plastic bag actuator. As shown, the relationship between pressure and torque can be interpolated with a linear relationship and therefore it is best to control plastic bags with pressure-torque relationship but not pressure-angle relationship. Given the pressure-torque relationship, at a certain pressure being read from the pressure sensor, it is possible to interpolate

how much torque is being applied. From the graph, it can also be observed that plastic bag actuators possess high torque of up to 4Nm

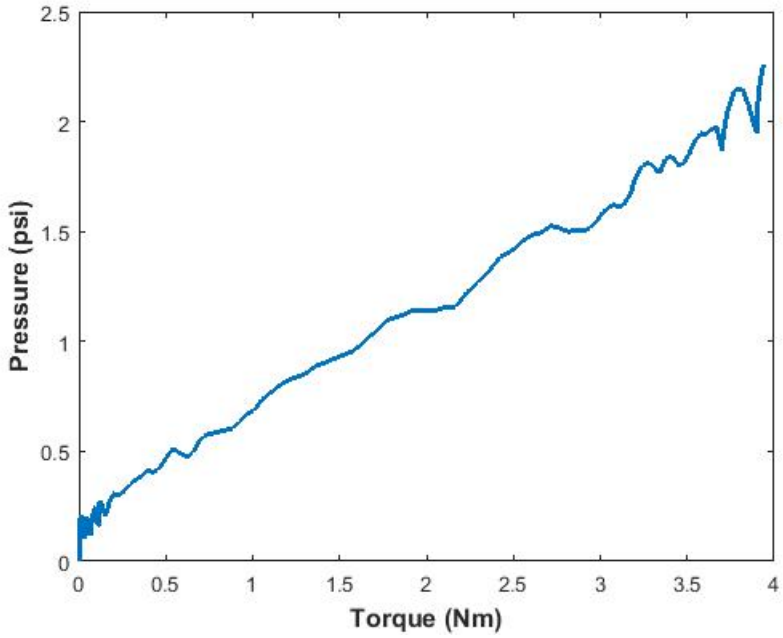


Figure 6.15: Air pressure as a function of torque for plastic bag actuator at 30°.

## 6.5 Muscle actuators

Isotonic contraction (muscle shortening at a constant force), maximal muscle force without shortening and contraction velocity were measured for SRM muscle actuators. As a way of characterizing the muscles, MI muscle was chosen as the standard while varying its parameter such as air channel height, $h_c$, length of muscle, $l$, length of wedge, $l_1$, number of wedges, $n$ and defining angle, $\theta$, to produce the other muscle actuators (M2 - M7). A table indicating measured isotonic contraction ratio of muscles M1-M8 is shown in Table 6.3. Another table showing the contraction speed expressed as contraction ratio per second is given in Table 6.4.

Graph 6.16 shows the pressure and contraction graphs for the M5 muscle. In all the muscles, vacuum pressure was regulated to -3psi. The graph shows vacuum pressure changing accordingly with the contraction ratio.

Figure 6.17 shows contraction ratio of M1 - M8 muscles under no load, 0.5Kg, 1.0Kg

Table 6.3: Mean and Standard deviation of isotonic contraction of the SRM muscles under different loads over 3 experiments.

| **Mean** | | | | | | | | |
|---|---|---|---|---|---|---|---|---|
| | M1 | M2 | M3 | M4 | M5 | M6 | M7 | M8 |
| **No load** | 0.48 | 0.224 | 0.58 | 0.17 | 0.40 | 0.59 | 0.65 | 0.51 |
| **0.5Kg** | 0.161 | 0.074 | 0.15 | 0.105 | 0.21 | 0.35 | 0.13 | 0.13 |
| **1.0Kg** | 0.092 | 0.053 | 0.091 | 0.045 | 0.113 | 0.135 | −0.022 | 0.0021 |
| **1.5Kg** | 0.082 | 0.035 | 0.054 | 0.042 | 0.096 | 0.0072 | | 0.002 |
| **Standard Deviation** | | | | | | | | |
| | M1 | M2 | M3 | M4 | M5 | M6 | M7 | M8 |
| **No load** | 0.01 | 0.011 | 0.012 | 0.011 | 0.014 | 0.01 | 0.013 | 0.011 |
| **0.5Kg** | 0.05 | 0.005 | 0.01 | 0.10 | 0.01 | 0.01 | 0.01 | 0.01 |
| **1.0Kg** | 0.006 | 0.021 | 0.019 | 0.026 | 0.004 | 0.107 | 0.005 | 0.01 |
| **1.5Kg** | 0.005 | 0.0309 | 0.005 | 0.014 | 0.007 | 0.002 | | 0.001 |

and 1.5Kg constant loads. As a general trend, the contraction ratio and speed reduced as the load increased, with the no load conditions having the highest contraction ratio overall. Isometric contraction occurs when the maximal load that can be held is reached, therefore, the load is just heavy enough that the muscle can no longer shorten but can still be held. Isometric contraction is making tension equal to the load and the muscle is not getting shorter. In maximal muscle force (without shortening), one cannot produce more force but the load can still be held up. If more weight is added at this stage, the muscle will begin to lengthen because the load has become greater than the tension that can be formed. This is called lengthening contraction: the muscles are still contracting but they are getting longer. Lengthening contraction was experienced by M7 muscle under 1.0Kg load (Table 6.3).

For the M1 muscle, the contraction ratio under 1.0Kg and 1.5Kg load is approximately the same but with a lower contraction speed of $0.017s^{-1}$ under 1.5Kg load as shown in Figure 6.17a.

The M2 muscle has its wedge angle changed to 67.5° as opposed to the M1 muscle with a 60° wedge. Contraction ratio is between 0.034 - 0.225 as shown in Figure 6.17b. As observed from the figure, contraction is in a less straight path especially for 1.0Kg and 1.5Kg loads. Isotonic contraction values are typically half of those of M1 muscles. The wedge angle is therefore a critical parameter to consider in designing SRM muscles because a slight change in wedge angle will have accumulative result on its performance.

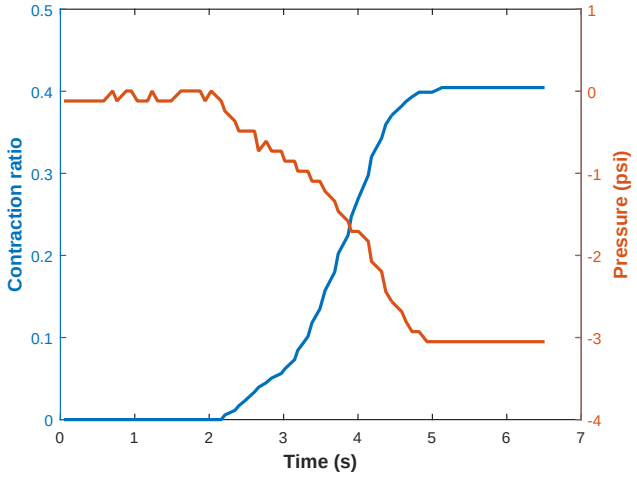


Figure 6.16: Air pressure and contraction of the M5 muscle. Vacuum pressure is regulated to -3psi for all SRM muscle actuators

Table 6.4: Soft muscle actuator maximum contraction velocity expressed as contraction ratio/time ($s^{-1}$) using the 6V DC vacuum pump.

| | M1 | M2 | M3 | M4 | M5 | M6 | M7 | M8 |
|---|---|---|---|---|---|---|---|---|
| **No load** | 0.11 | 0.063 | 0.126 | 0.178 | 0.146 | 0.118 | 0.203 | 0.217 |
| **0.5Kg** | 0.046 | 0.027 | 0.039 | 0.095 | 0.105 | 0.073 | 0.031 | 0.058 |
| **1.0Kg** | 0.028 | 0.016 | 0.015 | 0.045 | 0.050 | 0.027 | 0.005 | 0.002 |
| **1.5Kg** | 0.017 | 0.009 | 0.010 | 0.033 | 0.033 | 0.003 | −− | 0.001 |

The M3 muscle has its wedge angle parameter set as 75° with other parameters being the same. Similar to the observation of M2 muscle, the defining angle is an important parameter for SRM muscles. In this given angle, the ratio of contraction was 40% higher for the no load case compared with M1 (Figure 6.17c). However, for the other cases, the ratio was typically the same as M1. Changing the wedge angle has the direct effect of varying the breadth of the muscle, thereby resulting in more volume of the muscle. This is true for this M3 case. Though having a higher contraction under no load, this may not be a useful muscle for higher isotonic contraction. So careful consideration of the angle is essential for optimal performance.

The M4 muscle has the height of its air channel halved compared with the M1 muscle, while other parameters are the same. It generally has a lesser isotonic contraction ranging from 0.04 - 0.16 (Figure 6.17d) compared with M1 muscle. Therefore, the height of muscle channel is an important parameter to consider in the design of SRM

muscles; the length of wedge, $l_1$ should be greater or equal to the height of air channel, $h_c$ for better contraction values.

M5 SRM muscle has its number of air channels reduced to 7. Generally, its contraction ratio is about the same as with the M1 muscle (Figure 6.17e). This shows that the number of air channels will be the most suitable parameter to vary in order to produce same contraction values for an application that requires a change in length. This outcome is arrived at because varying the number of air channels will consequently result in change of the total length of the muscle while not significantly affecting the contraction ratio and speed.

The M6 muscle has twice the height of $h_c$ compared with M1 muscle. While it exhibits better contraction values under no load to 1.0Kg load cases compared with M1 (Figure 6.17f), it can be clearly observed that the contraction do not follow a linear path compared with M1. This becomes prominent with the 0.5Kg and 1.0Kg cases where the muscle contraction follows a curved path: it contracts a bit, reaches a peak where it stays for some time before contracting further. As a result of this observation, it can be deducted that while air channel height should be greater than the length of the wedge created by the angle of the muscle, it should be within a set allowable range in order to experience a more linear contraction path.

The M7 muscle is geometrically twice the length of M1 muscle. Its contraction ratio under the same vacuum pressure of -3psi is 50% higher than the M1 muscle and its speed is twice higher. This proves that just like skeletal muscles, summation of contractions in each air channel of the SRM muscle results in maximal force. Interestingly, M7 presents almost the same contraction ratio with M1 under 0.5Kg load. At 1.0Kg load, it can be observed from Figure 6.17g that this muscle begins to lengthen rather than shorten with a control pressure still set -3psi. Therefore, it can be observed that with a longer muscle, though contraction is higher under little loading conditions, performance drops drastically under load conditions as it begins to exhibit lengthening contraction. The M7 muscle is supposed to show the same contraction as the M1 muscle because it is twice the length of the M1 muscle, variance in result may be due to changes in the actuator because two actuators of the same mould and geometry do not guarantee the same performance due to hand fabrication.

The M8 muscle is not composed of wedge units but rectangular units with 4 air channels (Figure 4.20). The design of this muscle is made in order to compare wedged muscles with rectangular ones. While the M8 muscle exhibited the highest contraction speed

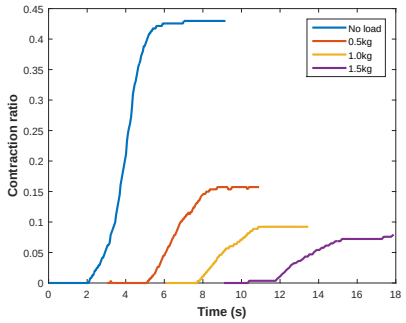


(a) M1

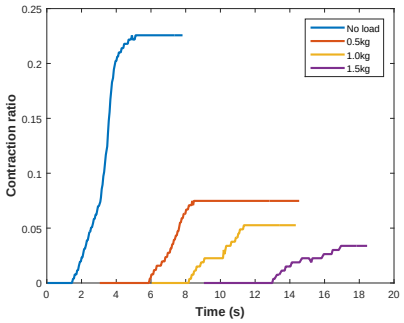


(b) M2

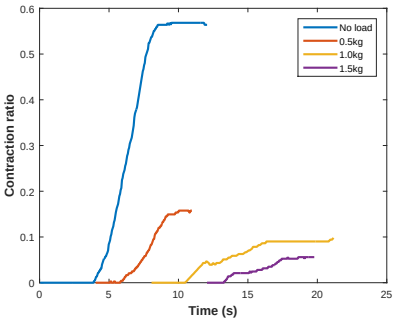


(c) M3

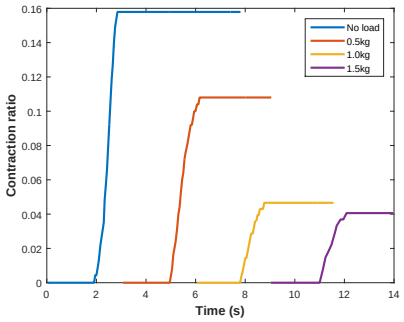


(d) M4

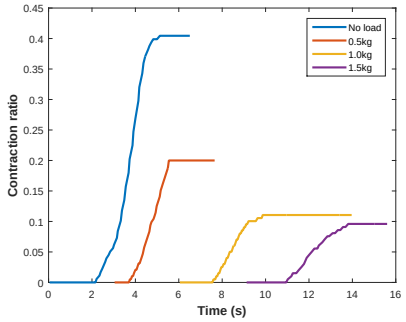


(e) M5

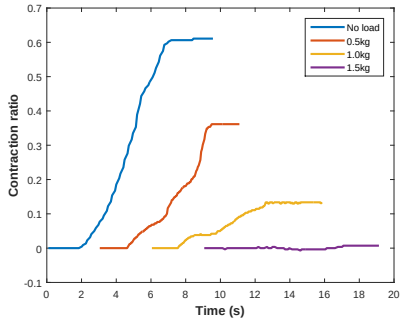


(f) M6

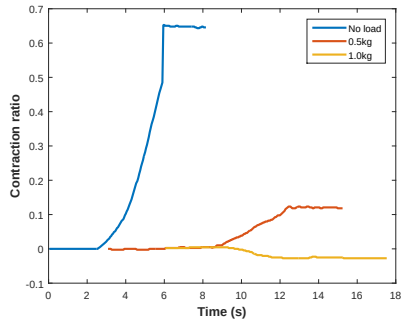


(g) M7

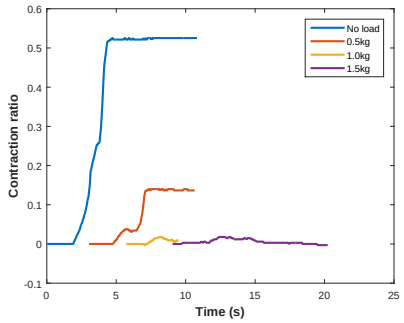


(h) M8

Figure 6.17: Contraction ratio and speed of soft muscles M1-M8 over time. (6.17a-6.17h).

(Table 6.4), the contraction of this muscle do not follow a straight path as per M1 - M7 muscles. This muscle, while contracting, twists its shape. This is largely due to the absence of a wedge, so it becomes unsuitable for applications requiring a straight contraction path. To implement 90° muscles that contract along a straight path, a more complicated geometry involving the work on vacuum operated linear muscle actuator [58] would be needed.

Also, the graphs of M8 contraction values (Figure 6.17h) show that with 0.5Kg load, muscle contraction graph is not linear because the muscle first contracts, then lengthens under the weight of the load before finally contracting further again, this may be due to the absence of a wedge coupled with large size of air channels. Another interesting observation is that it experiences a much larger amount of oscillations especially at larger loads compared with M1-M7 muscles. Additionally, the generation of bending motion will be impossible with M8 muscles.

## 6.6 Further Tests

Characterisation to show how properties of pressure source will affect readings from the pressure source, permeability of rubber actuators to air, repeatability in obtaining pressure readings from silicone rubber actuators and differences between plastic and rubber actuators are described in the following section.

### 6.6.1 Pressure source

Factors such as rating of the pump in terms of maximum pressure, flow rate and power rating will affect the time duration of the actuator to attain a desired position - a high power, high flow rate source will take a shorter time to reach a desired position. Figure 6.18 shows how a pump having the parameters specified in Table 6.5 responded to changes in pressure as recorded from the analogue pressure sensor while inflating. As observed, when pressure source is OFF, pressure sensor reading was stable, but experienced large fluctuations and hence unreliable sensor readings when pressure source is left ON. Pressure readings from 6VDC air pump is more stable when pressure source is ON compared with the 12VDC pump; fluctuations was within ±0.2 psi for a 6VDC air pump having flow rate of 2 liters per minute while fluctuations was within ±0.75psi for 12VDC air pump having a flow rate of 13 liters per minute. The 6VDC air pump

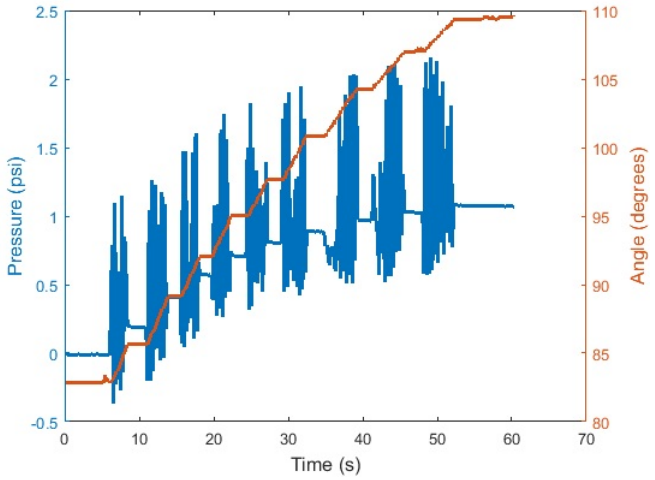


Figure 6.18: Angle and air pressure as a function of time using a 12VDC, high flow rate pump.

described in the introductory section was therefore used to collect characterisation data for all the soft actuators.

Table 6.5: Specification of 12V DC Air Pump.

| **Property** | **Specification** |
|---|---|
| Rated voltage | DC 12.0V |
| Rated current | <2000 mA |
| Charge time | <5s (rise from 0 – 5.8psi in 500cc capacity) |
| Tightness | < 0.1psi per minute |
| Noise | <60dB |
| Maximum pressure | >14.5psi |
| Air flow rate | 10.0 – 15 lpm |
| Pipe diameter | ⊘ 7.0mm |
| Model number | AJK-B12A2703 |
| External size | 60x113mm |

### 6.6.2 Repeatability Tests

Repeatability test was performed in order to determine how well rubber actuators produce the same result when a reading is collected multiple times. Figure 6.19 show graphs for braided and non-braided triangular actuators when readings were collected

multiple times. The fluctuations are seen in pressure readings due to the elastic nature of the silicone rubber: the walls are elastic and damping (dissipation of energy) occurs during inflation, when pressure source is turned off, fluctuations cease as shown. Fluctuations are also due to the flow rate of the pump, given the elastic body, the soft robot responds to the flow rate and speed of the pump, therefore, a high power pump with higher flow rate will experience larger fluctuations. Repeated experiments at the same conditions resulted in slight differences in readings as shown. It should also be noted that during the course of testing the actuators, they sometimes begin to leak so there is need to manufacture another one which will not be exactly the same due to hand moulding without the use of specialised equipments.

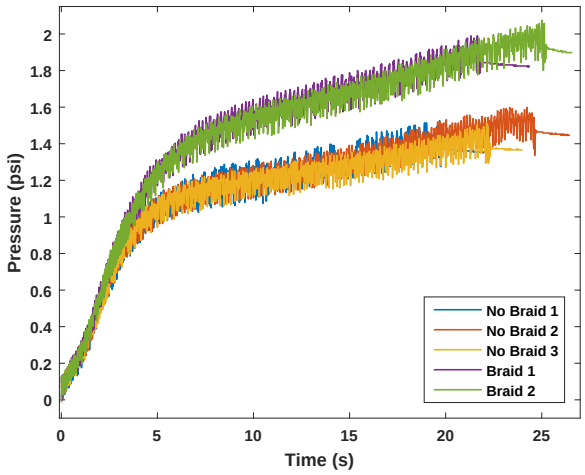


Figure 6.19: Graph to show repeatability in air pressure readings from silicone rubber actuators. Braid 1 and 2 represents the modules in which were reinforced with braided mesh. No Braid 1, 2 and 3 represents plain modules. The readings were captured with the 6VDC pump. Repeatability experiments were done for 1 sample repeated multiple times as illustrated.

A moving average carried out on the data in Figure 6.19 by averaging 50 samples to smoothen out fluctuations and to clearly observe each different measurement (Figure 6.20). The no braid and braid measurements were carried out under the same conditions (same pressure source and data acquisition). The two sets of soft actuators used are one with which a mesh network is embedded (Figure 4.11) and the other which is plain (Figure 4.6). From this graph, the inflation pressure is seen to be in two stages – a first stage at which there is a rapid increase in pressure which peaks at 1 psi (no braid) in 6.5s and 1.5 psi (braid) in 9s. After this stage, the pressure continues to

increase linearly albeit slowly. At this stage, it is observed that differences in readings for repeated experiment becomes noticeable and pronounced, a peak difference of 0.06 psi was measured. At the second phase, pressure attains 1.4 psi (no braid) in 24s with an increase of 0.4 psi in 18s. The pressure reaches about 2 psi in 24s (braid), meaning a gain of 0.5 psi in 15s. The drop in speed of air pressure increase at the second stage may be as a result of transition in sliding of rubber chains to the stretching of C-C bonds (See chapter 3).

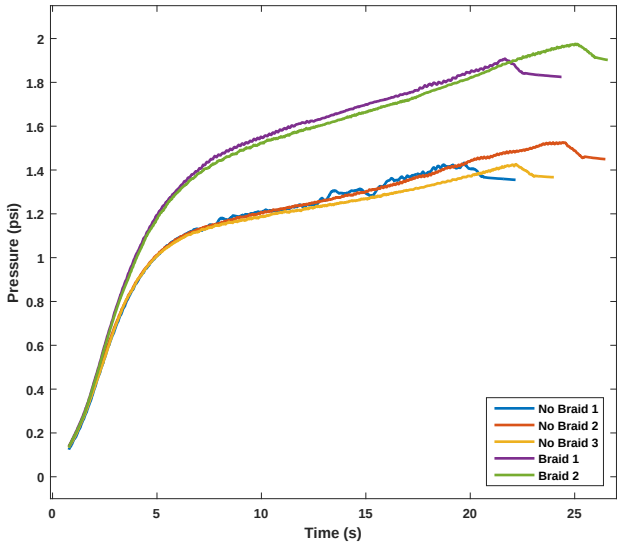


Figure 6.20: Moving average done over 50 samples of the graph in Figure 6.19.

It was observed that repeatability experiments conducted for soft actuators do not produce the same results due to a number of factors such as change in material properties as inflation–deflation cycles increases. It was also observed that low air pressure reading were measured because the soft elastic body increases in area when inflated which leads to a drop in pressure. Operating pressure for soft actuators are low because a comparably lower amount of force is induced owing to the highly elastic membrane. Therefore, a soft, highly extensible actuator having the same area with a rigid container will produce a relatively lower pressure reading compared with the rigid container.

Repeatability experiment of air pressure readings for plastic bag actuators was also carried out as shown in Figure 6.21. From the graph, there is a noticeable difference in the air pressure reading at the stage at which the pressure began to increase.

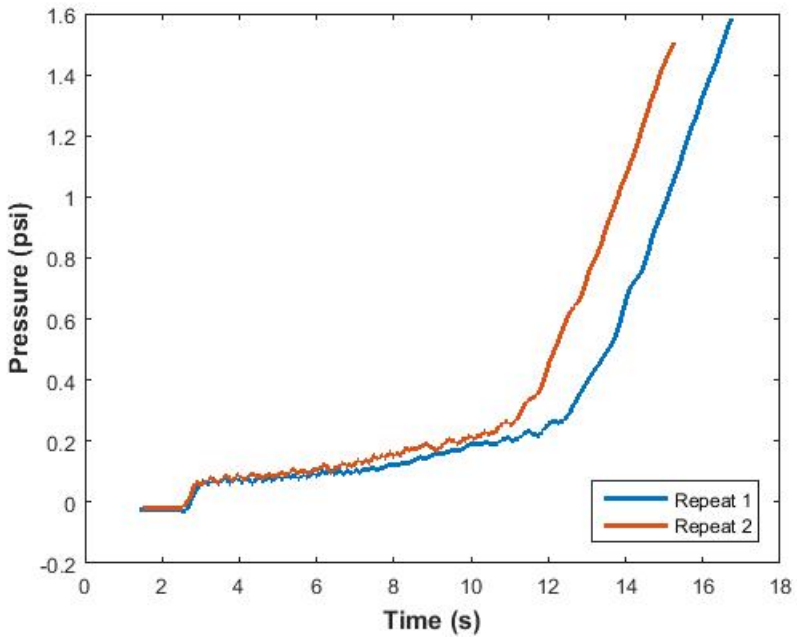


Figure 6.21: Graph to show repeatability in air pressure readings of plastic bag actuators for 1 sample.

### 6.6.3 Difference in plastic and rubber actuators

From the results presented thus far, it is observed that pressure-angle relationship for plastic bag actuators are non linear and so should be controlled with pressure-torque relationship while rubber actuators can be controlled by pressure–angle or pressure-torque relationship. It was found out that for plastic bag actuators, when the pressure source is turned off, though the system is air tight, a pressure reading of 0 is recorded. This is unlike silicone rubber actuators that show a reading that indicates the pressure of air inside the actuator. Due to this, data regarding permeability of air to plastic actuators could not be gathered. Additionally, a pressure reading of 0 was recorded because the experiment was conducted under no load conditions. Under load conditions, plastic bag actuators are suppose to give an air pressure reading that is indicative of its angle.

However, observations are seen in the pressure and angle when the pressure source is turned off for both plastic bag and silicone rubber actuator. From Figure 6.22, initially, the actuator was at an angle of 120° though pressure reads 0 because supply pressure is off even though the system is closed; as the supply pressure is turned back on at 8.5s, air pressure increased to 2.1psi and the angle increased after which it drops; at

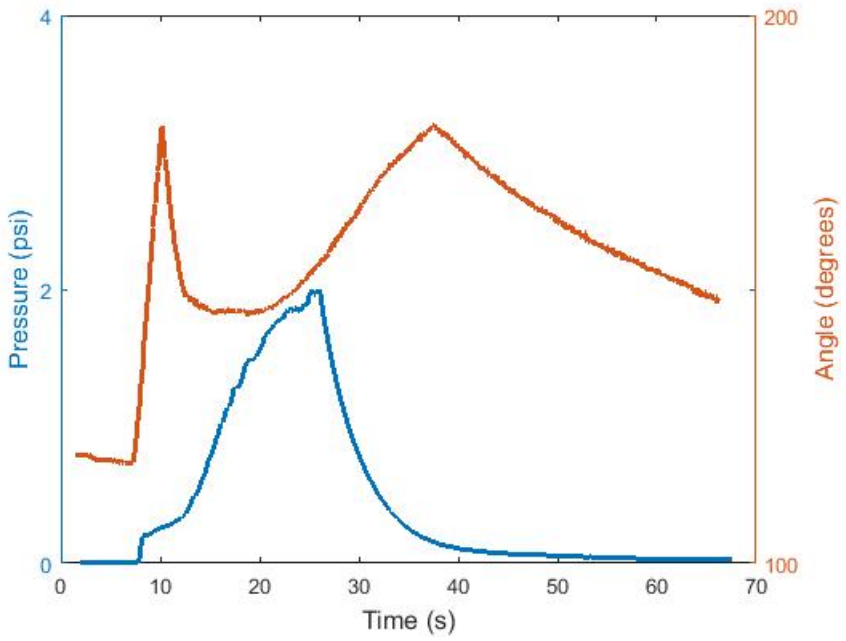


Figure 6.22: Angle and air pressure in an unloaded plastic bag actuator as a function of time.

the last stage, supply pressure is turned off again and the pressure drops to 0psi again but angle drops to 150°, not 0°. This graph further indicates the inability of plastic bag actuators to return to their original state when pressure source is removed unlike rubber actuators - an antagonist setup in which an antagonist pair pushes the bag to a given position would be highly necessitated in order for plastic actuators to overcome this difficulty.

From Figure 6.23, it can be observed that a silicone rubber actuator would return to its natural position as air is expelled from the system. The first stage is indicated by a flat line in pressure reading to show the stage at which pressure source is off but the system is closed (angle and pressure maintain the same value at this stage), later stages show when the system is open so that air leaves the soft actuator through the tubing, pressure gradually reduced to 0psi with corresponding decrease in angle to its natural position, albeit, non linearly.

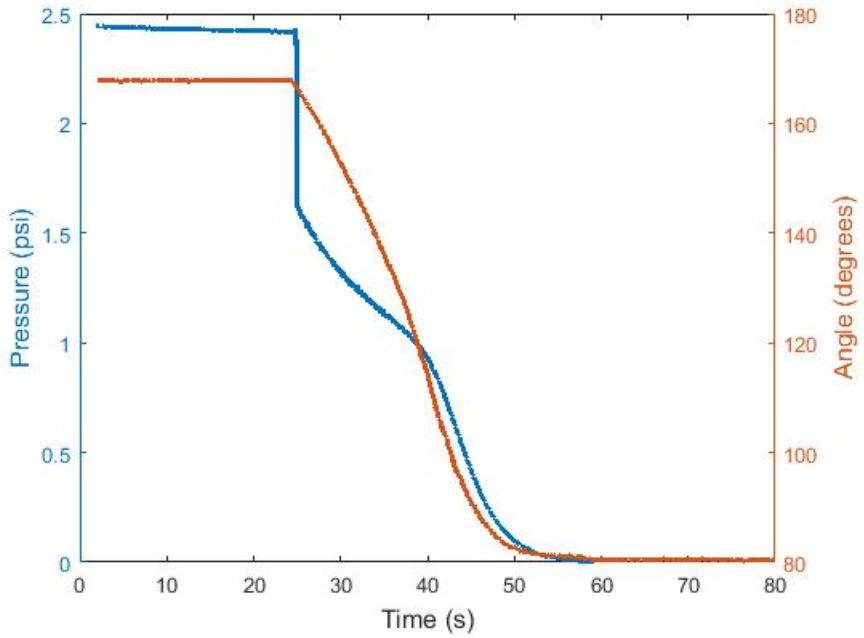


Figure 6.23: Angle and air pressure in silicone rubber actuator as a function of time as the system is left open for air to be exhausted from the actuator

## 6.7 Discussion

From the graphs of all the silicone rubber actuators, it was observed that the pressure rating is lower compared to what would be obtained when filling a rigid wall container with air. This is because as a stretchable material is being inflated, the structure is undergoing a volume expansion as a result of deformation of its structure. This volume expansion will also be reflected by an increase in surface area. As a result of this, the pressure reading will be reduced because of the relationship: $P = \frac{F}{A}$ where P = Pressure; F = Force and A = Area. Since the area is increasing, while the Force remains the same, pressure consequently has to be low. This observation is also reflected in the actuation time of the presented soft actuators to be very slow.

Conversely, negative air pressure results indicate a high operating vacuum pressure. This is due to the buckling phenomenon of rubbers when vacuum operated resulting from volume reduction which consequently increases the operating vacuum pressure.

The air pressure-volume model of Gent [163] served as a means to identify the bulging phenomenon associated with thin walled rubber tubes under inflation pressure. Experiments were conducted to validate the model by making plots of angle as a function of

pressure as shown in Figure 6.7. From observation of the graphs, the meshed triangular modules operated at a higher operating pressure compared with the other soft modules. The introduction of mesh had the effect of improving the torque output. In general, there were differences with Gent model compared to experimental results. This may be due to different shape of the actuator: the soft actuators have a triangular shape while the model assumes a spherical rubber. Also, the properties of silicone rubber such as strength and durability will change depending on the number of cycles of inflation, previous stresses the rubber has been subjected to and differences in manufacturing procedure.

The corrugated triangular actuator experienced low torque because soft silicone rubber was only used in its design, moulding was carried out by casting all its internal layers with silicone having the same material characteristics. While for the other actuators, the main structure was casted with high stiffness silicone while the low stiffness but highly extensible rubber was used for other enclosing faces of the triangle-shaped structure. Based on the presented results, interpolation data can be obtained using these characteristic graphs provided - parameters such as angle, torque or bending distance can then be inferred given a set pressure.

Though embedded mesh designs showed improved torque and pressure endurance, the introduction of embedded reinforcement to rubber is also a mode whereby the actuator would fail more easily and begin to experience leakage. This is because joining materials together with rubber, especially one that possesses significant difference in tensile stress constitute a point of weakness. Since the braided and corrugated designs had key advantages (mesh actuator had high torque while corrugated actuator had a wider range of motion) participant experiments were carried out with mesh and corrugated designs which will be presented in Chapter 8.

Plastic bag actuators have low tensile strength but high toughness, they also have a higher stiffness compared to silicone rubber which is observed by the high torque they generate. Despite some disadvantages of plastic bags actuators compared to rubber actuators as previously mentioned, they are light weight and possess high torque - these strengths will be exploited to actuate an exoskeleton that is originally passive (Chapter 9).

Bending robots were not as thoroughly analyzed as the triangular and muscle actuators because a significant portion of research work has focused on bending soft robots. The novelty of this PhD work comes in the design and characterisation of triangular and

muscle actuators. Bending soft robots have extensively been studied and also undergone studies to show its use to rehabilitate the fingers for gripping motion.

Novel artificial muscles made completely of soft silicone rubber that has no rigid parts which mimics the function and mechanism of the human muscle have also been characterized by varying key parameters such as angle, length and height of air channel in order to study optimum design variables that are responsible for its functionality and performance. From the results, it is shown that these fabricated muscles exhibit isotonic contraction and maximal muscle force (without shortening) is obtainable. Typically, maximal velocity and ratio of shortening occurs with zero load. A maximum contraction ratio of 67% and maximum contraction speed of $0.217s^{-1}$ was achieved. To mimic muscles in the human body, the designed artificial muscles are composed of a number of wedge-like units in series acting as the sarcomeres. The number of wedge units increases the contraction force. SRM muscles can be designed such that they can be arranged in parallel to increase the force generating capability just as how the amount of myofibrils in parallel determine the force capability of a skeletal muscle fiber.

## 6.8 Chapter Conclusion

This chapter focused on the characterisation of silicone rubber and plastic bag actuators in terms of torque output, air pressure rating and range of motion. In the next chapter, there will be a focus on the hardware and software controller approach adopted to control soft-bodied actuators to a desired pressure and position.

# Chapter 7

# Embedded Control Approach

A key challenge in soft robotics is controlling the large deformation experienced as a result of high compliance nature of soft robots. In this chapter, a study of hardware control component setup that drives the actuation of pneumatic soft actuators is first presented, then adopt a control strategy in software for regulating the amount of internal positive and negative air pressure inside the soft robot. Since the air pressure has a direct effect on the amount of deformation, the position of the robot is controlled

An embedded approach for actuating pneumatic soft robots is presented, with details of the setup and performance of the complete system was also demonstrated by building an embedded hardware and software control strategy to control internal air pressure (both positive and negative). This can be integrated into any specified soft robotic actuator requiring pneumatic actuation such as bending, triangular and muscle actuators. Pressure control was implemented with a piecewise linear controller, which is described with its performance shown. The hardware and software system presented in this chapter was used to actuate and control the bending, triangular and muscle actuators that was developed in Chapter 4. Thereafter, a two-staged control was implemented to move a soft robot to a desired position based on vision and pressure information.

## 7.1 Hardware Actuation System

The purpose of the hardware system is the regulation of compressed air from a pressure source such that the output pressure is directed to actuate a given soft robot. The use of electro-pneumatic regulator, air compressor or mechanical systems such as cylinders and piston arrangement for this purpose would lead to a bulky system, therefore, it

would be advantageous to make use of compact and portable hardware components. The following subsections describes the hardware implementation to actuate pneumatic soft robots.

### 7.1.1 Electro-pneumatics

Pneumatic circuits can be controlled by electric circuits, the interface between these two circuits may be a solenoid valve. Solenoid valves perform the same function as normal pneumatic valves but they are operated electrically. Inside the solenoid valve, there is a coil of wire through which an electric current is passed. It produces a magnetic field which attracts an iron armature, the movement of the armature operates the valve.

As illustrated in Figure 7.1, when the solenoid valve is on, an electric current will flow through the coil, the iron armature is attracted by magnetism. The solenoid has control of the valve, port 1 is connected to port 2 and air will flow to inflate the actuator. When the solenoid valve is off, the coil is de-energized and the spring has control of the valve. Port 2 is connected to port 3 and air flows out of the soft robot. The OFF and ON description is given as:

**Solenoid Operation Off:** When electric current is not flowing, a spring pushes the iron armature out of the coil. A seal connected to the armature blocks port 1, air can flow between ports 2 and 3 .

**Solenoid Operation On:** When current flows, the iron armature is attracted into the coil by a magnetic field. The spring pressure is overcome and the seal moves to block port 3, air can flow between port 1 and 2.

The solenoid valves used in this work have the specifications in Table 7.1.

### 7.1.2 Electro-pneumatic hardware setup

The main aim of this system is to regulate the pressure of compressed air from a pressure source such that a desired output pressure is directed to actuate the robot. The use of an electro-pneumatic regulator and air compressor for this purpose would be expensive. Furthermore, the use of mechanical systems such as cylinders, piston pump would be cumbersome and make the system bulky. For driving soft robot with a compact arrangement, solenoid valves which act as control switches for the flow of air

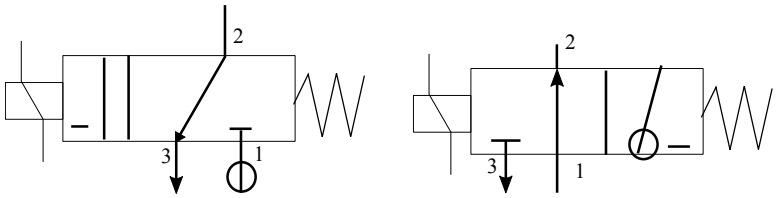


Figure 7.1: Solenoid valves ON and OFF position; the iron armature is attracted into the coil by a magnetic field. The spring pressure is overcome and the seal moves to block port 3, air can flow between port 1 and 2 for ON operation; a spring pushes the iron armature out of the coil. A seal connected to the armature blocks port 1, air can flow between ports 2 and 3 for OFF operation.

Table 7.1: Specifications of 2-way, 1-position solenoid valves

| **Property** | **Specification** |
|---|---|
| Rated voltage | DC 6.0V |
| Rated current | 375 ±10% mA |
| Resistance | 16 ± 10% Ω |
| Power | 2.25 ±10% W |
| Working pressure | < 6.5psi |
| Leakage | 0.06psi |
| Exhaust speed | < 3s (300cc tank, from 5.4psi to 0.3psi) |
| Pipe | ⊘ 3.0mm |
| Model number | AJK-F06A0504 |
| Dimension | 20x15x13mm |

into and out of the actuators are used. Two valves are required for one actuator: the first for inflation (inlet solenoid valve) while the other is for deflation (exhaust solenoid valve). This is a low pressure controller system that operates between about 0 to ±5psi.

The movement and deformation experienced by soft-bodied actuators is reliant on effective control of airflow into and out of the actuator. This is controlled by on/off solenoid valves that incorporate 2-way/1-position. The electro-pneumatic system is composed of an embedded electronic control on a Printed Circuit Board (PCB) and a compact structure to house the pneumatic system so that portability is ensured. 6V solenoid valve having a power rating of 2.25W, a maximum operating pressure of 350mmHg; exhaust speed of 4s and leakage of 3mmHg/minute was used. These solenoid valves are light-weight and compact so as to be suitably integrated. In the case of a high pressure application, high pressure valves would be needed - this would be achieved by either operating two solenoid valves in parallel as one logical valve or simply using valves with higher operating pressure.

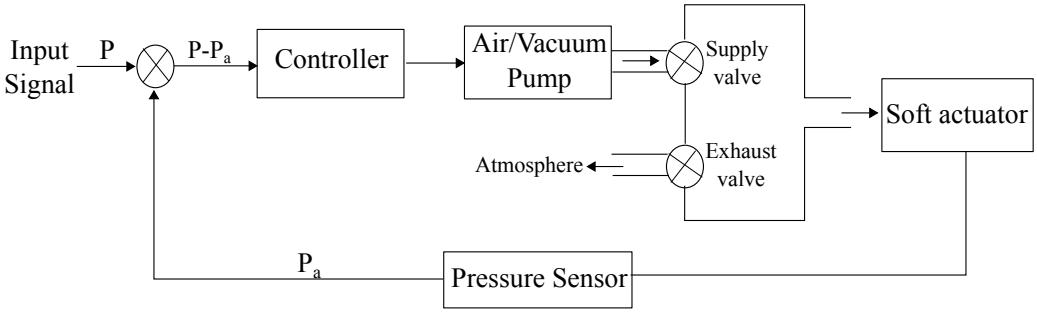


Figure 7.2: Block diagram of soft actuator pressure controller.

Figure 7.2 shows the block diagram of the electro-pneumatic setup to actuate soft robots: an input signal sets a desired pressure; the controller receives current air pressure in voltage units from the actuator by an ADC interface. When the input signal rises, compressed air from a pressure source passes through the inlet solenoid valve and changes to output pressure. The exhaust valve deflates the soft robot - this is essential to create a frequency at which a soft robot would inflate and deflate in order to create a specified rhythm of motion. The current pressure in the actuator is fed back via a pressure sensor, pressure corrections then occur to produce an output pressure that is equal to the set pressure. Pressure regulation is required to control motion of the soft robot and most importantly, prevent failure of silicone rubber due to over-inflation.

A Pulse Width Modulated (PWM) air pump controls output pressure inside the actu-

ator integrated with a pressure sensor. Pressure is controlled by varying the length of the duty cycle of the DC air pump, a duty cycle of 10ms was used. In order to write the duty cycle duration to control an air pump, a DAC is required. The output pressure into the soft actuator is also dependent on pressure difference, power supply ratings of valves and pump. For the inlet solenoid valve, pressure difference is given by a constant supply pressure and the actual pressure in the actuator. For the exhaust solenoid valve, pressure difference is between internal air pressure in the soft robot and atmospheric pressure.

### 7.1.3 Pressure Regulator Circuit

Figure 7.3 shows the arrangement of pump and valves for the actuation of soft robots in order to carry out inflation and deflation cycles. As shown, it consists of an air pump that acts as the pressure source; two solenoid valves (inlet and exhaust) and a pressure sensor to measure air pressure in the soft actuator.

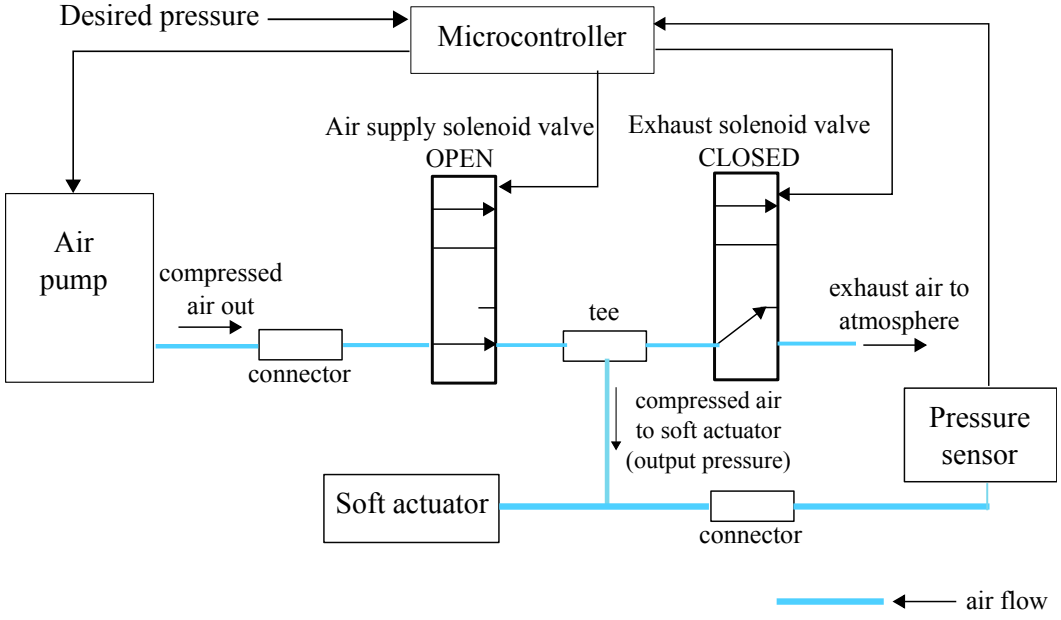


Figure 7.3: Circuit arrangement of soft robot pressure controller. Figure shows the arrangement of inlet and exhaust valves, pump, pressure sensor and soft robot.

Compressed air from the pump passes through the air supply solenoid valve and changes to output pressure when the air supply solenoid valve turns ON. In this way, air from the supply pump passes through the inlet valve and changes to output pressure. A PWM output is then produced on the output pin of the controller to increase or decrease the

speed of the pump in order to produce an output pressure equal to the desired pressure. The output pressure is fed back to the controller via the pressure sensor, this is to check if the desired pressure has become equal to the output pressure. Pressure corrections then occur to produce an output pressure that is equal to the set pressure.

More than one separate individual units of a soft actuator can be controlled using this system. This would be achieved by the addition of two valves for every separate air channel. This is a low pressure controller system that operates between 0 - ±5psi; since the pressure range of the pump as well as the solenoid valves are within this pressure range. Soft actuators based on Ecoflex 0030 silicone rubber operate within this pressure range and therefore this control system is suitable for the purpose. To achieve a high pressure system, high pressure pump and solenoid valves would be used.

### 7.1.4 Multichannel Arrangement

More than one separate individual units of a multichannel soft robot can be controlled using a multichannel arrangement. This is achieved by dividing the air coming from the pump and using two valves for each air channel; pressure and exhaust can be connected to one or more soft robot at a time. Using separate pressure control for each of the individual air channels illustrated in Figure 7.4 will tend to reduce failure of the soft robot through inflation and increase the obtainable range of motion. Each of the four air channels constituting wedge-shaped soft modules was controlled using this procedure. Figure 7.4b shows the hardware implementation comprising a multichannel arrangement for a four-channel soft robot. The complete circuit diagrams are found in the Appendix Section (Figure E.1 and E.2).

## 7.2 Piecewise linear pressure control system

Software controllers are usually based on bang-bang or PID control strategy. Figure 7.5 shows a Finite State Machine (FSM) based on a bang-bang controller to maintain air pressure inside a soft actuator. For example, to control internal air pressure between 0.7 psi to 0.9 psi, two pressure thresholds are used to prevent the pump from toggling on/off/on/off/on... too quickly. If the system were to be in the PUMP-off state (speed of air pump is reduced), then the system would remain in the PUMP-off state until the pressure drops below 0.7psi. If the system were to be in the PUMP-on state (air pump is inflating the robot at maximum duty cycle), then the system would remain

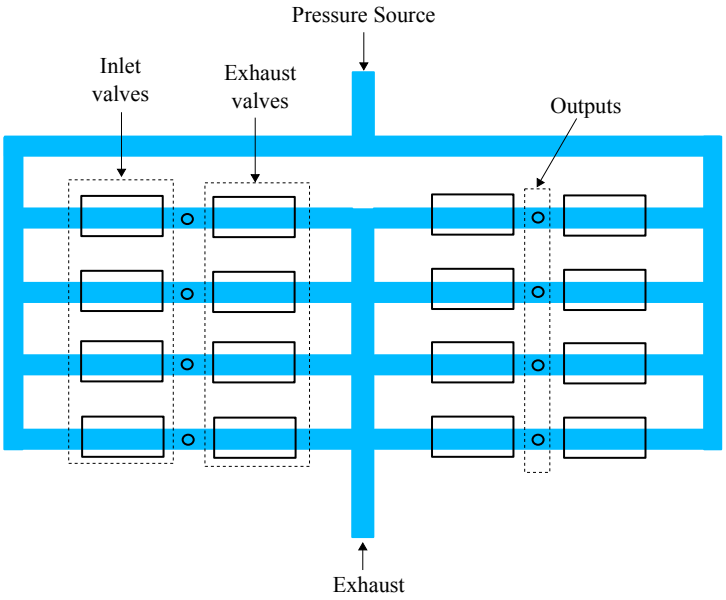


(a)

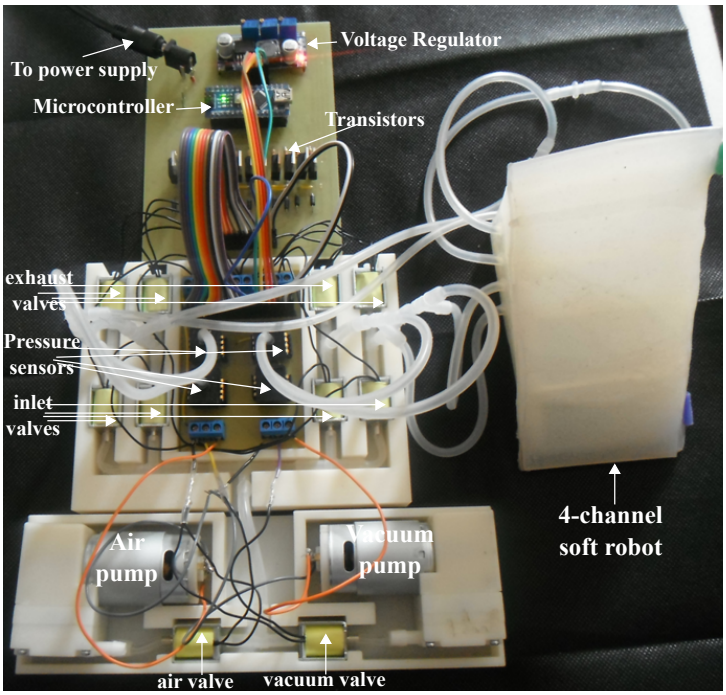


(b)

Figure 7.4: Hardware system for controlling soft robots with multi-channel network. (a) Arrangement showing network of valves using a single pressure source but feeding 8 outputs independently, Number of valves required is 2 × number of outputs. (b) Implementation of hardware control system for a 4-channel soft robot requiring 8 valves for independent control of air pressure inside each air channel. Positive and negative air sources are combined and then divided into four air channels to regulate air pressure inside individual channels.

in the PUMP-on state until the pressure rises above 0.9psi. Bang-bang controllers, though fast and easy to implement, suffer from large errors and inaccuracy. A PID control system having $P$, $PI$ or $PD$ variants are used as standards for controlling engineering systems. However, tuning the proportional, integral or derivative terms require a trial by error approach or can be determined from models built of the system. But pneumatic systems are highly non linear and more often that not, model control parameters developed are often not used in practical control. In this work, a software controller based on piecewise linear control for pressure was implemented.

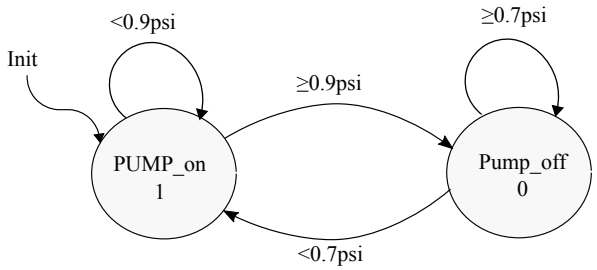


Figure 7.5: FSM to control pressure inside soft robot

Piecewise linear controller was chosen in this work to execute an embedded-based air pressure control system. Although PID controllers excel at being accurate and stable, they work well when a complete knowledge about the physical plant is known. Choosing the proper PID parameters requires expert knowledge about the plant. Piecewise linear controllers, on the other hand, are more robust and often used when complete knowledge about the plant is not known or can change dynamically which is the case of air pressure control system. Factors such as air leakage of the solenoid valves or leakage due to non-existence of perfectly air-tight system would cause the pressure control system to change dynamically. Program 2 shows the simplified algorithm for the piecewise linear control of air pressure [10].

The controller has two crisp inputs, $E$ and $D$. The error signal, $E$, is given by the difference in the desired and current pressure while $D$ is given by difference between the pressure at the current and previous time-step. The input membership sets are continuous piecewise-linear functions. Six input membership sets are produced from the crisp inputs, which are Slow, Fast, Ok, Down, Up and Constant. Slow, Fast and Ok input membership sets are obtained from $D$ while Down, Up and Constant input membership sets are obtained from $E$. Given these input membership sets. three output membership sets which are Increase, Same, Decrease are produced based on logic

**Algorithm 2** Pressure control piecewise linear algorithm

1: Define sampling frequency, $n$
2: Define change in output, $tn$
3: Given desired pressure, $P_d$
4: **for** every $n$ sample **do**
5: Read current pressure, $P$
6: Calculate crisp inputs, $E$ and $D$
7: $E = P_d - P$
8: $D = P(n) - P(n-1)$
9: Calculate input membership sets
10: Calculate output membership sets:
11: Increase, Same, Decrease
12: Calculate crisp output, $\delta N$
13: $\delta N = \frac{tn \times (Increase - Decrease)}{Decrease + Same + Increase}$
14: $N = N + \delta N$ ▷ $(0 \leq N \leq 255)$
15: Output $N$ to air/vacuum pump actuator
16: **end for**

functions. The six membership sets for the crisp inputs have the following meaning:

- Slow: True if the pressure is changing too slowly
- OK: True if the pressure is changing at the proper speed
- Fast: True if the pressure is changing too fast
- Up: True if the pressure is getting larger
- Constant: True if the pressure is remaining the same
- Down: True if the pressure is getting smaller

The three membership sets for the crisp output have the following meaning:

- Decrease: True if the pressure should be decreased
- Same: True if the pressure should remain the same
- Increase: True if the pressure should be increased

The membership sets for the output specifies the crisp output, $N$, as a function of the membership value. The output, $N$, of software controller is sent to the hardware controller which switches its output pins between 5V and 0V to create a PWM signal for

controlling the speed of the air pump. PWM works because the motor in the air and vacuum pumps have rotational inertia that filters out the fast switching. Therefore, the rotational inertia of the DC motor inside the pumps smooths out rapid pulses provided by PWM and the result is a slower axle rotation and consequently, regulating air pressure. For the case of solenoid valves, PWM will produce switching noise. This can be prevented by switching the valves either ON or OFF for inflation and deflation cycles while using PWM to control only the speed of the air/vacuum pump for air pressure control in the soft robot. PWM-mode is configured by output compare modules, as no operating system kernel is used, interrupt sub-routines worked very well to ensure correct timing of reading and writing of software commands.

To acquire voltage readings from the pressure sensor using the hardware control system, an accurate sampling rate was maintained for the purpose of reading data from the pressure sensor using 10-bit ADC conversion and outputting commands to the actuators. Since the time in between ADC samples must be equal and known in order for digital signal control to function properly, the ADC was configured to read samples at a periodic rate of 100Hz, piecewise linear software commands were likewise written to the DC pump actuator at a speed of 100Hz.

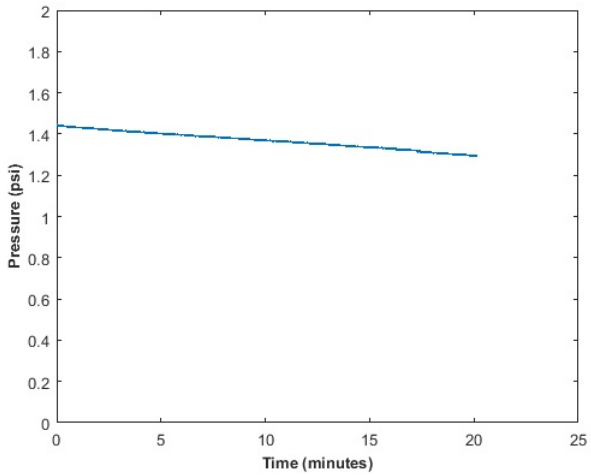


Figure 7.6: Air pressure in rubber actuator as a function of time when solenoid valve was in the holding (OFF) state and data collected for 20 minutes.

Before undertaking experiments involving control the performance of the solenoid valves in the holding (OFF) state was assessed. This was done by inflating a silicone rubber actuator to $\approx$ 1.4psi after which the solenoid valves was left in the holding state, air

pressure reading was then recorded for 20 minutes, the graph depicting the result is shown in Figure 7.6. It can be observed that a pressure drop of 0.12 psi is obtained after 20 minutes - this indicates the suitability of the valves so that they are well suited to carry out pressure control. This observation can be due to creep such that the elastic nature of the actuator produces material relaxation due to inflation pressure and consequently there has to be a drop in pressure. This result obtained can also be due to diffusion of air molecules that occurs through silicone rubber showing that it is not perfectly air tight even when the system is perfectly closed. Rubber actuators are not perfectly air-tight - air molecules slowly diffuse through microscopic pores of stretched rubber when filled with compressed air. This diffusion can be further explained by the spaghetti model of rubber as described in Chapter 3. This result can also be explained by material relaxation due to stretching of the rubber.

Figure 7.7a and 7.7b show graphs of the performance of the piecewise linear algorithm in regulating air pressure inside a rigid-bodied container between 0 - 5psi. From both graphs, it can be seen that the piecewise linear controller performed well in reaching and maintaining the desired pressure for varying amounts of time duration. On further observation, it was found out that any other controller with a simple threshold will perform the same way as the controller used here due to the relatively slow speed of the 6V air pump. An overshoot can be observed from Figure 7.7 because of the threshold set in the controller to be above the desired pressure.

Figure 7.8a and 7.8b show graphs representing the performance of the piecewise linear controller in regulating air pressure inside a soft robot between 0 - 1.5psi. It can be observed that it takes a longer time period for soft robots to attain a desired pressure compared to rigid wall container. Figure 7.8c is a zoomed in graph of Figure 7.8b which clearly shows that the piecewise linear controller is able to keep fluctuations within about $\pm$0.3psi from the desired positive pressure.

The embedded piecewise linear controller was also used to regulate negative air pressure inside silicone rubber actuator by replacing the air pump with a vacuum pump, negative air pressure was regulated between 0 to -5psi. From Figure 7.9, it can be observed that the controller was able to attain the desired negative pressure in 23.5s. Compared to regulating positive air pressure, a faster rate of attaining the desired negative pressure and lesser degree of fluctuations (within $\pm$ 0.05psi) is observed. The zoomed in graph (Figure 7.9b) clearly shows the path taken by the controller in reaching and maintaining the desired negative pressure.

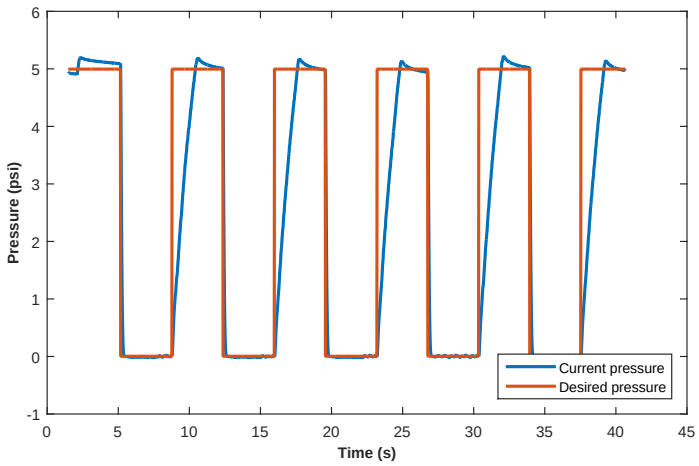


(a)

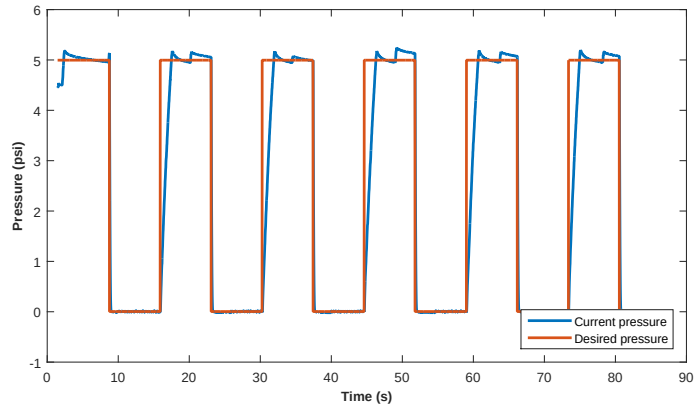


(b)

Figure 7.7: Air pressure as a function of time showing performance of the piecewise linear controller in regulating air pressure between 0 - 5psi for a rigid-bodied plastic container. (a) Time to maintain the desired pressure is 4s (b) Time to maintain the desired pressure is 8s.

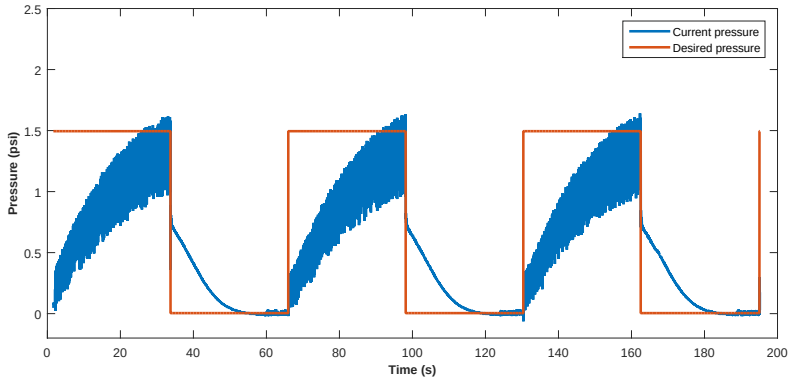


(a)

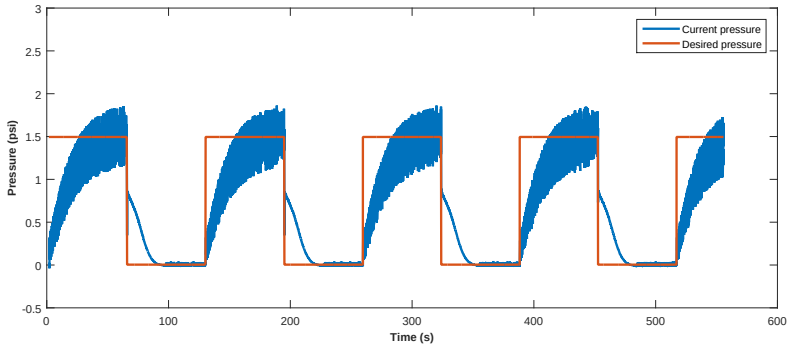


(b)

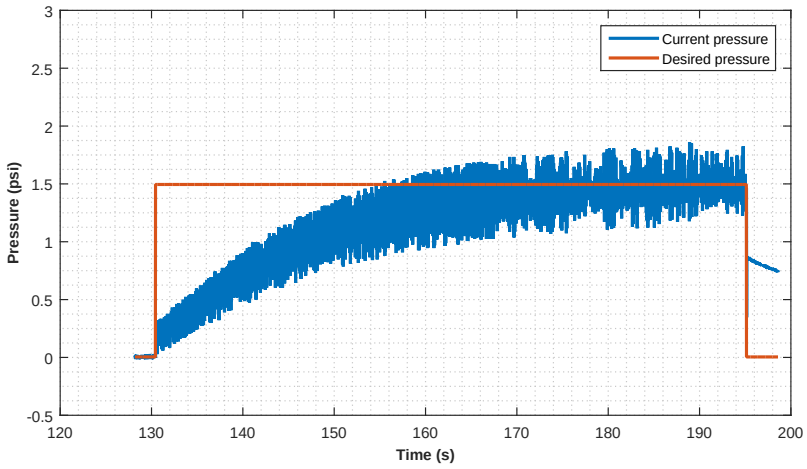


(c)

Figure 7.8: Air pressure as a function of time showing performance of the piecewise linear controller in regulating air pressure between 0 - 1.5psi for a soft-bodied robot. (a) Time to maintain the desired pressure is 30s. (b) Time to maintain the desired pressure is 65s. (c) Zoomed-in graph of Figure 7.8b from 120s to 200s.

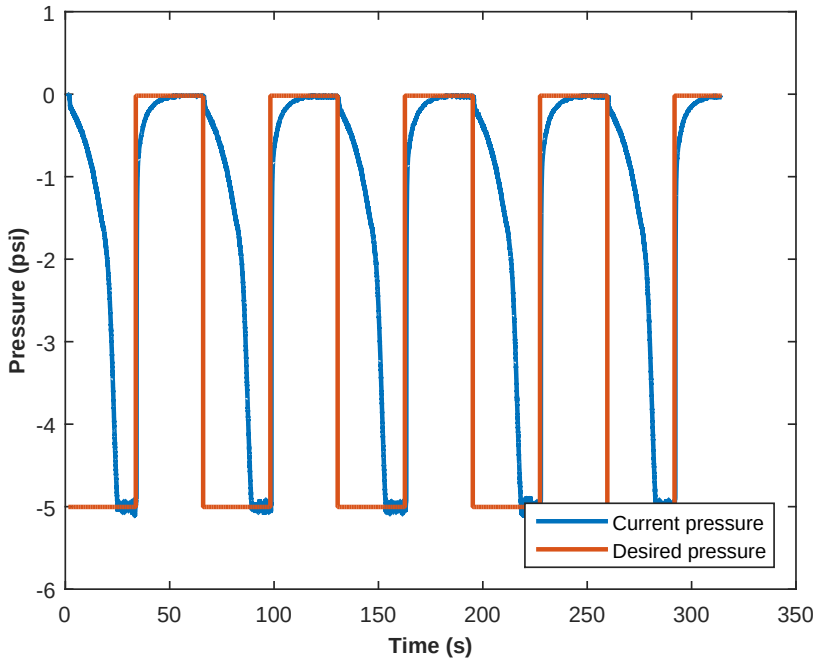


(a)

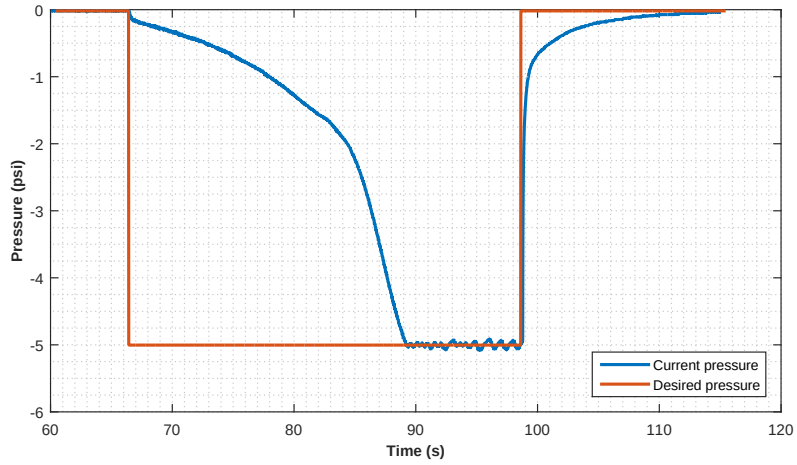


(b)

Figure 7.9: Air pressure as a function of time showing performance of the piecewise linear controller in regulating negative air pressure from 0 to -5psi for a soft-bodied robot. (a) Time to maintain the desired pressure is at a cycle rate of about 33s (b) Zoomed-in graph of Figure 7.9a from 60s to 120s.

Low pressure values were obtained because a soft elastic body increases in area when inflated which leads to a drop in pressure. Therefore, a soft, highly extensible actuator having the same area with a rigid container produces a relatively lower air pressure reading compared with the rigid container. Fig. 7.7a and 7.8a show graphs of a rigid container regulated from 0psi to 5.0psi and a soft robot inflated and regulated from 0psi to 1.5psi using piecewise linear controller respectively. This is because as a stretchable material is being inflated, the structure is undergoing a volume expansion as a result of deformation of its structure. This volume expansion will also be reflected by an increase in its surface area. As a result of this, the pressure reading will be reduced because of the relationship: $P = \frac{F}{A}$ where P = Pressure; F = Force and A = Area. Since the area is increasing, while the Force remains the same, pressure consequently has to be low. This observation is also reflected in the actuation time of soft actuators to be considerably slower given the hardware system. It was also observed that fluctuations in positive air pressure readings is obtained, this is due to the nature of the soft, elastic body being actuated as rigid wall containers do not show these fluctuations under the same piecewise linear controller. Conversely, negative air pressure results indicate a high operating vacuum pressure. This is due to the buckling phenomenon of rubbers when vacuum operated resulting from volume reduction which consequently increases the operating vacuum pressure.

## 7.3 Vision-Pressure Control

In this section, the controller setup to control the soft robot based on both visual information from a camera and pressure information is described. This implies that by specifying a desired position in visual space, the robot is then able to move to this desired position. The control system setup for SRM muscles is also described in this section.

The vision-pressure control system has four major parts (Figure 7.10): A camera, computer for visual processing, pressure regulation system and the wedge-shaped rubber actuator. The camera provides visual information, which is processed by an image processing software; pressure regulation system consisting of a pump (air and vacuum), by which pneumatic pressurization and depressurization can be obtained; inlet and exhaust solenoid valves; pressure sensor; and an electronic circuit.

A serial communication link is established to obtain the current angle measurement $q_0$

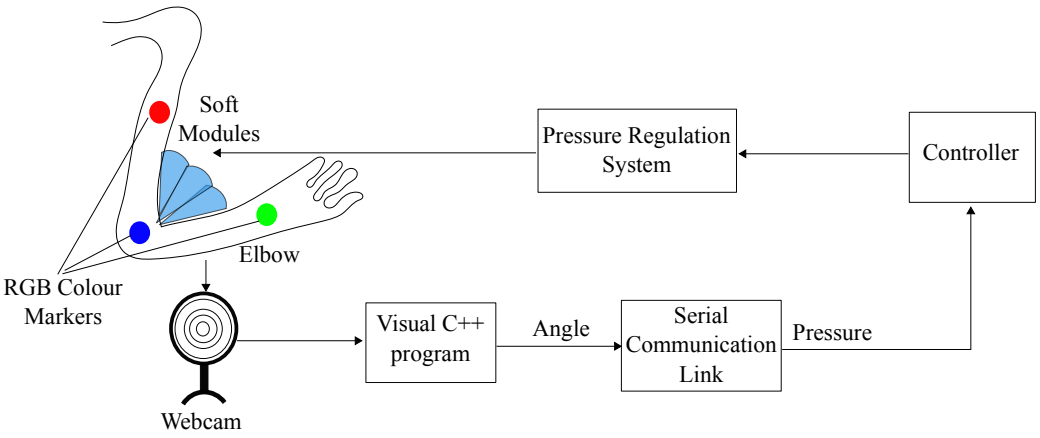


Figure 7.10: Schematic picture of vision-pressure control system. Wedge-shaped soft modules are attached to the elbow joint with red, blue and green colour markers positioned as shown, the Visual C++ program returns the angle of the elbow joint, the pressure sensor provides fedback by measuring the air pressure inside the modules.

from the visual processing program to the controller circuit which in turn would generate an appropriate PWM signal that would actuate the pump and valves to control the air pressure into the soft modules. This communication pathway was established through the USB interface of a PC as illustrated in Figure 7.10.

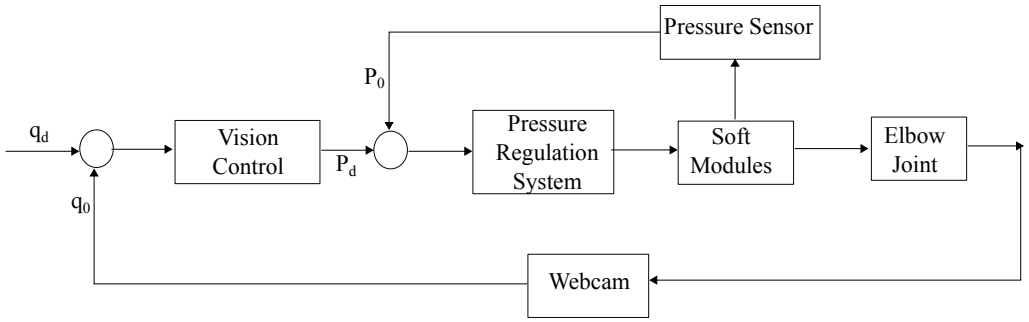


Figure 7.11: Block Diagram of Joint Control. The lower pressure control loop uses information from the pressure sensor to get the output pressure, $P_0$, while the higher visual control receives information of the current angle of the elbow, $q_0$, from the webcam.

A controller for visual feedback provided by the camera and control circuit are required to control the angle of the wedge-shaped robot. This visual-pressure control loop periodically receives discrepancies between the measured angle $q_0$ and the desired angle $q_d$ and uses a two-staged cascaded control approach to send a PWM signal to the pump and solenoid valves to resolve the difference. The difference between the measured and reference angle results in an error signal, which when passed to a high level vision con-

troller outputs a signal which is then used as setpoint that specifies the desired pressure to be obtained to move the robot to the desired position. Figure 7.11 shows the block diagram for the visual and pressure control. With this control strategy, an open loop control is possible by varying the amount of desired pressure, $P_d$, that is added to the output of the control loop. The pressure feedback signal is provided by the means of a pressure sensor to measure air pressure inside the soft robot. The output of this inner loop control corresponds to the duty cycle of the PWM signal that drives the pump. Figure 7.12 shows a graph in which a set angle of 120° is obtained.

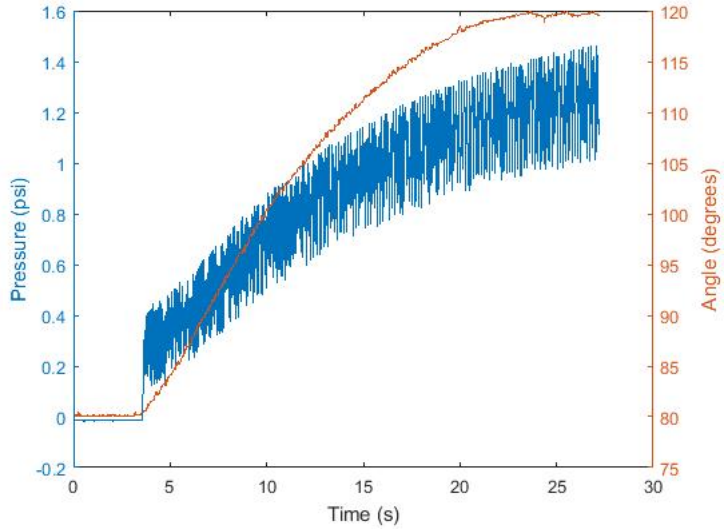


Figure 7.12: Angle and pressure as a function of time for vision-pressure control in which a set angle of 120° is obtained for actuator presented in Figure 4.11.

The control hardware setup for controlling SRM muscles is a modification of system just described to account for the vacuum pump. For a typical skeletal muscle, biological sensors are used to sense stretch and tension, the afferent motor neuron coiled around the muscle spindle senses stretch (muscle length and speed of stretch). It acts in reciprocal innervations causing contraction of stretched muscle and relaxation of antagonistic muscle. For the soft artificial muscle design, a computer vision system with the aid of a camera was setup as a sensor to measure velocity and contraction ratio. The afferent neuron associated with Golgi tendon organ senses tension generated by a human muscle. The Golgi tendon organ attaches muscle to the bones and are activated by contraction of the muscle. Measurement of tension was carried out by attaching predetermined weights at the end of the SRM muscles. The control system setup is

shown in Figure 7.13. The visual processing program measures the difference between the red and green colour markers in real time. The values measured using the visual processing system was verified with ground truth measurements.

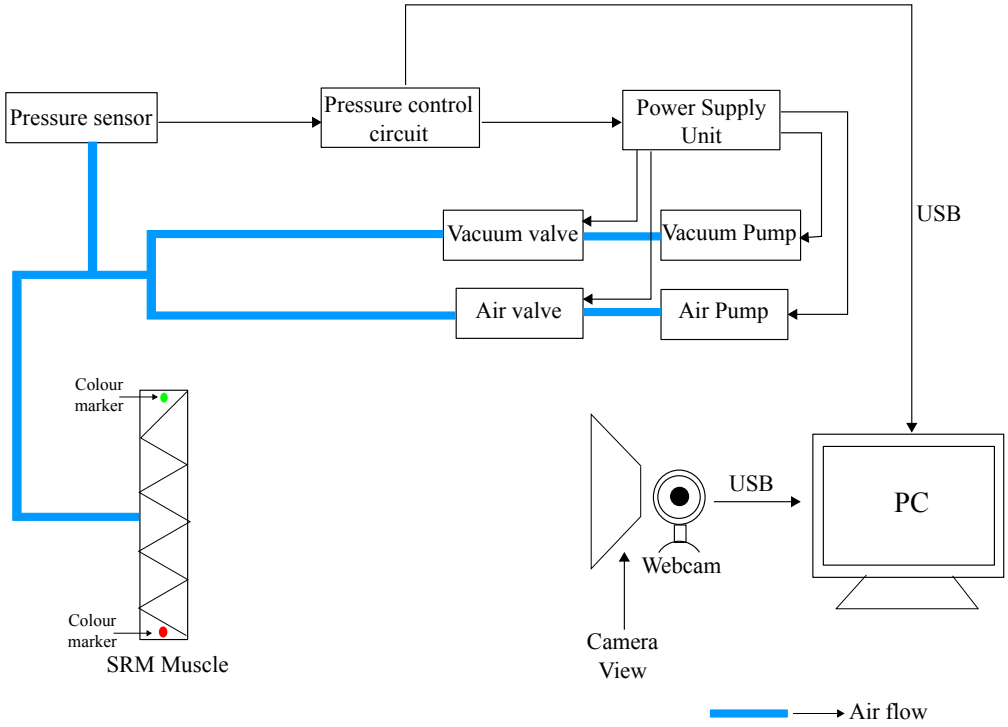


Figure 7.13: Control system setup for SRM muscles.

The soft artificial muscles are actuated by means of a vacuum pump, when the artificial muscle is unactuated, the structure is at standard atmospheric pressure. The actuation via a vacuum pump will expel air from the structure causing the muscle to contract. When air is introduced into the system through an air pump, the muscle goes back to its normal resting length.

## 7.4 Discussion

Controllers for pneumatic soft actuators need to involve pressurization and depressurization system as well as suitable control which has been presented using an electro-pneumatic setup. Though the use of fluidic drive piston-cylinder arrangement rather than solenoid valves would provide a more analog control of pressure by enabling precise analogue control of airflow into and out of the actuators, the results that have been presented in this work indicate the viability of the hardware components together with the

software control system in actuating and controlling positive and negative air pressure within silicone-based soft robots. This controller system can be used for a variety of pneumatic soft robots to achieve bending, rotary and contraction motions. Results also show the suitability and performance of the hardware and software system in actuating soft robots operating at low pressures, typically between -5 to +5psi. This pressure controller system can be modified to work with high pressure requirements such as an air compressor-air receiver arrangement which would be a high pressure system because the compressor and air tank are heavy duty accommodating more than 200psi.

In general, the more ambitious the requirements of control are, the more bulky the system will be and system compactness consequently reduces because the size of valves will affect compactness and portability requirements. This also applies to the time taken for the software control to run given the clock speed. The extent of compactness is also reliant on the degree of integration of control components such as sensors and valves. For a 2 or more actuator system such as robot requiring a multichannel pressure regulation, the number of transistors, pressure sensors and solenoid valves would increase accordingly. The compactness also depends on the tubing and cables needed for operation. Other pneumatic soft actuators such as McKibbean muscles can be controlled with this system, whereby each muscle will be actuated by 2 solenoid valves. This will also be required in cases requiring an antagonist setup or multi-finger actuators where each of the fingers requires a pair of solenoid valves for grasping tasks. For high pressure systems, the air source may be excluded from the control so as to reduce its size and weight. This would allow for the use of an air-tank containing compressed air as the pressure source. An air-tank arrangement may be superior in terms of speed and high pressure requirements but comes at the expense of being bulky and noisy. The solution employed in this work with the use of DC air and vacuum pumps allow for compact, light-weight, portable and a less noisy ($< 67dB$) pneumatic system.

It can be difficult to achieve high accuracy of pressure and visual measurements, which is due to the accuracy of the control and also due to some parameters of the solenoid valve such as leakage and exhaust speed as well as limited measurement accuracy through the use of visual information from a camera. Also, air leakage at the connecting point between the soft robot and the tubing; loose connection tubing between the pump, valves and pressure sensor can limit the accuracy of this system and should be properly taken care of. An embedded controller running at a higher clock frequency can be used so that tuning and improved quality of embedded control is realized.

Piecewise linear control strategy presents a promising approach since developed model parameters may not work in practice owing to a number of factors such as change in material properties as inflation-deflation cycles increases. It is also well known that the control of systems that use pneumatic air as actuation power is difficult due to non linearity of air compressibility, identifying the correct system model and unknown disturbances. The large deformation experienced by pneumatic soft robots means that air pressures set for a certain equilibrium position will depend on its current position. Therefore, air pressure will vary as position varies and vice versa. As a result of these highlighted reasons, the piecewise linear controller would provide a suitable control since it extrapolates from what it knows in the event of the unknown given unforeseen and unpredictable situations that have been described.

The presented system is modular in terms of mechanical modularity, supply of compressed air, electrical power supply and system integration as all of these are enclosed in a case to house the control components and PCB board. The control algorithms of this system can be easily modified to cover a wide range of movements such as bending, rotary or contraction motions performed for soft robots. Also, using separate pressure control for each air channel will tend to reduce failure of the soft robot as a result of inflation pressure and increase the range of obtainable movement.

## 7.5 Chapter Conclusion

The design of an embedded control circuit in hardware and software, operated as a pressure regulator system to perform pneumatic actuation of soft robots was presented. An approach to using this embedded system to actuate single and multiple air channels was demonstrated. The control hardware and software of this system can be easily modified to cover a wide range of movements such as for regulating the required positive and negative air pressure to attain a set bending or rotary angle or contraction amount for a given soft robot. The valve network involving a multichannel arrangement of valves is advantageous in its ability to control many outputs in parallel from a single pressure input. Finally, a two-stage controller involving vision and pressure was implemented so as to control the soft robot to a set position.

This chapter and the preceding ones focused on building and characterising the soft robotic system from the ground up including the actuators, control hardware and software. In the next two chapters, the focus is changed to the particular application of

the system that has thus been described, which is to use soft robotics for rehabilitating the upper limb.

# Chapter 8

# Elbow Rehabilitation Using Soft Robotic Modules

This focus of this chapter is on the study of the upper limb with a view to utilize soft robots to assist in necessary movements. The chapter also focuses on the use of the previously developed soft robots to achieve motion about the elbow joint to assist individuals with little or no muscular power so that when the therapist is away, a patient could simply wear the soft device and exercise at their convenience. This system is aimed at assisting in movement of the elbow by providing for elbow flexion and extension and has high safety integrity from the perspective of the patient because it is composed entirely of rubber, which is a compliant material and attached to the body via Velcro® strap fabric.

The design and validation of soft robots as an elbow joint assistive system is presented in this chapter. An overview of the anatomy of the upper limb and stroke is first provided, then the design and validation of the soft modules for elbow assistance is provided after.

## 8.1 Stroke and Anatomy of the Upper Limb

The motor control system of the brain consists of muscles and innervating neurons. The Somatic Motor Neuron (SMN) supplies skeletal muscles, likewise, sensory information from the skin, joints and all other parts of the body affected by that movement is sent back to the brain. Therefore, outgoing motor information and incoming sensory information is being integrated in a highly dynamic fashion whose end result produces a

final motor command which is sent to the primary motor cortex. A two-neuron system is required whenever there is a motor movement e.g. finger wiggling: the first neuron (CNS excitatory neuron) which has its cell body in the primary motor cortex sends an axon all the way down through the brainstem, to the spinal cord and then synapses with the second motor neuron whose cell body lives in the spinal cord and whose axon goes all the way down to the skeletal muscle (Figure 8.1). If there is a damage or injury to the axon of the SMN, there will be a paralysis of the skeletal muscle. A stroke occurs when there is an obstruction or breakage of middle cerebral artery which supplies blood to the motor cortex.

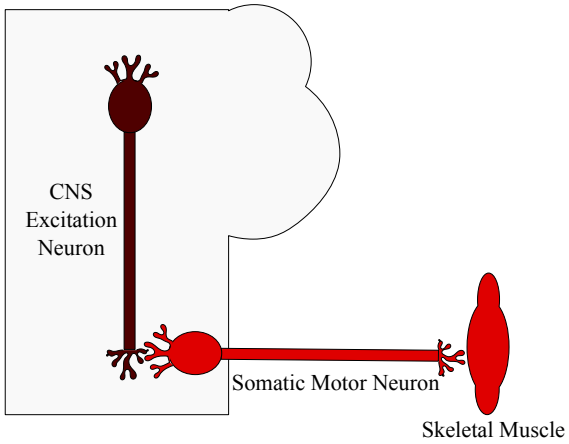


Figure 8.1: Two-neuron system responsible for motor activity.

### 8.1.1 Muscles

A muscle is a type of soft tissue that connects, supports or surrounds other structures or organs of the body. It converts chemical energy to kinetic energy through a process called cellular respiration. Muscles function by contracting, which under normal circumstances causes muscle shortening. Muscle contraction is triggered through electrical stimulation either by nerve impulse produced internally or electrically applied from the external environment. There are 3 types of muscles in the human body - skeletal muscle, cardiac muscle and smooth muscle. The human muscles form an integral part of the human body, constituting nearly half of the body weight. The skeletal muscle attaches to the prominence of 2 bones across a joint and pulls them closer together when it contracts. Usually, one bone will be relatively fixed, called the origin while the other bone would move more, called the insertion. The origin is the fixed point to which a

skeletal muscle attaches and the insertion is the movable point. Many skeletal muscles in the human body do not attach to a bone directly, but attach to bones via tendon which is inelastic in nature to allow force transmission. Figure 8.2 shows a schematic of skeletal muscle attachment to a bone.

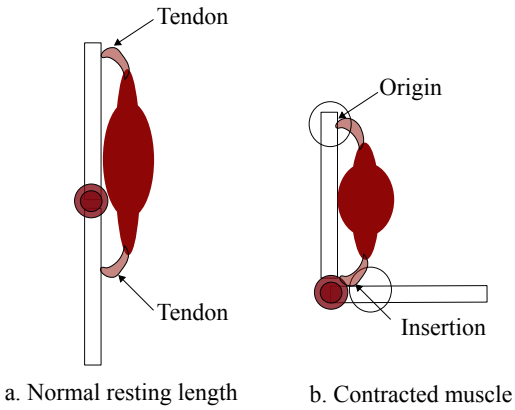


Figure 8.2: Skeletal muscle attachment to a bone.

The fundamental property of a muscle is contractility. Skeletal muscle fibers are very long multinuclear cells specialized for forceful short duration contractions. Limb muscles are controlled by the nervous system, a somatic motor neuron completes the pathway from the CNS to the skeletal muscle. The interface between an axon of a somatic motor nerve and a skeletal muscle cell membrane is the neuromuscular junction. When an action potential reaches the axon terminal of a somatic motor nerve, acetylcholine neurotransmitters are released which binds with acetylcholine receptors to depolarize the muscle cell, hence all muscle cells in the motor unit contract. Following muscle contraction, acetylcholinase enzymes in the synaptic cleft inactivate any residual neurotransmitter to prevent spontaneous contraction in the absence of a specific nerve impulse.

### 8.1.2 Joints

While the lower limb is adapted primarily for weight bearing and locomotion, the upper limb is adapted primarily for mobility and dexterity. In robotics, the kinematics of the human arm is modeled using a serial mechanism composed of seven revolute joints (Figure 8.3). The shoulder consists of a sequence of three revolute joints with intersecting axes coincident with the center of rotation. The fourth joint represents the elbow, while the last three joints take part in a spherical wrist [144].

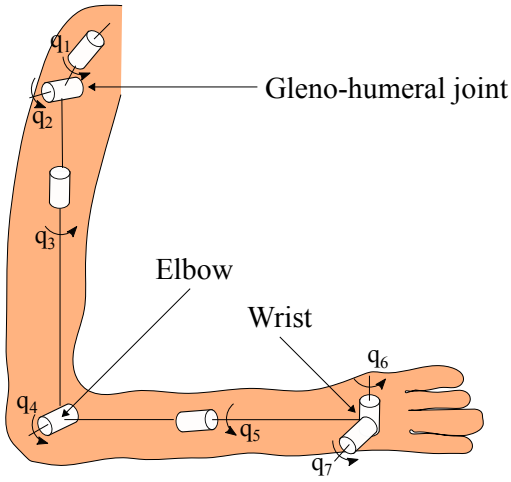


Figure 8.3: Kinematic modeling of human arm.

#### 8.1.2.1 Elbow Joint

The elbow joint is a synovial hinge joint consisting of the humeroulnar joint and the humeroradial joint. The elbow joint permits flexion and extension with only slight accessory motion in other axes. The elbow joint consists of a pair of articulations with contributions from the humerus, radius and ulna. Although three bones form the elbow joint, bone congruence is fairly exact, thereby making it among the most stable joints in the body. Flexion and extension of the forearm takes place at the elbow joint. Pronation and supination of the forearm takes place at the superior and inferior radial-ulna joint.

The elbow joint movement of a human body is modelled as a lever system consisting of a fulcrum, lever arm, load and effort; the fulcrum being the pivot point about which the rotational movement will occur. Movement occurs over the lever arm with effort being applied by a muscle against some load (a resistance to movement, for example, the weight of the arm against gravity or a load that needs to be lifted). The forearm is an example of a type 3 biomechanical lever system as shown in Figure 8.4. For a human elbow joint, the fulcrum is the elbow joint itself, the load is the weight of the forearm and other load being carried, the effort is applied by bicep muscles running from the shoulder and inserting down into the forearm very close to the elbow joint.

For this type 3 lever, the fulcrum is at one end of the lever system, the load is at the opposite end of the lever, while the effort is applied much closer to the fulcrum over a much shorter distance. The significance of this arrangement is that when the muscle is

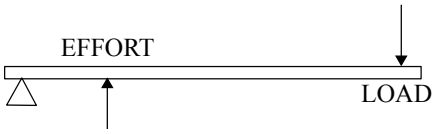


Figure 8.4: Type III lever system modelling of elbow joint movement.

contracted, a small distance of muscle contraction results in a much greater distance of movement at the forearm. The speed of contraction is enhanced by the length of the forearm lever, this is why it is referred to as a speed lever. As illustrated in Figure 8.5, the speed with which the load point moves is greater than the distance the effort point moves.

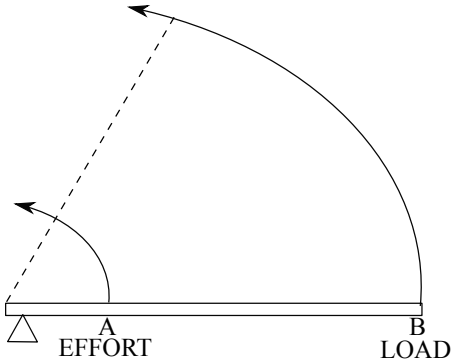


Figure 8.5: A small distance of muscle contraction at the point A (effort) results in a very much greater distance of movement at point B (forearm) for a type 3 lever system

This system operates at a mechanical disadvantage because a much greater effort is applied in order to move against a load. it implies a very powerful (bulky) muscle is needed close to the fulcrum to move an elbow joint quickly. A mechanical disadvantage system is advantageous because it allows for movement of body parts relative to each other without these bulky groups of muscles hindering movement. The fabricated soft muscles in this work would therefore have its effort point close to the pivot of a joint in order to deliver contraction force. Muscles can only shorten, in order to get it to be stretched back out again, an opposite force needs to be applied. Therefore, muscles need to be organized as antagonist pairs. Since the natural motion of an elbow joint is bidirectional (flexion and extension), this means two opposite actuators are needed. These two elements work together in an antagonistic archetype thereby simulating the biceps-triceps muscle system to provide bidirectional motion. This antagonistic arrangement is necessitated to prevent the use of only gravity to extend the forearm. The

force difference between the agonist and the antagonist actuators generates a positive or negative torque at the elbow joint.

#### 8.1.2.2 Other Joints

Other joints present in the upper limb include radioulnar, scapulothoracic and shoulder joint.

**Radioulnar Joints:** The proximal and distal radioulnar joints are synovial pivot joints permitting pronation and supination of the forearm and hand. During pronation and supination, the radial head pivots within the anular ligament and ulnar notch of the proximal radioulnar joint so that the distal radius swings laterally and medially around the ulnar head of the distal radioulnar joint, sturdy interosseous membrane unites and stabilizes the shafts of the radius and ulna during pronation and supination.

**Scapulothoracic joints:** A combination of the scapula on the chest wall, sternoclavicular and acromioclavicular joints is described as the scapulothoracic joint. The sternoclavicular joint is a synovial saddle joint and is the only bony articulation between the axial skeleton and the entire upper limb. Despite the lack of bone congruence, the sturdy ligaments of the sternoclavicular joint provide considerable stability. The acromioclavicular joint on the other hand is a synovial plane joint. The sternoclavicular and acromioclavicular joints permits gliding in several directions:

1. Elevation and depression: Elevation occurs when the scapula and upper limb glide superiorly. Depression occurs when the scapula and upper limb glide inferiorly. Elevation is movement in a superior (above) direction. Depression is movement in an inferior (below) direction.
2. Upward and downward rotation: Upward rotation of the scapula tilts the glenoid fossa superiorly, lengthening the reach upward. Downward rotation of the scapula tilts the glenoid fossa inferiorly, lengthening the reach downward
3. Protraction and retraction: Protraction occurs when the scapula and upper limb glide anteriorly while retraction occurs when the scapula and upper limb glide posteriorly.

**Shoulder Joint:** The shoulder (glenohumeral) joint is the most mobile joint in the human body, it is a synovial ball and socket joint between the glenoid fossa of the scapula and the head of the humerus. The surface of the humeral head is round and larger than the flat glenoid fossa of the scapula, so bone congruence is limited. The shoulder joint is least stable anteriorly and inferiorly and therefore most frequently dislocated. The joint permits motion in three axes: elevation and depression, abduction and adduction, internal rotation and external rotation.

1. Flexion and extension: Flexion occurs when the angle between the bones meeting at a joint decreases (becomes more acute); extension occurs when the angle between the bones meeting at a joint increases (becomes more obtuse)
2. Abduction and adduction: Abduction occurs when a limb moves away from the body midline; adduction occurs when a limb moves toward the body midline.
3. Internal rotation and external rotation: Internal rotation occurs when a limb or limb segment turns around its longitudinal axis toward the midline; external rotation occurs when a limb or limb segment turns around its longitudinal axis away from the midline.

### 8.1.3 Stroke & Neuroplasticity

The aim of this work is to use soft robotics to rehabilitate stroke patients whose muscles of their upper arm are weak. Stroke is a clinical diagnosis; it is the sudden onset and persistence beyond 24 hours of neurological signs and symptoms that can be explained by a vascular mechanism. If the middle cerebral artery blood vessel is blocked as a result of blood clot or there is an interruption of blood supply to the nervous tissue in the brain, it leads to ischemic stroke. The consequences of stroke can be devastating because the death of nerve cells following ischemic stroke is time dependent: a million nerve cells die per minute of vascular exclusion, even brief interruption of the blood supply to neurons can cause irreparable ischemic injury and cell death.

When there is upper motor neuron weakness in upper extremity cases of stroke, the extensors are weaker than the flexors, i.e. squeezing is possible because flexors are fine but fingers cannot be opened due to extensors being weak. Also, supination muscles

are weak so the arm pronates, the shoulder can be moved but not the fingers. Rehabilitation devices or therapy are often used in order to help in recovering muscular power. Prolonged exercising of the damaged limb could result in the regrowth of a pattern of neurons that would eventually aid recovery through neuroplasticity capability of the brain. Since motor nerve supply to a muscle is lost as a result of stroke, muscle paralysis occurs immediately and muscle atrophy can occur in weeks. Though damaged neurons cannot be replaced, neuronal processes may regenerate, hence the need for exercises to encourage recovery. Presently, about half of the people with ischemic stroke have a good neurological outcome after 3 months while the remaining half will be left with some disability [5], assistive devices are needed in both cases for recovery and assistance.

Aside stroke, other disorders affecting motor patterns in the limbs include arthrogryposis multiplex congenita, muscular dystrophy, spinal muscular atrophy, spinal cord injury and cerebral palsy [75].

## 8.2 Design Considerations for Elbow Motion Assistance

In this section, assistive motion for elbow joint flexion and extension is generated with the aid of wedge-shaped soft modules. The aim of an assistive robotic device is to provide a certain set of intensive/repetitive therapies to enhance motor recovery of patients, decreasing the amount of work of a therapist. During the intensive therapies of the upper limb, muscles are stretched and joints are rotated in order to recover the smooth and elastic functions of muscles. The sensory feedback signal then flows to somatosensory area of brain to facilitate the reorganisation of brain activity. These repetitive exercises are done by extending and flexing the upper limb by rotating the elbow joint through their range of motion. However, stroke patients are often unable to engage in these exercises on their own without having assistance from a physiotherapist.

Rigid robotic structures are often used to offer upper arm assistance. They are based on flexible joints connected by rigid links which makes them heavy with expensive and complicated control. Furthermore, they tend to be supported by a solid base on the ground. When the end-effector is attached to the human upper extremity, the base coordinates of body has to be fixed to the base coordinates of the robot. Because sudden changes of the base body coordinates might cause twist in extremity, the body of

patients has to be firmly fastened to secure the base coordinates of the body. However, this kind of constraint largely restricts the horizon of assistive devices. Moreover, these rigid devices require appropriate gravity balancing in proportion to the weight of the upper limb to offset gravity effects. All of these considerations lead to a set of design specifications required to be fulfilled by a soft wearable robotic assistive device in order to successfully assist in elbow motion.

**Compliance:** Pneumatic-type actuators are already compliant because of the inherent compliance of the actuator material and the compressibility of gases - compressibility enables absorption of unwanted forces.

**Visco-elastic property for passive motion:** To provide assistive motion, positional control is applied, and the amount of force to produce the desired motion should be controlled compliantly by visco-elastic property of the soft actuator.

**Structural transparency for active motion:** There should be little or no resistance in interactions with the robotic arm. The structural transparency is such that the mass of the actuator is so small that a patient performing spontaneous motion do not feel resistance in interactions with the robotic arm. A wearable actuator mass less than 0.5kg is desirable [54] with the advantage that a patient can take part in the rehabilitation in a natural setting.

**Wearable assistive robot:** It should not require the base coordinate system of robot to be grounded so that it does not constrain the motion of the main body. The soft assistive robot is designed such that the soft wedge-like inflatable units are assembled to produce torque. When the soft actuator is worn and actuated, its wedge angle along the arm will change which would act to generate a rotation, thereby assisting the movement of the upper limb; and the elastic modulus control of each module will contribute to compliant assistance. Other specifications such as intrinsic safety; comfort of fitting, adjustment and removal has to be considered during the design stage.

**Safe interaction:** A huge amount of tasks could be achieved when robots share the same workspace with humans, however, rigid robots usually require a strict division between the working area of the robot and human, since they normally do not fulfill lightweight and compliance requirements. For soft robots, high safety integrity for the user is ensured with a soft interface, likewise, low actuator mass

will reduce impact in case of a collision. Table 8.1 shows the basic information of the silicone based soft modules having braided mesh.

Table 8.1: Basic information of the braided mesh soft modules for elbow motion.

| **Characteristics** | **Value** |
|---|---|
| Weight | 0.18Kg |
| Degrees of Freedom | 1 (Elbow Flexion and Extension) |
| Assistive Torque | 3.7Nm |
| Range of Motion | $60° - 120°$ |
| Operating Pressure | -5 to 5 psi |

## 8.3 Wearable Attachment & Actuator Integration

The purpose of the soft robotic modules is for flexion and extension of the forearm at the elbow joint. Therefore, an attachment to the human body becomes fundamental in this design. For all devices to be worn on the body, the interface must be skin compatible. Attachments of the soft modules to the human upper limb were designed to facilitate large area of contact, stable fit, comfort of wearing and removal. Attachment was required to provide a smooth distribution of contact pressure over the entire length of the arm and forearm thereby minimizing the weight and discomfort and to provide a soft but secure attachment. These considerations are essential since the actuator is specifically designed for use for individuals with little or no muscular power. Figure 8.6 shows mesh silicone modules attached to a healthy participant with Velcro attachments. The attachment is made of an elastic fabric material with Velcro straps sewn on it. To join this fabric attachment to the silicone modules, two separately cured silicone layers with a thickness of about 1.5mm were made, the fabric was then embedded into these two layers with liquid silicone as adhesive.

The corrugated modules were also used but with attachment to the subject only at the forearm (Figure 8.7). This is because the corrugated modules can deliver a comparably low torque but move a joint through a sufficiently large range of motion. This arrangement reduces the weight of lifting since it is only the forearm that is being lifted, also, gravity is taken care of by placing the forearm on the table surface, this attachment method permits for sliding of the attachment. Generally, both the actuator geometry

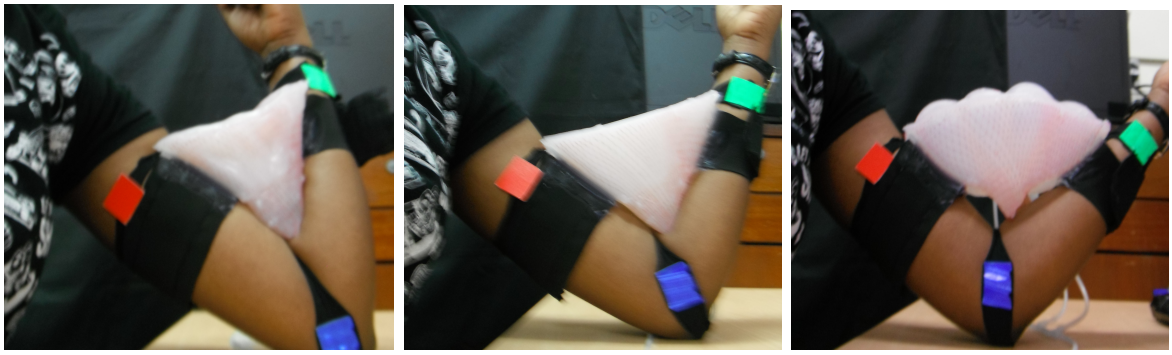

(a) Depressurised (b) Unactuated (c) Pressurised

Figure 8.6: Soft modules worn by a healthy participant. RGB Colour Markers used by the visual processing program to get the current angle, $q$, of the elbow. Angle is given by $q = \cos^{-1} \frac{l_1^2+l_2^2-l_3^2}{2l_1l_2}$. Where lengths $l_1$, $l_2$ and $l_3$ are calculated as the distance (in unit of pixels) between the centroid of the red and blue; blue and green; red and green colour markers respectively.

and attachment should be designed to suite the patient's geometry. For this work, a generic design was made for the purpose of participant experiments.


Figure 8.7: Corrugated soft modules worn by a participant a) unactuated b) actuated.

For the case of the SRM muscles, two M7 muscles were attached to a dummy hinge joint at the fixed and movable points to produce rotation of the joint (Figure 8.8). Attachment was through Velcro®straps sewn onto neoprene fabric material. The fabric was embedded inside silicone rubber to create a glue with the body of the muscles.

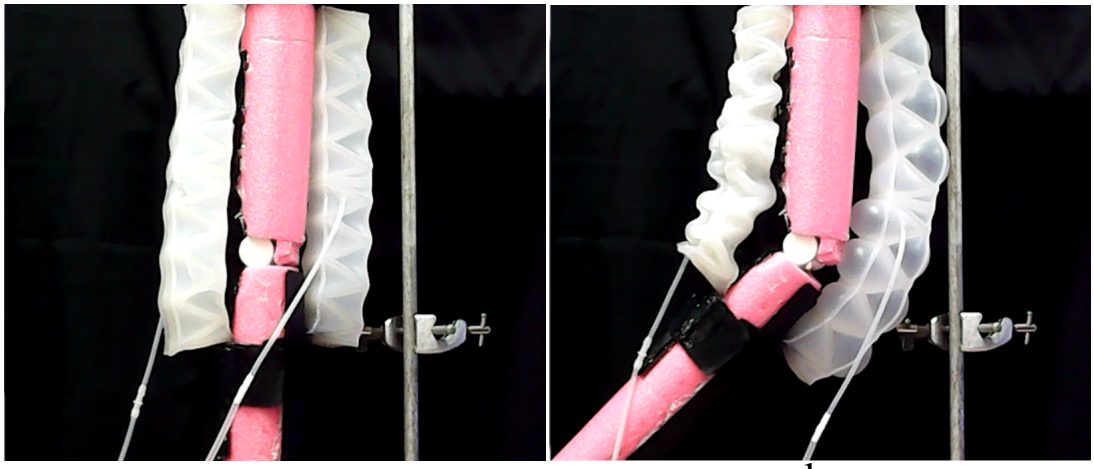


Figure 8.8: Muscles placed in antagonistic pair on a dummy hinge joint a. Antagonist pairs are not actuated b. Antagonist pairs are actuated to produce rotation of the joint, One muscle pair is contracting while the other pair is extending

## 8.4 Evaluation with healthy participants

Participants' experiments were conducted after approval by the local ethics research committee in the School of Biological Sciences, University of Reading (Reference Approval No: SBS16-17 15).

The soft modules of Figures 8.6 and 8.7 were tested with ten healthy subjects to assess its performance based on comfort, safety and usefulness of the actuator in providing elbow movements. A typical subject sits on a chair, puts his elbow on a table with a flexed initial state while actuation cycles are carried out. Male and female subjects within the age group of 21 – 36 years were recruited to assess the soft modules. Figure 8.9a shows the range of motion in mesh modules while Figure 8.9b shows pressure of air in the corrugated modules as a function of the range of motion in degrees for a subject. The actuation angle was measured as the internal elbow angle. The braided modules could move the elbow through an angle range of from 60° - 120°. The corrugated modules could move the elbow from the normal resting angle to between 30° - 40°.

The deformable elastic rubber conforms smoothly to the human skin so the soft robot easily interfaces with the human body, providing a safe feeling to the user when compared with the more traditional rigid robots. From participants' usability study, highlighted features of this soft module device include its portability, simplicity and ease of operation. Though only able to deliver smaller assistive torques compared to con-

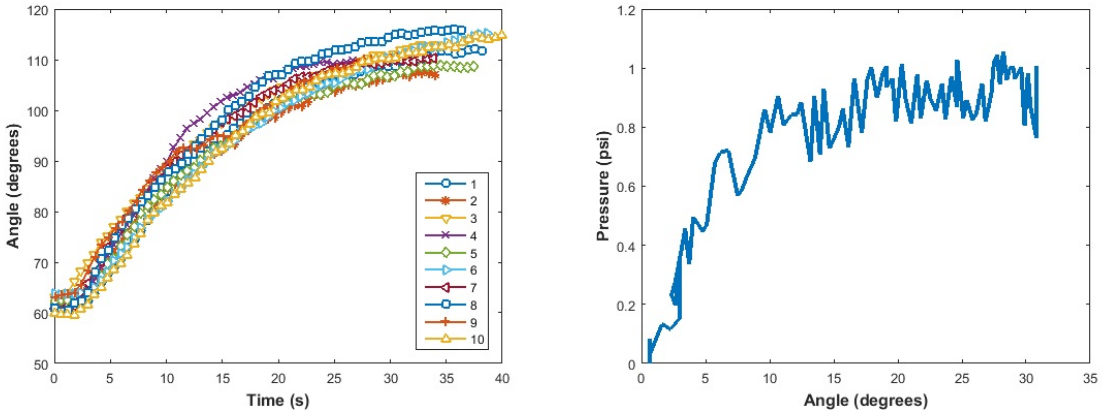


(a) (b)

Figure 8.9: (a) Range of motion in degrees of braided mesh modules worn on participants as a function of time. (b) Pressure of air in corrugated modules worn on a subject as a function of range of motion in degrees.

ventional assistive devices, the wearable, safe and compliant interaction with the user ensured ease of use. The boxplot of the participants' responses in terms of rating the soft robot in ease of assistance, comfort and safety is shown in Figure 8.10. This demonstrates the potential of the soft modules as an assistive aid to stroke patients. All the subjects agreed that soft robots should be used in rehabilitation. Participants were also positive about the use of visual information as seeing the motion of their elbow from the Webcam encouraged further motion and practise with the assistive soft actuators. The neoprene fabric with Velcro attachment enabled the rotary movement to be constrained within its working range of motion. The participants observed in this study observed that the braided mesh design gave a greater assistive force compared with the non-braided design.

## 8.5 Chapter Conclusion

An elbow joint soft rehabilitation device constructed solely from silicone rubber was implemented to demonstrate the use of the system as a motion and assistive device. This soft wearable device offers upper arm assistance by providing for rotary motion which corresponds to the natural motion of the movement of the human elbow. It can assist in movement of the elbow and can record pressure and angle of motion. This design and setup has an advantage over complex assistive systems, which often require

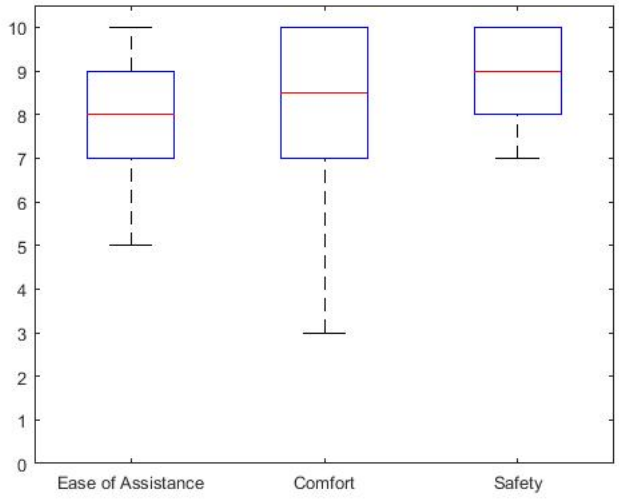


Figure 8.10: Box plot illustrating responses of 10 subjects that participated in the study; scores regarding rating of the soft modules in terms of assistance, comfort and safety are shown, scale is from 0 - 10.

several actuators, force sensors and specialised controllers, but comes at the expense of cost. Since soft robotic modules are composed of only compliant and soft materials, and operated with low air pressure, it is flexible and safe compared to hard robots. The system was designed to meet the specifications of light-weight, ease of wearing and adjustment and comparatively low mechanical complexity, which are essential for any wearable device. Finally, the results suggests the potential of the soft robots in making inexpensive and flexible robots that can work well with humans. The application of the SRM muscle for flexing and extending a rotary joint was also assessed which suggests its potential application in generating motion for individuals with weakened muscles.

This chapter focused on the study of the use of soft robotics to provide elbow assistive movements after providing a study on stroke and the anatomy of the upper limb. As seen from the study of joints in the human body, the shoulder joint is more complex than the elbow, therefore, a proper focus on the soft robotic strategy adopted for the movement of the shoulder will be presented in the following chapter.

# Chapter 9

# An application of soft robotics in Exoskeletons

The difficulty of designing a mechanism to move the shoulder relates to the need to allow a large range of motion and torque; a relatively high torque of about 20Nm would be required to elevate the arm in flexion or abduction. A shoulder assistive device should support isolated motions of flexion/extension and abduction/adduction motions as well as composite spatial motions since the shoulder joint is not an ideal 3RRR joint as was described in Chapter 8. Although the wedged-shaped actuator has been attached to actuate the shoulder joint as illustrated in Figure 9.1, taking into account a really complex kinematics of a shoulder joint as well as a wide range of motion, a free linkage solution making use of an exoskeleton should be preferred in assisting shoulder movements [165]. This chapter involves assessing the use of soft robots in assisting in shoulder motions through the use of an exoskeleton having four DoF (two at the shoulder joint and two at the elbow) which is actuated with soft actuators via compressed air.

The design specifications to be fulfilled by the shoulder assistive system include:

**Gravity compensation using exoskeleton:** Gravity balancing in proportion to the weight of the upper limb would be required to offset gravity effects.

**Degrees of freedom:** Two passive joints should shift the equilibrium plane of the upper limb, while two active joints should guide the wrist to its desired position.

**Viscoelastic property for passive motion:** To provide assistive motion, positional


Figure 9.1: Soft modules attached to the elbow and shoulder a) Depressurised b) Pressurised.

control is applied, and the amount of force to produce the desired motion should be controlled compliantly by viscoelastic property of the actuator.

**Structural transparency for active motion:** Structural transparency should be such that the mass of the robotic arm is so small that there are no restrictions in interacting with the robot arm.

## 9.1 Design of gravity compensating exoskeleton

The Wilmington Robotic Exoskeleton (WREX) which is a gravity compensating exoskeleton, was built to be used in conjunction with soft robots for assisting in shoulder motion. The original exoskeleton is a passive design with benefits of being light-weight and occupying less volume when compared to active gravity compensation designs equipped with motors that reduce safety and are more expensive. The structure of the exoskeleton is same as a balanced-arm lamp consisting a single forearm bar, one parallelogram and two tension spring sets. The exoskeleton works in a gravity reduced environment; the spring is essentially preventing the arm from falling by holding up the arm against gravity - adding or subtracting elastic bands accommodates users of different weights. The use of springs to counter gravity reduces weight of the structure but the disadvantage is that the overall assembly is no longer balanced, so an attachment to firmly clamp the structure to a ground base level so as to prevent it from tipping over is required.

The exoskeleton possesses four Degrees of Freedom (2 DoF at the shoulder and 2 DoF at the elbow joint), and was developed as shown in Figure 9.2 through 3D printing

and assembly. Since the exoskeleton works by offsetting gravity effects at the shoulder and elbow joint, a soft actuator which has a low amount of torque would be used to introduce an active design that can move the shoulder.

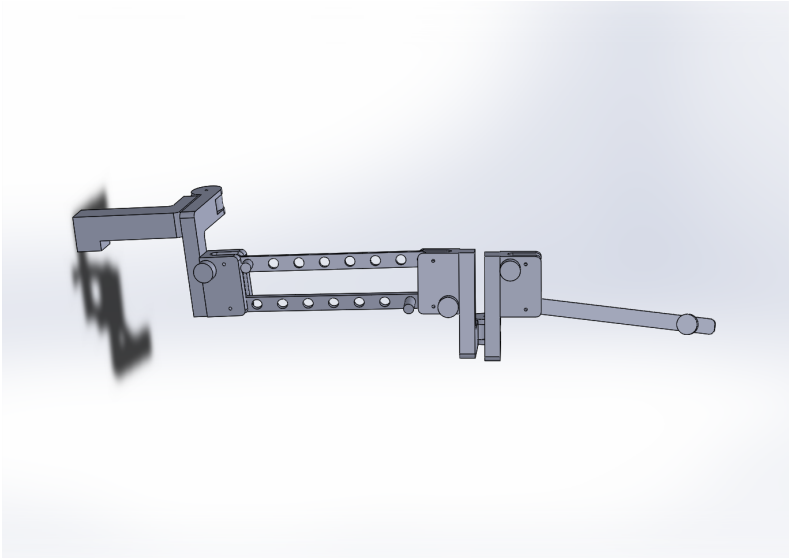

Figure 9.2: 3D Assembly of WREX, assembly consists of seven parts fastened together with the use of bolts and nuts.

The exoskeleton is a copy of the one built at Alfred I. duPont Hospital to help children with muscular dystrophy to elevate their arms passively. The WREX is a 2-link system and consists of an upper arm link constructed from hollow steel (or 3D printed plastic) rods into the shape of a parallelogram and a forearm link that is a single rod. Linear elastic bands serve as a linkage at these links to provide a balance and assist movements at the shoulder and elbow joint by passively offsetting gravity effects using elastic rubber bands. The device is particularly used for children with muscular dystrophy to elevate their arm so they can make use of the little residual strength they possess to move their arm in space. The device also benefit patients with muscular weakness conditions such as stroke and cerebral palsy. Because a large amount of torque is required to lift up the arm against gravity, a system that can offset gravity was chosen to be used with soft robots.

### 9.1.1 Kinematics

The kinematics of the WREX exoskeleton is described in this section. The WREX exoskeleton is a four DoF structure with two joints used for gravity compensation via

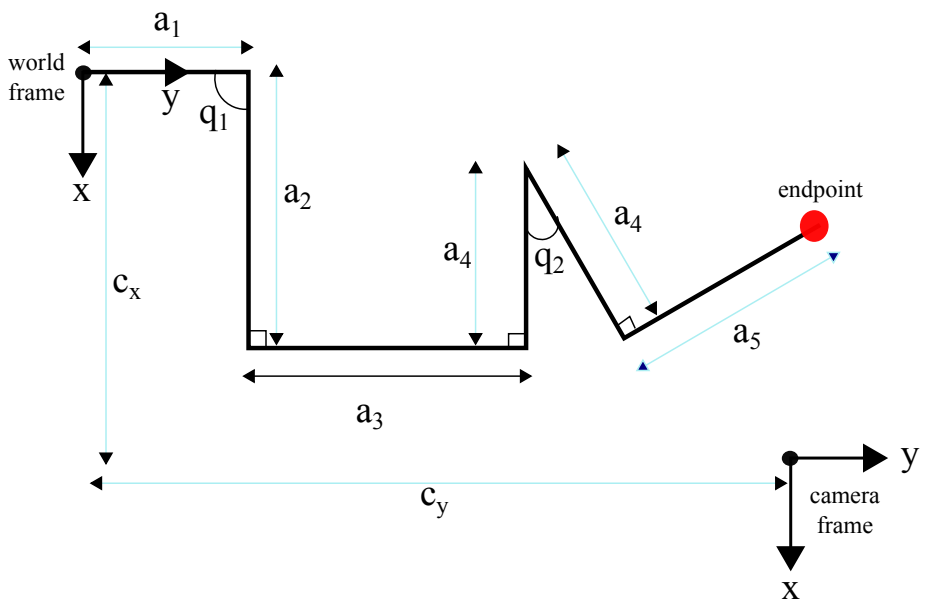


Figure 9.3: 2D representation of WREX.

rubber bands. Its kinematics can be considered as having two passive joints for gravity compensation, and two active joints for attachment of soft actuators, this reduces the kinematics to a 2D planar robot solution (Figure 9.3). Homogeneous transformation matrix from the world coordinate to the end effector coordinate, ${}^{W}T_{E}$, is given by:

$$ {}^{W}T_{E} = T_{y}(a_1)R(q_1)T(a_2, a_3)T_{x}(-a_4)R(q_2)T(a_4, a_5) \tag{9.1} $$

$$ {}^{W}T_{E} = \begin{bmatrix} T(0,0) & T(0,1) & T(0,2) \\ T(1,0) & T(1,1) & T(1,2) \\ 0 & 0 & 1 \end{bmatrix} $$

$$ \begin{aligned} T(0,0) &= \cos(q_1 + q_2) \\ T(0,1) &= -\sin(q_1 + q_2) \\ T(0,2) &= (a_2 - a_4)\cos q_1 - a_3 \sin q_1 + a_4 \cos(q_1 + q_2) + a_5 \sin(q_1 + q_2) \\ T(1,0) &= \sin(q_1 + q_2) \\ T(1,1) &= \cos(q_1 + q_2) \\ T(1,2) &= a_1 + (a_2 - a_4)\sin q_1 + a_3 \cos q_1 + a_4 \sin(q_1 + q_2) + a_5 \cos(q_1 + q_2) \end{aligned} $$

The following poses are defined: ${}^{W}T_{C}$: pose of the camera with respect to world coordinates; ${}^{W}T_{E}$: pose of the endpoint with respect to world coordinates; and ${}^{C}T_{E}$: pose of the camera with respect to world coordinates

$$\begin{aligned} {}^{C}T_{E} &= ({}^{W}T_{C})^{-1}.{}^{W}T_{E} \\ &=^{C} T_{W}.{}^{W}T_{E} =^{C} T_{E} \end{aligned} \tag{9.2}$$

$${}^{W}T_{C} = T(C_x, C_y)R(-90^\circ) = \begin{bmatrix} 0 & 1 & C_x \\ -1 & 0 & C_y \\ 0 & 0 & 1 \end{bmatrix}$$

$${}^{C}T_{W} = ({}^{W}T_{C})^{-1} = \begin{bmatrix} 0 & -1 & 0 \\ 1 & 0 & 0 \\ C_x & C_y & 1 \end{bmatrix} \tag{9.3}$$

$${}^{C}T_{E} = \begin{bmatrix} T_E(0,0) & T_E(0,1) & T_E(0,2) \\ T_E(1,0) & T_E(1,1) & T_E(1,2) \\ T_E(2,0) & T_E(2,1) & T_E(2,2) \end{bmatrix}$$

$$\begin{aligned} T_E(0,0) &= -\sin(q_1+q_2) \\ T_E(0,1) &= -\cos(q_1+q_2) \\ T_E(0,2) &= -[a_1 + (a_2+a_4)\sin q_1 + a_3\cos q_1 + a_4\sin(q_1+q_2) \\ &\quad + a_5\cos(q_1+q_2)] \\ T_E(1,0) &= \cos(q_1+q_2) \\ T_E(1,1) &= -\sin(q_1+q_2) \\ T_E(1,2) &= (a_2+a_4)\cos q_1 - a_3\sin q_1 + a_4\cos(q_1+q_2) + a_5\sin(q_1+q_2) \\ T_E(2,0) &= C_x\cos(q_1+q_2) + C_y\sin(q_1+q_2) \\ T_E(2,1) &= C_y\cos(q_1+q_2) - C_x\sin(q_1+q_2) \\ T_E(2,2) &= C_x[(a_2+a_4)\cos q_1 - a_3\sin q_1 + a_4\cos(q_1+q_2) + a_5\sin(q_1 \\ &\quad + q_2)] + C_y[a_1 + (a_2+a_4)\sin q_1 + a_3\cos q_1 + a_4\sin(q_1+q_2) + a_5\cos(q_1+q_2)] \end{aligned}$$

The position of the end point with respect to the camera is therefore given by variables $x, y, \theta$

$$\begin{aligned} x &= -[a_1 + (a_2 + a_4)\sin q_1 + a_3 \cos q_1 + a_4 \sin(q_1 + q_2) + a_5 \cos(q_1 + q_2)] \\ y &= (a_2 + a_4)\cos q_1 - a_3 \sin q_1 + a_4 \cos(q_1 + q_2) + a_5 \sin(q_1 + q_2) \\ \theta &= -\sin(q_1 + q_2).\frac{180}{\pi} \end{aligned} \tag{9.4}$$

The derivatives of $x$ and $y$ with respect to the joint angles $q_1$ and $q_2$ are:

$$\begin{aligned} \dot{x} = &-(a_2 + a_4)\dot{q}_1 \cos q_1 + a_3 \dot{q}_1 \sin q_1 - a_4(\dot{q}_1 + \dot{q}_2)\cos(q_1 + q_2) \\ &+a_5(\dot{q}_1 + \dot{q}_2)\sin(q_1 + q_2) \\ \dot{y} = &-(a_2 + a_4)\dot{q}_1 \sin q_1 - a_3 \dot{q}_1 \cos q_1 - a_4(\dot{q}_1 + \dot{q}_2)\sin(q_1 + q_2) \\ &+a_5(\dot{q}_1 + \dot{q}_2)\cos(q_1 + q_2) \end{aligned} \tag{9.5}$$

$$\begin{bmatrix} \dot{x} \\ \dot{y} \end{bmatrix} = \begin{bmatrix} J(0,0) & J(0,1) \\ J(1,0) & J(1,1) \end{bmatrix} \begin{bmatrix} \dot{q}_1 \\ \dot{q}_2 \end{bmatrix} \tag{9.6}$$

$$\begin{aligned} J(0,0) &= -(a_2 + a_4)\cos q_1 + a_3 \sin q_1 - a_4 \cos(q_1 + q_2) + a_5 \sin(q_1 + q_2) \\ J(0,1) &= -a_4 \cos(q_1 + q_2) + a_5 \sin(q_1 + q_2) \\ J(1,0) &= -(a_2 + a_4)\sin q_1 - a_3 \cos q_1 - a_4 \sin(q_1 + q_2) + a_5 \cos(q_1 + q_2) \\ J(1,1) &= a_4 \sin(q_1 + q_2) + a_5 \cos(q_1 + q_2) \end{aligned}$$

$$\begin{bmatrix} \dot{x} \\ \dot{y} \end{bmatrix} = J(\dot{q}_1, \dot{q}_2) \begin{bmatrix} \dot{q}_1 \\ \dot{q}_2 \end{bmatrix} \tag{9.7}$$

$J(\dot{q}_1, \dot{q}_2)$ is the Jacobian transformation matrix of the exoskeleton

### 9.1.2 Integration of soft actuators

Recall that rotary rubber actuators were fabricated in Chapter 4, Section 4.5. The purpose of developing these actuators was to apply them to a rotary joint such that it can be integrated with an exoskeleton structure such as the WREX to assist in shoul-

der motion. The rotary joint consists of two wings, one fixed and one moving part, connected in the middle through a rotary axis. By positive and negative pressure variations, the soft actuators expand and contract clockwise and counterclockwise achieving rotary motions. The integrated structure is shown in Figure 9.4a where two actuators are placed on the joint as an antagonist pair - when one pair is inflating, the other pair is deflating and vice versa as illustrated in Figure 9.4b and 9.4c.

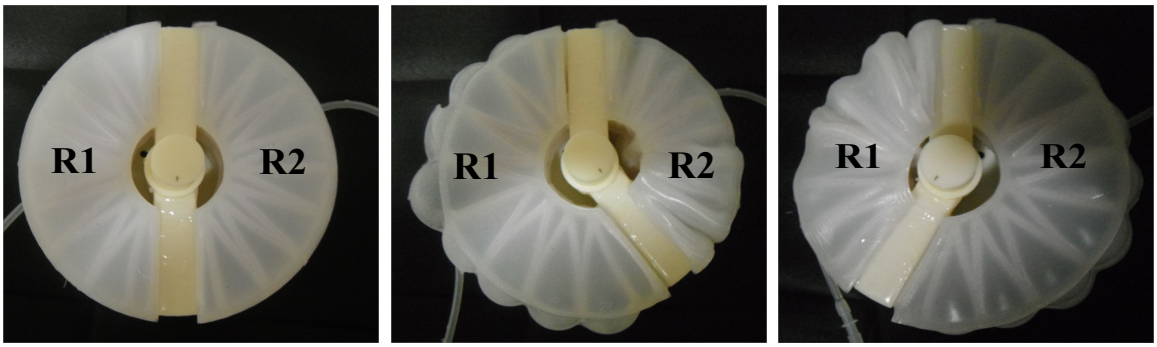


(a) (b) (c)

Figure 9.4: Rotary silicone rubber actuators placed to form an angle of 180° on a rotary joint as antagonist pair (a) Both rotary actuators are unactuated (b) R1 is undergoing pressurisation while R2 is being depressurised to rotate the joint counterclockwise (c) R1 is undergoing depressurisation while R2 is being pressurised to rotate the joint clockwise.

The soft actuators on their own cannot generate sufficient torque to assist the shoulder joint as previously discussed. This light weight gravity compensating exoskeleton was used in conjunction with the soft pneumatic actuators made from plastic bags. Pneumatically operated plastic bags was chosen for this purpose rather than elastomer designs so as to keep the overall weight of the exoskeleton low. Each silicone rubber rotary actuator of Figure 9.4 has a weight of 140g, two of these actuators are required for one joint (Figure 9.4a), but the WREX exoskeleton is light weight having a mass less than 500g. Low actuator mass is a design requirement for a wearable assistive system, hence the need to use a low mass soft actuator for the purpose. Moreover, the use of silicone rubber actuators will lead to an increased carrying weight to the user which would limit performance. Therefore, the use of plastic bags actuators with a weight less than 10g was chosen for this purpose as illustrated in Figure 9.5.

Inflatable plastic structures are lightweight, compact and flexible robotic designs driven by a pneumatic system. Compared with rubber actuators, inflatable bag actuators gen-

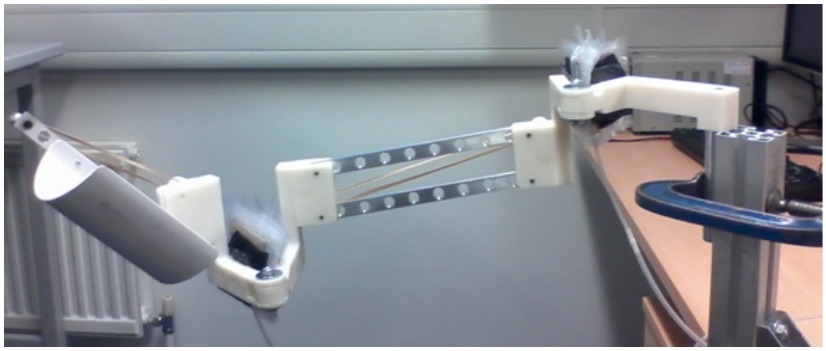

Figure 9.5: A light weight, passive 3D printed WREX exoskeleton having four degrees of freedom movement. Soft plastic bags attached to two joints with Velcro lead to the creation of two active joint to provide elbow and shoulder movement assistance. The plastic bag actuators when inflated with compressed air produces rotary motion of the joints.

erate a considerably larger torque compared with rubber actuators. The inflatable bags were controlled by a pressure regulation system developed in Chapter 7. The passive exoskeleton is powered by inflatable soft actuators made with ultra-light polyethylene sheets fabricated by heat sealing to form an air tight enclosure. Since the exoskeleton is already gravity compensated, the torques required to actuate joints are reduced so soft actuators which produce less torque compared with motors are well suited.

The polyurethane bags was integrated with the WREX by using hook and loop fasteners. To produce rotational movements that would ensure flexion and extension motions, positive and negative air pressure supplied by air and vacuum pumps respectively were used in control. The control system have been described in Chapter 7. Same with the rubber actuators, a software controller to reach a desired position was implemented to drive the integrated system based on pressure and visual information. The desired position vector, $X_d$, is designated on an external camera image, and tip position vector, $X$, is measured by a camera; the exoskeleton will then move to reduce the deviation, $X_d - X$, in the camera image based on the controller [140]: $\bar{J}(q)^T K_p(X_d - X) + \int K_i \bar{J}(q)^T (X_d - X)dt$, where $K_p$ and $K_i$ are proportional and integral gain matrix, $\bar{J}(q)$ is an approximate Jacobian matrix, $q$ is the vector of the joint angles.

## 9.2 Results

As an initial test, evaluation of the integrated system was carried out with calibrated weights to ascertain its ability to move under varying load conditions, thereafter, healthy participants were recruited to use and assess the functionality of the soft actuated exoskeleton.

### 9.2.1 Evaluation with calibrated weights

The workspace of the active system provided by the plastic bags was measured under loading conditions of no load, 0.5Kg, 1.0Kg and 1.5Kg as shown in Figure 9.6a. It can be observed that the exoskeleton has a little range of motion for all loading conditions, the air pressure information of the inflatable bags as they actuate the exoskeleton is shown in Figure 9.6b.

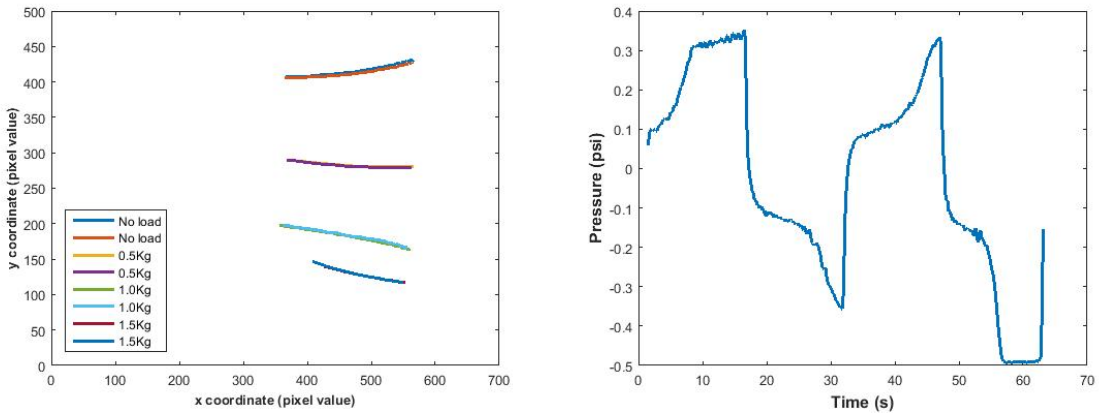


(a) (b)

Figure 9.6: (a) Workspace of exoskeleton actuated with plastic bags under different load conditions. (b) Air Pressure profile information as the exoskeleton moves.

### 9.2.2 Evaluation with healthy participants

Participants' experiments were conducted after approval by the local ethics research committee in the School of Biological Sciences, University of Reading (Reference Approval No: SBS16-17 15).

The performance of the integrated system was examined with healthy participants in terms of its ability to move the arm along its workspace due to its limited dynamic

range. For the system setup, the entire device is secured directly above the shoulder by attaching to a clamp stand while the forearm link is attached to the human body at the forearm via an elbow brace (Figures 9.7 and 9.8).

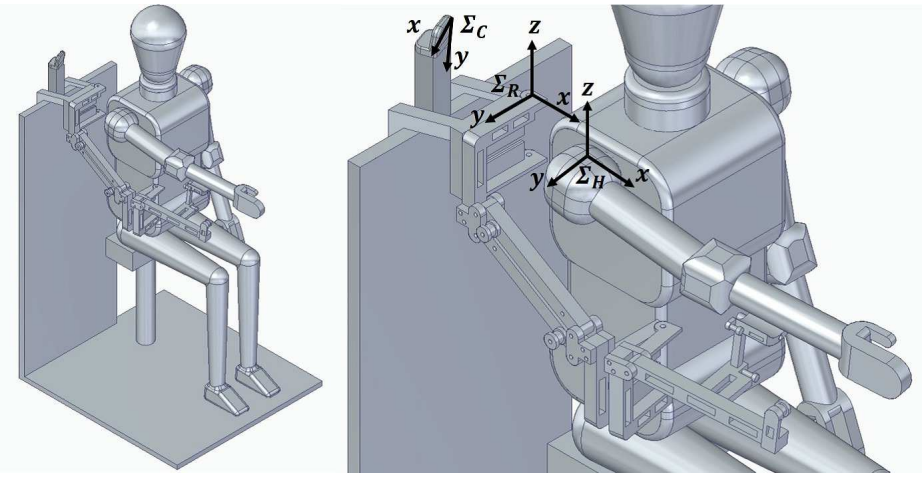


Figure 9.7: (a) Overall structure of the proposed exoskeleton with a participant. (b) Close-up picture of upper body. $\sum_R$ represents the base coordinate of the robot, $\sum_{C1}$ the camera coordinate used in the vision-based control law

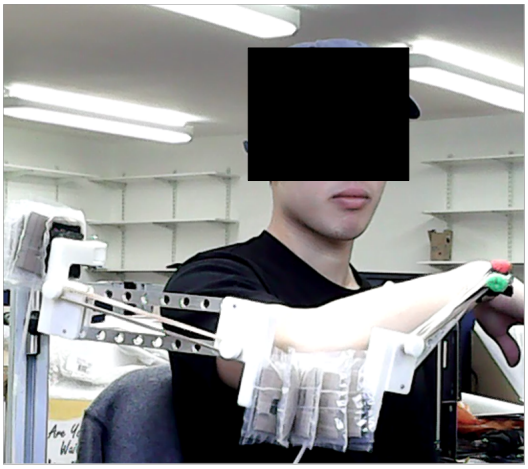

Figure 9.8: A participant places the arm on the exoskeleton actuated with plastic bags. Colour markers are used as trackers to measure the movement of the system.

Ten healthy volunteers consisting of both male and female subjects within the age group of 18 - 25 years were recruited for this experiment. A typical subject sits on a chair, puts his/her forearm on the elbow brace of the exoskeleton while actuation cycles are carried out to move the elbow and shoulder by inflation and vacuum deflation of the plastic

bags attached to the exoskeleton. After each participant has used the exoskeleton for movement tasks, a questionnaire is filled out in order to assess the ease of assistance, comfort and safety offered by the system. The range of movement of six out of the ten participants involved in the study is shown in Figure 9.9 while Figure 9.10 shows a boxplot of the responses of the ten subjects regarding assistance, comfort and safety. From the plot, the average rating for ease of assistance, comfort and safety are 7, 6.5 and 8 respectively on a scale of 0 - 10. It was observed that the mass of the arm would have an overall effect on the ease of the system in providing movement: while a low mass arm would provide a relatively easy assistance, heavy weight arms would provide a lesser amount of ease in moving the arm. Additionally, as a consequence of a larger amount of torque required to move the shoulder compared to the elbow, movement of the system at the shoulder joint is considerably lower.

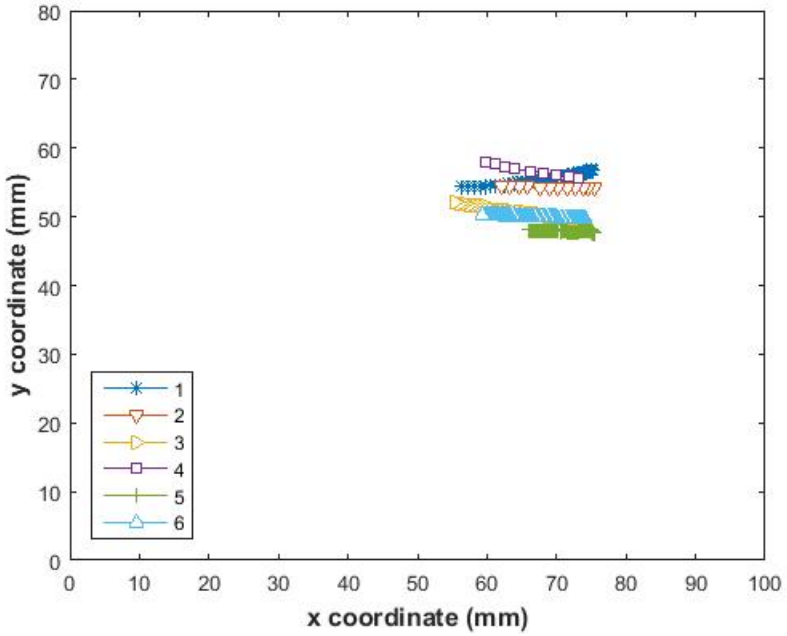


Figure 9.9: Tracking result of the endpoint of six participants involved in the study. Only 6 participants were recorded due to loss of camera tracking outside of its workspace for the remaining four participants.

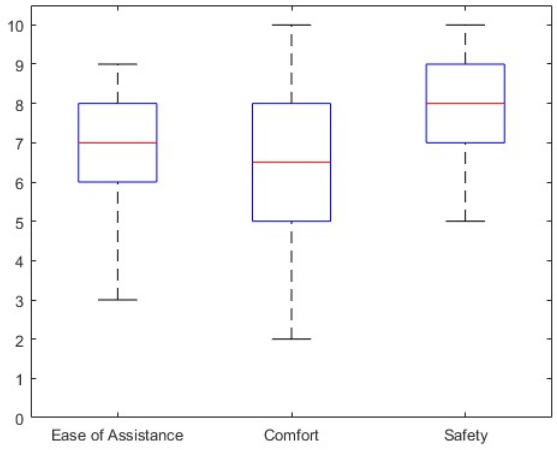


Figure 9.10: Box plot illustrating responses of 10 subjects that participated in the study; scores regarding rating of the exoskeleton actuated with plastic bags in terms of ease assistance, comfort and safety are shown, scale is from 0 – 10.

## 9.3 Chapter Conclusion

This chapter was on the implementation of the soft robotic strategy adopted to assist in shoulder motion, light weight plastic bags was preferred over silicone rubber actuators to reduce the overall weight of the integrated system. Assessment of the system in providing rotary motion was performed with healthy subjects. The next chapter is the concluding chapter of this thesis.

# Chapter 10

# Conclusion

The aim of this thesis was the development of custom made soft actuators that provide assistance to stroke patients during rehabilitation. Integrated with a compact control system, the actuators present promising prototypes for wearable, at-home elbow rehabilitation.

This work focused on the development and characterisation of soft-bodied actuators for upper limb assistance that exhibited bending, rotary and contraction motions. These actuators were constructed by a combination of material and geometrical parameters and relationships that have an overall effect on its method of actuation. To determine the range of motion and speed of the developed actuators, visual processing algorithms were employed so external sensors was used instead of internal sensors that may restrict the motion of the robot. The developed actuators were characterised in terms of air pressure, torque and range of movement. A portable controller implemented in hardware with the use of electro-pneumatics; and a software approach was implemented to regulate the amount of internal air pressure within the actuator. A higher level control making use of visual information from a camera and a combination of the lower level pressure control was then used to move the actuator to a specified position. The applications of these developed actuators were then studied for their use in providing upper limb assistance by assessing the actuators with healthy participants.

## 10.1 Contributions

The original contributions of this thesis to knowledge include the following:

**Rotary actuator designs:** Previous studies on soft robots manufactured with sili-

cone rubber often involve the design of bending actuators. In this work, an intensive study involving the design and characterisation of rubber based actuators that can produce rotary motion was carried out. This included variation in the number of modules and also variation in geometry e.g. pleated network design.

**Embedding braided mesh fabric:** A plain rubber sheet will bulge under inflation pressure which causes reduction in the efficiency of the actuator. A novel implementation that was introduced in this work involves embedding an interwoven mesh network into the rubber. This constrains the tension in only one direction, allowing the rubber actuator to do useful work along its direction of intended movement. This braided mesh network can also be embedded to act as a constraining layer for the case of a bending robot rather than using a different silicone grade or paper as per prior studies.

**Novel muscle actuators:** 100% silicone rubber actuators that contract upon actuation were fabricated and characterized in terms of speed, isotonic and isometric contraction. Popular muscle actuators in soft robotics are McKibben muscle types which have been extensively studied. The novel muscles that have been developed in this work have the capability to show interesting competitiveness with McKibben muscle and would also pave the way for further studies.

## 10.2 Future Work

In order to extend the results of this work, the following are recommended:

**FEM Modelling:** Finite Element Modelling and Analysis of the actuators developed in this work were not carried out as already discussed in Chapter 3. An extension of this work can be done to perform FEM analysis on these actuators.

**Range of motion:** It is desired that not only the torque but also the range of motion of the rotary actuators be improved. Therefore, another reinforcement strategy can be studied so as to improve the range of motion.

**Self-healing rubber:** Rubber fractures after repeated stresses involving series of inflation and deflation resulting in leakage. To make the actuators sustainable and marketable, introduction of nano materials that would make the actuator heal on its own following a fracture would be desirable. As the issue of air leakage

was a major re-occurrence throughout the development, characterisation and experimental stages in this work, this will lead to the development of smart soft actuators that are able to self heal when damaged.

**Standard sensor system:** Research efforts targeted towards developing standardized sensors for soft robotics are already in progress. This will relief the burden on the researcher in having to setup a standard measurement and sensor system to characterise novel soft actuators being produced.

**Smart rubber actuators:** Nano materials can be infused inside silicone rubber which would pave way for smart soft robots, i.e. soft robots that can accurately report their deformation and strain. This also follows from using sensors that would not limit the motion of the soft actuator. To move towards the aim of developing smart actuators, a completely soft battery cell made entirely out of silicone rubber was fabricated (see Appendix B), the main idea is that soft actuators will not require external source of power, rather, they can be powered internally.

This thesis focused on soft robotics for upper limb rehabilitation. The top performing rehabilitation actuators being used today are more than a thousand times stiffer than the human skin, while they work very well, the use of soft actuators which is close to nature is safe, comfortable as well as interesting. While upper limb disability is far too unique for there to be a single intervention for all, soft robotics show the promise of developing actuators that would encourage personalized form of assistance. Additionally, experience with patients requiring rehabilitation have shown that rehabilitation devices should be individualized to cater for the unique needs of the user. Through the contributions of this work, soft robotics show the promise that custom-made devices for upper-limb rehabilitation is possible. Integrating the soft robotic actuators with a compact control system will provide a promising adoption for a wearable, at home rehabilitation system for the upper limb.

# References


[1] Daniel Hernandez. LET'S GO SOFT: How soft robots will help sick kids walk and make the elderly stronger. `http://fusion.net/story/232380/soft-robotics-revolution/`, November 2015. Accessed: 2015-12-30.

[2] Karel Capek. Rossum's Universal Robots. `https://ebooks.adelaide.edu.au/c/capek/karel/rur/`, 1920. Accessed: 2016-01-12.

[3] Daniela Rus and Michael Tolley. Design, fabrication and control of soft robots. *Nature*, 521(7553):467–475, 2015.

[4] Andrew Marchese, Robert Katzschmann, and Daniela Rus. A Recipe for Soft Fluidic Elastomer Robots. *Soft Robotics*, 2(1):7–25, 2015.

[5] Machiel H.F. Van der Loos and David J. Reinkensmeyer. Rehabilitation and Health Care Robotics. In *Springer Handbook of Robotics*, pages 1223–1251. Springer Berlin Heidelberg, 2008.

[6] W.S. Harwin, A. Murgia, and E.K. Stokes. Assessing the effectiveness of robot facilitated neurorehabilitation for relearning motor skills following a stroke. *Medical & Biological Engineering & Computing*, 49(10):1093–1102, 2011.

[7] L.E.H. van Dokkuma, T. Ward, and I. Laffont. Brain computer interfaces for neurorehabilitation – its current status as a rehabilitation strategy post-stroke. *Annals of Physical and Rehabilitation Medicine*, 58(1):3–8, 2015.

[8] Victoria Oguntosin, W.S. Harwin, S. Kawamura, S.J. Nasuto, and Y. Hayashi. Development of a wearable assistive soft robotic device for elbow rehabilitation. In *2015 IEEE International Conference on Rehabilitation Robotics*, pages 747–752, Aug 2015.

[9] Victoria Oguntosin, S.J. Nasuto, and Y. Hayashi. A Compact Low-Cost Electronic Hardware Design for Actuating Soft Robots. pages 242–247, March 2015.

[10] Victoria Oguntosin, S.J. Nasuto, and Y. Hayashi. A Compact Low-Cost Electronic Hardware Design for Actuating Soft Robots. *International Journal of Simulation Systems, Science & Technology*, 16(3):1–11, 2016.

[11] Victoria Oguntosin, S.J. Nasuto, and Y. Hayashi. Embedded Fuzzy Logic Controller for Positive and Negative Pressure Control in Pneumatic Soft Robots. pages 63–68, Apr 2017.

[12] R. Alami, A. Albu-Schaeffer, A. Bicchi, R. Bischoff, R. Chatila, A. De Luca, A. De Santis, G. Giralt, J. Guiochet, G. Hirzinger, F. Ingrand, V. Lippiello, R. Mattone, D. Powell, S. Sen, B. Siciliano, G. Tonietti, and L. Villani. Safe and dependable physical human-robot interaction in anthropic domains: State of the art and challenges. In *IEEE/RSJ International Conference on Intelligent Robots and Systems*, pages 1–16, Oct 2006.

[13] J. F. Veneman, R. Ekkelenkamp, R. Kruidhof, F. C.T. van der Helm, and H. van der Kooij. A Series Elastic and Bowden-Cable Based Actuation System for Use as Torque Actuator in Exoskeleton-Type Robots. *The International Journal of Robotics Research*, 25(3):261–281, 2006.

[14] Cecilia Laschi. RoboSoft Working Paper. *RoboSoft*, (2):1–16, 2014.

[15] C. Laschi, M. Cianchetti, B. Mazzolai, L. Margheri, M. Follador, and P. Dario. Soft robot arm inspired by the octopus. *Advanced Robotics*, 26(7):709–727, 2012.

[16] M.W. Hannan and I.D. Walker. Kinematics and the implementation of an elephant's trunk manipulator and other continuum style robots. *Journal of Robotic Systems*, 20(2):45–63, 2003.

[17] Sangbae Kim, Cecilia Laschi, and Barry Trimmer. Soft robotics: a bioinspired evolution in robotics. *Trends in Biotechnology*, 31(5):287–294, 2013.

[18] Deepak Trivedi, Christopher D. Rahn, William M. Kier, and Ian D. Walker. Soft robotics: Biological inspiration, state of the art, and future research. *Applied Bionics and Biomechanics*, 5(3):99–117, 2008.

[19] Otherlab. Pneubotics. http://www.pneubotics.com/. Accessed: 2016-02-01.

[20] Michael T Tolley, Robert F Shepherd, Bobak Mosadegh, Kevin C Galloway, Michael Wehner, Michael Karpelson, Robert J Wood, and George M Whitesides. A resilient, untethered soft robot. *Soft Robotics*, 1(3):213–223, 2014.

[21] Kentaro Takagi, Masanori Yamamura, Zhi-Wei Luo, Masaki Onishi, Shinya Hirano, Kinji Asaka, and Yoshikazu Hayakawa. Development of a rajiform swimming robot using ionic polymer artificial muscles. In *IEEE/RSJ International Conference on Intelligent Robots and Systems*, pages 1861–1866, 2006.

[22] Takayuki Hoshi and Hiroyuki Shinoda. Robot skin based on touch-area-sensitive tactile element. In *IEEE International Conference on Robotics and Automation*, pages 3463–3468, 2006.

[23] I. Gaiser, R. Wiegand, O. Ivlev, A. Andres, H. Breitwieser, S. Schulz, and G. Bretthauer. Compliant Robotics and Automation with Flexible Fluidic Actuators and Inflatable Structures. http://www.intechopen.com/books/smart-actuation-and-sensing-systems-recent-advances-and-future-challenges/compliant-robotics-and-automation-with-flexible-fluidic-actuators-and-inflatable-structures, 2012. Accessed: 2016-12-15.

[24] Filip Ilievski, D. Mazzeo, Aaron, Robert F. Shepherd, Xin Chen, and George M. Whitesides. Soft Robotics for Chemists. *Angewandte Chemie International Edition*, 50(8):1890–1895, 2011.

[25] Jeong-Yun Sun, Xuanhe Zhao, Widusha R. K. Illeperuma, Ovijit Chaudhuri, Kyu Hwan Oh, David J. Mooney, Joost J. Vlassak, and Zhigang Suo. Highly stretchable and tough hydrogels. *Nature*, 489(7414):133–136, 2012.

[26] K.J. Kim and S. Tadokoro. Electroactive Polymers for Robotic Application: Artificial Muscles and Sensors. *Springer*, 2007.

[27] Shi Qiu, Hengchang Bi, Xiaohui Hu, Mingbo Wu, Yongfeng Li, and Litao Sun. Moldable clay-like unit for synthesis of highly elastic polydimethylsiloxane sponge with nanofiller modification. *RSC Advances*, 7(17):10479–10486, 2017.

[28] Carter S. Haines, Márcio D. Lima, Na Li, Geoffrey M. Spinks, and et al. Artificial Muscles from Fishing Line and Sewing Thread. *Science*, 343(6173):868–872, 2014.

[29] N.G. Tsagarakis and D.G. Caldwell. Improved modelling and assessment of pneumatic muscle actuators. In *2000 IEEE International Conference on Robotics and Automation*, volume 4, pages 3641–3646, 2000.

[30] D. Baiden, A. Wilkening, and O. Ivlev. Safety and handling concept for assistive robotic devices with pneumatic rotary soft-actuators. In *2011 IEEE/ASME International Conference on Advanced Intelligent Mechatronics*, pages 754–759, July 2011.

[31] Kim Hye-Jong, Y. Tanaka, A. Kawamura, S. Kawamura, and Y. Nishioka. Development of an inflatable robotic arm system controlled by a joystick. In *2015 24th IEEE International Symposium on Robot and Human Interactive Communication*, pages 664–669, Aug 2015.

[32] S. Schulz, C. Pylatiuk, A. Kargov, I. Gaiser, O. Schill, M. Reischl, U. Eck, and R. Rupp. Design of a Hybrid Powered Upper Limb Orthosis. In *World Congress on Medical Physics and Biomedical Engineering*, volume 25/IX of *IFMBE Proceedings*, pages 468–471. 2009.

[33] M. Cianchetti, A. Licofonte, M. Follador, F. Rogai, and C. Laschi. Bioinspired soft actuation system using shape memory alloys. *Actuators*, 3(3):226–244, 2014.

[34] S. Kim, E. Hawkes, K. Cho, M. Joldaz, J. Foleyz, and R. Wood. Micro artificial muscle fiber using NiTi spring for soft robotics. In *2009 IEEE/RSJ International Conference on Intelligent Robots and Systems*, pages 2228—-2234, Oct 2009.

[35] Ryan C. Chiechi, Emily A. Weiss, Michael D. Dickey, and George M. Whitesides. Eutectic Gallium–Indium (EGaIn): A Moldable Liquid Metal for Electrical Characterization of Self-Assembled Monolayers. *Angewandte Chemie International Edition*, 47(1):142–144, 2008.

[36] Chien-Chun Chen, Wen-Pin Shih, Pei-Zen Chang, Hsi-Mei Lai, Shing-Yun Chang, Pin-Chun Huang, and Huai-An Jeng. Onion artificial muscles. *Applied Physics Letters*, 106(18), 2015.

[37] Eric Brown, Nicholas Rodenberg, John Amend, Annan Mozeika, Erik Steltz, Mitchell R. Zakin, Hod Lipson, and Heinrich M. Jaeger. Universal robotic gripper based on the jamming of granular material. *Proceedings of the National Academy of Sciences*, 107(44):18809–18814, 2010.

[38] O. Ivlev. Soft fluidic actuators of rotary type for safe physical human-machine interaction. In *2009 IEEE International Conference on Rehabilitation Robotics*, pages 1–5, June 2009.

[39] Gustav Nyström, Andrew Marais, Erdem Karabulut, Lars Wågberg, Yi Cui, and Mahiar M. Hamedi. Self-assembled three-dimensional and compressible interdigitated thin-film supercapacitors and batteries. *Nature Communications*, 6(7259), 2015.

[40] K. Suzumori, S. Endo, T. Kanda, N. Kato, and H. Suzuki. A Bending Pneumatic Rubber Actuator Realizing Soft-bodied Manta Swimming Robot. In *IEEE International Conference on Robotics and Automation*, pages 4975–4980, April 2007.

[41] Harshal Arun Sonar and Jamie Paik. Soft pneumatic actuator skin with piezoelectric sensors for Vibrotactile feedback. *Frontiers in Robotics and AI*, 2(38), 2016.

[42] Y. She, C. Li, J. Cleary, and H. Su. Design and Fabrication of a Soft Robotic Hand With Embedded Actuators and Sensors. *Journal of Mechanisms and Robotics*, 7(2):1–9, 2015.

[43] Sangok Seok, C.D. Onal, Robert Wood, D. Rus, and S. Kim. Peristaltic locomotion with antagonistic actuators in soft robotics. In *2010 IEEE International Conference on Robotics and Automation*, pages 1228–1233, May 2010.

[44] Je-Sung Koh and Kyu-Jin Cho. Omega-Shaped Inchworm-Inspired Crawling Robot With Large-Index-and-Pitch (LIP) SMA Spring Actuators. *IEEE/ASME Transactions on Mechatronics*, 18(2):419–429, April 2013.

[45] T. Umedachi, V. Vikas, and B.A. Trimmer. Highly deformable 3-D printed soft robot generating inching and crawling locomotions with variable friction legs. In *2013 IEEE/RSJ International Conference on Intelligent Robots and Systems*, pages 4590–4595, Nov 2013.

[46] J Sárosi, I Biro, J Nemeth, and L Cveticanin. Dynamic modeling of a pneumatic muscle actuator with two-direction motion. *Mechanism and Machine Theory*, 85:25–34, 2015.

[47] B. Tondu and P. Lopez. Modeling and control of McKibben artificial muscle robot actuators. *IEEE Control Systems*, 20(2):15–38, Apr 2000.

[48] Heo Pilwon, S.J. Kim, and Kim Jung. Powered finger exoskeleton having partially open fingerpad for flexion force assistance. In *2013 IEEE/ASME International Conference on Advanced Intelligent Mechatronics*, pages 182–187, July 2013.

[49] Belforte, G. and Quaglia, G and Testore, F. and Eula, G. and Appendino, S. *Smart Textiles for Medicine and Healthcare*. 2007.

[50] A. Wilkening, D. Baiden, and O. Ivlev. Assistive control of motion therapy devices based on pneumatic soft-actuators with rotary elastic chambers. In *2011 IEEE International Conference on Rehabilitation Robotics*, pages 1–6, June 2011.

[51] Shunichi Kurumaya, Koichi Suzumori, Hiroyuki Nabae, and Shuichi Wakimoto. Musculoskeletal lower-limb robot driven by multifilament muscles. *ROBOMECH Journal*, 3(1):18, 2016.

[52] Y Sun, Yun Seong Song, and J. Paik. Characterization of silicone rubber based soft pneumatic actuators. In *2013 IEEE/RSJ International Conference on Intelligent Robots and Systems*, pages 4446–4453, Nov 2013.

[53] R.F. Shepherd, F. Ilievski, W. Choi, S.A. Morin, A.A. Stokes, A.D. Mazzeo, X. Chen, M. Wang, and G.M. Whitesides. Multi-gait soft robot. *PNAS*, 108(50):20400–20403, 2011.

[54] P. Polygerinos, S. Lyne, Wang Zheng, L.F. Nicolini, B. Mosadegh, G.M. Whitesides, and C.J. Walsh. Towards a soft pneumatic glove for hand rehabilitation. In *2013 IEEE/RSJ International Conference on Intelligent Robots and Systems*, pages 1512–1517, Nov 2013.

[55] A.D. Marchese, K. Komorowski, C.D. Onal, and D. Rus. Design and control of a soft and continuously deformable 2D robotic manipulation system. In *2014 IEEE International Conference on Robotics and Automation*, pages 2189–2196, May 2014.

[56] Raphael Deimel and Oliver Brock. A Compliant Hand Based on a Novel Pneumatic Actuator. In *2013 IEEE International Conference on Robotics and Automation*, pages 2039–2045, May 2013.

[57] John W. Monroe. Jointed assembly actuated by fluid pressure. `http://www.google.co.uk/patents/US5351602`, October 1994. Accessed: 2016-01-05.

[58] Dian Yang, Mohit S. Verma, Ju-Hee So, Bobak Mosadegh, Christoph Keplinger, Benjamin Lee, Fatemeh Khashai, Elton Lossner, Zhigang Suo, and George M. Whitesides. Buckling Pneumatic Linear Actuators Inspired by Muscle. *Advanced Materials Technologies*, 1(3):1600055, 2016.

[59] S. Sanan, J.B. Moidel, and C.G. Atkeson. Robots with inflatable links. In *IEEE/RSJ International Conference on Intelligent Robots and Systems*, pages 4331–4336, Oct 2009.

[60] R. Mutlu, G. Alici, and Weihua Li. Electroactive polymers as soft robotic actuators: Electromechanical modeling and identification. In *2013 IEEE/ASME International Conference on Advanced Intelligent Mechatronics*, pages 1096–1101, July 2013.

[61] G. Alici and D. Gunderson. A bio-inspired robotic locomotion system based on conducting polymer actuators. In *2009 IEEE/ASME International Conference on Advanced Intelligent Mechatronics*, pages 998–1004, July 2009.

[62] Jun Shintake, Samuel Rosset, Bryan Schubert, Dario Floreano, and Herbert Shea. Versatile Soft Grippers with Intrinsic Electroadhesion Based on Multifunctional Polymer Actuators. *Advanced Materials*, 28(2):231–238, 2016.

[63] Leonid Ionov. Hydrogel-based actuators: possibilities and limitations. *Materials Today*, 17(10):494 – 503, 2014.

[64] Huaping Tan and Kacey G. Marra. Injectable, Biodegradable Hydrogels for Tissue Engineering Applications. *Materials*, 3(3):1746, 2010.

[65] M. Manti, V. Cacucciolo, and M. Cianchetti. Stiffening in Soft Robotics: A Review of the State of the Art. *IEEE Robotics Automation Magazine*, 23(3):93–106, Sept 2016.

[66] N.G. Cheng, M.B. Lobovsky, S.J. Keating, A.M. Setapen, K.I. Gero, A.E. Hosoi, and K.D. Iagnemma. Design and Analysis of a Robust, Low-cost, Highly Articulated manipulator enabled by jamming of granular media. In *IEEE International Conference on Robotics and Automation*, pages 4328–4333, May 2012.

[67] Vincent Wall, Raphael Deimel, and Oliver Brock. Selective stiffening of soft actuators based on jamming. In *2015 IEEE International Conference on Robotics and Automation*, pages 252–257, 2015.

[68] Robert F. Shepherd, Adam A. Stokes, Jacob Freake, Jabulani Barber, Phillip W. Snyder, Aaron D. Mazzeo, Ludovico Cademartiri, Stephen A. Morin, and George M. Whitesides. Using Explosions to Power a Soft Robot. *Angewandte Chemie International Edition*, 52(10):2892–2896, 2013.

[69] Bobak Mosadegh, Aaron D. Mazzeo, Robert F. Shepherd, Stephen A. Morin, Unmukt Gupta, Idin Zhalehdoust Sani, David Lai, Shuichi Takayama, and George M. Whitesides. Control of soft machines using actuators operated by a Braille display. *Lab Chip*, 14:189–199, 2014.

[70] Y. Mengüç, Y.L. Park, H. Pei, D. Vogt, P. M. Aubin, E. Winchell, L. Fluke, L. Stirling, R. J. Wood, and C. J. Walsh. Wearable soft sensing suit for human gait measurement. *The International Journal of Robotics Research*, 33(14):1748—-1764, 2014.

[71] Bryan N. Peele, Thomas J. Wallin, Huichan Zhao, and Robert F. Shepherd. 3D printing antagonistic systems of artificial muscle using projection stereolithography. *Bioinspiration & Biomimetics*, 10(5):055003, 2015.

[72] Younan Xia and George M. Whitesides. Soft Lithography. *Annual Review of Materials Science*, 28(1):153–184, 1998.

[73] Robert K. Katzschmann, Andrew D. Marchese, and Daniela Rus. Autonomous Object Manipulation Using a Soft Planar Grasping Manipulator. *Soft Robotics*, 2(4):155–164, 2015.

[74] Hod Lipson and Melba Kurman. *Fabricated: The New World of 3D Printing.* 2013.

[75] Tariq Rahman, Whitney Sample, Shanmuga Jayakumar, Marilyn Marnie King, Jin Yong Wee, Rahamim Seliktar, Michael Alexander, Mena Scavina, and Alisa Clark. Passive exoskeletons for assisting limb movement. *Journal of Rehabilitation Research & Development*, 43(5):583–590, 2006.

[76] Hong Kai Yap, Hui Yong Ng, and Chen-Hua Yeow. High-Force Soft Printable Pneumatics for Soft Robotic Applications. *Soft Robotics*, 3(3):144–158, 2016.

[77] Jorge G Cham, Sean A. Bailey, Jonathan E. Clark, Robert J. Full, and Mark R. Cutkosky. Fast and Robust: Hexapedal Robots via Shape Deposition Manufacturing. *The International Journal of Robotics Research*, 21(10-11):869–882, 2002.

[78] A.M. Dollar and R.D. Howe. A robust compliant grasper via shape deposition manufacturing. *IEEE/ASME Transactions on Mechatronics*, 11(2):154–161, April 2006.

[79] Joshua Gafford, Ye Ding, Andrew Harris, Terrence McKenna, Panagiotis Polygerinos, Dónal Holland, Arthur J. Moser, and Conor J. Walsh. Shape Deposition Manufacturing of a Soft, Atraumatic, Deployable Surgical Grasper. In *Proceedings of Design of Medical Devices Conference 2014*, Minneapolis, MN, 7-10 April 2014.

[80] Sindy K.Y. Tang and George M. Whitesides. Basic Microfluidic and Soft Lithographic Techniques. *Access Engineering*, 2010.

[81] Michael D. Dickey, Ryan C. Chiechi, Ryan J. Larsen, Emily A. Weiss, David A. Weitz, and George M. Whitesides. Eutectic Gallium-Indium (EGaIn): A Liquid Metal Alloy for the Formation of Stable Structures in Microchannels at Room Temperature. *Advanced Functional Materials*, 18(7):1097–1104, 2008.

[82] R. Adam Bilodeau, Edward L. White, and Rebecca K. Kramer. Monolithic fabrication of sensors and actuators in a soft robotic gripper. In *2015 IEEE/RSJ International Conference on Intelligent Robots and Systems*, pages 2324–2329, Sept 2015.

[83] Y. Tenzer, L.P. Jentoft, and R.D. Howe. The Feel of MEMS Barometers: Inexpensive and Easily Customized Tactile Array Sensors. *IEEE Robotics Automation Magazine*, 21(3):89–95, Sept 2014.

[84] L.P. Jentoft, Y. Tenzer, D. Vogt, Liu Jia, R.J. Wood, and R.D. Howe. Flexible, stretchable tactile arrays from MEMS barometers. In *16th International Conference on Advanced Robotics*, pages 1–6, Nov 2013.

[85] W. Felt, K.Y. Chin, and C.D. Remy. Contraction Sensing with Smart Braid McKibben Muscles. *IEEE/ASME Transactions on Mechatronics*, 21(3):1201–1209, 2015.

[86] W. Felt and C.D. Remy. Smart braid: Air muscles that measure force and displacement. In *IEEE/RSJ International Conference on Intelligent Robots and Systems*, pages 2821–2826, Sept 2014.

[87] C. Larson, B. Peele, S. Li, S. Robinson, M. Totaro, L. Beccai, B. Mazzolai, and R. Shepherd. Highly stretchable electroluminescent skin for optical signaling and tactile sensing. *Science*, 351(6277):1071–1074, 2016.

[88] Martin Weigel, Tong Lu, Gilles Bailly, Antti Oulasvirta, Carmel Majidi, and Jürgen Steimle. iSkin: Flexible, Stretchable and Visually Customizable On-Body Touch Sensors for Mobile Computing. In *Proceedings of the 33rd Annual ACM Conference on Human Factors in Computing Systems*, pages 2991–3000, 2015.

[89] Malin Eriksson, Annsofie Torgnysdotter, and Lars Wagberg. Surface Modification of Wood Fibers Using the Polyelectrolyte Multilayer Technique: Effects on Fiber Joint and Paper Strength Properties. *Industrial & Engineering Chemistry Research*, 45(15):5279–5286, 2006.

[90] Victoria Oguntosin, S.J. Nasuto, and Y. Hayashi. Implementation of a design concept of a moulded, soft battery cell. In *2016 12th Conference on Ph.D. Research in Microelectronics and Electronics*, pages 1–4, June 2016.

[91] Paxton Maeder-York, Tyler Clites, Emily Boggs, Ryan Neff, Panagiotis Polygerinos, Dónal Holland, Leia Stirling, Kevin C. Galloway, Catherine Wee, and Conor J. Walsh. Biologically Inspired Soft Robot for Thumb Rehabilitation. In *ASME Design of Medical Devices Conference*, Minneapolis, MN, Apr 2014.

[92] B.M. Haworth. *The Characterisation of Soft Robotic Actuators: design, build and behaviour*. 2012. M.Sc. thesis.

[93] N. Napp, B. Araki, M.T. Tolley, R. Nagpal, and R.J. Wood. Simple passive valves for addressable pneumatic actuation. In *2014 IEEE International Conference on Robotics and Automation*, pages 1440–1445, May 2014.

[94] E. Mattar. Biomimetic Dexterous Hands: Human Like Multi-fingered Robotics Hand Control. In *2012 International Conference on Computer Modelling and Simulation*, pages 193–200, March 2012.

[95] Ramses V. Martinez, Carina R. Fish, Xin Chen, and George M. Whitesides. Elastomeric Origami: Programmable Paper-Elastomer Composites as Pneumatic Actuators. *Advanced Functional Materials*, 22(7):1376–1384, 2012.

[96] M. Mihajlov, Matthias Hubner, O. Ivlev, and A. Graser. Modeling and Control of Fluidic Robotic Joints with natural compliance. In *IEEE International Conference on Control Applications Computer Aided Control System Design*, pages 2498–2503, Oct 2006.

[97] M. Jordan, D. Pietrusky, M. Mihajlov, and O. Ivlev. Precise position and trajectory control of pneumatic soft-actuators for assistance robots and motion therapy devices. In *IEEE International Conference on Rehabilitation Robotics*, pages 663–668, June 2009.

[98] A. Wilkening, M. Mihajlov, and O. Ivlev. Model-based pressure and torque control for innovative pneumatic soft-actuators. In *Proceedings of International Conference on Fluid Power*, pages 291–302, 2010.

[99] P. Polygerinos, Z. Wang, J.T.B. Overvelde, K.C. Galloway, R.J. Wood, K. Bertoldi, and C.J. Walsh. Modeling of soft fiber-reinforced bending actuators. *IEEE Transactions on Robotics*, 3(31):778–789, 2015.

[100] Ricardo Morales, FranciscoJavier Badesa, Nicolás García-Aracil, JoséMaría Sabater, and Carlos Pérez-Vidal. Pneumatic robotic systems for upper limb rehabilitation. *Medical & Biological Engineering & Computing*, 49(10):1145–1156, 2011.

[101] Fumiya Iida and Cecilia Laschi. Soft Robotics: Challenges and Perspectives. *Procedia Computer Science*, 7:99–102, 2011.

[102] A.T. Asbeck, S.M.M. De Rossi, I. Galiana, Ye Ding, and C.J. Walsh. Stronger, Smarter, Softer: Next-Generation Wearable Robots. *IEEE Robotics Automation Magazine*, 21(4):22–33, Dec 2014.

[103] I. Vanderniepen, R. Van Ham, J. Naudet, M. Van Damme, B. Vanderborght, R. Versluys, and D. Lefeber. Novel Compliant Actuator for Safe and Ergonomic Rehabilitation Robots - Design of a Powered Elbow Orthosis. In *2007 IEEE International Conference on Rehabilitation Robotics*, pages 790–797, June 2007.

[104] D. Kim. Compliant motion control for a compliant rehabilitation system. In *2015 IEEE International Conference on Rehabilitation Robotics*, pages 422–427, Aug 2015.

[105] Y. Hayashi, K. Nagai, K. Ito, S.J. Nasuto, R.C.V. Loureiro, and W.S. Harwin. A feasible study of EEG-driven assistive robotic system for stroke rehabilitation. In *International Conference on Biomedical Robotics and Biomechatronics*, pages 1733–1739, June 2012.

[106] D. Fix James. 2002.

[107] N.G. Kutner, R. Zhang, A.J. Butler, S.L. Wolf, and J.L. Alberts. Quality-of-life change associated with robotic-assisted therapy to improve hand motor function in patients with subacute stroke: a randomized clinical trial. *Physical Therapy*, 90(4):493–504, Apr 2014.

[108] H.I. Krebs, B.T. Volpe, M.L. Aisen, and N. Hogan. Increasing productivity and quality of care: Robot-aided neuro-rehabilitation. *Journal of Rehabilitation Research and Development*, 37(6):493–504, 2000.

[109] Ramses V. Martinez, Jamie L. Branch, Carina R. Fish, Lihua Jin, Robert F. Shepherd, Rui M. D. Nunes, Zhigang Suo, and George M. Whitesides. Robotic Tentacles with Three-Dimensional Mobility Based on Flexible Elastomers. *Advanced Materials*, 25(2), 2013.

[110] G.R. Johnson, D.A. Carus, G. Parrini, S. Scattareggia Marchese, and R Valeggi. The design of a five-degree-of-freedom powered orthosis for the upper limb. *Proceedings of the Institution of Mechanical Engineers, Part H: Journal of Engineering in Medicine*, 215(3):275–284, 2001.

[111] H.I. Krebs, B.T. Volpe, D. Lynch, and N. Hogan. Stroke rehabilitation: an argument in favor of a robotic gym. In *International Conference on Rehabilitation Robotics*, pages 219–222, June 2005.

[112] Tobias Nef, Matjaz Mihelj, and Robert Riener. ARMin: a robot for patient-cooperative arm therapy. *Medical & Biological Engineering & Computing*, 45(9):887–900, 2007.

[113] Peter S. Lum, Charles G. Burgar, Machiel Van der Loos, Peggy C. Shor, Matra Majmundar, and Ruth Yap. MIME robotic device for upper-limb neurorehabilitation in subacute stroke subjects: A follow-up study. *Journal of Rehabilitation Research & Development*, 43(5):631–642, 2006.

[114] Susan Coote, Brendan Murphy, William Harwin, and Emma Stokes. The effect of the GENTLE/s robot-mediated therapy system on arm function after stroke. *Clinical Rehabilitation*, 22(5):395—405, 2008.

[115] T. Rahman, R. Ramanathan, R. Seliktar, and W. Harwin. A Simple Technique to Passively Gravity-Balance Articulated Mechanisms. *Journal of Mechanical Design*, 117(4):655–658, 1995.

[116] A. Gopalswamy, P. Gupta, and M. Vidyasagar. A new parallelogram linkage configuration for gravity compensation using torsional springs. In *IEEE International Conference on Robotics and Automation*, pages 664–669, May 1992.

[117] Stratasysfdm. 3D-Printed Magic Arms. `https://www.youtube.com/watch?v=WoZ2BgPVtA0`. Accessed: 2015-03-17.

[118] Tariq Rahman, Whitney Sample, Rahamim Seliktar, Michael Alexander, and Mena Scavina. A body-powered functional upper limb orthosis. *Journal of Rehabilitation Research and Development*, 37(6):675–680, 2000.

[119] A.H.A. Stienen, E.E.G. Hekman, F.C.T. van der Helm, G.B. Prange, M.J.A. Jannink, A.M.M. Aalsma, and H. van der Kooij. Freebal: dedicated gravity compensation for the upper extremities. In *IEEE 10th International Conference on Rehabilitation Robotics*, pages 804–808, June 2007.

[120] Gill A. Pratt, Matthew M. Williamson, Peter Dillworth, Jerry Pratt, and Anne Wright. *Stiffness isn't everything*, pages 253–262. Springer Berlin Heidelberg, Berlin, Heidelberg, 1997.

[121] S. Wolf, G. Grioli, O. Eiberger, W. Friedl, M. Grebenstein, H. Höppner, E. Burdet, D. G. Caldwell, R. Carloni, M. G. Catalano, D. Lefeber, S. Stramigioli, N. Tsagarakis, M. Van Damme, R. Van Ham, B. Vanderborght, L. C. Visser, A. Bicchi, and A. Albu-Schäffer. Variable Stiffness Actuators: Review on Design and Components. *IEEE/ASME Transactions on Mechatronics*, 21(5):2418–2430, 2016.

[122] P.R. Culmer, A.E. Jackson, S. Makower, R. Richardson, J.A. Cozens, M.C. Levesley, and B.B. Bhakta. A Control Strategy for Upper Limb Robotic Rehabilitation With a Dual Robot System. *IEEE/ASME Transactions on Mechatronics*, 15(4):575–585, Aug 2010.

[123] Kai Yap Hong, Hoon Lim Jeong, F. Nasrallah, J.C.H. Goh, and R.C.H. Yeow. A soft exoskeleton for hand assistive and rehabilitation application using pneumatic actuators with variable stiffness. In *2015 IEEE International Conference on Robotics and Automation*, pages 4967–4972, May 2015.

[124] K. Suzumori, S. Iikura, and H. Tanaka. Applying a flexible microactuator to robotic mechanisms. *IEEE Control Systems*, 12(1):21–27, Feb 1992.

[125] Yun Seong Song, Yi Sun, R. van den Brand, J. von Zitzewitz, S. Micera, G. Courtine, and J. Paik. Soft robot for gait rehabilitation of spinalized rodents. In *2013 IEEE/RSJ International Conference on Intelligent Robots and Systems*, pages 971–976, Nov 2013.

[126] R. Boian, A. Sherman, C. Han, A. Merians, G. Burdea, S. Adamovich, M. Recce, M. Tremaine, and H. Poizner. Virtual-reality-based post-stroke hand rehabilitation. *Stud Health Technol Inform*, 85:64–70, 2002.

[127] M. Wehner, B. Quinlivan, P.M. Aubin, E. Martinez-Villalpando, M. Baumann, L. Stirling, K. Holt, R. Wood, and C. Walsh. A lightweight soft exosuit for gait assistance. In *2013 IEEE International Conference on Robotics and Automation*, pages 3362–3369, May 2013.

[128] Frank Daerden and Dirk Lefeber. The Concept and Design of Pleated Pneumatic Artificial Muscles. *International Journal of Fluid Power*, 2(3):41–50, 2001.

[129] P. Beyl, K. Knaepen, S. Duerinck, M. Van Damme, B. Vanderborght, R. Meeusen, and D. Lefeber. Safe and Compliant Guidance by a Powered Knee Exoskeleton for Robot-Assisted Rehabilitation of Gait. *Advanced Robotics*, 25(5):513–535, 2011.

[130] S. Schulz, B. Schmitz, R. Wiegand, C. Pylatiuk, and M. Reischl. The Hybrid Fluidic Driven Upper Limb Orthosis-OrthoJacket. In *Proceedings of the MyoElectric Controls/Powered Prosthetics Symposium Fredericton*, pages 1–6, 2011.

[131] C. J. Nycz, T. Bützer, O. Lambercy, J. Arata, G. S. Fischer, and R. Gassert. Design and Characterization of a Lightweight and Fully Portable Remote Actuation System for Use With a Hand Exoskeleton. *IEEE Robotics and Automation Letters*, 1(2):976–983, July 2016.

[132] J.W. Valvano. Embedded microcomputer systems: Real time interfacing. Cengage Learning-Engineering, third edition, 2011.

[133] Pump. Designing a Pneumatic Pump. `http://www.math.nus.edu.sg/~bao/teach/ma3264/documents/pump.pdf`. Accessed: 2015-12-09.

[134] L.A. Zadeh. Fuzzy Sets and Systems. *International Journal of General Systems*, 17(2):129–138, 1990.

[135] K. Hirota and M. Sugeno. *Industrial Applications of Fuzzy Technology in the World*, volume 2. 1995.

[136] D. Pelusi, R. Mascella, L. Tallini, L. Vazquez, and D. Diaz. Control of Drum Boiler dynamics via an optimized fuzzy controller. *International Journal of Simulation: Systems, Science and Technology*, 17(33):1–7, 2016.

[137] D. Pelusi. PID and intelligent controllers for optimal timing performances of industrial actuators. *International Journal of Simulation: Systems, Science and Technology*, 13(2):1–7, 2012.

[138] G. R. Gossweiler, C. L. Brown, G. B. Hewage, E. Sapiro-Gheiler, W. J. Trautman, G. W. Welshofer, and S. L. Craig. Mechanochemically Active Soft Robots. *ACS Applied Material Interfaces*, 7(40):22431–22435, 2015.

[139] B. Jones and I. Walker. Kinematics for multisection continuum robots. *IEEE Transactions on Robotics*, 22(1):43–55, 2006.

[140] S. Hirai, K. Shimizu, and S. Kawamura. Vision-based motion control of pneumatic group actuators. In *IEEE International Conference on Robotics and Automation*, volume 3, pages 2842–2847, 2002.

[141] L.C. Visser, R. Carloni, and S. Stramigioli. Vision based motion control for a humanoid head. In *IEEE/RSJ International Conference on Intelligent Robots and Systems*, pages 5469–5474, Oct 2009.

[142] A. Vandini, A. Salerno, C.J. Payne, and Yang Guang-Zhong. Vision-based motion control of a flexible robot for surgical applications. In *2014 IEEE International Conference on Robotics and Automation*, pages 6205–6211, May 2014.

[143] M. Inaba, K. Nagasaka, F. Kanehiro, S. Kagami, and H. Inoue. Real-time vision-based control of swing motion by a human-form robot using the remote-brained approach. In *IEEE/RSJ International Conference on Intelligent Robots and Systems*, volume 1, pages 15–22, Nov 1996.

[144] A.M. Zanchettin, L. Bascetta, and P. Rocco. Achieving Humanlike Motion: Resolving Redundancy for Anthropomorphic Industrial Manipulators. *IEEE Robotics Automation Magazine*, 20(4):131–138, 2013.

[145] S. Patil, J. S. Nadar, J. Gada, S. Motghare, and S. S. Nair. Comparison of Various Stereo Vision Cost Aggregation Methods. *International Journal of Engineering and Innovative Technology*, 2(8):222–226, 2013.

[146] S. Hinterstoisser, S. Holzer, C. Cagniart, S. Ilic, K. Konolige, N. Navab, and V. Lepetit. Multimodal templates for real-time detection of texture-less objects in heavily cluttered scenes. In *2011 IEEE International Conference on Computer Vision*, pages 858–865, Nov 2011.

[147] Xiaoyong Shen, Li Xu, Qi Zhang, and Jiaya Jia. Multi-modal and Multi-spectral Registration for Natural Images. In *Lecture Notes in Computer Science*, volume 8692, pages 309–324. 2014.

[148] Jasmine Banks and Peter Corke. Quantitative Evaluation of Matching Methods and Validity Measures for Stereo Vision. *The International Journal of Robotics Research*, 20(7):512–532, 2001.

[149] Maxime Lhuillier and Long Quan. Quasi-Dense Reconstruction from Image Sequence. In *Lecture Notes in Computer Science*, volume 2351, pages 125–139. 2002.

[150] V. Pradeep, C. Rhemann, S. Izadi, C. Zach, M. Bleyer, and S. Bathiche. MonoFusion: Real-time 3D reconstruction of small scenes with a single web camera. In *2013 IEEE International Symposium on Mixed and Augmented Reality*, pages 83–88, Oct 2013.

[151] M. Danelljan, F.S. Khan, M. Felsberg, and J. van de Weijer. Adaptive Color Attributes for Real-Time Visual Tracking. In *2014 IEEE Conference on Computer Vision and Pattern Recognition*, pages 1090–1097, June 2014.

[152] Dong Wang, Huchuan Lu, and Ming-Hsuan Yang. Least Soft-Threshold Squares Tracking. In *IEEE Conference on Computer Vision and Pattern Recognition*, pages 2371–2378, June 2013.

[153] A. E. Hoerl and R. W. Kennard. Ridge regression: Biased estimation for nonorthogonal problems. *Technometrics*, 121:55–67, 1970.

[154] C. Nissler, N. Mouriki, C. Castellini, V. Belagiannis, and N. Navab. OMG: Introducing optical myography as a new human machine interface for hand amputees. In *2015 IEEE International Conference on Rehabilitation Robotics*, pages 937–942, Aug 2015.

[155] Herbert Bay, Tinne Tuytelaars, and Luc Van Gool. SURF: Speeded Up Robust Features. In *Lecture Notes in Computer Science*, volume 3951, pages 404–417. 2006.

[156] Yan Ke and R. Sukthankar. PCA-SIFT: a more distinctive representation for local image descriptors. In *IEEE Conference on Computer Vision and Pattern Recognition*, volume 2, pages 506–513, June 2004.

[157] E. Olson. AprilTag: A robust and flexible visual fiducial system. In *2011 IEEE International Conference on Robotics and Automation*, pages 3400–3407, May 2011.

[158] A. Kawamura, M. Tachibana, S. Yamate, and S. Kawamura. Encoderless robot motion control using vision sensor and back electromotive force. In *2014*

*IEEE/RSJ International Conference on Intelligent Robots and Systems*, pages 1609–1615, Sept 2014.

[159] R. Nishida and S. Kawamura. A new feedback robot control method based on position/image sensor integration. In *2012 IEEE/RSJ International Conference on Intelligent Robots and Systems*, pages 5012–5017, Oct 2012.

[160] Alan N. Gent. Elasticity. In *Engineering with Rubber*, pages 37–88. Hanser, third edition, 2012.

[161] Easy Composites. Technical Datasheet. `http://easycomposites.co.uk/downloads/TDS/EC-TDS-Addition-Cure-Silicone-Rubber.pdf`. Accessed: 2016-12-22.

[162] Smooth-On. Ecoflex Series. `https://www.smooth-on.com/tb/files/ECOFLEX_SERIES_TB.pdf`. Accessed: 2016-12-22.

[163] A.N. Gent. Elastic instabilities in rubber. *International Journal of Non-Linear Mechanics*, 40(2–3):165–175, 2005.

[164] Honeywell. ASDX Series Silicon Pressure Sensors. `http://www.farnell.com/datasheets/1850579.pdf?_ga=1.244440389.115337667.1482958853`. Accessed: 2014-12-22.

[165] Oleg Ivlev. Motion Therapy Devices based on Rotary Soft Fluidic Actuators - Concept and Prototyping. In *Technically Assisted Rehabilitation*, 2009.

# Appendix A

# Practical Discussions

This appendix chapter is dedicated to providing discussions about key information and challenges that impacted on the work in general. Discussion regarding the failures encountered while working with silicone rubber for attachment design as well as for pneumatic actuation purposes are presented. A major reoccurring issue is air leakage with a number of factors contributing as would be discussed.

## A.1 Air Leakage

The fundamental problem that is encountered in any fluid-based design e.g. in pneumatics systems is leakage. Leakage can occur as a result of several factors presented by the following:

One is the leakage as a result of air bubbles in cured silicone rubber. If air is dissolved in the mixed liquid silicone rubber, holes created as a result of the bubbles will remain in the cured form. These locations create potential failure points and would continue to degenerate as the interior cavity of the rubber actuator is inflated with air pressure. Conditions where a degassing vacuum chamber in used do not guarantee the complete removal of air bubbles if curing is carried out under standard atmospheric conditions as air is soon introduced into the liquid rubber. This is because rubber consists of interwoven long chain molecules possessing a relatively large amount of free volume as a result of few crosslinks, which gives rise to high permeability and absorption of gases from the atmosphere when in liquid state.

Second is air leakage as a result of joining two different silicone grades with each other. Two identical elastomers adhere when glued together with the same uncured elastomer

as long as both surfaces remain in intimate contact. This excellent adhesion is due to interdiffusion of curatives during the early stages of cure that allow interfacial crosslinks to form. Although liquid silicone bonds well with cured silicone with excellent adhesion to each other, the difference in tensile properties created as a result of the different grades of silicone causes there to be increased stress on the silicone layer with a lesser tensile strength. The result of this is failure and hence leakage in the soft silicone part when subjected to high air pressure while the hard silicone part is left undamaged. While one can argue that the combination of both silicone grades should the subjected to reasonable air pressure limit which is within the working range of the soft silicone, a compromise has to be reached because this solution would lead to a reduction in performance especially in the case of the bending robot where the bend is on the hard silicone layer and increased pressure leads to an increase of bending angle.

Third is leakage at the insertion position of air tubing with the soft robot. While this can be easily curtailed by using silicone tubing as liquid silicone could then be used to seal open edges which together with the silicone tube would produce an excellent seal, it is noteworthy to mention this so that an individual starting out with silicone rubber actuators do not make use of polyurethane hose to feed air directly into a silicone rubber actuator. This should be ensured so that time is not wasted unnecessarily in fixing what could be easily prevented.

Forth is air leakage resulting from the limitations of the actuation components such as the air pump, vacuum pump and control solenoid valves. The specifications including leakage parameters of the hardware control components used in this work as obtained from the corresponding datasheets have already been specified in the characterisation chapter. Readers willing to follow up on this work should note that the hardware control components chosen will have significant effect on the results obtained not only in terms of the extent of air leakage but also actuation speed.

Silicone rubber or rubbers in general experience a strikingly non-uniform deformation under large deformations especially if the layer is thin (typically $< 1.5mm$). This can also be observed from some of the pictures that have been presented where one portion of the rubber is highly distended (bulging) while the rest remains less inflated (Figures 4.22, 8.8, 9.1, 9.4b). Other illustrative pictures are seen in Figure A.1. This phenomenon has been found to be neither as a consequence of deficiency in manufacturing procedure, nor as a result of weakness of the rubber material itself but have been found to be comparable with Eulerian buckling - arising from the unique ability of rubber to undergo

large elastic deformations. The part undergoing bulging can grow very large and failure would occur as this affected portion can no longer withstand any slight increase in air pressure, hence air leakage would occur soon after. It was this experience that gave rise to the reinforcement of rubber with interwoven mesh which comes at the expense of reduction in the range of movement that should normally be expected.

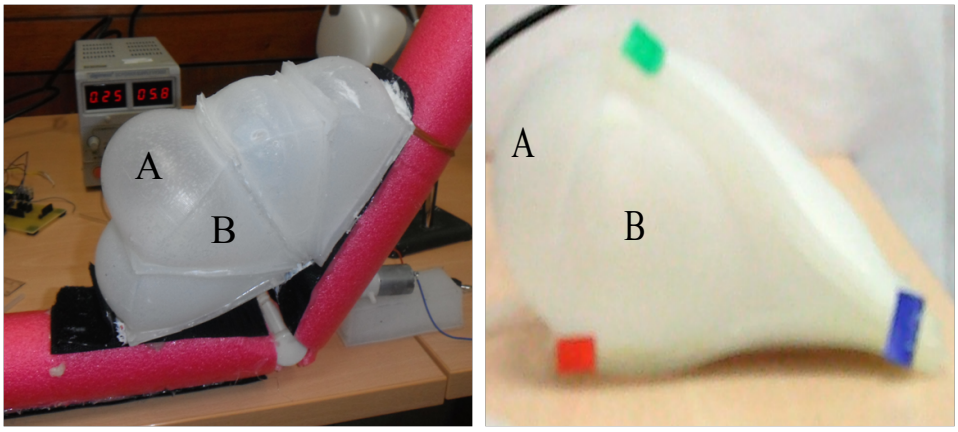


(a) (b)

Figure A.1: For both actuators, face A of the actuator is highly distended while face B and other modules are less inflated. As soon as this happens, the highly distended face will grow weaker at a fast rate and would fail.

Even under perfect conditions, air leakage is normally expected because the structure of silicone rubber as a polymer consist of long molecules that tangle up like cooked spaghetti meaning that there are spaces or "free volume" in between its molecular chains so that gas molecules pass through the cured compound as was discussed in Chapter 3. This reoccurring issue of air leakage offers a potential research direction in which soft actuators are able to repair themselves when damaged instead of the user or manufacturer having to repair it.

## A.2 Attachment

The purpose of the soft actuators that have been developed was towards the goal of assisting upper-limb motion, therefore attachment method was an important parameter to be considered. This section discusses the developmental process that was arrived at in designing various attachments used.

To solve the problem of attachment, silicone rubber were first considered being that silicone constitutes the actuator material itself and also to ensure comfort of wearing and secure fitting. This was achieved by making the arm bands moulded with soft silicone rubber while the forearm was fabricated using hard silicone. This was done because soft silicone has high extension ratio and could stretch to more than 500% of its original length, therefore would be comfortable to the user when wearing and adjusting. However, the downside of this method is that the attachment is not firm due to increased elasticity. That was why the forearm attachment was moulded using hard silicone to create a firm attachment while making it easy to take off since it is worn about the wrist. In spite of this solution, the area of contact with the skin was not large enough and therefore, attachment was not very stable.

Another solution was the use of only Velcro to attach to a dummy joint as illustrated in Figure A.1a. The result of this approach is that the soft actuator begins to slide out of place as it undergoes inflation and as the angle begins to increase. Furthermore, it is impossible to implement this attachment method to the surface of the human skin.

The chosen solution was through the use of Neoprene fabric with Velcro straps consisting of hook and loop fasteners sewn on the fabric. To adhere this fabric with silicone rubber, Neoprene fabric was embedded into two separate cured silicone layers each 2mm thick, with liquid silicone used as glue in between. Neoprene fabric is well suited for contact with the human skin because it is elastic and resilient. Neoprene fabric is stretchable so the change in modulus of elasticity from silicone rubber to the fabric is much less and so bonding forms well. A minor issue with this approach is that after prolonged use, the bond between neoprene fabric and silicone rubber begins to wear away because the location at which silicone rubber is joined with another material other than silicone constitutes a potential failure location. Another problem associated with the Velcro method of attachment was that the fixed attachment provided by this design led to constraining the elbow such that it moves only through the range of motion provided by the level of flexibility at which the arm and forearm were fastened even though the range of extension of the soft modules was still considerable. This led to the attachment method where the assistive actuator was glued to a PETG plastic sheet then placed on a supporting table while a user places his/her forearm on the actuator.

# Appendix B

# Publications

This chapter presents publications of this work which are being submitted and have been published in peer review conferences and journals. These papers are shown in the next pages.

# Appendix C

# Ethical Approval & Risk assessment

This appendix chapter presents the ethical approval and associated material that was used to conduct the participants experiments in Sections 8.4 and 9.2.2. The application includes submission, information, consent and questionnaire forms used. It also includes the risk assessment form for silicone rubber actuator production; these forms are presented in the following pages.

**SBS Local Research Ethics Committee**

University of Reading

# Project Submission Form

Note All sections of this form should be completed. Please continue on separate sheets if necessary.

Principal Investigator: Dr. Yoshikatsu Hayashi

School: Biomedical Engineering Section, School of Biological Sciences

Title of Project: Development of Soft Modular Robotics

Proposed starting date: January 30, 2017

Brief description of Project:

Soft robotics is an emerging field in robotics that makes use of squishy, compliant and elastic materials such as rubber. These materials exhibit large deformation and similar to inflatable toys. Soft robots are flexible, compliant and resilient, they offer little resistance to compressive forces and therefore fully adapted to be used in direct attachment with the skin. These features provide inherent safety from the perspective of the user. In comparison with rigid-bodied robots, soft robots have a number of advantages such as possessing extremely low inertias, which reduces the metabolic cost of wearing them; They intrinsically transmit moments through biological joints since they only apply tensile forces; Since they are composed of elastic material, they are easy to put on and take off. Recently, soft robots have received increasing attention due to their obvious advantages of high flexibility and safety. To work towards the goal of providing assistive motion using soft robots, we have proposed a new paradigm of assistive devices that make use of 100% silicone rubber and interface with the body through this soft structure. We also use soft plastic bag actuators to actuate the passive, light weight Wilmington Robotic Exoskeleton (WREX) in order to provide elbow and shoulder assistance.

I confirm that to the best of my knowledge I have made known all information relevant to the School Research Ethics Committee and I undertake to inform the Committee of any such information which subsequently becomes available whether before or after the research has begun.

I confirm that a list of the names and addresses of the subjects in this project will be compiled and that this, together with a copy of the Consent Form, will be retained within the School for a minimum of five years after the date that the project is completed.

Signed

…… (Investigator) Date……

…… (Head of School) Date……

…… (Student -where applicable) Date……

**Checklist**

1. This form will be submitted to the School Research Ethics Committee and will subsequently, if approved, be signed by my Head of School (or authorized Head of Department) ☑

2. The Consent form includes a statement to the effect that the application has been reviewed by the University Research Ethics Committee and has been given a favourable ethical opinion for conduct ☑

3. I have made, and explained within this application, arrangements for any confidential material generated by the research to be stored securely within the University and, where appropriate, subsequently disposed of securely. ☑

4. I have made arrangements for expenses to be paid to participants in the research, if any, OR, if not, I have explained why not. ☑

5. EITHER

   (a) The proposed research does not involve the taking of blood samples; ☑

   OR

   (b) For anyone whose proximity to the blood samples brings a risk of Hepatitis B, documentary evidence of protection prior to the risk of exposure will be retained by the Head of School. ☐

   Signed ……. (Head of School or authorized Head of Department)
   Date…….

6. EITHER

   (a) The proposed research does not involve the storage of human tissue, as defined by the Human Tissue Act 2004; ☑

   OR

   (b) I have explained within the application how the requirements of the Human Tissue Act 2004 will be met. ☐

7. EITHER

   (a) The proposed research will not generate any information about the health of participants; ☑

   OR

   (b) In the circumstance that any test reveals an abnormal result, I will inform the participant and, with the participant's consent, also inform their GP, providing a copy of those results to each and identifying by name and date of birth; ☐

OR

(c) I have explained within the application why (b) above is not appropriate. ☐

8. EITHER

(a) the proposed research does not involve children under the age of 5; ☑

OR

(b) My Head of School has given details of the proposed research to the University's insurance officer, and the research will not proceed until I have confirmation that insurance cover is in place. ☐

Signed ……. (Head of School or authorised Head of Department)
Date……..

This form and further relevant information (consent form and information sheet) should be returned electronically to: Dr. M. Alejandra Perotti (m.a.perotti@reading.ac.uk). You will be notified of the Committee's decision as quickly as possible, and you should not proceed with the project until a favourable ethical opinion has been passed.

School of Biological Sciences

APPLICATION FORM

| SECTION 1: APPLICATION DETAILS |
|---|
| |
| 1.1<br>Project Title: Development of Soft Modular Robotics<br>Proposed start date: 30/01/2017 Proposed end date: 28/02/2017 |
| 1.2<br>Principal Investigator [supervisor name, if student project] Dr Yoshikatsu Hayashi<br>Office room number: 157 Internal telephone: 01183785024<br>Email address: y.hayashi@reading.ac.uk<br><br>Other applicants (role): Victoria Oguntosin (PhD Student)<br>Department: Biomedical Engineering<br>Email address: v.w.oguntosin@pgr.reading.ac.uk |
| 1.3<br>Project Submission Declaration<br><br>I confirm that to the best of my knowledge I have made known all information relevant to the Research Ethics Committee and I undertake to inform the Committee of any such information which subsequently becomes available whether before or after the research has begun.<br><br>I understand that it is a legal requirement that both staff and students undergo Criminal Records Checks when in a position of trust (i.e. when working with children or vulnerable adults).<br><br>I confirm that a list of the names and addresses of the subjects in this project will be compiled and that this, together with a copy of the Consent Form, will be retained within the School for a minimum of five years after the date that the project is completed.<br><br>Signed…… (Principal Investigator) Date:……<br>Signed…… (Student) Date:…… |
| 1.4<br>University Research Ethics Committee Applications<br><br>Projects expected to require review by the University Research Ethics Committee must be reviewed by the Chair of the School Ethics Committee or the Head of School before submission.<br><br>Signed……N/A…… (Chair of School Committee) Date:…N/A……<br>Signed……N/A…… (Head of School) Date:…N/A…… |
| 1.5 |

External research ethics committees

Please provide details below of other external research ethics committees to which this project has been submitted, or from whom approval has already been granted [e.g. NHS Committee]

| Name of committee | Date of submission/approval | Reference | Status |
|---|---|---|---|
| N/A | N/A | | |
| | | | |

SECTION 2: PROJECT DETAILS

2.1

**Lay Summary**

Soft Module
This study aims to evaluate the usability of a novel soft robotic module for providing elbow movement assistance. The soft robot consists of a wedged-shaped silicone rubber actuator (as shown in Addendum, Fig 1) actuated by means of low air pressure pneumatics. The actuator material is elastic and highly stretchable, similar to rubber-based air balloons toys and is very safe for use near humans. The working air pressure is less than 3psi and the maximum torque is 2.7Nm, which is a relatively small range of the force, thus, will not damage the joints. The soft actuator is designed to be wearable via neoprene Velcro attachments. It is designed for elbow flexion and extension motions. To obtain visual information regarding angle of motion, colour tracking is done.

Exoskeleton
This study aims to evaluate the usability of soft plastic bag actuators (Addendum, Fig 2a) for providing elbow and shoulder movement assistance. The exoskeleton is a 3D printed structure with four degrees of freedom (Addendum, Fig 2b), two joints make use of elastic rubber bands to lift the arms against gravity. This exoskeleton is a replica design of the WREX exoskeleton which have been commercialised to assist children with muscular dystrophy to move their upper limb using the little residual strength they possess. The original device is completely passive, having no actuators. We modified the exoskeleton by introducing soft plastic bag actuators driven by means of low air pressure pneumatics. The actuator material is polythene plastic similar to bags used in groceries shopping and is very safe for use near humans. The working air pressure is less than 3psi and the maximum torque it can produce is 4Nm, which is a relatively small range of the force, thus, will not damage the joints. The structure is designed for shoulder and elbow planar movements. To acquire data relating to reaching motions, colour tracking is carried out.

2.2

**Procedures**

In this study, the subjects will be attached to the soft robot and exoskeleton for

10 minutes respectively while actuation to move the robot for reaching tasks will be carried out. At the end of a session, a subject will then be required to appraise their experience with the soft robot by answering a questionnaire and/or few verbal questions. There will be a video recording of only the motion of the participant while action cycles are performed.

The details of the experimental procedure are given below:

- After providing written informed consent, the participant will be physically shown the soft actuator and exoskeleton. Then there will be an oral explanation of the expected functionality. A video will also be shown demonstrating the expected movement. There will be a demonstration of how to stop the system at any time during the task.
- The investigator will then attach the soft robot and exoskeleton to the subject, the colour markers will also be worn on the subject. The investigator will ask to ensure the robot is comfortably positioned, on receiving an affirmative response, the experiment will begin.
- When the subject is ready, the investigator will first start the control system to execute reaching, flexion and extension movements to run for 10 minutes. Pressure and visual tracking information to measure angle of motion will be recorded during this period.
- After completing the above task, the subject will be required to judge their experience with the soft robot by filling out a questionnaire (see attached questionnaire) and/or few verbal questions. Concretely, they will be questioned about the usability, comfort and safety while using the soft robot.

2.3

**Location and Duration:**

The study will be conducted at University of Reading, Systems Engineering building, Room 187. The expected duration of a subject participation in the study is approximately 20 minutes.

2.4

**Funding**

This project is a self-funded project, not supported by any external sources

2.5 **Ethical Issues**

**a. Benefits:**
There are no benefits to taking part in this research. The participants will gain state-of-the-art knowledge of soft robotics research being conducted at University of Reading, and may derive satisfaction from helping to improve the soft assistive module.

**b. Risks to participants:**
The risks include the following: Injury resulting from contact with the soft actuator or exoskeleton; Irritation of silicone rubber; Anxiety related to the robot's proximity to the participant; Breach of confidentiality

**c. Risk management:**

To minimize risk of injury for the soft modules:

The soft actuator is made completely of stretchable rubber actuated with air pressure. This concept can be thought of as air balloons commonly used by children as toys which is unlikely to cause physical injury. Preliminary investigations by soft robotics researchers support this intuition, and this has also been our experience in the development of soft robots. Furthermore, an attachment of this soft actuator is also made of elastic neoprene material which is a stretchable fabric clothing. Therefore, accidental physical contact with the soft robot poses minimal risk to the subject.

To minimize risk of injury for the exoskeleton:
The exoskeleton is a 3D printed structure with ABS plastic material. The exoskeleton is a replica of the WREX which have been approved for use by children to help in elevating their upper arm. The plastic bag is a polythene plastic material actuated with air pressure. This concept of actuation is similar to inflatable toys used by children which is unlikely to cause physical injury. Preliminary investigations by researchers that developed the exoskeleton support this intuition, and this has also been our experience since the development of the exoskeleton with plastic bag actuation. Therefore, accidental physical contact with the system poses minimal risk to the subject.

To minimize risk of irritation for the soft modules:
Cured silicone rubber is skin safe and poses no irritation when in contact with the skin. Also the neoprene fabric used as attachment is a safe clothing material and unlikely to cause irritation. Furthermore, the soft robot will be kept in a clean environment.

To minimize anxiety:
Subjects will be informed of the functionalities of the soft robot and exoskeleton before interacting with it, a video recording of the expected movement will also be shown to the subjects prior to the start of the experiment. In addition, the control system for the soft actuator is pre-programmed to work within low air pressure (not exceed 3 psi operating pressure). The soft robot can likewise be controlled with the use of a controller circuit consisting of the air pumps and valves by the investigator using keyboard and ON/OFF control switch. Also, the participating subject can control the circuit using the switch. Furthermore, all power to the soft robot can be completely shut off at any time by the investigator using the power supply switch. On disconnecting the air tubes of the soft actuator from the connector that feeds into the air pump, the soft actuator loses all torque and does not maintain its position but rather gradually returns to its rest position. On disconnecting the air tubes, the exoskeleton becomes passive. The participant can easily remove the arm from the exoskeleton as there are no fasteners to attach the arm to the exoskeleton

To minimize risk of breach of confidentiality:
All study data will be coded by assigning a unique case number. The information linking the case number to the subject's identity will be stored electronically in a secure machine managed by the university servers. The study data and consent forms will be stored in separate secure cabinets at

University of Reading, Brain Embodiment Lab, with access available only to the investigators involved in the study. All email correspondence with prospective subjects will be carried out via the secure university email account that is accessible by only the investigator of the study. The electronic data recorded from each participant will be stored safely on internal university servers. As part of the video recording, the face of the participants will not be recorded, only the motion of the elbow will be recorded.

**d. Degree of physical or psychological risk:**
The risks identified in 2.5c above are minimal risks. The probability and magnitude of harm or discomfort anticipated have been minimized by various materials, hardware design choices and by following ethics protocol.

2.6

**Deception**

This research will not involve any kind of deception. No data will be omitted and correct information will be provided to the participants and in research publications.

2.7

**Payment**

Participants will be compensated for this study with £5 in cash

2.8

**Data storage, data protection and confidentiality**

Data protection and confidentiality will be ensured during and after the experimentation. Data collected in this experiment is of two categories- 1) Digital: air pressure data, videos and 2) Hard copy: participant consent form and anonymised questionnaire.

**a. Questionnaires:**
A questionnaire relating to subject assessment of the soft actuator in providing shoulder and elbow movements will be filled by the participants. Personal identifiers such as name, signature, age and gender will be collected. These will be translated into a unique identifier. The questionnaires will be anonymised using the participant's unique identifier. Electronic files will be stored for 10 years, in password protected university computer, accessible by only the investigators assigned to the study. Questionnaires will be stored securely in a separate locked cabinet in BEL. BEL is a restricted access laboratory and only BEL researchers performing experiments will have access to the consent form cabinet and questionnaire cabinet. Questionnaires will be destroyed 5 years after completion of the project.

**b. Photos and Videos:**
Video recording of only the elbow movement of the participant will be made. Participants' unique identifiers will not be included in these recordings. Videos of the experiment will also be anonymised and stored in the secure shared BEL drive detailed above. Photos and videos would only be taken upon receiving explicit written consent from the participants and they can opt out of it. Under no circumstances, the participant will be identifiable in the photos or videos. Face of the participant will not be captured and hence will not be visible in the imagery. Only with explicit written consent from the participants, their imagery might be used in the scientific publications and the

rules of the scientific journal for sharing will apply.

**c. Consent forms:**
Consent form is the only document that will contain participant's name. Signed consent forms will be stored securely in the locked cabinet storage facility in BEL which is exclusively for the consent forms. No other information will be stored along with these consent forms in this cabinet. Consent forms will not be shared with the third parties. Consent forms will be destroyed after 6 years following the date of completion of the experiment. Data sharing will be in accordance with research data management policy set out by the University of Reading (http://www.reading.ac.uk/web/files/reas/RDM_Policy_1-0.pdf)

**d. Data Access:**
Only the investigators assigned to this study will have access to the data obtained.

**e. Protection of participant confidentiality and secure research records:**
All study data will be coded by assigning a unique case number. The information linking the case number to the subject's identity will be stored electronically in a secure machine managed by the university password protected servers. The study questionnaire data and consent forms will be stored in separate secure cabinets at University of Reading, Brain Embodiment Lab, with access available only to the investigators involved in the study.

**f. Process for monitoring data to ensure that study goals are met:**
Analysis on the data collected will be performed by the investigators involved in the study. Weekly meetings to review the study progress will be held to ensure study procedures are being followed and to discuss any unforeseen concerns that might have arisen during the study.

2.9

**Consent**

Consent forms will be used (see attached consent form), presented in paper format. Subjects participate in this study of their own free will. They may at any time withdraw without providing reason.

SECTION 3: PARTICIPANTS DETAILS

3.1

**a. Class:**
Subjects are required to be healthy adults volunteers, aged 18 and over, without any disability

**b. Number of participants:**
A small sample of 10 participants will be recruited. There has been no analysis to determine the sample size. We anticipate that this small number of participants will be sufficient.

**c. Estimate ratio of males to females:**
50:50

**d. Inclusion and Exclusion Criteria:**
Inclusion criteria:

- Age 18 and over
- Able to read and understand the nature of the study and consent process

| | |
|---|---|
| | Exclusion criteria:<br>• Any physical or mental disability |
| 3.2 | **Participant Recruitment**<br><br>Participants will be solicited using flyers at University of Reading (see attached flyer) |

## Addendum:
## Development of Soft Modular Robotics

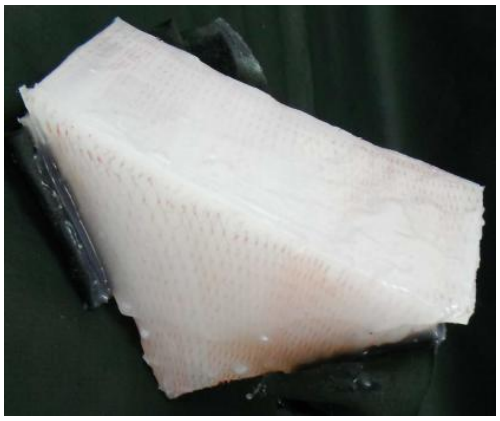

Fig 1: Soft Robotic Module designed for providing elbow movement assistance. Fabric neoprene attachment is used to attach to the participant to make it wearable. The soft module is actuated with air pressure which causes its angle to change.

Fig 2a: Polythene plastic bag used to actuate the exoskeleton to cause rotary motion

Fig 2b: A light weight, passive 3D printed WREX exoskeleton having four degrees of freedom movement. Soft plastic bags attached to two joints lead to the creation of two active joint to provide elbow and shoulder movement assistance. The plastic bag actuators when inflated with compressed air produce rotary motion of the joints.

*Researcher (principal)*: Dr. Yoshikatsu Hayashi
*Email*: y.hayashi@reading.ac.uk
*Phone*: +44 (0) 01183785024

*Researcher (role)*: Victoria Oguntosin (PhD Student)
*Email*: v.w.oguntosin@pgr.reading.ac.uk

University of Reading
**School of Biological Sciences**
Biomedical Engineering Section
University of Reading
Reading RG6 6AY

*Phone:* +44 (0) 118 378 8072
*email:* biosciences@reading.ac.uk

# INFORMATION SHEET

## Project Title: Development of Soft Modular Robotics

### Background

The purpose of this study is to evaluate the usability of assistive soft robots for providing elbow movement assistance. Data obtained from the study will be used to analyse, improve the design usability and functionality of the device.

The soft robot consists of a wedged-shaped silicone rubber actuator controlled by means of low air pressure pneumatics. The actuator material is elastic and highly stretchable, similar to rubber-based air balloons toys and is very safe for use near humans. The working air pressure is less than 3psi and the maximum torque is 2.7Nm. The soft actuator is designed to be wearable via neoprene Velcro attachments. It is designed for elbow flexion and extension motions. To obtain visual information regarding angle of motion, colour tracking is done.

The purpose of this study is also to evaluate the usability of soft plastic bag actuators with an exoskeleton for providing shoulder and elbow movement assistance. Data obtained from the study will be used to analyse, improve the design usability and functionality of the soft actuator. The exoskeleton is a 3D printed structure with four degrees of freedom; two joints make use of elastic rubber bands to lift the arms against gravity. This exoskeleton is a replica design of the WREX exoskeleton which have been commercialised to assist children with muscular dystrophy to move their upper limb using the little residual strength they possess. The original device is completely passive, having no actuators. We modified the exoskeleton by introducing soft plastic bag actuators driven by means of low air pressure pneumatics. The actuator material is polythene plastic similar to bags used in groceries shopping and is very safe for use near humans. The working air pressure is less than 3psi and the maximum torque it can produce is 4Nm, which is a relatively small range of the force, thus, will not damage the joints. The structure is designed for shoulder and elbow planar movements. To acquire data relating to reaching motions, colour tracking is carried out.

### Why are we doing this study?

Soft robots are flexible, compliant and resilient. They offer little resistance to compressive forces and therefore are fully adapted to be used in direct attachment with the skin. These features provide inherent safety from the perspective of the user. In comparison with rigid-bodied robots, soft robots have a number of advantages such as possessing extremely low inertias, which reduces the metabolic cost of wearing them. This study will help in studying the use of soft robots for providing elbow movements.

This study will also help in studying the use of soft plastic bag actuators for providing shoulder and elbow movements for healthy adults.

### What is the purpose of the study?

The purpose of this study is to gather preliminary evidence of the usability of a novel soft robotic module and plastic bag actuators for providing shoulder and elbow movement assistance to healthy adults. Data obtained from the study will be used to analyse, improve the design usability and functionality of the device.

**Who is eligible to participate in the study? Why have I been invited?**

Participants are required to be healthy adult volunteers, aged 18 and over.

**How can you be involved?**

You will wear the soft robot and exoskeleton for 10 minutes respectively while actuation to move the robot for reaching tasks will be carried out. At the end of a session, you will then be required to appraise your experience with the soft robot by answering a questionnaire and/or a few verbal questions. There will be a video recording of only your motion while action cycles are performed.

You can email Victoria Oguntosin at v.w.oguntosin@pgr.reading.ac.uk regarding participation.

**Do I have to take part?**

Subjects participate in this study of their own free will. You may at any time withdraw without providing reason and this will be without detriment.

**What will be involved if you take part?**

The details of the experimental procedure are given below:

- After providing written informed consent, you will be physically shown the soft actuator and exoskeleton. Then there will be an oral explanation of the expected functionality of the soft robot. A video will also be shown demonstrating the expected movement of the soft actuator. There will be a demonstration of how to stop the soft robot at any time during the task.
- The investigator will then attach the soft robot to your elbow, colour markers will also be worn. For the exoskeleton, the investigator will ask the subject to place the arm at the attachment point of exoskeleton. The investigator will ask to ensure the robot is comfortably positioned. On receiving an affirmative response, the experiment will begin.
- When you are ready, the investigator will first start the control system to execute flexion and extension movements to run for 10 minutes. Pressure and visual tracking information will be recorded during this period.
- After completing the above task, you will be asked to judge your experience with the system by filling out a questionnaire and/or a few verbal questions. Concretely, you will be questioned about the usability, comfort and safety while using the soft robot and exoskeleton.

**Confidentiality, storage and disposal of information**

You will be asked to provide your name and to sign a consent form so that we can keep a record of your participation in this study. All data recorded will be stored safely on internal university servers,

password protected. Ethical information and other paper work filled out will be stored in separate, secured and locked cabinets located in Brain Embodiment Lab.

**Are there any benefits/risks to taking part [e.g. health]?**

There are no benefits or health risks to taking part in this experiment. You will gain state-of-the-art knowledge of the soft robotics research being conducted at University of Reading.

**What expenses/payment or equivalent be made for participation in the study?**

You will be remunerated for your time and participation with £5.

**What will the results of the study be used for?**

The results of this study will contribute towards PhD research and scientific publications. Additionally, this experiment will also help in improving the soft robotic module. Any published results obtained from the study may be sent to you if you desire.

**Who has reviewed the study?**

This project has been subject to ethical review, according to the procedures specified by the University Research Ethics Committee and has been given a favourable ethical opinion for conduct.

**Contact details for further questions:**

Experiments and the research will be conducted by Victoria Oguntosin (v.w.oguntosin@pgr.reading.ac.uk) who is currently a 3rd year PhD student with Brain Embodiment Lab. Victoria is supervised by Dr Yoshikatsu Hayashi and Prof Slawomir Nasuto.

*Contact details*:

PI Name: Dr Yoshikatsu Hayashi

Email: y.hayashi@reading.ac.uk

Phone: +44 (0) 01183785024

**In the event of a complaint:**

If you have any comments or if you have a complaint, you can contact the Chair of the Ethics Committee of the School of Biological Sciences, Dr M. Alejandra Perotti Email: m.a.perotti@reading.ac.uk

**Thank you for your help.**

**Research Ethics Committee**

University of Reading

# Consent Form for Participation in Research

1. I have read and had explained to me by **Victoria Oguntosin** the accompanying Information Sheet relating to the project on **"Development of Soft Modular Robotics"**

2. I have had explained to me the purposes of the project and what will be required of me, and any questions I have had have been answered to my satisfaction. I agree to the arrangements described in the Information Sheet in so far as they relate to my participation.

3. I understand that participation is entirely voluntary and that I have the right to withdraw from the project any time, and that this will be without detriment.

   Optional Permission

   I understand that the researchers may want to use portions of any video recording for illustrative reasons in presentations of this work for scientific or educational purposes; I give my permission to do so provided that my name will not appear.
   ☐YES ☐NO (Please initial here _____)

4. This project has been subject to ethical review, according to the procedures specified by the University Research Ethics Committee and has been given a favourable ethical opinion for conduct.

5. I have received a copy of this Consent Form and the accompanying Information Sheet.

   Name……..

   Signed……

   Date……....

Investigator Contact Details:

Dr Yoshikatsu Hayashi
✉ y.hayashi@reading.ac.uk
☎ 01183785024

Victoria Oguntosin
✉ v.w.oguntosin@pgr.reading.ac.uk

University of Reading

## Development of Soft Modular Robotics

## Questionnaire

1. Rate the level of ease disabled persons will be able to move with the assistance of the soft actuator based on your experience with it. Tick one box.

| | | | | | | | | | |
|---|---|---|---|---|---|---|---|---|---|
| 1 extremely difficult | 2 | 3 | 4 | 5 | 6 | 7 | 8 | 9 | 10 extremely easy |

2. Overall, rate your level of comfort while using the soft modules. Tick one box.

| | | | | | | | | | |
|---|---|---|---|---|---|---|---|---|---|
| 1 totally uncomfortable | 2 | 3 | 4 | 5 | 6 | 7 | 8 | 9 | 10 totally comfortable |

3. How cautious were you about safety when using the soft robot. Tick one box.

| | | | | | | | | | |
|---|---|---|---|---|---|---|---|---|---|
| 1 extremely cautious | 2 | 3 | 4 | 5 | 6 | 7 | 8 | 9 | 10 definitely not cautious |

4. Imagine a situation that you were using this soft robot to provide you with elbow assistance. Do you think soft robots should be used in rehabilitation?
   ☐ Yes ☐ No

5. In general, to what extent would you prefer having a robot versus a human to provide assistance with moving or exercising your elbow, if you needed assistance?
   ☐ I definitely prefer robot
   ☐ I probably prefer robot
   ☐ I have no preference
   ☐ I probably prefer human
   ☐ I definitely prefer human
   ☐ I prefer the robot and human equally

6. Please describe the reason for your choice in Question 5
   _____
   _____
   _____

## Background Information

Please answer the following questions. All of your answers will be treated confidentially. **If you do not wish to answer a question, please leave it blank.** Thank you in advance for your help.

**Gender:** ☐ Male ☐ Female

**Age**…… (Should be more than 18 years old)

University of Reading

## Development of Soft Modular Robotics

## Questionnaire

1. Rate the level of ease disabled persons will be able to move with the assistance of the exoskeleton based on your experience with it. Tick one box.

| | | | | | | | | | |
|---|---|---|---|---|---|---|---|---|---|
| 1 extremely difficult | 2 | 3 | 4 | 5 | 6 | 7 | 8 | 9 | 10 extremely easy |

2. Overall, rate your level of comfort while using the exoskeleton. Tick one box.

| | | | | | | | | | |
|---|---|---|---|---|---|---|---|---|---|
| 1 totally uncomfortable | 2 | 3 | 4 | 5 | 6 | 7 | 8 | 9 | 10 totally comfortable |

3. How cautious were you about safety when using the exoskeleton with the plastic bag actuators. Tick one box.

| | | | | | | | | | |
|---|---|---|---|---|---|---|---|---|---|
| 1 extremely cautious | 2 | 3 | 4 | 5 | 6 | 7 | 8 | 9 | 10 definitely not cautious |

4. Imagine a situation that you were using this exoskeleton to provide you with shoulder and elbow assistance. Do you think this system should be used in rehabilitation?
   ☐ Yes ☐ No

5. In general, to what extent would you prefer having a robot versus a human to provide assistance with moving or exercising your shoulder and elbow, if you needed assistance?
   ☐ I definitely prefer robot
   ☐ I probably prefer robot
   ☐ I have no preference
   ☐ I probably prefer human
   ☐ I definitely prefer human
   ☐ I prefer the robot and human equally

6. Please describe the reason for your choice in Question 5
   _____
   _____
   _____

## Background Information

Please answer the following questions. All of your answers will be treated confidentially. **If you do not wish to answer a question, please leave it blank.** Thank you in advance for your help.

**Gender:** ☐ Male ☐ Female

**Age**…… (Should be more than 18 years old)

# PROJECT/ACTIVITY RISK ASSESSMENT FORM (RA2)

| | |
|---|---|
| **School/Service/Department:** | School of System Engineering |
| **Assessment Reference No.** | |
| **Assessment date:** | 03/07/2014 |
| **Activity assessed:**<br>*Please make sure this adequately describes the activity that you are assessing, including the location* | Production of soft actuators which involves moulding and handling of silicone in Engineering Building, room B05 and mechanical workshop, also involves the use of air pneumatics |
| **Person(s) at risk** | Student handling the materials, Victoria Oguntosin |

| Task/ Activity<br>*List significant steps in the activity.*<br>*Consider doing a separate risk assessment for each step, if the Task/Activity breaks down into substantial sub-components (in which case, delete this column)* | Hazard | Specific person(s) at risk<br>*If already listed above, leave blank, or delete this column* | Existing control | Impact* | Probability* | Risk outcome* | Additional controls required | Action by whom | By when |
|---|---|---|---|---|---|---|---|---|---|
| Handling and mixing parts A and B of silicone liquid<br><br>Operating a pneumatic system | Skin and eyes irritation<br><br>Airline coming loose<br>Sudden release of air | | Safety goggles, gloves and lab-coat available<br><br>Follow lab rules | Broadly acceptable<br><br>Broadly acceptable | Unlikely<br><br>Unlikely | Min or<br><br>Min or | | | |

# Appendix D

# Parts and Moulds

This chapter shows 3D CAD representation, 3D printed parts and moulds used in producing rubber actuators.

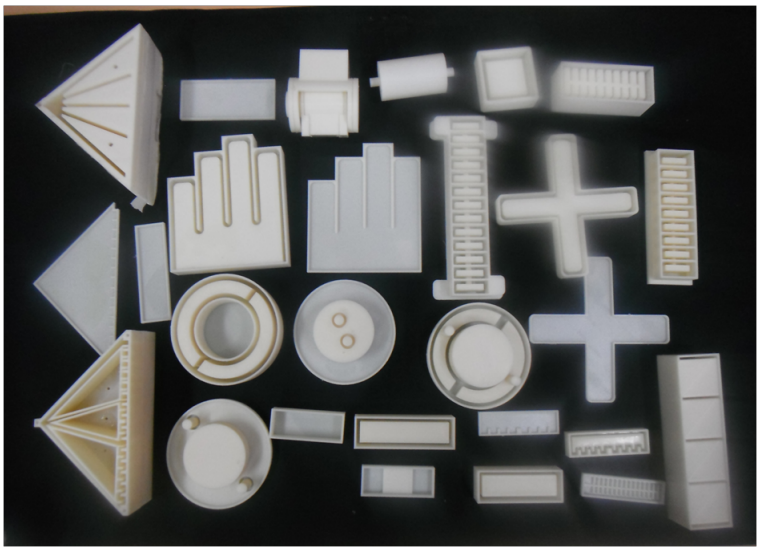

Figure D.1: Some 3D designs printed with ABS plastic.

Figure D.2: Some silicone soft robots produced using the 3D printed shapes in Fig. D.1.

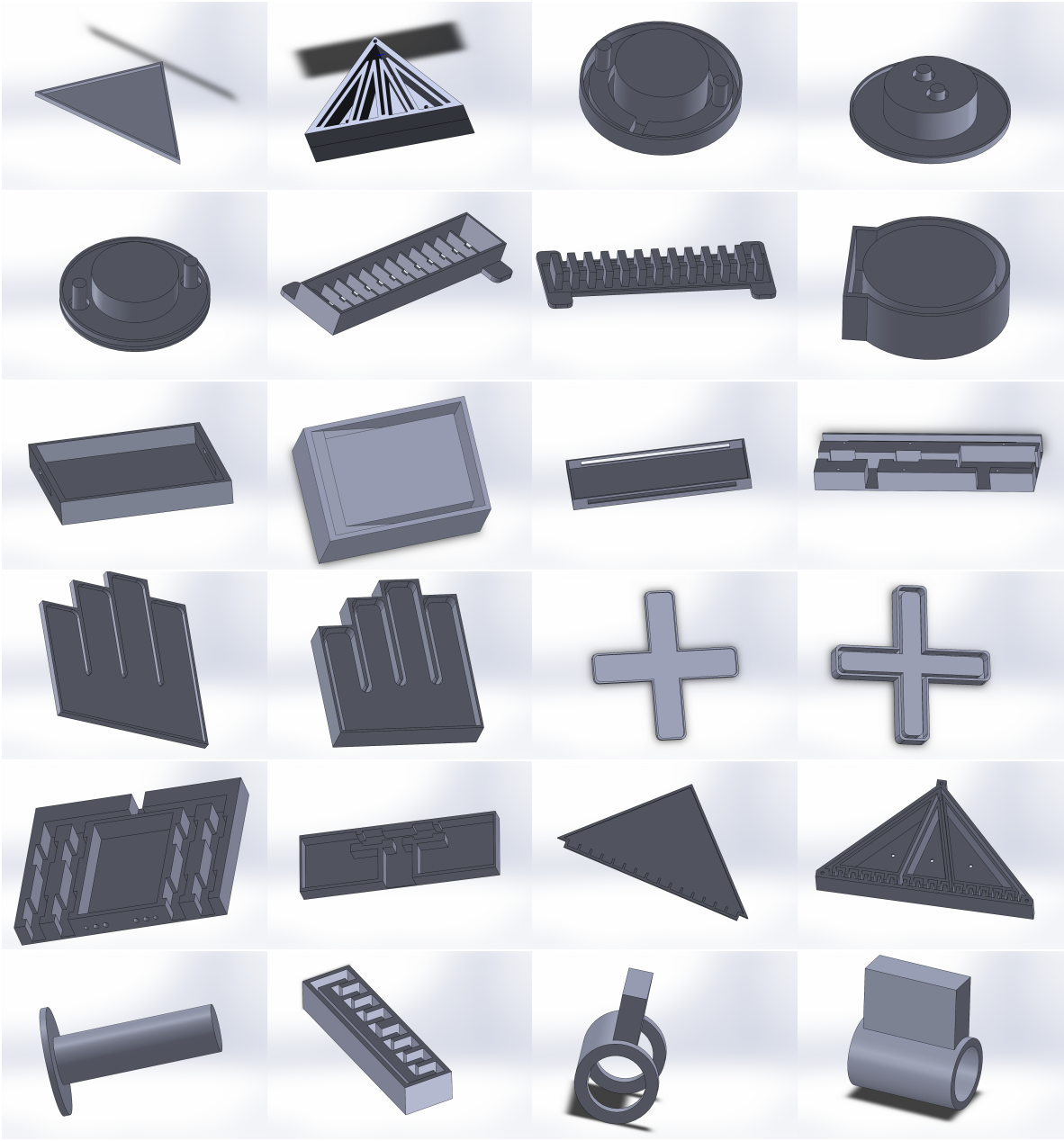

Figure D.3: Some designed SolidWorks parts, includes moulds, dummy joints, casing enclosure for hardware control components.

# Appendix E

# Circuit diagrams

This chapter shows the complete circuit diagrams for the hardware controller presented in Section 7.1.2; and are shown in the following pages.

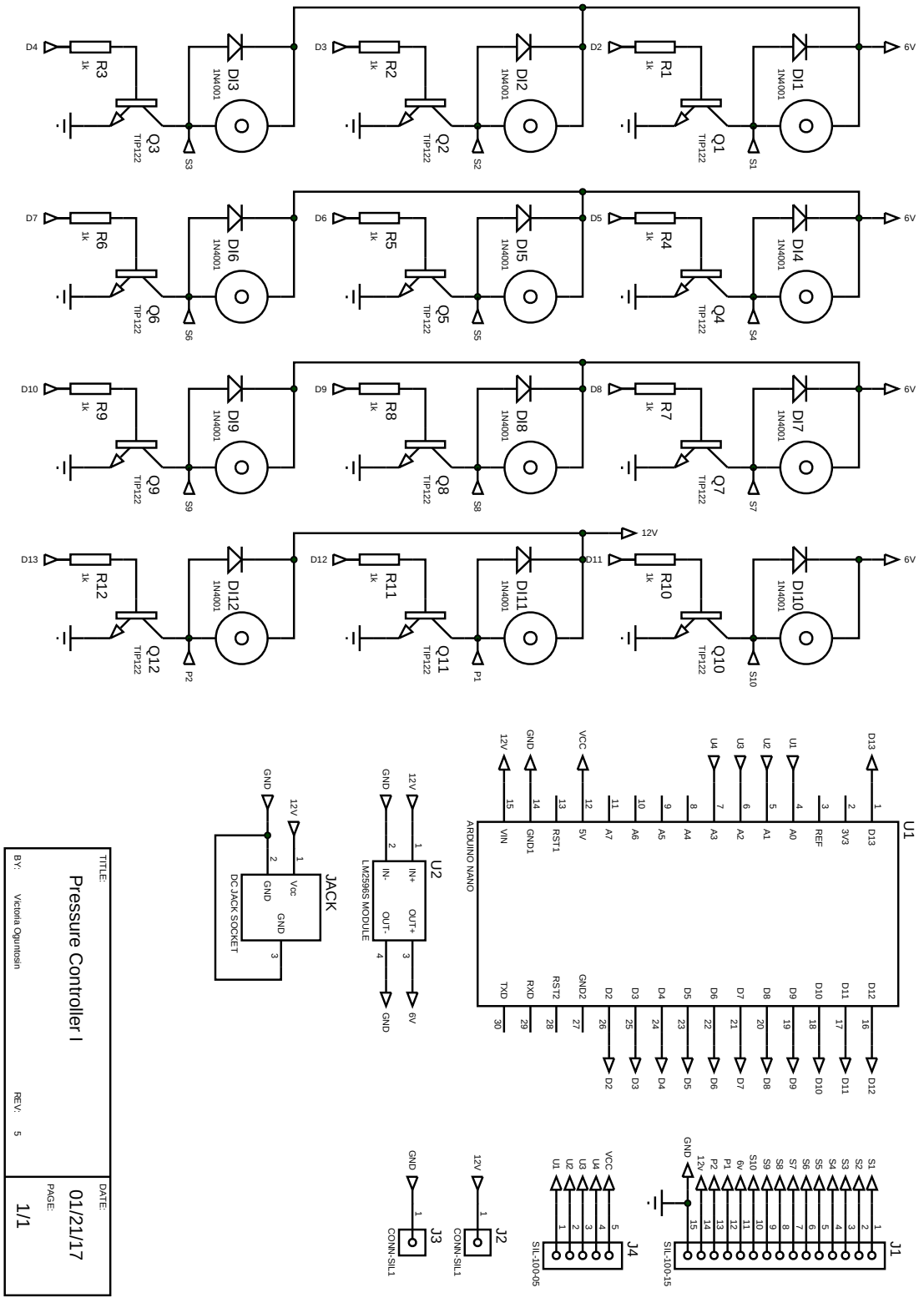


Figure E.1: Circuit Diagram I

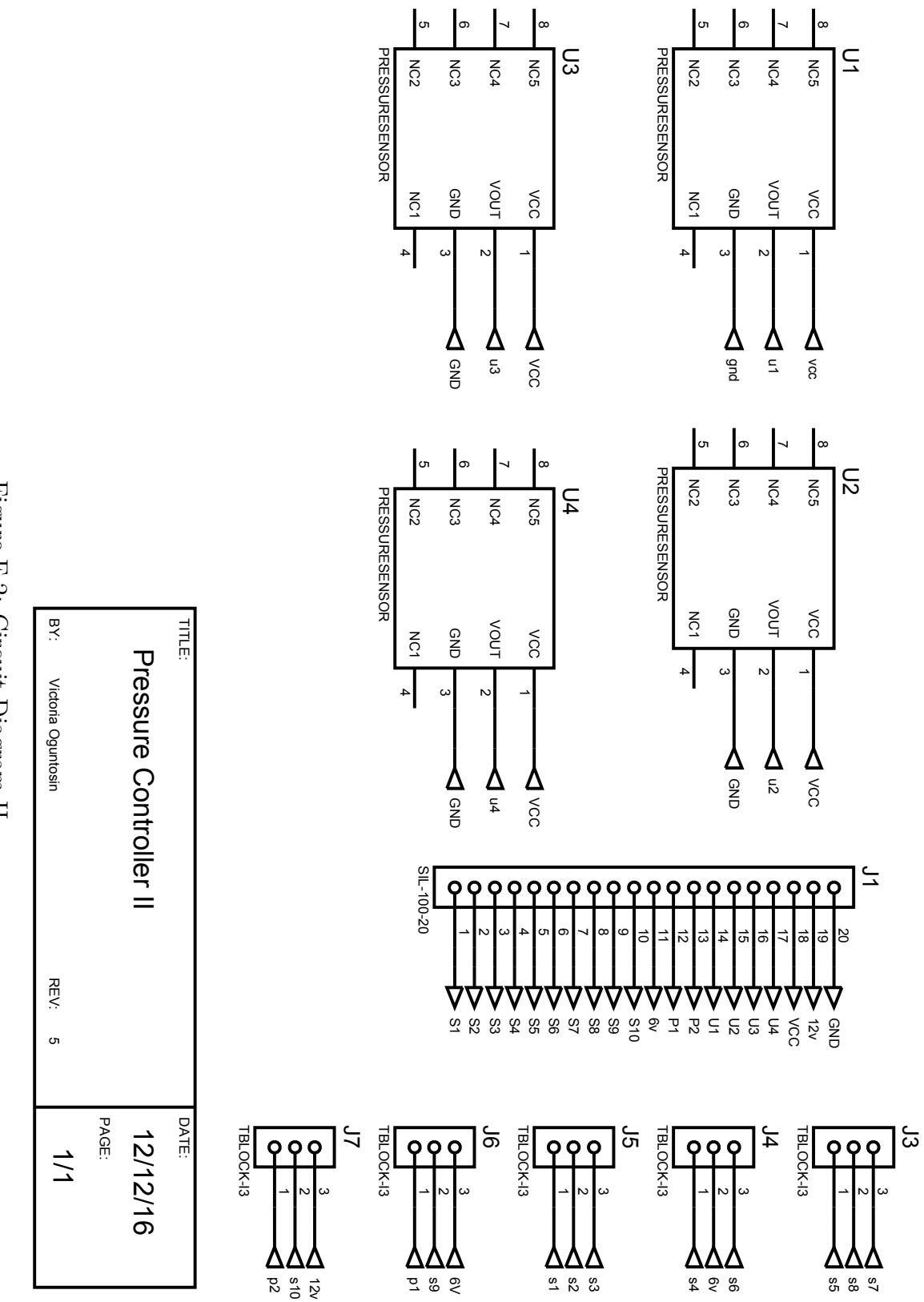


Figure E.2: Circuit Diagram II

# Appendix F

# Program Codes

Listing F.1: Microsoft Visual C++ Visual Processing Program

```
#include <iostream>
#include "SerialClass.h"
#include <string>

#include <stdio.h>
#include <stdlib.h>

#include <math.h>
#include <Windows.h>

#include <conio.h>

#include <opencv2/core/core.hpp>
#include <opencv2/highgui/highgui.hpp>
#include <opencv2/imgproc/imgproc.hpp>

using namespace std;

#define FRAME_WIDTH  320
#define FRAME_HEIGHT 240

#define PI 3.14159265

int thresh = 100;

FILE *fp  = fopen( "Data.csv", "w" );
int main(int argc, char** argv)  {

   fprintf(fp, "Angle,Pressure,Time[ms]\n");
   _int64 nowTime = 0;

   Serial* SP = new Serial("COM4"); //adjust as needed
   if (SP->IsConnected())
```

```
34    printf("We're connected");
35
36    char incomingData[256] = "";  //pre-allocate memory
37    int dataLength = 256;
38    int readResult = 0;
39
40    cv::VideoCapture mycamera(0); //capture video from webcam
41
42    if(!mycamera.isOpened()) {
43       printf("ERROR: Could not open webcam");
44       return -1;
45    }
46
47    //Create a window to display the images from the webcam
48    cv::namedWindow("MyWebcam", CV_WINDOW_AUTOSIZE);
49
50    int posX_red = 0; int posY_red = 0;
51    int posX_blue = 0;   int posY_blue = 0;
52    int posX_green = 0;  int posY_green = 0;
53
54    float length1 = 0;
55    float length2 = 0;
56    float length3 = 0;
57
58    float q = 0.0;
59    float qd = 180.0;
60
61    double dt = 0.001;
62    double error = 0.0;
63    double previous_error = 0.0; double integral = 0.0;
64    double derivative = 0.0;
65    int Kp = 1; int Ki = 1; int Kd = 1;
66    double output = 0.0;
67
68    cv::Mat src_img;
69    cv::Mat smooth_img;
70    cv::Mat hsv_img;
71
72    cv::Mat thresholded_img;
73    cv::Mat red_thresh_img;
74    cv::Mat red_threshold_output;
75    cv::Mat red_thresholded_img;
76    cv::Mat blue_thresh_img;
77    cv::Mat blue_threshold_output;
78    cv::Mat blue_thresholded_img;
79    cv::Mat green_thresh_img;
80    cv::Mat green_threshold_output;
81    cv::Mat green_thresholded_img;
82
83    while(1) {
84       mycamera >> src_img; //Capture next frame from the webcam
85
```

```
86      cv::medianBlur(src_img, smooth_img, 7);   //medianblur
87      cv::cvtColor(smooth_img, hsv_img, CV_BGR2HSV);  //RGB-HSV
88
89      cv::inRange(hsv_img, cv::Scalar(130, 165, 124),
90      cv::Scalar(179, 255, 255), red_thresh_img);
91      cv::inRange(hsv_img, cv::Scalar(111, 103, 85),
92      cv::Scalar(127, 255, 255), blue_thresh_img);
93      cv::inRange(hsv_img, cv::Scalar(71, 69, 154),
94      cv::Scalar(117, 255, 255), green_thresh_img);
95
96      // Detect edges using Threshold
97      cv::threshold( red_thresh_img, red_threshold_output,
98      thresh, 255, cv::THRESH_BINARY );
99      cv::threshold( blue_thresh_img, blue_threshold_output,
100     thresh, 255, cv::THRESH_BINARY );
101     cv::threshold( green_thresh_img, green_threshold_output,
102     thresh, 255, cv::THRESH_BINARY );
103
104     red_thresholded_img = red_threshold_output.clone();
105     blue_thresholded_img = blue_threshold_output.clone();
106     green_thresholded_img = green_threshold_output.clone();
107
108     // Get the red moments
109     vector<cv::Moments> mu_r(contours_red.size() );
110     for( int i = 0; i < contours_red.size(); i++ ) {
111        mu_r[i] = moments( contours_red[i], false );
112     }
113
114     // Get the blue moments
115     vector<cv::Moments> mu_b(contours_blue.size() );
116     for( int i = 0; i < contours_blue.size(); i++ ) {
117        mu_b[i] = moments( contours_blue[i], false );
118     }
119
120     // Get the green moments
121     vector<cv::Moments> mu_g(contours_green.size() );
122     for( int i = 0; i < contours_green.size(); i++ ) {
123        mu_g[i] = moments( contours_green[i], false );
124     }
125
126     //  Get the red mass centers:
127     vector<cv::Point2f> mc_r( contours_red.size() );
128     for( int i = 0; i < contours_red.size(); i++ ) {
129        mc_r[i] = cv::Point2f( mu_r[i].m10/mu_r[i].m00,
130        mu_r[i].m01/mu_r[i].m00 );
131        posX_red = mu_r[i].m10/mu_r[i].m00;
132        posY_red = mu_r[i].m01/mu_r[i].m00;
133     }
134
135     //  Get the blue mass centers:
136     vector<cv::Point2f> mc_b( contours_blue.size() );
137     for( int i = 0; i < contours_blue.size(); i++ ) {
```

```
138         mc_b[i] = cv::Point2f( mu_b[i].m10/mu_b[i].m00,
139         mu_b[i].m01/mu_b[i].m00 );
140         posX_blue = mu_b[i].m10/mu_b[i].m00;
141         posY_blue = mu_b[i].m01/mu_b[i].m00;
142      }
143
144      //  Get the green mass centers:
145      vector<cv::Point2f> mc_g( contours_green.size() );
146      for( int i = 0; i < contours_green.size(); i++ ) {
147         mc_g[i] = cv::Point2f( mu_g[i].m10/mu_g[i].m00,
148         mu_g[i].m01/mu_g[i].m00 );
149         posX_green = mu_g[i].m10/mu_g[i].m00;
150         posY_green = mu_g[i].m01/mu_g[i].m00;
151      }
152
153      // find the lengths: colour blue should be at the center
154      length1 = sqrt(pow((posX_red - posX_blue),2.0) +
155      pow((posY_red - posY_blue),2.0));
156      length2 = sqrt(pow((posX_blue - posX_green),2.0) +
157       pow((posY_blue - posY_green),2.0));
158      length3 = sqrt(pow((posX_red - posX_green),2.0) +
159      pow((posY_red - posY_green),2.0));
160
161      // calculate the current angle q
162      q = acos( (pow(length1, 2) + pow(length2, 2) -
163      pow(length3, 2))/(2*length1*length2) ) * 180/PI;
164
165      printf(" Angle: %f\n", q);
166
167      error = qd - q;
168      if ( error > 0 && error < 180) {
169         integral = integral + error*dt;
170         derivative = (error - previous_error)/dt;
171         output = Kp*error + Ki*integral + Kd*derivative;
172         previous_error = error;
173      }
174      printf(" PID Output: %f\n", output);
175      readResult = SP->ReadData(incomingData,dataLength);
176      std::string test(incomingData);
177
178      int k = atoi(incomingData);
179      nowTime = cv::getTickCount();
180      printf("Angle: %f\tPressure: %d\tTime: %d\n", q,k,nowTime);
181      fprintf(fp, "%f,%d,%d\n",q,k,nowTime);
182
183      cv::imshow("VISION-A", src_img);
184      cv::imshow("Red", red_threshold_output);
185      cv::imshow( "Blue", blue_threshold_output );
186      cv::imshow( "Green", green_threshold_output );
187
188      if (cv::waitKey(30) == 27) break;
189   }
```

```
190
191     fclose(fp);
192
193     return 0;
194 }
```

Listing F.2: Arduino Program

```
1  int sensorValue = 0;
2  float sensorVoltage;
3  float pressure = 0.0;
4  int incomingByte = 0;   // for incoming serial data
5
6  int airPump = 5;
7  int airValve = 9;
8  int vacuumPump = 6;
9  int  vacuumValve = 7;
10
11 int S1 = 2;   //S1
12 int S2 = 3;   //S2
13 int S3 = 4;   //S3
14 int S4 = 5;   //S4
15 int S5 = 6;   //S5
16 int S6 = 7;   //S6
17 int S7 = 8;   //S7
18 int S8 = 9;   //S8
19 int S9 = 10; //S9
20 int S10 = 11; //S10
21 int P1 = 12; //P1
22 int P2 = 13; //P2
23
24 void setup() {
25       Serial.begin(9600);
26       //set pins as outputs
27       pinMode(airPump, OUTPUT);          // air pump
28       pinMode(vacuumPump, OUTPUT);       // vacuum pump
29       pinMode(airValve, OUTPUT);         // air valve
30       pinMode(vacuumValve, OUTPUT);     // exhaust valve
31       pinMode(13, OUTPUT);
32
33       pinMode(S1, OUTPUT);    //S1
34       pinMode(S2, OUTPUT);    //S2
35       pinMode (S3, OUTPUT);    //S3
36       pinMode (S4, OUTPUT);    //S4
37       pinMode(S5, OUTPUT);      //S5
38       pinMode(S6, OUTPUT);    //S6
39       pinMode (S7, OUTPUT);    //S7
40       pinMode (S8, OUTPUT);    //S8
41       pinMode(S9, OUTPUT);    //S9
42       pinMode(S10, OUTPUT);    //S10
43       pinMode (P1, OUTPUT);    //P1
44       pinMode (P2, OUTPUT);    //P2
```

```
45    }
46
47    void loop() {
48       pressure = ( ( ( ( (analogRead(A0) * 5.00) / 1023) -
49        (0.10 * 5 )) * 5.0 ) / (0.8 * 5 ) );
50
51       digitalWrite(airPump, HIGH);
52       digitalWrite(airValve, HIGH);
53
54       digitalWrite(vacuumPump, LOW);
55       digitalWrite(vacuumValve, LOW);
56       delay(25000);
57
58       digitalWrite(airPump, LOW);
59       digitalWrite(airValve, LOW);
60
61       digitalWrite(vacuumPump, HIGH);
62       digitalWrite(vacuumValve, HIGH);
63       delay(15000);
64
65       digitalWrite(P1, HIGH);
66       digitalWrite(S9, HIGH);
67
68       digitalWrite(P2, LOW);
69       digitalWrite(S10, LOW);
70
71       digitalWrite(S1, HIGH);
72       digitalWrite(S3, LOW);
73
74       digitalWrite(S2, HIGH);
75       digitalWrite(S6, LOW);
76
77       digitalWrite(S5, HIGH);
78       digitalWrite(S7, LOW);
79
80       digitalWrite(S8, HIGH);
81       digitalWrite(S4, LOW);
82
83       Serial.println(analogRead(A0));  // the current pressure
84
85       if (Serial.available() > 0) {
86           incomingByte = Serial.parseInt();
87       }
88
89 }
```